

---

# **SYNTHESIS AND CHARACTERIZATION OF METHOTREXATE LOADED ZINC OXIDE NANO PARTICLES FOR EFFICIENT DELIVERY TO BREAST CANCER CELLS**

A THESIS

SUBMITTED TO

SVKM'S NARSEE MONJEE INSTITUTE OF MANAGEMENT STUDIES

(NMIMS) DEEMED-TO-UNIVERSITY

FOR THE DEGREE OF

**DOCTOR OF PHILOSOPHY  
IN  
BIOLOGICAL SCIENCE**

BY

**Mr. MITESH MANOJKUMAR JOSHI**

UNDER THE SUPERVISION OF

**Dr. PURVI BHATT**



**SUNANDAN DIVATIA  
SCHOOL OF SCIENCE**

**SUNANDAN DIVATIA SCHOOL OF SCIENCE**

SVKM's Narsee Monjee Institute of Management Studies (NMIMS) Deemed-to-University,

V.L. Mehta Road, Vile Parle (West), Mumbai – 400056, India.

**JULY 2024**

---

---

# **SYNTHESIS AND CHARACTERIZATION OF METHOTREXATE LOADED ZINC OXIDE NANO PARTICLES FOR EFFICIENT DELIVERY TO BREAST CANCER CELLS**

A THESIS

SUBMITTED TO

SVKM'S NARSEE MONJEE INSTITUTE OF MANAGEMENT STUDIES

(NMIMS) DEEMED-TO-UNIVERSITY

FOR THE DEGREE OF

**DOCTOR OF PHILOSOPHY**

**IN**

**BIOLOGICAL SCIENCES**

BY

**Mr. MITESH MANOJKUMAR JOSHI**

**Project Guide**

**Dr. Purvi Bhatt**

**Dean**

**Dr. B. Jayakumar Singh**



**SUNANDAN DIVATIA  
SCHOOL OF SCIENCE**

**SUNANDAN DIVATIA SCHOOL OF SCIENCE**

SVKM's Narsee Monjee Institute of Management Studies (NMIMS) Deemed-to-University,

V.L. Mehta Road, Vile Parle (West), Mumbai – 400056, India.

**JULY 2024**

---

---

## DECLARATION BY THE STUDENT

This is to certify work embodied in the thesis “**SYNTHESIS AND CHARACTERIZATION OF METHOTREXATE LOADED ZINC OXIDE NANO PARTICLES FOR EFFICIENT DELIVERY TO BREAST CANCER CELLS**” for the award of the Degree of Doctor of Philosophy in Biological Sciences is my contribution to the research work carried out under the supervision of ‘Dr. Purvi Bhatt.’ The work has not been submitted for the award of any other degree/to any other University. Wherever a reference has been made to earlier reported findings, it has been cited in the thesis. The thesis fulfills the requirements of the ordinance relating to the award of the Ph.D. degree of the University.

**Mr. Mitesh Manojkumar Joshi**

Place: Mumbai

Date:

Forwarded by

**Dr. Purvi Bhatt**

Associate Professor, H.O.D Biological Sciences,  
Sunandan Divatia School of Science,  
SVKM's Narsee Monjee Institute of Management Studies (NMIMS)  
Deemed-to-University V.L. Mehta Road,  
Vile Parle (West), Mumbai-400056

---

---

---

## CERTIFICATE

This is to certify that the work described in this thesis entitled “**SYNTHESIS AND CHARACTERIZATION OF METHOTREXATE LOADED ZINC OXIDE NANO PARTICLES FOR EFFICIENT DELIVERY TO BREAST CANCER CELLS**” has been carried out by Mr. Mitesh Manojkumar Joshi under my supervision. I certify that this is his Bonafide work. The work described is original and has not been submitted for any degree to this or any other University.

-----  
**Dr. B. Jayakumar Singh**  
Dean

Date:

-----  
**Dr. Purvi Bhatt**  
Project Guide

Date:

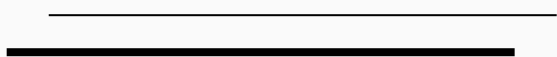
**SUNANDAN DIVATIA SCHOOL OF SCIENCE**  
**SVKM's Narsee Monjee Institute of Management Studies (NMIMS)**  
**Deemed-to-University, V. L. Mehta Road,**  
**Vile-Parle (West), Mumbai – 400056.**

---

---



*This Thesis is  
Dedicated  
To My  
Mummy, Pappa  
&  
Sister*



### Acknowledgements

As I sit down to write these acknowledgments, I find myself overwhelmed with a mix of emotions with gratitude, nostalgia, and a touch of joy. This journey, which culminates in the completion of this thesis, has been a transformative experience. It has tested my limits, expanded my horizons, and brought me face to face with both challenges and triumphs. Throughout this process, I have been fortunate to receive support from numerous individuals and institutions, without whom this achievement would not have been possible. Each person mentioned herein has left a lasting impression in every aspect of this work in their own unique way, and I gratefully acknowledge each of their contributions and support.

"I dedicate this thesis to my beloved parents **Rekha Joshi, Manoj Joshi** and my sister **Kinjal Pandya**, whose unwavering love and constant encouragement have been my guiding light throughout this challenging yet rewarding journey. Their faith and support in me have spurred me on even during moments of doubt. Their sacrifices have provided me with the foundation upon which I have built my academic pursuits. This work is a testament to their unwavering support, and I forever cherish their presence in my life."

To start with first I extend my sincere gratitude to my esteemed advisor, guide and mentor **Dr. Purvi Bhatt**, for her invaluable guidance, mentorship, and unwavering belief in my potential. Your expertise, critical insights, continuous encouragement, and push, have shaped and refined my research, making this thesis a reality. Ma'am has always pushed me to limits so that I can achieve the success. I'll always be thankful for you for your teachings and constructive comments.

Then comes another important pillar my doctoral committee members, whose advise, and constructive feedback have remained instrumental in shaping this doctoral work. **Dr. K.C. Barick**, Scientific Officer, BARC with all the help required regarding synthesis protocol and always humbly answering my queries with patience. **Professor Padma Devarajan**, Professor and Dean Research & Innovation, ICT, Mumbai for giving critical comments has really pushed me to next level and for helping us out with procurement of Methotrexate from industry. They have made sure that project reaches to its highest standards and maintains the quality research.

Also, I would like to specially thank **Dr. Aparna Khanna** ex-dean, Sunandan Divatia School of Science and **Dr. Dhananjaya Saranath**, Ex-Emeritus Professor, Sunandan Divatia School of Science for providing a stimulating academic research environment and the resources

necessary for conducting my research. From providing permissions, resolving our complaints and being the constant source of motivation, they have inculcated good research attitude in me. I will forever be grateful for their contribution in the initial phase of the work.

I am deeply indebted to the exceptional guidance and inspiration I have received from my faculties of Sunandan Divatia School of Science, that includes **Dr. Ekta Khattar** for always being that ray of hope, source of guidance, encouragement and putting faith in me with respect to all sort of responsibilities. Thank you for being the research scholar's faculty and constantly being on our side for any help. I feel grateful to have faculty like **Dr. Brijesh Sukumaran**, for his valuable guidance and expertise in tissue culture lab that laid the foundation of my PhD. For solving any technical queries to biostatistics problems, he has always been the helping faculty with great enthusiasm for life. **Dr. Harinder Singh** for always trusting me with responsibilities and believing in me. He has always heard PhD scholars including me and guided me for right things. **Dr. Prasad Pethe**, ex-faculty, for making my pre-PhD experience enriching and resourceful in the short duration. His dedication to his work and enthusiasm to teach was truly remarkable that has left lasting impression on me. Special thanks are due to **Mrs. Madhuri Khanolkar** for being there for me always from day 1. It won't be exaggeration if I say without the help of her this wouldn't have been possible. Thank you, for all the moral, mental and academic support received for past 7 years. For always understanding my feelings and allowing me to share my feeling and encouraging me to finish PhD with right mindset. I would also like to thank the other past and present administrative staff of Sunandan Divatia School of Science starting with **Mrs. Manasi Naik** for handling all the academic records and providing me with all the necessary support in same regards. **Dr. Vinod Malap** for always be ready to help and showing kind gesture towards me and keeping the environment happy and positive. Special thanks to other staff members like **Mrs. Karuna Dhamane** for helping me with all the administrative work and arranging all of our meetings on time. This part will be incomplete without mentioning **Sushma maushi**, and **Sonu** for giving me so much of love and affection and a lot of coffee on many low days. Always being there with me right from morning to late till evening and all the fun parties, examination duties and many more memories with them. Without them this PhD would not have been this easy to go. I have my extreme affection to them. **Dharmesh Bhai** for always helping with printing and other helps along with special coffee treats.

I would also like to thank **Madhura Ma'am**, SAIF, Indian Institute of Technology Bombay for their help with the flow cytometry experiments. They have been very accommodating

---

and very helpful all throughout my visits there. Special mention to SAIF, IIT-B for all the technical analysis facilities. Also, not to forget **Mrs. Geeta Pai** and **Mrs. Pooja** from Central instrumentation lab, Shobhaben Pratapbhai Patel School of Pharmacy & Technology Management for all the help regarding all the analysis of DLS, Zeta and DSC. I humbly thank all of you for all your support and contribution.

I would here by like to express my deepest gratitude to **Khandelwal Laboratories Pvt. Ltd**, Mumbai, India for providing me with Methotrexate gift sample. Without their help this work would not have reached here.

Here comes the most important people of my life and it won't be an exaggeration if I say without you guys, I couldn't have imagined to finish my PhD. Thank you for being my chosen family, the ones who celebrated my every success and embraced me through every hurdle. Starting with **Dr. Shriya Sawant** you are my crime partner, travel partner and the best friend I found. I have learnt a lot from you. Special thanks to you for always being there on the bad days and sharing food by my side. Your laughter has been my refuge, your advice my guiding light, and your companionship an invaluable gift. This thesis would not be the same without your incredible presence in my life, and I dedicate it to you with heartfelt appreciation. **Dr. Asmita Kamble** you need special mention too, for all this long unending journey and especially last year, things would not have fallen into place without your help. Thanks to your advices, knowledge and patients with me. I cannot thank you enough for being my most loyal audience to laugh on my petty jokes and keeping my morals high. Thank you for the help till the last day of submission and post that too literally. **Dr. Jasmeet Kaur Viridi**, for your invaluable inputs in experimental analysis and into some heavy-duty discussions too. To be **Dr. Ruchita Joshi**, **Ms. Meenakshi Shukla** and **Mrs. Hiral Hindocha** for our special breakfast times and laughter sessions, that have brightened my darkest days, and your belief in me has kept me going when doubt threatened to overwhelm. This thesis is a testament to the power of true friendship, and I am eternally grateful to have you all by my side.

A special mention to my beloved colleague-cum-friend to be **Dr. Alok Singh**, without his help the whole of animal work would not be possible. He was extremely helpful, kind and supportive throughout the study duration. His intellectual inputs have helped me to complete my animal work without any glitches.

My deepest appreciation goes to my research group, starting with my seniors who have mentored me at various stages during this journey, **Dr. Maneka Hoonjan**, and **Dr. Sania**

---



---

**Laheri.** always grateful for being my elder sisters at workplace and constantly motivating me to keep going. I'm really blessed to have seniors (Didi) like you guys and all the pep-talks and always being there to listen my problems. **Mr. Nimish Moramkar, Ms. Rezina Billimoria and Ms. Anuradha Panigrahi** for their unwavering support and companionship throughout this academic pursuit. Thank you for being my sounding board, my confidantes, and my partners in crime. It was great to have juniors like you guys.

To the dearest lab mates of Lab 509, **Dr. Kavita, Nikita, Evieann, Neha, Meghna, Rebecca, Shrey and Miloni.** Your companionship, collaboration, and intellectual discussions have enriched my experience and fueled my passion for research. I am grateful for the supportive and stimulating environment you have fostered. How can I forget all the potlucks, Diwali/Christmas parties and celebration of all the colorful festival days would have reminded dull without you all being involved. Your constant poke to complete all my task on time including my thesis. Thank you, guys. With some I had tiffs and with some laughs but, at the end we all were ONE. From going to academic conferences to college events and parties everything is colorful and memorable to me. My final years of PhD would not be same without you all. Few other special mentions here are **Ms. Prachi Shah** for her invaluable support for experimental design and analysis specifically for Western blot. **Dr. Shruti Bhatkalkar and Dr. Viral Mehta** for their input and support during the initial days of project. My other fellow seniors that need mention here are **Mr. Mayank Shah** for my guiding light into SDSOS and helping me with work and academic parts. **Dr. Niloufer Dumasia and Dr. Ruchita Shelat** for teaching me most important asset required in cell biology i.e Tissue culture training and being the sweetest seniors whom I can rely on. Other few important seniors too who together have made this whole journey memorable are **Dr. Vrundali, Zoya, Amruta, Dr. Nishant, Dr. Yashika and Dr. Swati.**

This journey has been enriched by the company and alliance of my fellow seniors, juniors, and my dearest students. Thank you for the countless hours of brainstorming sessions, shared learning experiences, and moments of laughter and support. To my fellow researchers, your insights and constructive criticism have helped to refine my research and shape this thesis into its final form. I am grateful to be part of such a vibrant and intellectually stimulating community.

---

I would like to thank SVKM's Narsee Monjee Institute of Management Studies (NMIMS) Deemed-to-be-University, for providing me with Doctoral fellowship/Scholarship. This really helped me with crucial financial support that I was looking forward to.

This journey has been enriched by the camaraderie and support of my fellow students whom I have taught. Thank you for sharing your knowledge, resources, and laughter. Finally, to the university staff and everyone who has played a role in this journey: I extend my sincere gratitude to the administrative staff, librarians, and technicians who have made this experience possible. Your dedication to the university community has created an environment that fosters academic excellence.

Research participants: I would like to express my sincere gratitude to all the participants who volunteered their time and effort for my research study. Your participation was essential to the success of this research. And my kind condolences to all the Mice that were sacrificed in the animal studies and my deepest gratitude towards them. Without them the animal study wouldn't have been possible.

I dedicate this thesis to each one of you, friends, family, relatives and close friends.

Thank you, Mahadev, for being a part of my journey and all the blessings.

- Mitesh Manojkumar Joshi

# Abstract

---

**Abstract**

Breast cancer is the most common cancer among women and is the second leading cause of cancer-related deaths in women, following lung cancer. Early detection and treatment play a crucial role in improving survival rates. However, metastasis and cancer resistance to therapies continue to contribute to cancer mortality. Triple-negative breast cancer (TNBC) is a type of breast cancer that does not have any hormonal receptors or HER2, which makes it more difficult to treat. Combination therapy, which involves the use of multiple agents that target different genes, disease pathways, or cell-cycle checkpoints, has shown promise in enhancing the efficacy of standard single-agent treatments.

Folic acid receptor (FAR) is a molecular marker that is highly expressed in certain cancers, including breast cancer. Targeting FAR allows for the specific delivery of antitumor agents to FAR-overexpressing cancer cells while minimizing non-specific tissue absorption. Methotrexate (MTX) is a commonly used chemotherapy drug that has shown potential in targeting FAR-overexpressing cells. Nanotechnology offers passive and active targeting strategies to enhance drug concentration within cancer cells and reduce toxicity to normal cells. Zinc oxide nanoparticles (ZnONPs) have proved its efficacy as a potential anticancer agent for various different cancer types in vitro. ZnONPs are cytotoxic as they release soluble  $\text{Zn}^{+2}$  ions in the surrounding environment which is the major factor involved into ZnONPs related toxicity.

In this study, we aimed to develop a novel system combining ZnONPs and MTX to enhance therapeutic effectiveness and minimize side effects. The synthesized MTX-ZnONPs were characterized using various techniques, revealing hexagonal crystal morphology with an average size of 30 nm and positive Zeta potential. A drug release study demonstrated biphasic drug release, with approximately 90% of the drug released within 24 hours.

Biocompatibility studies confirmed that the MTX-ZnONPs were safe for use in blood, showing no hemolysis or aggregation of blood cells. Furthermore, MTT cell viability assay revealed higher cytotoxicity of MTX-ZnONPs compared to MTX alone in breast cancer cell lines, indicating enhanced anticancer potential. Bare ZnONPs exhibited increased toxicity in control breast cells (MCF-10A) compared to MTX-ZnONPs. In addition, MTX showed different efficacy of MTX-ZnONPs against different types of breast cancer cells MCF-7 and MDA-MB-231 irrespective of their sensitivity to MTX.

---

Additional analysis, such as AO/EB staining, cell cycle analysis, and Annexin V FITC/PI assay, supported the MTT results and demonstrated dose-dependent effects of MTX-ZnONPs, revealing distinct morphological changes associated with apoptosis and necrosis. Along with this western blot data revealed that MTX-ZnONPs show intrinsic pathway activation leading to apoptosis in MCF-7 while, in MDA-MB-231 it shows necrotic death similar to results of Annexin V-FITC/PI assay. In-vivo acute oral toxicity studies in mice showed no signs of toxicity or mortality, even at the highest dose tested, suggesting that MTX-ZnONPs are not toxic to animals.

Overall, the findings of this study highlight the potential of MTX-ZnONPs as an effective and safe nanocarrier for both MTX sensitive and resistant breast cancer cells. The enhanced cytotoxicity, selectivity towards cancer cells, and biocompatibility observed in vitro, along with the absence of acute toxicity in vivo, provide a promising outlook for the application of MTX-ZnONPs in breast cancer treatment. However, further investigations are required to evaluate its long-term safety and efficacy for potential clinical use in cancer treatment.

---

**Table of contents**


---

List of Abbreviations		i
List of Figures		v
List of Tables		x
Chapter 1	Introduction	1
Chapter 2	Review of Literature	9
2.1	Breast cancer	10
2.1.1	Epidemiology of breast cancer	10
2.1.2	Anatomy of female breast	11
2.1.3	Common breast conditions	12
2.1.4	Breast cancer and risk factors	13
2.1.5	Pathogenesis of breast cancer	14
2.1.6	Diagnosis of breast cancer	18
2.1.6.1	Clinical Breast Imaging Techniques	18
2.1.6.2	Biomarkers for breast cancer detection	19
2.1.7	Treatment of breast cancer	21
2.1.7.1	Surgery	22
2.1.7.2	Radiation	23
2.1.7.3	Chemotherapy	24
2.1.7.4	Hormone therapy	26
2.1.7.5	Targeted therapy	28
2.1.7.6	Immuno therapy	29
2.2	Methotrexate (MTX)	30
2.2.1	Structure and mechanism of action	30
2.2.2	Role in cancer and other malignancies	34
2.2.3	Toxicity	35
2.2.4	Newer approach	37
2.3	Nanotechnology and its applications	41
2.3.1	What is nanotechnology?	41

2.3.2	Applications of nanotechnology in cancer	43
<b>2.4</b>	<b>Zinc oxide nanoparticles (ZnONPs)</b>	<b>46</b>
2.4.1	Biological role of Zinc (Zn)	46
2.4.2	ZnONPs properties	47
2.4.3	ZnONPs synthesis route	49
2.4.4	ZnONPs mechanism of action	52
2.4.5	ZnONPs anticancer application/drug delivery application	54
<b>Chapter 3</b>	<b>Rationale, Aim and Objectives</b>	<b>56</b>
3.1	Rationale	57
3.2	Aim	57
3.3	Objectives	57
<b>Chapter 4</b>	<b>Synthesis, Characterization, and drug release study of nanoparticles</b>	<b>58</b>
<b>4.1</b>	<b>Introduction</b>	<b>59</b>
4.1.1	Synthesis of nanoparticles	59
4.1.2	Characterization of nanoparticles	60
4.1.2.1	UV-Vis Spectroscopy	60
4.1.2.2	Fourier Transform Infrared (FTIR) spectroscopy	60
4.1.2.3	X-Ray Diffraction (XRD)	60
4.1.2.4	Inductively coupled plasma-atomic absorption spectroscopy (ICP-AES)	61
4.1.2.5	Zeta potential and Dynamic light scattering (DLS)	61
4.1.2.6	Energy dispersive spectroscopy (EDS)-mapping	61
4.1.2.7	High-resolution transmission electron microscopy (HR-TEM)	61
<b>4.2</b>	<b>Materials and Methods</b>	<b>62</b>
4.2.1	Synthesis of Bare ZnONPs	62
4.2.2	Synthesis of Methotrexate loaded Zinc oxide nanoparticles (MTX-ZnONPs)	62
4.2.3	MTX loading efficiency	63
4.2.4	Characterization	63

4.2.2.1	UV-Vis Spectroscopy	63
4.2.2.2	FTIR spectroscopy	63
4.2.2.3	XRD	63
4.2.2.4	ICP-AES	64
4.2.2.5	Zeta potential and DLS	64
4.2.2.6	EDS-mapping	64
4.2.2.7	HR-TEM	64
4.2.2.8	Stability of NPs	64
4.2.5	Drug release study of MTX-ZnONPs	64
<b>4.3</b>	<b>Results</b>	<b>65</b>
4.3.1	UV-Vis Spectroscopic analysis	65
4.3.2	Fourier Transform Infrared Spectroscopic analysis	66
4.3.3	X-Ray Diffraction analysis	69
4.3.4	Inductively coupled plasma-atomic absorption spectroscopic analysis	70
4.3.5	Zeta potential and DLS analysis	71
4.3.6	Energy Dispersive Spectroscopy-Mapping analysis	72
4.3.7	High Resolution-Transmission Electron Microscopic analysis	73
4.3.8	Stability analysis of NPs	76
4.3.9	Drug release study of MTX-ZnONPs	77
<b>4.4</b>	<b>Discussion</b>	<b>78</b>
<b>4.5</b>	<b>Conclusion</b>	<b>82</b>
<b>Chapter 5</b>	<b>In-vitro study to evaluate the anti-cancer activity of Methotrexate loaded Zinc oxide nanoparticles on breast cancer cell lines</b>	<b>83</b>
<b>5.1</b>	<b>Introduction</b>	<b>84</b>
5.1.1	MTT Cellular viability assay	85
5.1.2	Acridine Orange/ Ethidium Bromide (AO/EB) viability staining	86



5.1.3	Cell cycle analysis by Propidium Iodide (PI) staining	88
5.1.4	Annexin V-FITC- Propidium Iodide assay	90
5.1.5	Western blot analysis	92
<b>5.2</b>	<b>Materials and Methods</b>	<b>95</b>
5.2.1	Cell lines	95
5.2.2	Chemicals and reagents	96
5.2.3	Cell culture methodology	96
5.2.3.1	Heat inactivation of FBS	96
5.2.3.2	Preparation of complete media	97
5.2.3.3	Maintenance of cell lines	97
5.2.4	MTT Cellular viability assay (in vitro cell cytotoxicity assay)	101
5.2.5	Acridine Orange/ Ethidium Bromide (AO/EB) viability staining	101
5.2.6	Cell cycle analysis by flowcytometry	102
5.2.7	Annexin V FITC- Propidium Iodide assay	102
5.2.8	Western blot analysis	103
<b>5.3</b>	<b>Results</b>	<b>103</b>
5.3.1	MTT Cellular viability assay (in vitro cell cytotoxicity assay)	103
5.3.2	Acridine Orange/ Ethidium Bromide (AO/EB) viability staining	106
5.3.3	Cell cycle analysis by flowcytometry	110
5.3.4	Annexin V FITC- Propidium Iodide assay	113
5.3.5	Western blot analysis	116
<b>5.4</b>	<b>Discussion</b>	<b>119</b>
<b>5.5</b>	<b>Conclusion</b>	<b>122</b>
<b>Chapter 6</b>	<b>Blood biocompatibility studies</b>	<b>123</b>
<b>6.1</b>	<b>Introduction</b>	<b>124</b>

<b>6.2</b>	<b>Materials and Methods</b>	<b>125</b>
6.2.1	Hemolysis study	125
6.2.2	Blood cell aggregation study	125
<b>6.3</b>	<b>Results</b>	<b>126</b>
6.3.1	Hemolysis study	126
6.3.2	Blood cell aggregation study	128
<b>6.4</b>	<b>Discussion</b>	<b>130</b>
<b>6.5</b>	<b>Conclusion</b>	<b>131</b>
<b>Chapter 7</b>	<b>In-vivo acute oral toxicity study</b>	<b>132</b>
<b>7.1</b>	<b>Introduction</b>	<b>133</b>
<b>7.2</b>	<b>Materials and Methods</b>	<b>134</b>
7.2.1	Animal ethics approval	134
7.2.2	Animal experimentation & housing	135
7.2.3	Experimental design	135
7.2.4	Observations	136
<b>7.3</b>	<b>Results</b>	<b>136</b>
<b>7.4</b>	<b>Discussion</b>	<b>141</b>
<b>7.5</b>	<b>Conclusion</b>	<b>141</b>
<b>Chapter 8</b>	<b>Summary and Conclusion</b>	<b>142</b>
	<b>Bibliography</b>	<b>145</b>
	<b>Appendix</b>	<b>175</b>
	<b>List of Conferences/ Workshops/ Award(s)</b>	<b>189</b>
	<b>List of Publications</b>	<b>192</b>
	<b>Synopsis</b>	<b>194</b>

---

**List of Abbreviations**

ADM	Adriamycin
AgNPs	Silver nanoparticles
ALL	acute lymphoblastic leukemia
ALND	Axillary lymph node dissection
ALP	Alkaline phosphatase
ALT	Alanine aminotransferase
AML	Acute myelogenous leukemia
AO	Acridine Orange
AST	Aspartate aminotransferase
ATR	Attenuated total reflection
AuNPs	Gold nanoparticles
BCS	Breast-conserving surgery
BSA	Bovine Serum Albumin
BUS	Breast ultrasound
CDK	Cyclin dependent kinases
CEM	Contrast enhanced mammography
CNTs	Carbon nanotubes
CPCSEA	Committee for the Purpose of Control and Supervision of Experiments on Animals
CR	Cumulative Release
CS	Chitosan
CSCs	Cancer stem cells
CTCs	Circulating Tumor Cells
CTX	Cyclophosphamide
CTX	DNA-binding domain
DCIS	Ductal carcinoma in situ
DDS	Drug delivery system
DHFR	Dihydrofolate reductase
DLS	Dynamic light scattering

---

DMARDs	Disease-modifying antirheumatic drugs
DMEM	Dulbecco's Modified Eagle's Medium
DOX	Doxorubicin
DPBS	Dulbecco's Phosphate Buffered Saline
EB	Ethidium bromide
EBRT	External beam radiation therapy
EDS	Energy dispersive spectroscopy
E <sub>g</sub>	Band gap energy
EGFR	Epidermal growth factors
EPR	Enhanced permeability and retention
ER	Estrogen receptor
FA	Folic acid
FAR	Folic acid receptor
FBS	Foetal bovine serum
FDA	Food and Drug Administration
FITC	Fluorescein isothiocyanate
FSH	Follicle-stimulating hormone
FTIR	Fourier transform infrared spectroscopy
FWHM	Full width at half maximum
GGT	Gamma-glutamyltransferase
GHS	Globally Harmonized System
GRAS	Generally regarded as safe
HER2	Human epidermal receptor 2
HOMO	Highest occupied molecular orbital
HRP	Horseradish peroxidase
HRT	Hormone replacement therapy
HR-TEM	High-resolution transmission electron microscopy
IARC	International agency for research on cancer
IBC	Inflammatory breast cancer
ICP-AES	Inductively Coupled Plasma-Atomic Emission Spectrometry

IEC	Institutional Ethics Committee
IEP	Iso electric point
LD <sub>50</sub>	Lethal dose 50
LH	Luteinizing hormone
LUMO	Lowest occupied molecular orbital
LV	Leucovorin
mAb	Monoclonal antibodies
MEGM	Mammary Epithelial Cell Growth Medium
MOM	Mitochondrial outer membrane
MRI	Magnetic resonance imaging
MTX	Methotrexate
MTX-ZnONPs	Methotrexate loaded Zinc oxide nanoparticles
NCCS	National Centre for Cell Sciences
NFDM	Nonfat dried milk
NHL	Non-Hodgkin lymphoma
NPs	Nanoparticles
OECD	The Organization for Economic Cooperation and Development
PEG	Polyethylene glycol
PEG-400	Poly ethylene glycol 400
PEI	Poly ethylene imine
PI	Propidium iodide
PR	Progesterone receptor
PRP	Platelet-rich plasma
PS	Phosphatidylserine
PVA	Poly vinyl alcohol
PVDF	Polyvinylidene fluoride
QDs	Quantum dots
RBCs	Red blood cells
RCF	Reduced folate carrier 1
ROS	Reactive oxygen species

RT	Room temperature
SAED	Selected area electron diffraction
SCLC	Small cell lung cancer
SEM	scanning electron microscope
SLNB	Sentinel lymph node biopsy
SPIONs	Super para magnetic nanoparticles
TEA	Tri ethyl amine
TiO <sub>2</sub> NPs	Titanium dioxide nanoparticles
TiONPs	Titanium dioxide nanoparticles
TNBC	Triple negative breast cancer
UV-Vis	Ultraviolet-visible
VCR	Vincristine
WBCs	White blood cells
XRD	X-ray diffraction
Zinc	Zn
ZnONPs	Zinc oxide nanoparticles

## List of Figures

Figure No.	Figure Caption	Page No.
1.1	Distribution of Incidence and Mortality for the 10 Most Common Cancers globally in 2020 for Both Sexes (Source: Globocan, 2020)	3
1.2	Burden of breast cancer in female population in World and India (a) Estimated number of new incident cases in world, (b & c) estimated number of new incident cases and deaths in India 2020 (Source: Globocan, 2020)	4
2.1	Estimated number of prevalent cases of Cancer in India (Source: Globocan, 2020)	10
2.2	Female breast anatomy- side view (Source- Johns Hopkins Medicine)	11
2.3	Structural similarities between Folic acid and Methotrexate molecule (Source: Halik et al., 2021)	31
2.4	Graphical representation of Methotrexate's mechanism of action. (FAR; Folic acid receptor. RCF; reduced folate carrier. MTX(GLU 1-7); methotrexate polyglutamates. FPGS; folypolyglutamyl synthase. DHFR; dihydrofolate reductase. DHF; dihydrofolate. THF; tetrahydrofolate. 5,10-CH <sub>2</sub> -THF; 5,10-methylenetetrahydrofolate. 5-CH <sub>3</sub> -THF; 5-methyltetrahydrofolate. MTHFR; methylenetetrahydrofolate reductase. dUMP; deoxyuridine monophosphate. dTMP; deoxythymidine monophosphate. GGH; $\gamma$ -glutamyl hydrolase. ATIC; AICAR formyltransferase. AICAR; 5-aminoimidazole 4-carboxamide ribonucleotide. FAICAR; 10-formyl AICAR.)	33
2.5	Graphical presentation of nanoscale comparison of various entities for comparison purpose. (Source: Bayda et al., 2020)	42
2.6	Applications of nano science in the fields of Chemistry, biology and physics (Source: Bayda et al., 2020)	45
2.7	ZnONPs mechanism of action (Source: Bisht and Rayamajhi, 2016)	53
4.1	UV-Vis spectroscopic analysis of bulk ZnO, bare ZnONPs, MTX-ZnONPs and MTX showing their respective normalized spectra in the range of 200-800 nm wavelength. Inset showing Tauc's plot of bare ZnONPs for bandgap energy measurement.	66
4.2	FTIR spectroscopy analysis of bare ZnONPs (red), MTX-ZNONPs (blue) and MTX (pink) showing their respective spectra when recorded in the wavelength range of 4000-400 cm <sup>-1</sup> .	68
4.3	XRD analysis of bare ZnONPs, MTX-ZnONPs and MTX revealing their respective diffraction spectrum recorded in the range of 20- 80 2 $\theta$ angle.	70

4.4	Zeta potential and Dynamic Light Scattering (DLS) analysis of bare ZnONPs and MTX-ZnONPs. (a) Zeta potential of bare ZnONPs and MTX-ZnONPs was analyzed across wide pH range and plotted, (b) DLS analysis of bare ZnONPs and MTX-ZnONPs size distribution data in histogram.	71
4.5	EDS mapping images of (a) bare ZnONPs; (b) MTX-ZnONPs, showing Zinc (blue), Oxygen (green) and Carbon (red). (Right) showing EDS spectrum with elemental values in table, (left) EDS micrographs showing each element mapped with different colors.	73
4.6	HR-TEM analysis of nanosystems showing HR-TEM of image of (a) bare ZnONPs and (e) MTX-ZnONPs; size distribution curve of (b) bare ZnONPs and (f) MTX-ZnONPs; crystal lattice structure of (c) bare ZnONPs and (g) MTX-ZnONPs; SAED pattern of (d) bare ZnONPs and (h) MTX-ZnONPs.	75
4.7	Physical stability study for color, flow and texture study of bare ZnONPs and MTX-ZnONPs at two different time points.	77
4.8	Drug release study of MTX-ZnONPs conducted in PBS at pH 7.4 and pH 5.0	78
5.1	A simplified overview of the principle behind MTT assay. Viable cells take up the yellow tetrazolium dye MTT (3-(4,5-dimethylthiazol-2-yl)-2,5-diphenyltetrazolium bromide) which is reduced to purple formazan crystals by mitochondrial dehydrogenase enzymes. Chemical structure of MTT and its reduced form, formazan. The tetrazole ring in MTT (1) is converted to a formazan by cellular enzymes. The red arrows indicate the reduction process, while the dashed lines and minus symbol represent factors that can disrupt MTT reduction or hinder uptake, leading to inaccurate OD measurements. It also illustrates various factors that can affect MTT assay measurements. (Source: Ghasemi et al., 2021)	86
5.2	Morphological difference between apoptosis and necrosis of a cell. On the left side notice the blebs being made and eaten by a phagocyte as fate of cells in apoptosis. Right hand side of image shows swelling, inflammatory response, and leak leaks everywhere which will induce inflammation and possible organ failure. (Source: Robbins and Cotran pathologic basis of disease, 9th ed.)	87
5.3	The cell cycle is divided into four main phases: G1 (growth phase 1), S (synthesis phase), G2 (growth phase 2), and M (mitotic phase). Each phase plays a crucial role in preparing the cell for division. This histogram on right depicts the results of a cell cycle analysis using propidium iodide (PI) staining, a common method for quantifying cellular DNA content using flow cytometer. The horizontal axis represents the relative fluorescence intensity of PI, which is proportional to the amount of DNA present in each cell. The vertical axis represents the number of cells detected at each fluorescence intensity level. Cells in G1 have 2n DNA content, having already duplicated their DNA in the previous cell cycle. During the S phase, DNA replication occurs, leading to a doubling of DNA content to 4n. Cells in G2 maintain 4n DNA	89



	content, preparing for mitosis. Mitosis involves cell division, resulting in daughter cells with $2n$ DNA content each.	
5.4	This schematic diagram illustrates the principle of Annexin V-FITC/PI staining, a common method for identifying and differentiating healthy, early apoptotic, and late apoptotic cells. (a) Illustrates a normal healthy cell membrane. The phospholipid bilayer of the cell membrane is shown as a smooth, uninterrupted structure. Neither Annexin V-FITC (green) nor PI (red) can enter the cell, resulting in no fluorescence signal, (b) Represents an early stage apoptotic cell membrane. Early in apoptosis, phosphatidylserine (PS) flips from the inner leaflet to the outer leaflet of the plasma membrane. Annexin V-FITC, with high affinity for PS, binds to the exposed PS on the cell surface, resulting in green fluorescence. PI remains excluded due to the intact plasma membrane, resulting in no red fluorescence, (c) Shows a late stage apoptotic cell membrane. In late apoptosis or necrosis, the plasma membrane loses its integrity and permeability. Both Annexin V-FITC and PI can enter the cell. Annexin V-FITC binds to PS, while PI binds to DNA, resulting in a double-positive signal with green and red fluorescence. (Source: <a href="https://www.dojindo.com/">https://www.dojindo.com/</a> )	91
5.5	Intrinsic and Extrinsic Apoptosis Pathways in cell leading to apoptosis: This diagram depicts two main pathways of programmed cell death, or apoptosis: the intrinsic pathway and the extrinsic pathway. Both pathways ultimately lead to the activation of caspases, which dismantle the cell's essential components, resulting in cell death. In intrinsic pathway the stress signals trigger the release of cytochrome c from the mitochondria into the cytosol. Cytochrome c binds to Apaf-1, forming a complex that activates caspase-9. Caspase-9 activates downstream caspases (caspase-3, caspase-7), leading to the execution of apoptosis. Extrinsic pathway is initiated by external signals called death ligands, such as Fas ligand or $\text{TNF-}\alpha$ , binding to their specific receptors on the cell surface. Death receptor binding induces the clustering and activation of caspase-8 or caspase-10. imilar to the intrinsic pathway, activated caspase-8/10 triggers the downstream caspases (caspase-3, caspase-7), leading to apoptosis execution. (Source: Wanner, E., Thoppil, H., & Riabowol, K. 2020).	93
5.6	Phase contrast microscopy images of the cell lines MCF-10A, MCF-7 and MDA-MB-231 as observed under $10\times$ , $20\times$ and $40\times$ magnifications.	99
5.7	Effect of bare ZnONPs, MTX-ZnONPs and MTX on mitochondrial function in (a) MCF-10A (b) MCF-7 (c) MDA-MB-231 cells. Cell viability was determined by the MTT reduction assay after 24 hrs and 48 hrs. Data presented are mean $\pm$ SD. Asterisk above columns indicate statistically significant difference compared to bare ZnONPs ( $***=p < 0.001$ , $**=p < 0.01$ , $*=p < 0.05$ )	105

5.8	AO/EB dual staining of MCF-10A cells for live dead cell screening treated with bare ZnONPs, MTX-ZnONPs and MTX at concentration range of 10-30 $\mu\text{g}/\text{mL}$ . Magnification: 20X	107
5.9	AO/EB dual staining of MCF-7 cells for live dead cell screening treated with bare ZnONPs, MTX-ZnONPs and MTX at concentration range of 2.5-7.5 $\mu\text{g}/\text{mL}$ . Magnification: 20	108
5.10	AO/EB dual staining of MDA-MB-231 cells for live dead cell screening treated with bare ZnONPs, MTX-ZnONPs and MTX at concentration range of 40-60 $\mu\text{g}/\text{mL}$ . Magnification: 20X	109
5.11	Cell cycle analysis by PI staining for MCF-7 cells treated with bare ZnONPs, MTX-ZnONPs and MTX for 24 hrs. Data is presented as Bar graph (left) and Histogram (right). Asterisk in the columns indicate statistically significant difference compared to control group (* $p \leq 0.05$ ; ** $p \leq 0.01$ ; *** $p \leq 0.001$ )	111
5.12	Cell cycle analysis by PI staining for MDA-MB-231 cells treated with bare ZnONPs, MTX-ZnONPs and MTX for 24 hrs. Data is presented as Bar graph (left) and Histogram (right). Asterisk in the columns indicate statistically significant difference compared to control group (* $p \leq 0.05$ ; ** $p \leq 0.01$ ; *** $p \leq 0.001$ )	112
5.13	Apoptosis analysis by Annexin V-FITC/ PI for MCF-7 cells treated with bare ZnONPs, MTX-ZnONPs and MTX for 24 hrs. Data is presented as Bar graph (left) and Scatter plot (right). Asterisk in the columns indicate statistically significant difference compared to control group (* $p \leq 0.05$ ; ** $p \leq 0.01$ ; *** $p \leq 0.001$ )	114
5.14	Apoptosis analysis by Annexin V-FITC/ PI for MDA-MB-231 cells treated with bare ZnONPs, MTX-ZnONPs and MTX for 24 hrs. Data is presented as Bar graph (left) and Scatter plot (right). Asterisk in the columns indicate statistically significant difference compared to control group (* $p \leq 0.05$ ; ** $p \leq 0.01$ ; *** $p \leq 0.001$ )	116
5.15	Western blot analysis for MCF-7 cells treated with bare ZnONPs, MTX-ZnONPs and MTX for 24 hrs. Asterisk in the columns indicate statistically significant difference compared to control group (* $p \leq 0.05$ ; ** $p \leq 0.01$ ; *** $p \leq 0.001$ )	118
5.16	Western blot analysis for MDA-MB-231 cells treated with bare ZnONPs, MTX-ZnONPs and MTX for 24 hrs. Asterisk in the columns indicate statistically significant difference compared to control group (* $p \leq 0.05$ ; ** $p \leq 0.01$ ; *** $p \leq 0.001$ )	120
6.1	RBC hemolysis study of Bare ZnONPs, MTX-ZnONPs and MTX. (a) visual presentation of hemolysis assay in tubes; (b) graphical presentation of % hemolysis when plotted against concentration.	122

6.2	Blood cell aggregation assay performed with bare ZnONPs, MTX–ZnONPs and MTX at 200 µg/ ml. Graphical presentation of % hemolysis and visual presentation of the test. (Magnification 40X)	129
7.1	Experimental protocol used as per OCED TG 425 guideline.	136

---



---

List of Tables

<b>Table No.</b>	<b>Table Title</b>	<b>Page No.</b>
2.1	Chemotherapy drug classes and mode of action	25
2.2	Summary of Novel nanocarriers used for MTX delivery.	40
4.1	List of all the functional groups identified based on FTIR spectrum analysis of bare ZnONPs, MTX-ZnONPs and MTX.	67
4.2	Zn <sup>+2</sup> concentration determined from ICP-AES analysis of bare ZnONPs and MTX-ZnONPs	70
4.3	Observation table of colloidal stability study for bare ZnONPs and MTX-ZnONPs.	76
5. 1	Optimized conditions for maintenance of cell lines	100
7.1	Animal grouping scheme as per experimental protocol	135
7.2	Effect of MTX-ZnONPs different doses on body weight of mice	137
7.3	Observation table for physical parameters and behavioral patterns recorded for mice treated with 55 mg/ kg group.	138
7.4	Observation table for physical parameters and behavioral patterns recorded for mice treated with 175 mg/ kg group.	139
7.5	Observation table for physical parameters and behavioral patterns recorded for mice treated with 550 mg/ kg group.	140

# Chapter 1

# Introduction

---

## Introduction

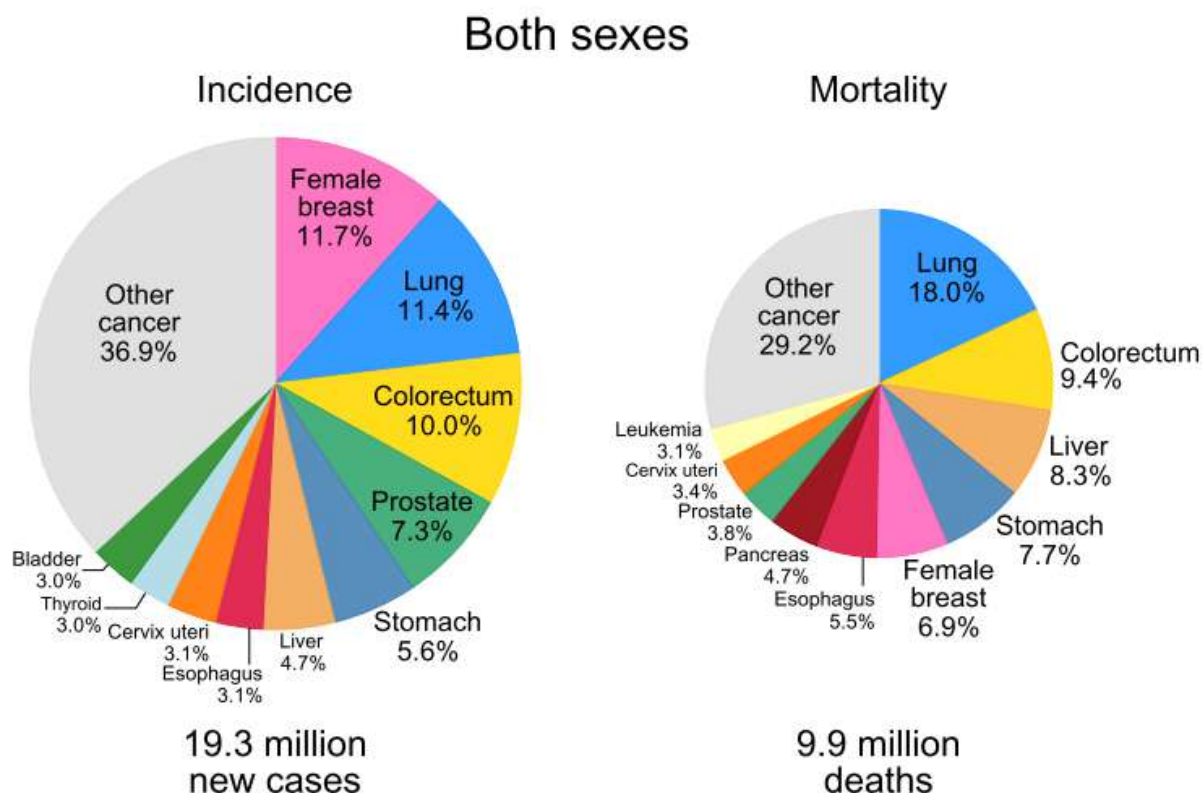
Cancer that's mainly characterized as uncontrolled growth and spread of abnormal cells is one of the highly talked and researched non communicable disease with globally highest number of reported cases and death. Cancer being multifactorial and very dynamic in its nature has become challenge to healthcare and research industry. Cancer is among the key disease's humans are dealing since the ancient times to till today's morden era. Cancer has emerged as an issue of global concern and a major cause of death across the globe (Understanding Cancer - National Cancer Institute, 2016). Cancer can be caused due to mutation in somatic cell that eventually on accumulation changes the functioning of few pivotal genes to healthy functioning of cell. When a normal cell loses its control over cell cycle it becomes immortal and gains the ability of uninterrupted division. These changes mainly occur due to mutations in the genes known as Oncogenes or Tumor suppressor gene which lead to change in sensitive mechanism of cell to go for uncontrolled cell division which we call cancer. These mutations can be caused due to internal or external factors eventually leading to activation of array of metabolic and genetic pathways giving rise to new neoplastic cells. Cancer cells shows some typical features like uninterrupted proliferation, evasion of apoptosis, invasion, and angiogenesis (Khanna and Berek, 2015). Cancer can develop in any part of body where every cell has potential to develop as cancer cell. These cells then form tumor, a mass of uncontrolled growth of cells exception is blood cancers where tumors are not formed. The rate at which cancer cases are increasing across the globe is very disturbing and controlling mortality rate has come as a challenge. The 5-year prevalence rate for cancer incidence is expected to reach 43.8 million by the year of 2023 which is almost twice the current count. Lung cancer, colorectal cancer, stomach cancer, hepatocellular carcinoma and breast cancer remain top cancers with high mortality rates together accounts for almost 50% of total deaths reported across the globe (Ferlay et al., 2019). Cancer cells typically show two major types:

**Benign tumors:** in this type of tumor generally do not spread to other tissues or organs of the body. These could be fibromas, adenomas, hemangiomas, papillomas, osteochondromas etc.

**Malignant tumors:** Where cells of neoplasm acquire ability to get detach and spread to other distant sites in body via lymphatic or blood system, a phenomenon known as metastasis.

Based on type of cancer cells involved it can either be invasive viz. (invasive lobular or invasive ductal carcinomas) or non-invasive viz. (carcinoma in-situ). Majority of cancers are metastatic, and they remain undetected for very long time and thus difficult to diagnose and thus one of the prime causes of death. Metastatic tumors remain difficult to treat and thus chances of

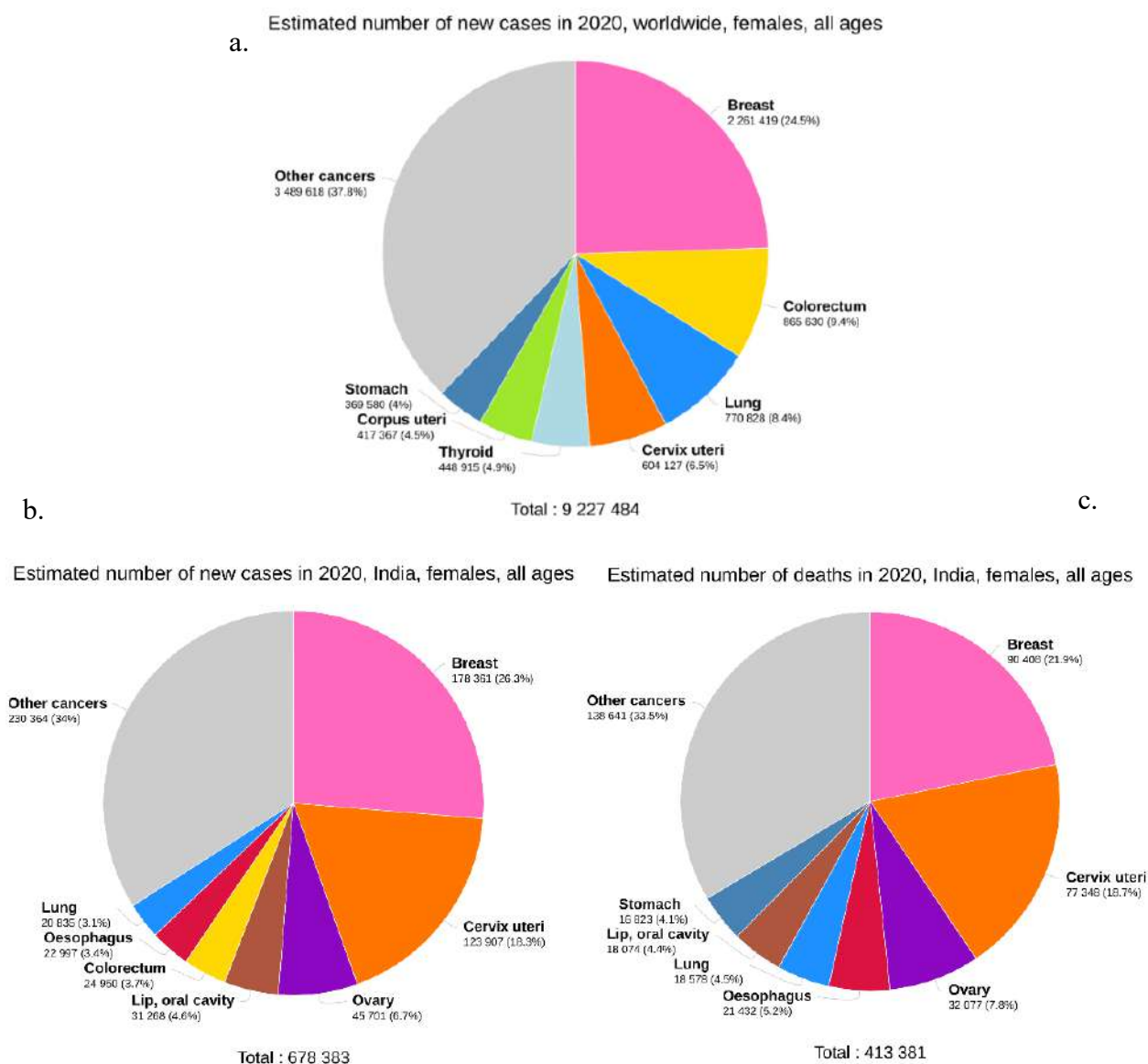
relapse remain fair. Data from the International Agency for Research on Cancer (IARC) suggests that one-in-six females and one-in-five males will develop cancer in their lifetime and one-in-eleven females and one-in-eight males will die because of it. GLOBOCAN, 2020 data reveals that, number of new cancer cases have escalated from 18.1 million in 2018 to 19.3 million in 2020.



**Figure 1.1** Distribution of Incidence and Mortality for the 10 Most Common Cancers globally in 2020 for Both Sexes (Source: Globocan, 2020)

On the same note, mortality rate all over the world has gone to 9.9 million deaths. According to the report breast cancer (11.7%), lung cancer (11.4%), colorectum cancer (10.0%) followed by prostate cancer (7.3%) and stomach cancer (5.6%) are the top five globally reported cancer which accounts for nearly half of the of the total reported cases worldwide **Figure 1.1**. Epidemiologically, Asia accounts for the 49.3% new cancer cases and highest numbers of deaths at 58.3% followed by Europe and America. With 2.3 million new incidence cases, breast cancer has surpassed the lung cancer and globally becomes the leading cause of cancer in both sexes and even in females with incident rate of 11.7% and 24.5% respectively (**Figure 1.2**). Worldwide cancer related deaths breast cancer ranks 5<sup>th</sup> considering both sexes at 6.9% and chief cause of death in women with 15.5%. Breast cancer is the most frequently diagnosed

cancer in women, In India, breast cancer cases are responsible for 1/4<sup>th</sup> of all the cases reported with an incidence rate of 26.3% and highest cancer related deaths in females are also reported by breast cancer with mortality rate of 21.9% (Sung et al., 2021).



**Figure 1.2** Burden of breast cancer in female population in World and India (a) Estimated number of new incident cases in world, (b & c) estimated number of new incident cases and deaths in India 2020 (Source: Globocan, 2020)

Breast cancer is a heterogenous solid tumor in nature with increasing challenge to diagnosis and treatments. Breast cancer can be of different types depending on the type of breast tissues involved in it. Breast cancer can be developed in any region of breast like lobules which are the glands that produce milk, ducts are the tissues that carries milk from lobules to nipple and connective tissues that also have fat tissues in it responsible for structural and supporting other



---

tissues. Based on the tumor location it can be called as invasive lobular carcinoma and invasive ductal carcinoma which are aggressive types where cancer cells can spread from one tissue to other. Ductal carcinoma in situ (DCIS) is the most common type of breast cancer which is seen amongst females (Cindy B. Matsen, 2013).

Tumor cells can become invasive anytime and can metastasise to different regions of body. Based on how the cancer spreads, it is divided into stages, grade, and its biomarker status to understand its clinical progression and treatment options. Breast cancer cells also show expression of certain types of receptors on it like Estrogen receptor (ER), Progesterone receptor (PR) and human epidermal growth factor 2 (HER2) that are hence called ER<sup>+</sup>, PR<sup>+</sup> and HER2<sup>+</sup> breast cancer. Whereas in some cases all three types of receptors are present or absent they can be called as triple positive breast cancer or triple negative breast cancer (TNBC). Presence or absence of these receptors on tumor cells can decide the course of treatment (Parsa et al., 2016). MCF-7 cell line represents the most common subtype of breast cancer (ER-positive, HER2-negative) and exhibits slower growth and less aggressive behaviour with higher MTX sensitivity. MCF-7 is one of the most extensively studied breast cancer cell lines, with an abundant data on its biology and response to various anti-cancer agents. This facilitates data interpretation and comparison with previous studies (Shandiz et al., 2021). MDA-MB-231 represents a more aggressive subtype of breast cancer being a type of TNBC. MDA-MB-231 cells exhibit a high migratory and invasive capacity, characteristic of advanced breast cancer. This cell line also shows high MTX resistance providing a contrasting model to MCF-7 and allows for evaluation of MTX efficacy against a more challenging, therapy-resistant phenotype (Dawood, 2016).

Diagnosis route for breast cancer still follows the classical methods like physical examination being the primary followed by mammogram to advanced tests like MRI scan, bone scan, CT scan, breast biopsy or blood tests (Hutchinson, 2010). Treatment strategy available for breast cancer can be surgery, radiation therapy, chemotherapy, hormonal therapy, and targeted therapy. Surgery is possible only in early stages of cancer where tumor size is small, operatable, and not metastasized. Radiation therapy leads to secondary complications. Chemotherapy is used as an adjuvant therapy along with other types of therapy to minimize the risk of cancer relapse. Different classes of anti-cancer drugs are used like alkylating agents, antimetabolite, hormonal or biological like monoclonal antibodies (mAbs) depending on the grade and biomarker type of cancer (Cindy B. Matsen, 2013).

---

---

The main goal of using anti-neoplastic drugs is to achieve maximum plasma concentration at lower dose to get show maximum effect on cancer cells and leaving healthy cells almost unharmed, but this has always remained as a challenge due to inherent physiochemical properties of drug. Conventional chemotherapeutic agents in use comes with quite a lot of limitations such as non-specific distribution and targeting in addition to life threatening side effects and resistance in cancer cells. To minimize toxicity and resistance problem, targeted therapies are seen as a solution. Targeting the molecular markers on cancer cell is so far the best strategy available that can help differentiate between cancerous and non-cancerous cells, specifically deliver the drug to tumor specific sites and enhance its tumor site accumulation (Sha Jin, 2013). Folic acid receptor (FAR) are best molecular markers available on vast majority of cancer cells whose expression level increases 20-30 folds in certain cancers like ovarian, breast, cervical etc for their increasing demand of folic acid. FAR overexpression levels can be explained by the rapidly dividing and growing cells which have exceptional requirements for synthesis of nucleic acids and metabolism. By targeting FAR overexpressing cancer cells with class of antimetabolite drugs like Methotrexate (MTX), can help deliver the therapeutic agent specifically to these cells and avoiding non-specific tissue targeting (Cheung et al., 2016; Fasehee et al., 2016). In the current study, Methotrexate, a known anti-folate agent was explored for its role in targeting cells overexpressing folic acid receptor. MTX is an analogue of folic acid molecule with minor changes in the structure, it also binds to the same site of folic acid on FAR and internalized in the cell.

Nanotechnology offers both passive and active targeting strategies that can enhance the intracellular concentration of drugs in cancer cells and at the same time avoid toxicity to normal cells. Use of nanoparticles along with drug has advantage of using two different strategies to target cancer cells. Nanotechnology is extending its roots deep into the fields of medical science, technology and research providing niche to develop further advancements. More than six decades back in time physicist, Dr. Richard Feynman conceived the first ever idea of “nanotechnology” in his famous paper ‘There’s Plenty of Room at the Bottom’ (Feynman, 1997) and ever since nanotechnology has taken a leap in several areas (Manoranjan Arakha, 2018). Nanomaterials have received greater attention due to remarkable and distinct electric, optical, and mechanical properties with high surface area to volume ratio, size, shape, and quantum confinement effect. The crux of the field is molecule at its nanoscale than its bulk counterpart which changes the optical, mechanical, and biological properties making them more attractive for various applications. Going by conventional definition, nanoparticles (NPs)

---

can be defined as any particle having size range of 1–100 nm in at least one dimensions. Nanomaterials can be of different types like carbon nanomaterials: carbon nano tubes (CNTs), carbon nano wire. Metal/ metal oxide nanoparticles: Gold nanoparticle (AuNPs), Silver nanoparticles (AgNPs), Zinc oxide nanoparticles (ZnONPs), Titanium dioxide nanoparticles (TiO<sub>2</sub>NPs), Super para magnetic nanoparticles (SPIONs) etc. Polymeric nanoparticles which are made up of organic/ synthetic/ natural polymers or in combination, optimal for drug delivery application (Anselmo and Mitragotri, 2019; Hobson, 2009). Of the several NPs that have been tested positive for their anticancer potential in vitro, Zinc oxide (ZnO) amongst them has proved its efficacy as a potential anticancer agent for various cancers. ZnO is a white powder with USFDA approved “Generally Regarded as Safe” (GRAS) status for human external application. ZnO in its bulk form is used in many cosmetic and medical ointments and food additives. ZnONPs offers attractive properties such as easy synthesis, biocompatibility UV absorption, antimicrobial activity, anticancer activity, preferential killing of cancer cells by reactive oxygen species (ROS) generation leading to apoptosis (Xiong, 2013). ZnONPs are better anticancer agents compared to its bulk counterpart owing to its nanoparticle properties like small size, shape and large surface area and large bandgap energy (ZnO is being used in various different forms like quantum dots, nanoparticles, nanocomposite etc. for imaging, detection and as a treatment agent for various different cancer types (Shobhaa et al., 2017). ZnONPs cytotoxicity is attributed to its release of soluble Zn<sup>+2</sup> ions in the surrounding environment which is the major route for generation of ROS in cell. ZnONPs being positively charged selectively attracted towards cancer cells and leads to membrane destabilization and impaired permeability of cells. Increased ions in the cell leads to generation of reactive oxygen species (ROS) in the cell which generates oxidative stress on the cell and DNA damage, protein damage and ultimately apoptosis of cell (Wingett et al., 2016).

Nanotechnology offers both passive and active targeting strategies that can enhance the intracellular concentration of drugs in cancer cells and at the same time avoid toxicity to normal cells (Sarkar et al., 2018). Several NPs that have been tested in vitro; ZnONPs has proved its efficacy as a potential anti-cancer agent for various cancer types. ZnONPs offers attractive properties such as easy synthesis, biocompatibility, and preferential killing of cancer cells, by ROS generation, DNA damage, leading to apoptosis (Singh et al., 2020). By combining the ZnONPs and MTX, as novel system, we anticipate that the system will enhance the therapeutic effectiveness and minimize the side effects by individual systems when used alone. Also, this study will also highlight the potential of new nano formulations effectiveness against cell lines

---

---

showing variable sensitivity to MTX (MCF-7-MTX sensitive; MDA-MB-231- MTX resistant). Therefore, this study has the potential to contribute significantly towards the development of more targeted and efficient cancer treatments. Using series of characterizations, in-vitro and in-vivo analysis we aim to study the efficacy and anti-cancer potential of this combination system against breast cancer cells.

# Chapter 2

# Review of Literature

---



---

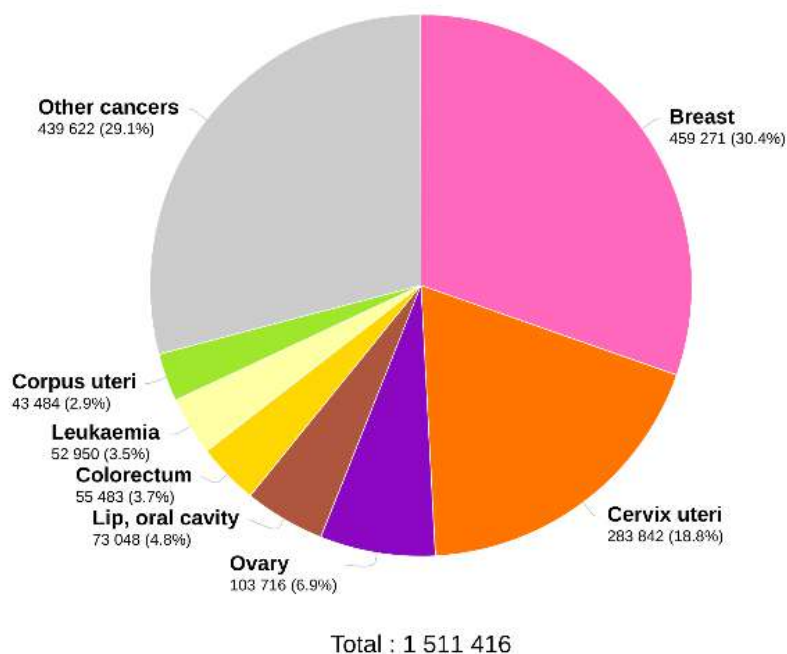
## Review of Literature

### 2.1 Breast cancer

#### 2.1.1 Epidemiology of breast cancer

Breast cancer is the most common cancer in females worldwide, with more new cases diagnosed each year than any other type of cancer. In 2020, there were an estimated 2.3 million new cases of breast cancer, representing 11.7% of all cancer cases (Arnold et al., 2022). Age-adjusted breast cancer incident rates in India are lower than in the United Kingdom. It is estimated that by year 2025, estimated number of breast cancer cases will account for approximately 30% of the total cancer burden followed by cervical cancer in India and world both (**Figure 2.1**). However, the mortality rate is similar. This suggests that breast cancer is being diagnosed at a later stage in India, which is leading to poorer outcomes. There is a significant increase in the incidence and cancer-associated morbidity and mortality in the Indian subcontinent, as described in global and Indian studies (Malvia et al., 2017). As seen from the GLOBOCAN 2020 data that of all cancers, almost one third of burden will be contributed by breast cancer only globally and even in Indian subcontinent (Sung et al., 2021).

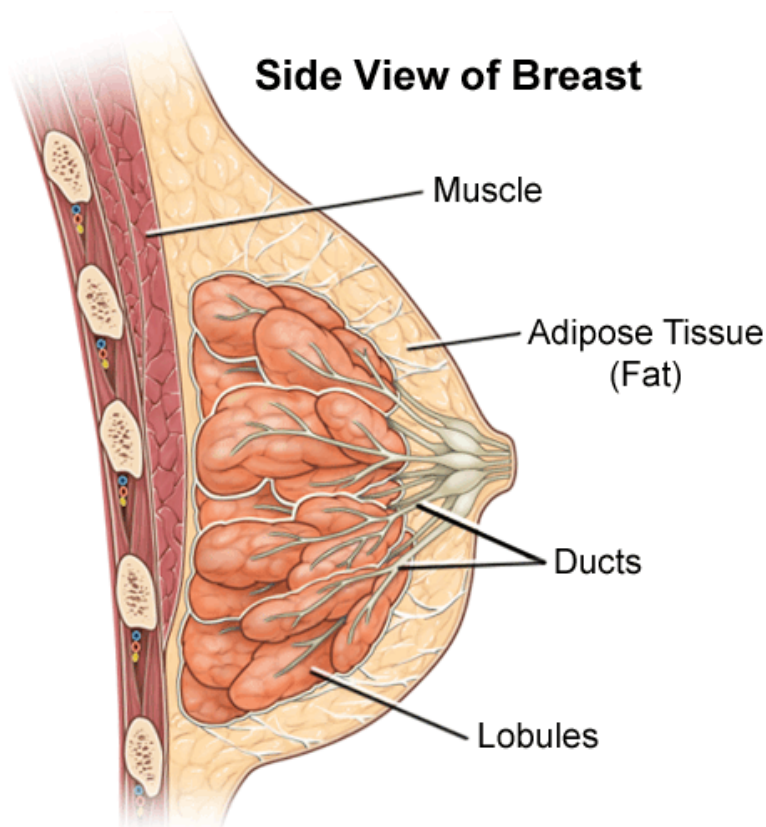
Estimated number of prevalent cases (5-year) in 2020, India, females, all ages



**Figure 2.1** Estimated number of prevalent cases of Cancer in India (Source: Globocan, 2020)

### 2.1.2 Anatomy of female breast

Breasts are found in both males and females and is made up of adipose tissue, a type of fat tissues that makes up the breast. Typically, female breasts are more glandular than male breasts. They are held in place and attached to the front of the chest wall by ligaments on either side of the sternum. They are located on the pectoralis major, the major chest muscle on top of the ribcage. They do not have any muscles in them. Each breast is made up of 15-20 circularly arranged lobes which are covered in adipose tissues around it, giving them its size and shape. These lobes are connected to each other via small ducts carrying milk at the tip of the breast also known as nipple. Area around nipple which is generally little darker in color known as areola. There are lymphatic and blood vessels in every breast. Lymph is a liquid, nearly colourless fluid that is carried by the lymph vessels. Between lymph nodes, lymph is carried by lymph veins. Small, bean-shaped structures called lymph nodes are used to store and filter white blood cells, which aid in the body's defence against illness and infection. There are clusters of lymph nodes in the chest, axilla (under the arm), and above the collarbone that are located close to the breast (Jesinger, 2014; Pandya and Moore, 2011).



**Figure 2.2** Female breast anatomy- side view (Source- Johns Hopkins Medicine)

---

### 2.1.3 Common breast conditions

There are many common breast conditions, both benign (non-cancerous) and malignant (cancerous). Some of the most common benign breast conditions include:

**Fibrocystic breast changes:** This is a condition that causes lumpiness, thickening, and swelling in the breasts. It is most common in women between the ages of 20 and 50.

**Fibroadenomas:** Fibroadenomas are round, rubbery, solid lumps that move easily when pushed. They are most common in women in their late teens and early 20s.

**Intraductal papillomas:** These are growths similar to warts that can develop in the milk ducts. They can cause a bloody or milky discharge from the nipple.

**Mastitis:** This is an infection of the breast tissue. It is most common in women who are breastfeeding.

Some of the most common malignant breast conditions include:

**Breast cancer:** Breast cancer is the most common cancer among women. It can occur at any age, but is most common in women over the age of 50. Carcinomas, or tumors that originate in the epithelial cells lining organs and tissues throughout the body, account for the majority of breast cancer cases. Adenocarcinomas, which originate in cells in the ducts (the milk ducts) or the lobules, are typically the more specific type of carcinomas that arise in the breast (glands in the breast that make milk). A pre-cancerous condition known as in situ breast cancer (also known as ductal carcinoma in situ, or DCIS) begins in a milk duct and has not spread to the surrounding breast tissue. Any type of breast cancer that has expanded (invaded) into the surrounding breast tissue is referred to as invasive (or infiltrating) breast cancer (Dr.R.Sarin and ICMR group, 2016). Triple-negative breast cancer (TNBC) is an aggressive form of invasive breast cancer in which the cancer cells produce either too little or too much of the HER2 protein in addition to lacking ER or PR receptors. (On all three tests, the cells come out "negative.") It makes up 15% of all cases of breast cancer and can be challenging to cure (Dawood, 2010).

**Inflammatory breast cancer (IBC):** This is a rare, aggressive and very painful condition of breast cancer that causes the breast to become swollen, tender and red. Perhaps more than 1% to 5% of all breast tumors are inflammatory breast cancers (IBCs). It is a form of invasive ductal carcinoma, although there are differences in its symptoms, prognosis, and course of treatment. IBC results in breast inflammation symptoms such as redness and swelling, which

---



are brought on by cancer cells obstructing local lymph veins and making the breast appear "inflamed" (Masuda et al., 2013).

**Paget disease of the breast:** This is a rare condition of breast cancer that impacts the nipple and surrounding area, areola. The areola and nipple skin frequently have a red, scaly, and crusty appearance. The nipple may be leaking yellow or bloody fluid. The nipple may appear flat or twisted at times. It may also itch or burn. If the condition doesn't get better, doctor may attempt treating it for eczema before recommending a biopsy (Lim et al., 2011).

It is important to see a doctor if you notice any changes in your breasts, such as a lump, pain, or discharge. Early detection and treatment of breast cancer can improve the chances of survival.

### 2.1.4 Breast cancer and risk factors

BC continues to be a leading public health concern worldwide and is the most prevalent form of cancer in the world today. Breast cancer is a disease that starts in the cells of breast which grows out of control. Breast cancer statistic and global concerns are already discussed earlier. In general, breast cancer survivors have an excellent prognosis, especially if they receive an early diagnosis. This is probably due to early identification, screening, and better treatment. Several distinct variables are necessary for survival. Several factors are known to contribute in increasing the risk of breast cancer includes (Malvia et al., 2017; Sun et al., 2017):

Epidemiologically it was found out in several studies that married women had few times lesser risk to develop breast cancer than single women. Not only that even women having kids and breast-feeding women's show lesser risk to develop breast cancer (Lipworth et al., 2000).

**Age:** this remains to be one of the most important risk factors contributing to the increased chances to develop breast cancer. Overall risk to develop cancer is higher in old age compared to young age considering over exposure to the carcinogens for longer period of time. After the age of 40 risk increases to develop breast cancer hence, regular screening and monitoring for signs and symptoms is recommended (Tafari et al., 2023).

**Lifestyle factors:** The risk of breast cancer can be increased by modern lifestyle factors like excessive alcohol use and dietary fat consumption. Alcohol consumption can stimulate the estrogen receptor pathways and raise blood levels of hormones related to estrogen. Typical western diet high in fat, particularly saturated fat, is linked to mortality and a poor prognosis

for people with breast cancer. Smoking, especially at a young age, has been linked to an increased risk of breast cancer (Feng et al., 2018a).

**Reproductive factors:** The risk of breast cancer can be increased by reproductive factors like early menarche, delayed menopause, first pregnancy after the age of 30, and low parity. An increased risk of post-menopausal breast cancer is linked to being overweight and obese (Feng et al., 2018b).

**Hormonal factors:** Birth control pills and contraceptive pills are amongst the major high-risk factor for induce breast cancer in women. Estrogens, both endogenous and exogenous, are linked to an increased risk of breast cancer. The ovary typically produces endogenous estrogen, whereas oral contraceptives and hormone replacement therapy (HRT) are the main exogenous estrogen sources. HRT use has been linked to an increased risk of breast cancer, according to numerous studies (Tafari et al., 2023).

**Genetic factors:** Family history accounts for close to 25% of all breast cancer cases. Women are more likely to contract the condition if their mother or sister has the disease. The mutations of breast cancer-related genes like BRCA1 and BRCA2 are partly responsible for the inherited likelihood for breast cancer. BRCA1 and BRCA2 mutation carriers have cumulative risks of 50 and 70 percent for breast cancer, respectively. In men's breast cancer, BRCA2 mutations are more common than BRCA1 mutations. BRCA1 mutation carriers will experience more severe consequences than BRCA2 mutation carriers (Khanna and Berek, 2015; Kotsopoulos et al., 2012).

### 2.1.5 Pathogenesis of breast cancer

A striking similarity emerges at the molecular level between the intricate choreography of normal development and the aberrant dance of cancer progression. Precise signaling pathways orchestrate human development, enabling cells to converse with each other and their surroundings. Remarkably, these very pathways are often commandeered or sabotaged by cancer cells, including cancer stem cells (CSCs) (Takahashi-Yanaga and Kahn, 2010). Essentially, cancer exploits genetic and epigenetic manipulations to break free from the shackles that normally control cell behavior – proliferation, survival, and movement. Many of these alterations target signaling pathways governing crucial processes like cell division, death, differentiation, and motility. Overactive mutations in genes called proto-oncogenes can hyperactivate these pathways, while inactivation of tumor suppressors silences vital negative regulators. This section explores into three key signaling pathways that both coordinate normal

---

---

breast tissue development and influence CSC functions: estrogen receptor (ER) signaling, HER2 signaling, and the canonical Wnt pathway (Shah, Rupen, Kelly Rosso, 2014).

- **ER signaling and ER-positive breast cancer:** Estrogen receptors, a diverse family, exist in two main forms: membrane-bound receptors, primarily G protein-coupled, and nuclear receptors, including ER $\alpha$  and ER $\beta$ . Both ER subtypes act as master switches, activating or repressing target genes once their ligands bind. While sharing core structural features crucial for their fundamental roles, ER $\alpha$  and ER $\beta$  employ distinct elements for signal transduction, ensuring receptor-specific actions. Both types possess six functional domains with varying degrees of similarity and retain the ability to form partnerships, known as heterodimers. The most highly conserved region, with a staggering 96% identity, is the DNA-binding domain (DBD). This crucial domain mediates the interaction of ER dimers with specific DNA sequences called estrogen response elements (EREs) within target genes (Wang and Tang, 2022).

One of the most well-defined processes by which ER $\alpha$  promotes the growth of breast cancer cells is its close association with cyclin D1. This important contributor, cyclin D1, facilitates the vital G1 to S phase transition in many cancer cells by acting as a strong activator for cyclin-dependent kinases (CDKs) 4 and 6. The complex feedback loop that forms between ER $\alpha$  and cyclin D1 may be the key to comprehending resistance to antiestrogen treatment. This realization makes it possible to investigating the possibility of combining hormone therapy and selective CDK4/6 inhibitors in ER-positive patients, which may result in a more successful course of treatment (Hernando et al., 2021).

- **HER2 signaling and HER2-positive breast cancer:** Beyond the ER's role, another protein family reigns in the occurrence of breast cancer: the Human Epidermal Growth Factor Receptors (EGFRs), also known as HERs (Yook et al., 2020). These four powerful players, numbered 1 to 4, hold control over both normal tissues and many cancer types. Among them, HER2 (or HER2/neu, c-ERBB2) stands out as a particularly potent figure. Like its EGFR members, HER2 is a receptor tyrosine kinase, a large molecule with three distinct domains: a ligand-binding crown, a transmembrane bridge, and an intracellular domain (Loibl and Gianni, 2017). But unlike the others, HER2 remains perpetually available, making it the preferred ligand for forming alliances with other molecules. This constant activation grants HER2 the power to influence numerous cellular functions through diverse pathways. A dimerization occurs when a ligand attaches itself to HER2, bringing two HER2 molecules

together. This interaction sparks a cascade of phosphorylation events within HER2's intracellular domain, activating molecules like the MAPK and PI3K signaling pathways. These pathways, potent forces, are heavily involved in the initiation of breast tumorigenesis. In summary, HER2 is a strong candidate in the fight against breast cancer because of its distinct, status and capacity to create strong relationships. Understanding its intricate mechanism is crucial for devising effective treatment strategies to and restore balance (Karami Fath et al., 2022).

The HER2 protein, which is overexpressed in many tumor cells, is in charge and regulates unchecked growth and development. Its overexpression gives it the ability to control a wide range of cellular processes via complex signaling pathways. Modern medicine's cornerstone, targeted medicines, have been developed which specifically target this protein. New findings have shown novel pathways that extend its hold on breast cancer (Arteaga et al., 2011).

- **Wnt/ $\beta$ -catenin signaling in breast cancer:** Instead of merely depending on genetic abnormalities, Wnt signaling shows aberrant activity in breast cancer, possibly via an autocrine loop. Although there are few activating mutations in Wnt system components, around half of clinical cases had higher levels of the crucial downstream effector  $\beta$ -catenin, indicating alternative pathways of pathway activation (Meszaros and Patocs, 2020). The positive regulator Dvl exhibits amplification in about 50% of breast tumors. On the other hand, the complex role of Wnt dysregulation in the advancement of breast cancer is further highlighted by the downregulation of Wnt inhibitors, such as Dickkopf 1 (DKK1) in the presence of metastasis and Frizzled-related protein 1 (FRP1) in 78% of malignancies. In addition, changes in the tumor suppressor APC have been found in as many as 50% of breast cancer cases, which adds to the dysregulated Wnt signaling pathway (Kaur et al., 2020).

The Wnt/ $\beta$ -catenin pathway was markedly hyperactivated in basal-like breast cancers, and a higher level of nuclear  $\beta$ -catenin was associated with a poor prognosis. Activated  $\beta$ -catenin is known to promote triple-negative breast cancer, but in vivo investigations have shown that it also aids in the growth of HER2-positive mammary tumors. Treatment approaches focused on reactivating silent Wnt inhibitors through processes such reversing DNA methylation and miRNA repression have showed promise in reducing tumor growth, given the varied pro-oncogenic capacity of Wnt ligands. Furthermore, it has been shown that Wnt pathway activation is associated with increased radiation resistance in both human breast cancer cell lines and mouse mammary gland progenitor cells. This suggests that the Wnt pathway may

play a role in resistance to current anticancer therapies by influencing populations of stem and progenitor cells (Mukherjee and Panda, 2020; Takahashi-Yanaga and Kahn, 2010).

- **BRCA1/2 mutations in breast cancer:** For certain people, the predisposition to develop breast or ovarian cancer could be genetically linked. A specific concern is mutations in the breast cancer susceptibility genes BRCA1 and BRCA2 (Feng et al., 2018). These mutations have a crucial role in breast cancer, as evidenced by the fact that up to 20 percent of women with a family history of the condition carry them. The prevalence of BRCA mutations is much higher in the Ashkenazi Jewish community, believed to be between 30 and 35 percent (Stadler et al., 2012). They are therefore at a higher risk of developing ovarian and breast cancer. In contrast, the overall population has a substantially reduced risk, which emphasizes the significance of specific preventative interventions and genetic screening for people of Ashkenazi heritage. Interestingly, only 4.5 percent of Ashkenazi Jewish males with breast cancer have BRCA1 mutations, even though BRCA2 mutations account for 14% of male instances of breast cancer overall. This points to a gendered predisposition within this population, indicating the need for additional investigation into the mechanisms underlying (Manchanda et al., 2015).

The BRCA proteins work together to repair DNA damage by homology-directed repair (HDR), which inhibits the development of cancer. This process is similar each other's tumor-suppressive mechanism. Thus, loss of function and/or deletion mutations in the BRCA genes reduce the efficacy of DNA repair and may facilitate the development of malignant cells, thereby raising the risk of breast cancer by a factor of 5–6. Though BRCA mutations can be inherited and contribute to a certain number of familial cases, researchers have not found any difference in the risk of breast cancer among carriers with or without an intimate family history. A recent study suggests that smoking may also marginally increase the risk of breast cancer and other cancers in those with the BRCA mutation. The accuracy of identifying the high-risk group and the efficacy of preventative treatments will both be enhanced by these findings. Clinical data hint at a curious connection between BRCA1 mutations and a specific type of breast cancer: the basal-like variety. Notably, BRCA1-linked breast cancers lacking estrogen receptor (ER) or EGFR2 (ERBB2) overexpression often exhibit the telltale markers of basal epithelial cells, a characteristic already associated with ER/ERBB2-negative tumors (Teng et al., 2011).

---

### 2.1.6 Diagnosis of breast cancer

In order to detect early-stage breast cancer, researchers have investigated a variety of diagnostic methods including mammography, Magnetic resonance imaging (MRI), ultrasonography, PET, and breast magnetic resonance imaging (Shah, Rupen, Kelly Rosso, 2014).

#### 2.1.6.1 Clinical Breast Imaging Techniques

##### 1. Mammography

Mammography remains a cornerstone in the fight against breast cancer. Its ability to detect tumors at an early stage, coupled with advancements in technology and personalized screening practices, continues to contribute to improved patient outcomes. While annual mammograms remain a common recommendation for women starting at age 40, concerns exist regarding their limitations. These include relatively high false-positive and false-negative rates, particularly for younger women with dense breast tissue. Sensitivity can also be impacted by individual factors like personal history and radiologist expertise. Additionally, mammograms utilize ionizing radiation and can be uncomfortable for some patients. Recent research suggests the impact of mammograms on reducing breast cancer mortality may be lower than previously estimated (Pötsch et al., 2022). Contrast-enhanced mammography (CEM), which focuses on tumor blood vessel development, presents a potential alternative or complementary tool. While it involves slightly higher radiation exposure than traditional mammograms due to the use of contrast injections, CEM demonstrates improved sensitivity and performance compared to both mammograms and ultrasound. This suggests potentially greater accuracy in cancer detection (Ghaderi et al., 2019).

##### 2. Ultrasound

Breast ultrasound (BUS) leverages sound waves to visualize internal breast structures, aiding in the detection of potential abnormalities. Its widespread availability and relatively low cost make it a valuable tool in the fight against breast cancer. The primary strength of BUS lies in its ability to differentiate between fluid-filled cysts and solid masses, which can be challenging for mammography, especially in women with dense breast tissue. This allows for more accurate assessment of suspicious findings and can be particularly beneficial for individuals with a high risk of developing breast cancer (Huang et al., 2017).

However, BUS is not without limitations. Compared to mammography, its overall cancer detection rate is lower, primarily due to the similar acoustic properties of healthy and cancerous tissues. Additionally, the effectiveness of BUS heavily relies on the expertise of the performing

---

radiologist, as subtle interpretations of the generated images are crucial for accurate diagnosis. Therefore, while BUS serves as a valuable complement to mammography, particularly for high-risk women, pregnant individuals, and those unsuitable for mammograms, it should not be viewed as a complete replacement. Combined use of both modalities can optimize sensitivity and specificity for early cancer detection, while acknowledging the potential for increased biopsy rates associated with this approach (Ilesanmi et al., 2021; Xian et al., 2018).

### 3. MRI

MRI has emerged as a powerful tool in healthcare, but its application in breast cancer detection carries unique benefits and limitations. Unlike mammograms and ultrasounds that rely on X-rays or sound waves, MRI leverages strong magnetic fields and radiofrequency signals to create detailed cross-sectional images of the breast tissue. This technology offers high sensitivity, making it adept at identifying even small tumors, especially in women with elevated breast cancer risk (Ghaderi et al., 2019).

Overall, while not a replacement for established screening methods like mammograms and ultrasounds, MRI plays a valuable role in targeted breast cancer diagnosis, particularly for high-risk women. Ongoing research continues to refine and optimize MRI technology, aiming to improve its specificity and affordability. These holds promise for expanding its application in the future, potentially benefiting a wider range of women in the fight against breast cancer (Jesinger, 2014).

#### 2.1.6.2 Biomarkers for breast cancer detection

##### 1. Protein biomarkers

While traditional biopsy remains the gold standard for cancer diagnosis, the search for reliable non-invasive methods continues. Protein biomarkers, naturally occurring molecules in the body, have emerged as promising candidates for early detection and prognosis in breast cancer. Some potential players and the challenges associated with their clinical application are:

- **CA15-3:** This traditional biomarker, while not ideal for early detection, excels in tracking tumor recurrence and assessing treatment effectiveness in advanced stages (Salama et al., 2020).
- **PD-L1 status:** If diagnosed with advanced-stage or metastatic triple-negative breast cancer, they may run a test to see whether the cancer is PD-L1-positive in order to determine whether the immunotherapy drug Keytruda will be helpful (Makówka and Kotowicz, 2023).

- 
- **CA 27-29 levels:** Breast cancer has the ability to release the protein known as cancer antigen 27-29 (CA 27-29). Elevated CA 27-29 levels may indicate an increase in metastatic breast cancer (Makówka and Kotowicz, 2023).
  - **CEA levels:** The protein known as carcinoembryonic antigen, or CEA, is a marker for colon cancer. It can be applied to ascertain whether breast cancer has progressed to other body parts.
  - **CA 125 levels:** The presence of ovarian cancer results in the production of CA 125, or cancer antigen 125. Elevated levels could indicate a recurrence of breast cancer (Salama et al., 2020).
  - **HER2:** Overexpressed in roughly 30% of breast cancers, HER2 levels offer valuable insights into:
    - Prognosis: Higher levels often indicate a more aggressive course of the disease, informing treatment decisions and patient prognoses.
    - Treatment Selection: HER2 positivity opens doors to targeted therapies like Herceptin, offering personalized options for better outcomes.
    - Disease Monitoring: Tracking HER2 levels alongside other factors like tumor size and lymph node involvement provides a comprehensive picture of disease progression and potential relapses (Nahta and O'Regan, 2012).

## 2. Gene biomarkers

The fight against breast cancer goes beyond simply detecting tumors. Understanding the underlying genetic and molecular mechanisms plays a crucial role in diagnosis, prognosis, and treatment .

- **BRCA1 and BRCA2:** These tumor suppressor genes fix double-strand breaks in DNA, acting as security guards. These genes' defenses are compromised by mutations, which can raise the risk of breast cancer by 21–40%. Researchers such as Rasheed et al. have created very efficient graphene-based sensors to identify these changes, leading to customized risk assessment and preventive actions (Roberts et al., 2020).
  - **p53:** This "guardian angel" gene also contributes to DNA repair and inhibits the development of cancer. About 30 to 35 percent of breast tumors have mutations in p53, making it a useful target for detection and therapy . A possible method for detecting these
-



---

alterations and directing treatment choices is the use of DNA biosensors (Dumay et al., 2013; Goh et al., 2011).

- **Cell-Free Tumor DNA (cfDNA):** Imagine little bits of DNA that are secreted by cancer cells and travel through the bloodstream like silent secrets. The analysis of these cfDNA fragments has enormous potential for non-invasive breast cancer diagnosis. cfDNA holds promise as a real-time cancer monitoring "liquid biopsy." Not only are elevated amounts of cfDNA shown in advanced cancer cases, but they have also been proposed as a diagnostic tool for breast cancer and other cancers too. Although research is still in its early stages, studies that cfDNA levels could be connected to the advancement of cancer, providing important clues about the disease's pathophysiology (Hashad et al., 2012).
- **MicroRNAs (miRNAs):** These tiny molecules fine-tune gene expression, acting as master regulators of cellular activity. Specific miRNAs, like miR-21, have been linked to breast cancer. Electrochemical nano biosensors, as explored offer an extremely sensitive way to detect these miRNAs, potentially leading to early detection and better prognosis (Fu et al., 2011).

### 2.1.7 Treatment of breast cancer

Conquering breast cancer requires a multi-pronged approach, tailoring treatments to the specific stage and characteristics of the disease. Treatment strategy is influenced by breast cancer biology and behavior. While some tumors are larger and develop more slowly, others are smaller and grow faster. Options for treatment and advice are highly personalized and based on a number of variables, such as:

- Tumor staging
- Tumors subtype (hormonal status)
- Age, overall health, menopausal status, and preferences of the patient
- Other mutations and diagnostic data

Although, BC treatment can be divided into three different approaches to understand them individually are like:

- Local treatment i.e., they target the tumor without harming the surrounding tissue involving radiation and surgery. The majority of breast cancer patients will undergo surgery to remove the tumor. In certain cases, additional treatments may be required in

addition to surgery, either before or after the procedure, depending on the kind and stage of the breast cancer (Fitoussi et al., 2010).

- Systemic treatments i.e medications used to treat breast cancer are referred to as systemic therapy, because they can penetrate cancer cells virtually anywhere in the body. Certain medications can be administered orally, intramuscularly, or directly into the bloodstream. Several pharmacological treatments for breast cancer may be employed, depending on its form. Chemotherapy, hormone therapy, targeted therapy and immune therapy are covered under this approach (Serrano-Olvera, 2011).
- Treatment by stage i.e, where stage of breast cancer is considered as primary option to choose the treatment plan considering other factors personalized to patient.

### 2.1.7.1 Surgery

The large number of breast cancer patients get surgery as part of their treatments. Depending on the circumstances, many forms of breast surgery may be performed for various purposes. To remove breast cancer, there are two primary forms of surgery:

**Breast-conserving surgery:** The goal of breast-conserving surgery is to remove the malignancy while leaving some normal tissue in place. In this case the breast portion that has the malignancy is only removed. The location, size, and other variables of the tumor determine how much breast needs to be removed. Other names for this procedure include segmental mastectomy, quadrantectomy, lumpectomy, or partial mastectomy (Li et al., 2003).

**Mastectomy:** A mastectomy is a surgical procedure in which the entire breast, along with any surrounding tissues, is removed. Mastectomies can be of various different kinds involving removal of either one of the breasts or a double mastectomy where surgery is performed on certain women to remove both breasts.

As a part of surgery or separately also sometimes during a biopsy, one or more lymph nodes in the underarm (axillary) area will be removed and examined in the laboratory to determine if the cancer spread. Sentinel lymph node biopsy (SLNB) is a surgical technique where a dye is injected, and only the lymph node or lymph nodes under the arm that have absorbed the dye are removed. It is expected that the malignancy will spread to these lymph nodes initially. Limiting the number of lymph nodes removed reduces the possibility of adverse events following axillary lymph node dissection, such as lymphedema, or swollen arms. During an Axillary lymph node dissection (ALND) operation, the surgeon removes a large number of

---

underarm lymph nodes (often fewer than 20) without the use of a dye. Although ALND is not performed as frequently as it formerly was, in certain circumstances it may still be the most effective method of examining the lymph nodes (Dr.R.Sarin and ICMR group, 2016; Hutchinson, 2010).

### 2.1.7.2 Radiation

A vital part of treating breast cancer is radiation therapy, which is frequently administered following surgery to eradicate any cancer cells that may still be present and lower the chance of recurrence. This type of treatment uses radiation, such as high-energy X-rays or particles, to target and kill remaining tumor cells with the least amount of damage to nearby healthy tissue (Baskar et al., 2012). Radiation therapy are mainly of two types: External beam radiation therapy (EBRT) and Brachytherapy

**EBRT:** EBRT is a method of delivering radiation therapy externally by means of a machine that focuses radiation beams at the site of tumor. It is mostly employed in the treatment of breast cancer because it enables focused radiation therapy to the afflicted breast tissue without seriously harming the surrounding healthy tissues. Treatment for breast cancer with EBRT is common, particularly while the disease is still in its early stages. Following breast-conserving surgery, this type of radiation therapy is frequently used to target any cancer cells that may still be present and lower the chance of recurrence. Breast-conserving surgery is becoming a common choice for the local treatment of early-stage invasive breast cancer as multiple studies have demonstrated that it produces overall survival rates that are comparable to mastectomy when combined with external beam radiation therapy. All things considered, EBRT is a valuable all-encompassing approach to treating breast cancer, improving outcomes and assisting with long-term disease management (Brown et al., 2015; Terheyden et al., 2016).

**Brachytherapy:** Another method of administering radiation therapy is brachytherapy, sometimes referred to as internal radiation. A device carrying radioactive seeds or pellets is inserted into the breast tissue in the location where the cancer was excised for a brief period of time rather than directing radiation beams from outside the body. As partial breast irradiation, brachytherapy alone (instead of radiation to the entire breast) can be utilized for some women who underwent breast-conserving surgery (BCS). The patient pool for brachytherapy may be narrowed due to tumor location, size, and other considerations (Kindts et al., 2019).

Brachytherapy comes in two primary varieties that are used to treat breast cancer: High Dose Rate (HDR) and Low Dose Rate (LDR). A high-intensity radioactive source, like Ir192, is

---

---

inserted into the breast tissue during HDR brachytherapy and left there for a brief while typically a few minutes. In LDR brachytherapy, low-intensity radioactive sources are positioned over extended periods of time, typically ranging from days to weeks. In situations of BCS, brachytherapy used as a boost following external beam radiation has demonstrated efficacy in lowering the risk of local recurrence. When combined with BCS, it is a well-researched alternative for patients with early-stage breast cancer and has been proven to have survival rates comparable to mastectomy (Smith et al., 2014).

### 2.1.7.3 Chemotherapy

Chemotherapy hinders cell division, upregulates cellular apoptosis and thereby ceases tumor growth. It is used as an adjuvant therapy to surgery or radiation therapy in early and advanced cancers to improve patient outcome and occasionally as a part of monotherapy regime to minimize the risk of relapses. Chemotherapy when used before surgery in order to control the size of tumor or some other complications it is called as neo-adjuvant chemotherapy. For metastatic cancers, chemotherapy has a benefit of being given systematically so as to reach all tissues and effectively kill cancer cells disseminated to other parts of body. Anti-cancer drugs classified under different classes like alkylating agent, antimetabolites, plant alkaloids, antitumor antibiotics, hormonal and other miscellaneous (**Table 2.1**). hinders cell division, upregulates cellular apoptosis and thereby ceases tumor growth. It is used as an adjuvant therapy to surgery or radiation therapy in early and advanced cancers to improve patient outcome and occasionally as a part of monotherapy regime to minimize the risk of relapses. It has been observed that, long-term use of alkylating agents can also lead to secondary malignancies like leukemia in some cases. Toxicity to bone marrow cells, reproductive cells are some of the major concerns for the use of these agents (Boivin, 1990; Davies, 2001). Next class of drugs are antimetabolite as name suggests they interfere with the DNA & RNA synthesis and thus creating imbalance in cellular machinery leading to cell death. Toxicity associated with these drugs are also against some of the rapidly dividing normal cells of the body like hair follicle cells, intestinal mucosa and bone marrow cells. Hepatotoxicity and renal toxicity are also seen with majority of these drugs but, once treatment is stopped the toxicity can be minimized (Chabner et al., 2005a; Corrie, 2008; Sudhakar, 2009). Plant alkaloids are derived from plant products that mainly works on M phase mitosis of cell cycle and inhibits cell division. These drugs act by interfering with microtubule polymerization and thus leading to cells arrested in cell division stage. Lung cancer, breast cancer, lymphoma, leukemia are some of the cancers treated using these drugs. Toxicity associated with these drugs are with

---

hematopoietic cells, neurological and reproductive system. Increased resistance to taxel group of drug is growing concern (Corrie, 2008; Krause, 2019). Antitumor antibiotics also known as Anthracyclines are special class of drugs derived from *Streptomyces* spp. These drugs work by interfering with DNA/ RNA synthesis and thus hindering protein synthesis essential for cells normal functioning. Major toxicity issues with these drugs are cardiotoxicity with critical dosage. Post treatment malignancies can also be seen in some cases (Mukherjee et al., 2012).

**Table 2.1** Chemotherapy drug classes and mode of action

Drug Class	Examples	Mode of action	References
Alkylating agents	Nitrogen mustard, Cyclophosphamide, Chlorambucil, Cisplatin, Carboplatin	Crosslinking DNA, Nicks in DNA,	(Chabner et al., 2005a; Corrie, 2008; Jerzy Einhorn, 1985)
Antimetabolites	Aminopterin, Methotrexate, 5-Fluorouracil(5-FU), 6-Mercaptopurine(6-MP)	Interfere with the DNA & RNA synthesis	(Chabner et al., 2005a; Corrie, 2008; Sudhakar, 2009)
Plant Alkaloids	Vincristine, Vinblastine, Paclitaxel, Docetaxel	Inhibits cell division, Microtubule polymerization	(Krause, 2019; Morris and Fornier, 2008; Zhang and Kanakkanthara, 2020)
Antibiotics	Daunorubicin, Doxorubicin, Epirubicin, Mitoxantrone, Anthracyclines, Bleomycin	DNA intercalation, DNA adduct formation, Inhibiting DNA synthesis	(Bhattacharya and Mukherjee, 2015; Gao et al., 2020)
Hormonal agents	Anastrozole, Tamoxifen, Toremifene, leuprolide, Flutamide	Blocks hormone production, alters the hormone, prevents hormone attachment to receptor	(Lorizio et al., 2012; Yasui et al., 2016)

Hormonal drugs work by two ways by blocking the production of hormone in body or by interfering with hormone synthesis. These drugs can be only used for hormone positive cancers like prostate, breast, ovarian cancers etc. and not for any hormone receptor negative cancers (Lorizio et al., 2012; Yasui et al., 2016). Cancer chemotherapy has oodles of side effects which adversely affects the patient's undergoing chemotherapy. These cytotoxic drugs not only affect cancer cells but, they also target normal cells or tissues and show non-specific toxicity which

---

leads to serious side effects. Depending on the type of cancer, dose and duration of chemotherapy side effects can vary from mild symptoms like nausea, hair loss, vomiting, fatigue, hot flashes, weight loss etc. to severe symptoms like secondary malignancy, hepatotoxicity, cardiotoxicity, renal toxicity etc. Even chemoresistance is seen to be rapidly acquired in many cancer type and treatments are becoming more and more difficult (Florea and Büsselberg, 2013; Holohan et al., 2013; Thanki et al., 2013).

### 2.1.7.4 Hormone therapy

Hormones like progesterone and estrogen can have an impact on certain forms of breast cancer. Because of their protein receptors, which bind to progesterone and estrogen, breast cancer cells are able to proliferate. Hormone or endocrine therapies work by preventing these hormones from binding to these receptors. By using hormone therapy, cancer cells can be reached in virtually any part of the body, not just the breast. It is advised for female patients whose malignancies are positive for hormone receptors. It is ineffective for women whose tumors lack hormone receptors (these tumors are called hormone receptor-negative). Adjuvant therapy, or hormone therapy, is frequently given following surgery to help lower the chance of the cancer returning (Narod, 2011). Occasionally, it begins prior to surgery (as neoadjuvant therapy). Cancer that has returned after treatment or spread to other body areas can also be treated with hormone therapy. In order to slow down or stop the growth of hormone receptor-positive breast cancer cells, hormone treatment aims to inhibit the effects of these hormones or reduce their levels in the body. Treatment options for breast cancer include a variety of hormone therapies:

**Selective Estrogen Receptor Modulators (SERMs):** A class of medications known as SERMs functions as an antagonist of the estrogen receptor in some tissues and an agonist in others. They are frequently used to treat estrogen-related diseases such as osteoporosis, breast cancer, and menopausal symptoms. SERMs that are well-known include raloxifene and tamoxifen. These medications function by attaching themselves to the body's estrogen receptors, which can either increase or block the effects of estrogen. Because of their dual activity, SERMs are useful in treating a variety of illnesses because they can have distinct effects in different tissues. Taking tamoxifen can help reduce the chances of breast cancer developing in women who are at high risk. It also minimizes the likelihood of developing additional DCIS in both breasts or invasive breast cancer. Tamoxifen can help women with hormone receptor-positive invasive breast cancer who have had surgery reduce the likelihood that the cancer will return and increase their chances of living a longer life (Fei et al., 2021; Patel and Bihani, 2018).

---

---

**Aromatase Inhibitors (AIs):** A class of drugs known as AIs is used to treat hormone receptor-positive breast cancer, especially in postmenopausal women. These medications function by blocking the enzyme aromatase, which is in charge of converting the body's production of androgens hormones made by the adrenal glands into estrogens, or female sex hormones. AIs lower the body's estrogen levels by preventing this conversion, which can aid in halting or slowing the growth of hormone receptor-positive breast cancer cells. AIs are of several types including an oral AI is letrozole, also marketed as Femara. It is used to treat postmenopausal women with metastatic breast cancer and as adjuvant therapy for early-stage hormone receptor-positive breast cancer. One AI that is administered orally is Anastrozole (Arimidex) (Gnant et al., 2021). It is frequently used in postmenopausal women with hormone receptor-positive early breast cancer as adjuvant therapy, which is medicine administered after primary treatment to reduce the chance of the cancer returning. Advanced breast cancer may also be treated with anastrozole (Chumsri, Saranya, Timothy Howes, Ting Bao, Gauri Sabnis, 2011; Goss et al., 2016).

**Selective Estrogen Receptor Degraders (SERDs):** A class of medications known as SERDs targets the ER to be destroyed by the cell's mechanism for breaking down proteins. This strategy provides a novel means of inhibiting the impact of ER on cancer cells, specifically in hormone-positive breast cancer. Fulvestrant is one SERD example that is authorized for the treatment of metastatic breast cancer. The goal of ongoing research is to create novel, more potent SERDs to help patients with hormone receptor-positive breast cancer achieve better results. Among the medications included in this category are Fulvestrant, which is authorized for the treatment of metastatic breast cancer. Research is also being done to create novel and more potent SERDs in order to enhance the prognosis of patients with hormone receptor-positive breast cancer (Wang and Tang, 2022).

**Luteinizing Hormone-Releasing Hormone (LHRH) Agonists:** A class of Leuprolide and goserelin Leuprolide and goserelin drugs known as LHRH agonists is used to treat hormone receptor-positive breast cancer, especially in premenopausal women. These medications function by inhibiting the release of luteinizing hormone (LH) and follicle-stimulating hormone (FSH) from the pituitary gland, which lowers the body's synthesis of estrogen. Hormones called LH and FSH cause the ovaries to create more estrogen thus indirectly controlling the estrogen levels in the body. Leuprolide and goserelin (Zoladex) are common LHRH medications (Lupron). In premenopausal women, they can be used as hormone therapy in combination with other hormone medications such as Fulvestrant, aromatase inhibitors, and

---

---

tamoxifen. Although these drugs are usually well tolerated, they can have menopause-like adverse effects, including weakening of the bones, hot flashes, and dry vagina (osteoporosis) (Kim et al., 2023; Liu et al., 2013).

### 2.1.7.5 Targeted therapy

Targeted therapies using biological agents such as monoclonal antibodies (mAb) are specific towards a particular cancer cell protein. Targeting such proteins impedes cancer cell survival and limits proliferation. In early 1990, research showed potential role of mAbs to target cancer cells and paved a way towards new therapeutic approach. The first mAb approved for cancer treatment was in the year 1997, Rituximab (Rituxan<sup>®</sup>) against CD-20 antigen of B-lymphocyte for B cell related malignancies (Pérez-Herrero and Fernández-Medarde, 2015). These mAb based treatment relies on identifying a cellular target e.g. Antigen or a receptor present on the cell against which the antibody can be raised and is the most critical part of work. mAbs works by averting ligand receptor interaction or activating immunological response towards cells. Presently mAbs used in cancer are differ types as showed in (Figure 1) like **a**. Directed towards a certain domain of a receptor which has role in cell proliferation thus hindering the signal transduction E.g. Cetuximab (Erbitux<sup>®</sup>) against Erythrocyte growth factor receptor (EGFR) and Trastuzumab (Herceptin<sup>®</sup>) against Human epidermal growth factor receptor-2 (HER-2) receptor, Ipilimumab (Yervoy<sup>®</sup>) binds to CTLA-4 coreceptor on T-cell which intern prevents the T-cell inactivation by not allow it to interact with B7, **b**. mAbs are used to target against cellular antigen to augment the immunogenic response by body's own immune system to kill the neoplastic cells E.g. Rituximab (Rituxan<sup>®</sup>) as discussed earlier and Alemtuzumab (Campath<sup>®</sup>) against CD-52 antigen on B- cell for Chronic lymphocytic leukemia (CLL) (Ke and Shen, 2017), **c**. In another strategy mAbs are used as a delivery vehicle to carry the non-human enzyme to the cancer site where it can activate the prodrug/drug and kill the cancer cells, this strategy is known as “antibody-directed enzyme prodrug therapy” (ADEPT). Different clinical studies are going around the world for multiple cancer at different stages and we hope soon it will be available (Padma, 2015), **d**. In another approach again delivery potential of mAbs have been explored to carry the cytotoxic drugs or radioisotopes to neoplastic cells making it selective and avoiding non specificity to other tissues and organs E.g. <sup>131</sup>I-tositumomab (Bexxar<sup>®</sup>) and <sup>90</sup>Y-Ibritumomab tiuxetan (Zevalin<sup>®</sup>) uses radioisotopes of Iodine and Yttrium respectively, conjugated to mAbs against CD-20 receptor, on B-cell for non-Hodgkin's type of lymphomas, Gemtuzumab ozogamicin (Mylotarg<sup>®</sup>) is a drug in which mAb against CD-33 is conjugate with cytotoxic drug molecule calicheamicin. CD-33 antigen is

---



---

majorly seen on the blast cells in acute myelogenous leukemia (AML) patients and even present on normal myeloid cells. Not only cancers of blood but other cancers like breast cancer, CRC and lung cancers are also been addressed using mAbs based treatment mode (Serrano-Olvera, 2011b). Certain drawbacks even mAbs show which limits its use like, few of the targeted antigen or receptors are found universally expressed on both cancer and normal cells sometimes differ in expression levels, this led to inhibited activity of normal cells and hinder their function which leads to secondary side effects. Fevers, chills, arthralgia, myalgia, rashes and in some cases increased immunological reactions to immune suppression also seen. With few specific types of mAbs based therapy increased cardiac effects are seen like, myocardial ischemia, myocardial infarction, arrhythmia. Regardless of this, targeted therapies are much safer than the traditional cytotoxic chemotherapy drugs. Other than mAbs small molecule inhibitors and immunotoxins are some other targeted therapies currently in application for cancer treatment with its own potentials and limitations (Price and Rao, 2013; Serrano-Olvera, 2011b).

### 2.1.7.6 Immuno therapy

The use of medications to strengthen a person's immune system so it can more efficiently identify and eliminate cancer cells is known as immunotherapy. To improve the immune response, immunotherapy usually targets particular proteins that are part of the immune system. The side effects of these medications differ from those of chemotherapy (Farkona et al., 2016).

The immune system's capacity to prevent itself from targeting the body's normal cells is a crucial component. It accomplishes this by utilizing proteins on immune cells called "checkpoints," which must be activated or inactive in order to initiate an immunological response. These checkpoints are occasionally used by breast cancer cells to deter immune system attacks. Medication aimed at these checkpoint proteins aids in reestablishing the immune system's defense against breast cancer cells. There are forms of breast cancer that can be treated with immunotherapy (Kirkwood et al., 2012).

**Checkpoint Inhibitors:** These medications work by targeting proteins on cancerous or immunological cells to aid the immune system in identifying and eliminating cancerous cells. Pembrolizumab, also known as KEYTRUDA® (Tong et al., 2018), is a checkpoint inhibitor that specifically targets T cells' PD-1 protein. Another checkpoint inhibitor, atezolizumab (TECENTRIQ®), targets the PD-L1 protein on cancer cells (Reddy et al., 2020).

**mAbs:** These are chemicals made in laboratories that aid the immune system in identifying and combating cancerous cells. Trastuzumab (Herceptin) (Dawood, 2016), this mAb targets

---

---

HER2-positive breast cancer cells; it is not a conventional immunotherapy. Other examples are already covered in Targeted therapy section of the chapter.

**Adoptive cell transfer:** This strategy aims to strengthen T cells' innate capacity to combat malignancy. Through genetic engineering, T cells a subset of white blood cells—can be made more capable of identifying and eliminating cancerous cells. This process is known as chimeric antigen receptor (CAR) T-cell therapy. Because CAR T-cell therapy modifies T cells' genes to enable them to fight cancer, it is occasionally referred to as a form of cell-based gene therapy. Even in cases where other forms of cancer treatment are no longer effective, this kind of treatment can be quite beneficial. The US Food and Drug Administration (FDA) has authorised CAR T-cell therapy for the treatment of multiple myeloma and certain types of leukemias and lymphomas. Usually, CAR T-cell therapy is employed following the failure of conventional forms of treatment. Tisagenlecleucel (Kymriah™) and Axicabtagene ciloleucel (Yescarta™) are two of the examples of FDA-approved CAR-T cell therapy for B- cell lymphomas (Meng et al., 2021; Weinstein B et al., 2021).

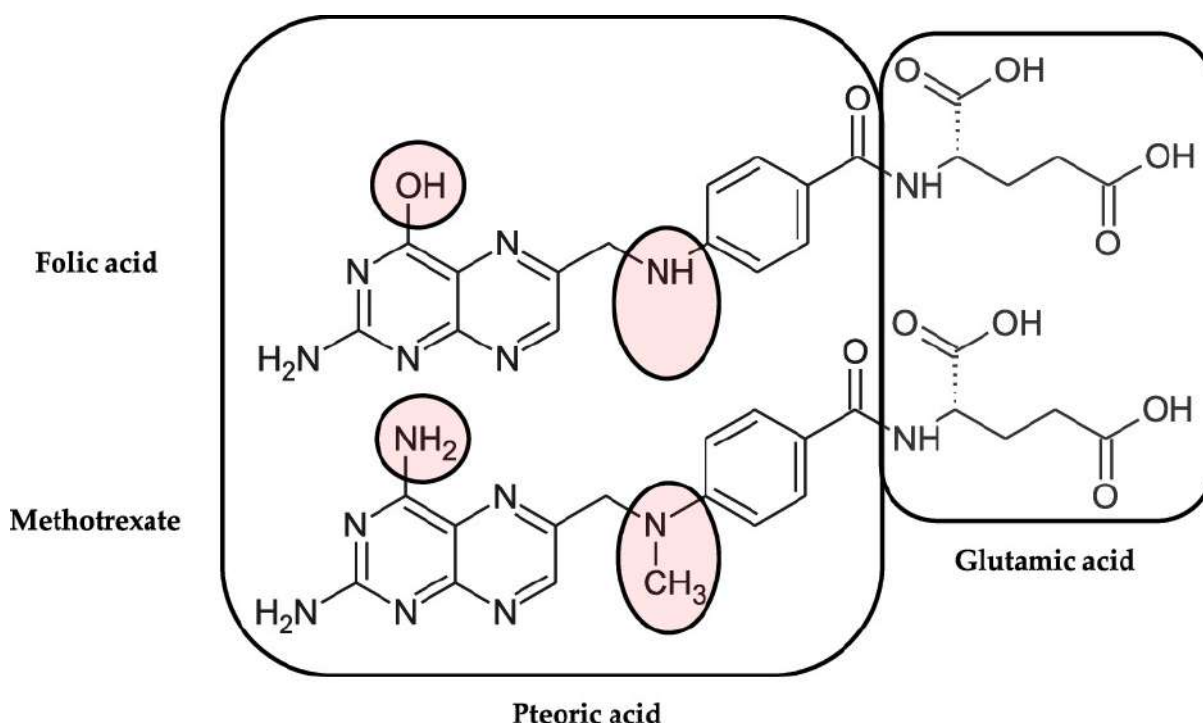
## 2.2 Methotrexate (MTX)

### 2.2.1 Structure and mechanism of action

Treatment for cancer has historically involved the use of MTX, a synthetic organic compound, potent chemotherapeutic medication. It was first developed by Dr. Yellapragada Subbarow an Indian origin scientist in the early 1950s as a therapy for pediatric leukemia (Bagri et al., 2023). MTX is an analogue of aminopterin which was first used in the treatment of acute leukemia in 1947. However, because of its better therapeutic index, amethopterin was marketed as MTX. Ever since, it has been extensively utilized to treat a wide range of solid tumors, such as malignancies of the head and neck, esophagus, breast, and lung (Khan et al., 2012).

MTX shares structural similarities with folic acid (FA) which is a Vitamin B9 essential for human body. MTX is a antagonist to FA belongs to the class of drugs known as antimetabolites, and its essential action is disruption of DNA synthesis and repair, making them effective in inhibiting the growth of cancer cells. MTX's chemical structure is made up of a pteridine ring, which is connected to a p-aminobenzoic acid moiety and is typical of derivatives of folate. Because of its structure, MTX can competitively inhibit dihydrofolate reductase (DHFR), which prevents rapidly dividing cells of body like cancer cells, bone marrow cells, and skin cells from synthesizing proteins, RNA, and DNA. The conversion of deoxyuridine to thymidine requires tetrahydrofolic acid which is, during this process, oxidized to dihydrofolic acid. The

kinetics of this system are dependent on the reconversion of dihydrofolic acid to the tetrahydro form by the enzyme DHFR. It is at this site that MTX exerts its action by electrostatic binding of the enzyme for which it has an affinity 100,000 times that of the substrate (Bedoui et al., 2019). Thus, the synthesis of thymidine and formation of DNA is prevented. Fortunately, the addition of exogenous formyl tetrahydrofolic acid, folic acid or folinic acid (Leucovorin) bypasses this block and allows the continued production of thymidine-an effect which has been utilized to therapeutic advantage in serious case of MTX toxicity. In this way MTX probably affects both normal and malignant cells by inhibiting cell division mainly in the S phase of the cell cycle ultimately halting DNA synthesis and kills cells in the S phase of the cell cycle thus causing a block at the G1-S transition (Hamed et al., 2022; Nogueira et al., 2018).



**Figure 2.3** Structural similarities between Folic acid and Methotrexate molecule (Source: Halik et al., 2021)

Following MTX infusion, the primary metabolite in serum is 7-hydroxymethotrexate (7-OH-MTX), which is responsible for both toxicity and activity of MTX. Soon after the infusion, 7-OH-MTX concentrations in plasma are higher than those of the parent molecule. Citation63 MTX and 7-OH-MTX demonstrate first-order pharmacokinetic characteristics. Citation62 Renal excretion of MTX involves both active tubular reabsorption and secretion as well as passive glomerular filtration. MTX is eliminated by the kidneys more quickly than 7-OH-MTX (Ren et al., 2019).

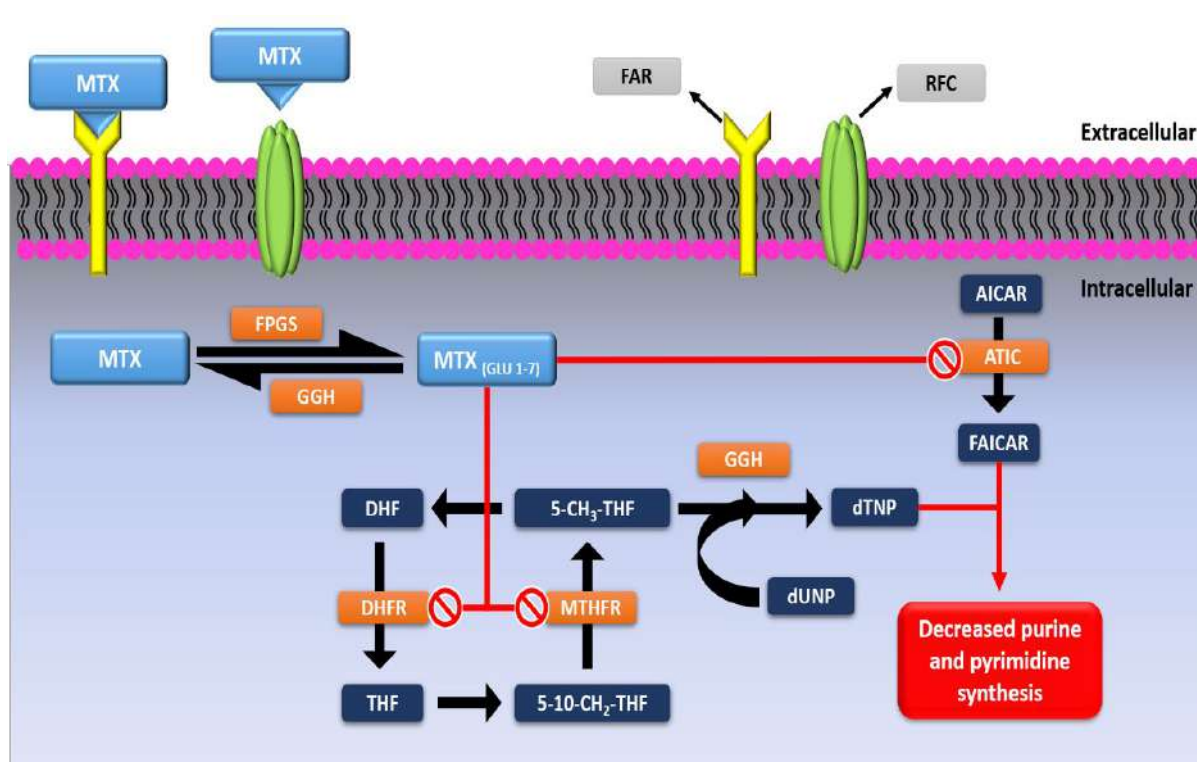
---

The ATP-binding cassette transporter reduced folate carrier 1 (RFC1) primarily follows cellular MTX entry. To a little degree, MTX further employs receptor-mediated endocytosis through the means of folate receptors (FRs), which are membrane proteins anchored by glycosyl-phosphatidyl-inositol (GPI) and capable of internalizing bound folates and folate conjugates. FRs are overexpressed in 90% of ovarian carcinomas, and some other FR positive hypoxic cancer strains possess epithelial cell lining, including breast, lung, cervical, oral, and pancreatic cancer (Hagner and Joerger, 2010). Research has indicated that the overexpression of FR $\alpha$  could potentially provide cancer cells with an advantage in proliferation through mechanisms that are both connected to and separate from folate uptake. For DNA replication and cell division, normal cells also express FR; however, cancer cells express FR 500 times more frequently than healthy cells (Vivek et al., 2017). This increases cellular uptake of anti-folate class of drug by activating multiple endocytic pathways and decreases drug resistance in cancer. These factors have drawn attention to folic acid-based targeting ligands. It has been documented that solid tumor such ovarian, lung, and breast carcinomas overexpress FR $\alpha$ . Conversely, FR $\alpha$  is only found in modest quantities on the apical surfaces of a few organs, including the kidney, lung, and choroid plexus, in normal human tissues (Nogueira et al., 2018; Xie et al., 2013).

Because it is strongly ionized and typically hydrophilic, MTX passes biological barriers relatively poorly. Intracellular folypolyglutamyl synthase (FPGS) metabolizes MTX to a polyglutamate derivative called MTX<sub>Glu</sub>. Compared to the original MTX form, MTX<sub>Glu</sub> exhibits a much longer cell residence time and higher bioactivity. This is a crucial pharmacokinetic phase that establishes the drug's defined action and designates MTX as a type 1 prodrug representation that goes through intracellular bioactivation. MTX is not as effective as MTX<sub>Glu</sub> as an anti-folate drug since it has a much stronger ability to inhibit DHFR (**Figure 2.4**). By blocking folate-related enzymes, primarily DHFR, which catalyse the conversion of dihydrofolate (DHF) to tetrahydrofolate (THF), MTX indirectly slows cell division. THF is crucial for the synthesis, maintenance, and replication of DNA strands and functions as a major coenzyme in several transmethylation processes in the pyrimidine and purine nucleotide production pathways. When MTX inhibits intracellular THF synthesis, cell growth and its associated metabolic equilibrium are disrupted. Additionally, it inhibits other enzymes involved in the de novo production of purine and pyrimidine nucleotides, such as Methyl tetra hydro folate reductase (MTHFR) converting 5-methyltetrahydrofolate (5-CH<sub>3</sub>-THF) to 5,10-methylenetetrahydrofolate (5,10-CH<sub>2</sub>-THF), a crucial step in deoxythymidine monophosphate

---

(dTNP) synthesis. Other enzymes inhibited too are amido-phosphoribosyl transferase, 5-aminoimidazole-4-carboxamide ribonucleotide transformylase (AICART), and thymidylate synthase (TYMS). As a result, MTX<sub>Glu</sub> is the one that exhausts the precursors needed for the synthesis of DNA and RNA, which are essential for proliferation of cells, causing disruptions in DNA synthesis and eventually leading to cell death (**Figure 2.4**). The fact that MTX activity is most noticeable in cells that are actively dividing, primarily in the S phase of the cell cycle, is not surprising. In fact, the multiplying cancer cells are the ones most vulnerable to the cytotoxic effect of this medication, suggesting a connection between folate antagonistic activity and MTX's anti-tumor activity (Chan and Cronstein, 2013; Wong and Choi, 2015).



**Figure 2.4** Graphical representation of Methotrexate's mechanism of action. (FAR; Folic acid receptor. RFC; reduced folate carrier. MTX<sub>(GLU 1-7)</sub>; methotrexate polyglutamates. FPGS; folylpolyglutamyl synthase. DHFR; dihydrofolate reductase. DHF; dihydrofolate. THF; tetrahydrofolate. 5,10-CH<sub>2</sub>-THF; 5,10-methylenetetrahydrofolate. 5-CH<sub>3</sub>-THF; 5-methyltetrahydrofolate. MTHFR; methylenetetrahydrofolate reductase. dUMP; deoxyuridine monophosphate. dTMP; deoxythymidine monophosphate. GGH;  $\gamma$ -glutamyl hydrolase. ATIC; AICAR formyltransferase. AICAR; 5-aminoimidazole 4-carboxamide ribonucleotide. FAICAR; 10-formyl AICAR.)

---

### 2.2.2 Role in cancer and other malignancies

In particular, a significant advancement in cancer therapy was the switch from high dosage MTX (HDMTX) therapy of 0.5–5 g/week to low dose MTX (LDMTX) therapy of 7.5–25 mg/week for RA and psoriasis. A few years later, it was discovered that MTX was one of the best disease-modifying antirheumatic drugs (DMARDs) used for psoriasis and RA patients significantly when given a LDMTX (1-2 mg/day). However, starting in the middle of the 1980s, MTX was used in RA clinical applications as DMARDs (Cutolo et al., 2001).

About 70 years ago, anti-folates- the first class of anti-metabolites was presented to the clinic. One of the earliest classes of antineoplastic medicines to be created were folate antagonists. Childhood acute lymphoblastic leukemia (ALL) was brought into cure in 1948 with the use of the 4-amino derivative of FA (aminopterin), and the related drug MTX is now a key part of today's cancer treatment (Khan et al., 2012). MTX is FDA-approved for treating ALL, either in combination with other medications or on its alone, to treat patients with various forms of hematologic malignancies as well as to treat ALL that has progressed to the central nervous system (CNS) or to stop it from spreading there. Advanced mycosis fungoides (MF) or advanced non-Hodgkin lymphoma (NHL) and many other cancer types, such as brain tumors, breast cancer, hepatoma, lung cancer, lymphomas. Some types of head, neck, and esophagogastric carcinomas, gastric cancer, osteosarcoma that has not spread to other body parts or after primary tumor surgery, prostate and bladder cancers, or gestational trophoblastic neoplasia, are also approved for treatment with MTX (Bryan, 2012; Marika Grönroos, et al., 2006). When treating early-stage breast cancer, MTX is used either alone or in combination with other medications, surgery, and other therapies. Treatment for metastatic breast cancer involves a variety of combination regimens, including vincristine (VCR), adriamycin (ADM), cyclophosphamide (CTX), MTX, 5-fluorouracil (5-FU) (CMF), 5-FU, and CTX in combination with 5-FU and tegafur followed by LV rescue (MUL). The researchers demonstrated, based on experimental data, that the traditional CMF regimen is safe and has a significant impact on how early breast cancer patients respond to treatment (Chabner et al., 2005b; Hamed et al., 2022).

While chemotherapy, including MTX, is utilized both pre and post-operatively for lung malignancies, surgical resection remains choice of treatment method. The chemotherapeutics etoposide, vincristine, or Adriamycin were usually included in the regimens along with the medications MTX, CTX, and lomustine for small cell lung cancer (SCLC). A combination of all the medications listed above, followed by chest radiation therapy, proved to be the most

successful regimen. Patients responded effectively to the treatment, which also produced a significant tumour response rate (Mazzaferro et al., 2013).

MTX was introduced to the area of rheumatology in recent years, and it has significantly improved the clinical state and prognosis of many patients with inflammatory disorders, including RA. As of right now, MTX is the first-line medication recommended for treating RA. It can be taken either alone or in conjunction with conventional or biologic DMARD. Starting in the middle of the 1980s, MTX was the first medication used in clinical RA applications (Cutolo et al., 2001). Nowadays, MTX is frequently used in conjunction with other medications to treat a variety of neoplasms, including severe and resistant forms of autoimmune diseases, such as RA, psoriasis, myasthenia gravis, Crohn's disease, multiple sclerosis, polyarticular juvenile idiopathic arthritis, and even an ectopic pregnancy (Khan et al., 2012). Recent research revealed that MTX-treated RA patients had low levels of circulating purines and pyrimidines, which in turn affected their potential for DNA and RNA synthesis as well as cell proliferation. Deregulation of mononucleotide precursors of nucleic acid, specifically at the stage of methylation of dUMP into dTMP by thymidylate synthase, is another factor contributing to disruption of DNA synthesis and suppression of cell proliferation in the inflammation triggering cells in the joints. A new study confirmed that MTX suppressed human PBMC TS activity in vitro at low doses explaining its role in reducing inflammation in RA patients (Abolmaali et al., 2013; Kyvsgaard et al., 2021).

### 2.2.3 Toxicity

The inadequate bioavailability of many available chemotherapeutic drugs presents a significant obstacle, restricting their development and hindering their full therapeutic potential in vivo. Methotrexate (MTX), for instance, suffers from both poor aqueous solubility and limited bioavailability. Further compounding this issue, within 24 hours of intravenous treatment, 80–90% of the administered dose is eliminated unchanged in the urine, indicating inadequate absorption of the native substance. The remaining 10-20% of the absorbed drug is susceptible to rapid degradation in the bloodstream and exhibits toxicity towards healthy tissues (Yang et al., 2015). These limitations restrict the drug's effectiveness, resulting in decreased patient compliance, reduced quality of life, and substantial dose reductions, ultimately compromising its efficacy and potentially leading to life-threatening events (Kakkar et al., 2015). If MTX is used incorrectly, it can become toxic. The most of the fairly uncommon mortality brought on by MTX are due to severe myelosuppression, the most dangerous side effect. Pneumonitis, liver fibrosis, homoeopathy, inhibition of the bone marrow, and alopecia are other adverse

---

---

effects. Risk factors associated with MTX include hyperglycemia, renal disease, hepatitis, and being overweight (Hamed et al., 2022). Hepatotoxic MTX has the potential to induce cirrhosis and hepatitis. Many of HDMTX's side effects are extremely dangerous and could jeopardize the lives of patients. Early discovery, careful observation, and rescue dosages all contribute to the reduction of toxicity. Regarding MTX first-pass metabolism, 80–90% of the medication is eliminated unaltered in the urine. A certain proportion of hepatic component plays significant role for MTX clearance. The "Common Toxicity Criteria for Adverse Events" guidelines, developed by the National Cancer Institute (NCI), provide a clear description of hepatotoxicity (Roberts et al., 2020). These recommendations take into account increases in liver enzymes, such as alkaline phosphatase, gamma-glutamyltransferase (GGT), alanine aminotransferase (ALT), and aspartate aminotransferase (AST) and alkaline phosphatase (ALP) (Bath et al., 2014). Urine with a higher pH will have more MTX and its metabolites soluble in it, while MTX and its metabolites are insoluble in acidic urine. MTX crystals, on the other hand, develop in an acidic pH and cause abrupt renal failure. Numerous risk factors, including low alkalinization, inadequate hydration, prolonged methotrexate use, and low rescue dose, are to blame for the high prevalence of toxicity. Moreover, medications that obstruct methotrexate's renal tubular excretion delay the drug's clearance, which increases the risk of renal damage (Marika Grönroos et al., 2006). Within one to three weeks, hematologic toxicity manifests and then goes away in three weeks. Clinically, toxicity develops as severe leukopenia followed by thrombocytopenia; the toxicity can be either acute or persistent. Moreover, because of the possibility of dying, up to 25% of patients with hematological toxicities stop receiving treatment. One MTX toxicity that is hard to avoid is pancytopenia, which can strike suddenly during treatment (Feinsilber et al., 2018).

Apart from these toxicities, neurotoxicity, GIT toxicity and pulmonary toxicity are some other common complications associated with HDMTX treatment which can be controlled to an certain extent with the help of LV (Hagner and Joerger, 2010).

### 2.2.4 Newer approach

Many studies in the field of drug delivery have been conducted to overcome drug resistance in addition to improving drug efficacy and pharmacokinetics, circulation in the blood, controlled release, and therapeutic window in order to deliver MTX in an efficient manner. Furthermore, it has been proposed that MTX's hybridization with nanocarriers may lead to significant advancements in nanomedicine. Numerous nonviral nanovehicles, including inorganic and organic/polymer nanovehicles, are now accessible. Difficulties related to MTX, such as

---



---

delivery routes, frequent long-term doses, and insufficient targeting options, frequently result in less-than-ideal outcomes, non-adherence from patients, and systemic adverse responses. Recent years have seen a number of attempts employing nanotechnology to address those limitations. These nanotechnology approaches reduce nonspecific targeting, circumvent first passage metabolism, and enhance drug efficacy, among other benefits. However, while long-term effective medicines are still lacking, this continues to rank highest among unmet needs (Khan et al., 2012; Patel et al., 2021). **Table 2.2** summarizes different types of novel formulations used for MTX delivery.

**Microspheres:** Microspheres are made with less adverse effects and enhanced pharmacological action with extended release. Under near-infrared (NIR) laser irradiation, a succession of LM-and/or MTX-loaded microspheres were prepared by chitosan (CS) and formaldehyde was utilized to accomplish cancer chemophotothermal synergistic therapy. Moreover, intratumoral injections of the CS/LM/MTX microspheres were given to animals carrying tumors. When paired with MTX's drug release, these microspheres exhibited increased anticancer efficacy in vivo. These microspheres also exhibit good biocompatibility and minimal toxicity, both of which are important for in vivo procedures. Therefore, the microspheres loaded with LM and/or MTX demonstrated superior potential for cancer chemophotothermal synergistic therapy when combined with NIR laser irradiation (Fan et al., 2020).

**Nanogel:** Avasatthi et al. synthesized a hot homogenized nanogel made up of MXT-loaded nanostructured lipid carrier (MXTNLC), and they assessed its ability to reduce psoriasis symptoms in an imiquimod-induced psoriasis model (Patel et al., 2021).

**Hydrogel:** In a study conducted on 14 adult patients with palmoplantar lesions, Kumar et al. examined the safety and effectiveness of a recently marketed topical MXT (0.25 %) formulation in a hydrogel substrate. According to their findings, MXT 0.25% in a hydrophilic gel is well tolerated but has limited efficacy in managing psoriasis lesions on the palms and soles (Patel et al., 2021).

**Liposomes:** Liposomes are the self-assembling amphiphilic molecules that are widely created from different lipids (phospholipids and cholesterol) in bilayers with a water-soluble membrane-containing element and a hydrophilic bond within and outside of the bilayers. Because liposomes have unique internal and external surface features, they have been thoroughly studied as medication and gene delivery vehicles. Drug molecules usually reside in

---

---

the liposome's core, and the outside surface can be altered based on the specific development objective for each drug delivery system (DDS) type. The physicochemical properties and in vitro permeability of deformable liposomes entrapped with MXT were examined by Srisuk and colleagues. They created lipid vesicles using PC and oleic acid (OA) and compared them to traditional liposomes made from PC and CH using the thin-film hydration approach and entrapped with MXT. Deformable MXT liposomes encapsulated in PC or hydrogenated lecithin with dipotassium glycyrrhizinate surfactant were studied by (Trotta et al., 2004).

**Metal nanoparticles:** The biological compatibility, functionalizable surfaces, simple interaction with drug molecules, and tunable dimensions and forms of metal nanoparticles, such as gold (AuNPs) and silver (AgNPs), made them useful as DDS. The in vivo anticancer effects and invitro cytotoxic effects of MTX-conjugated AuNPs were described by (Rahman et al., Chloroauric acid was reduced with sodium citrate to create MTX-AuNPs, which were then conjugated with MTX. Lewis lung carcinoma (LL2) cell culture line was used to test the anticancer effects of free MTX and MTX-AuNPs. It was confirmed that in LL2 cells, the anticancer efficacy of MTX–AuNPs was much stronger (more than 17-fold sensitive) than that of free MTX. Compared to the free MTX-treated or PBS-treated control groups, the tumor volume was considerably decreased in the MTX–AuNP-treated mouse group (Chen et al., 2007). In one of the other study the ultrafine AuNPs were used for enhanced and safe delivery of MTX drug to the breast cancer cells. Smaller size of AuNPs were pegylated to functionalize the surface and enhanced uptake of particles. MTX loaded AuNPs showed better targeting and killing in comparison to only AuNPs and free MTX. Free MTX has problem with fast renal clearance and reducing toxicity which were easily tackled by combining the drug with nano platform (Naz et al., 2019).

**Metal oxide nanoparticles:** Different types of metal, metal oxide and non-metal oxide nanoparticles like gold nanoparticles (AuNPs), silver nanoparticles (AgNPs), iron oxide nanoparticles (IONPs), zinc oxide nanoparticles (ZnONPs), quantum dots (QD's), silica nanoparticles, carbon nanotubes and nano shells etc. are covered under Inorganic nanoparticles. Inorganic nanoparticles are more popular in the areas of biomedicine, imaging, drug delivery system, diagnosis, optics and even electronics. Due to high stability, biocompatible nature and unique size shape properties at nanoscale level makes them ideal candidate for DDS (Bhattacharyya et al., 2011). Because of their enormous surface areas, spherical shape, and metal oxides particularly iron oxide nanoparticles (IONPs) and ZnONPs have been proposed as DDS. Nosrati et al, used L-lysine coated IONPs as a carrier for the delivery of MTX to

---

MCF-7 breast cancer cells. In comparison to free MTX, IONP-MTX showed enhanced cytotoxicity to MCF-7 cells and thus can be seen as a potential agent against various different FR positive cancer cells (Nosrati et al., 2017).

**Carbon nanomaterials:** Carbon atoms grouped in a particular configuration, such as carbon nanotubes (CNTs) or graphene, make up carbon nanomaterials. Because of their unique geometry, carbon nanomaterials have a high surface area and can effectively carry pharmaceutical compounds, such as methotrexate, to cancer cells by encapsulating them within their structure (Fabbro et al., 2012). In addition to medication administration, biological labeling, bioimaging, and electronic applications, carbon-based materials, such as NPs, nanotubes, and graphene, have been extensively researched. The synthesis of MTX-conjugated fluorescent carbon nanoparticles (CNPs-MTX), which have demonstrated potential in enhancing MTX's pharmacokinetic characteristics, is one instance of this. One easy and environmentally friendly way to produce ultra-small sized CNPs on a wide scale is through the synthesis from glucose or sucrose using an ultrasonic technique under strong oxidative conditions. Evaluations of CNPs-MTX's bioactivity show that they are quite biocompatible, and CNPs-MTX combinations show encouraging cytotoxic effects on the human lung cancer cell line (H157) (Ajmal et al., 2015).

**Table 2.2** Summary of Novel nanocarriers used for methotrexate delivery.

Nanocarrier	System formulation	IC50 value	Results	References
<b>Liposome</b>	PEG-P(HPMA-LA)-PDMA, Anis-PEG-P(HPMA-LA)- PDMA	4.811M(H460)	100% survival rate after 45 days	(Yang et al., 2016)
	Phospholipon 90G + Cholesterol (70%: 30%)	2.15 mg/ ml (BT-474)	Enhanced cytotoxic activity on cancer cell line in contrast to free MTX	(Dastjerd NT et al., 2021)
<b>Nanogel</b>	Chitin nanogel	0.046 mg/ml (THP-1 and HaCaT)	Substantial degree of toxicity on cancer cells, with no systemic or cutaneous toxicities in vivo	(Panonnummal and Sabitha, 2018)
	Poly(acrylic acid)-poly(vinyl amine) block copolymer	-	Improved and selective cytotoxic activity against human breast cancer cells MCF-7	(Dehvari et al., 2019)
	Dendritic polyglycerol (dPG)	75 and 100 µg/ mL (Hela and MCF-7)	Better antitumor activity than free MTX	(Zhang et al., 2015)
<b>Dendrimer</b>	PAMAMandOEG	8.91 g/mL(MCF-7)	High tumour growth suppression and enhanced blood compatibility	(Zhao et al., 2016)
	Glucosamine-conjugated PEPE	2.14 and 2.79 µM (U 87 MG and U 343 MGa)	Transport of MTX over the BBB and into the central necrotic areas	(Dhanikula et al., 2008)
<b>Metal nanoparticle</b>	AuNPs	100 µg/ mL (A549)	Enhanced controlled release and anticancer activity	(Wang et al., 2016)
	PEG and AgNPs	258.6 lg/mL (MCF-7)	Reduced hemolytic toxicity in contrast to unbound MTX	(Muhammad et al., 2016)
<b>Carbon Nanomaterial</b>	AF488/647, FA and 99Tc coated multiwalled CNT	2.13 lg/mL (A549) 1.95 l g/mL (MCF-7)	Theragnostic application with high□ antitumor activity	(Das et al., 2013)
	Graphene oxide	50 ng/mL (A549)	Enhanced water stability and controlled release	(Du et al., 2013)
	Dopamine, graphene oxide	15.33 lg/mL (MCF-7) 83.73 lg/mL (HEK-293)	Sustained release and DA helps to target the nanocarrier to cancer cells	(Masoudipour et al., 2017)

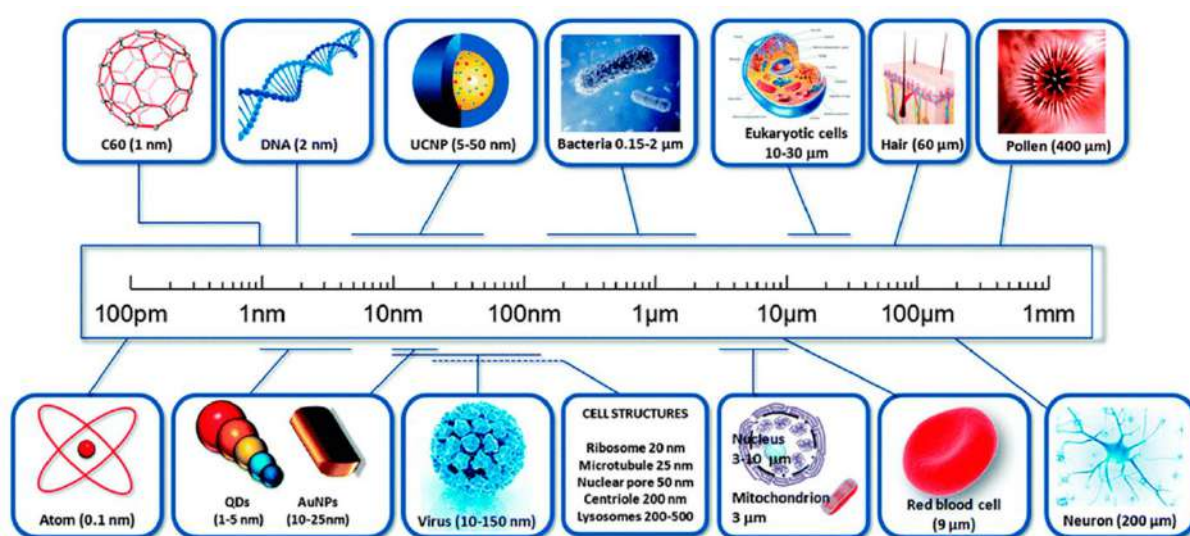
---

### 2.3 Nanotechnology and its applications

#### 2.3.1 What is nanotechnology?

Nanoscience and nanotechnology these two terms, though often used interchangeably, have distinct meanings. Nanoscience is the exploration and understanding of matter at the atomic and molecular level, focusing on the unique properties and behaviors that emerge at this minuscule scale. Think of it as peering into a hidden world, deciphering the language of the tiniest building blocks. Alternatively, nanotechnology takes matters beyond. The creation of novel materials, tools, and technologies is the practical application of this nanoscale knowledge. Imagine creating materials for spacecraft that are both extraordinarily strong and light, creating small robots that can directly administer medication to sick cells, or even creating solar cells that can capture sunlight almost perfectly are some of the real-life applications of the same. 'Nano' represents a one thousand millionth of a meter ( $10^{-9}$  m) (**Figure 2.5**). It is a Greek prefix that means dwarf or something very small. By definition, NPs are shaped like any other particle with size range of 1–100 nm; that is, they are specifically the size that fall between bulk materials and quantum dots or atomic/molecular structures (Mansoori, 2017). The different new features of these nano-sized particles, which are connected to a high surface area to volume ratio and/or quantum phenomena, result in unique physical and chemical properties. The Nobel Prizes given for the discovery of several NPs including Henry Rohrer in 1986 for the invention of the scanning tunneling microscope (Adams and Barbante, 2013), Kroto et al. in 1985 for the discovery of fullerene (Kroto, 1992), and Geim and Novoselov in 2010 for the discovery of graphene (Geim and Novoselov, 2009) led to the widespread acceptance of nanotechnology. Long before Taniguchi coined the term "nanotechnology" in 1974, physicist Richard Feynman gave a talk titled "There's Plenty of Room at the Bottom" on December 29, 1959, at an American Physical Society meeting at the California Institute of Technology (Feynman, 1997). This talk laid the foundation for the ideas and concepts underlying nanoscience and nanotechnology. This innovative concept opened up new avenues for thought, and Feynman's theories have since been validated. He is regarded as the founding father of modern nanotechnology because of these factors. NPs have gained attention in the biomedical field due to its small size, superior efficiency and increased physiochemical properties. While human exposure to nanoparticles has always existed, the industrial revolution saw a sharp rise in this attention. They can be synthesized from various metals, non-metals & polymers (Wang, 1999). Early 2000s, nanotechnology started to become more and more popular and research into engineered nanomaterial escalated. NPs have certain

exceptional characteristics like larger surface area to volume ratio, small size, structural properties and extended blood circulation time comparatively which makes them ideal candidate for various medical and clinical application. NPs began to get incorporated into different commercial products by that time like the use of ZnONPs and Titanium dioxide nanoparticles ( $\text{TiO}_2\text{NPs}$ ) in various sunscreens and lotions (Janer et al., 2014), AgNPs in various medical applications (Santamaria, 2012). Various different nanoplatforms like metal NPs, inorganic NPs, dendrimers, liposomes, polymeric NPs, nano devices, nanocomposites, nanocarriers etc. are under research for imaging, diagnostic and even treatment for various diseases including cancer.



**Figure 2.5** Graphical presentation of nanoscale comparison of various entities for comparison purpose. (Source: Bayda et al., 2020)

Nowadays, nanotechnology has a constant impact on people's lives. There are a wide range of possible advantages. However, there is a great deal of worry about the possible health and environmental concerns due to the broad human exposure to nanoparticles. As a result of these worries, new scientific fields including nanotoxicology and nanomedicine have emerged. The study of possible harmful health effects of NPs is known as nanotoxicology (Oberdörster, 2010). The field of nanomedicine, encompassing subfields like biomaterials, bioengineering, biosensors, and bioimaging, emerged to investigate the potential advantages and hazards associated with nanoparticles utilized in medical devices and medicine. Improved medication distribution, antimicrobial coatings for medical equipment, decreased inflammation, better surgical tissue repair, and the identification of cancer cells in circulation are just a few of the

---

possible advantages of medical nanomaterials (Domingues et al., 2022; Zhao and Castranova, 2011a).

### 2.3.2 Applications of nanotechnology in cancer

Different branches of science contribute to the field of nanoscience and nanotechnology applications are chemistry, physics, biology, material science, engineering, and biotechnology as shown in **Figure 2.6**. It's the amalgamation of all these different science in various combination pays way to the generation of wide varieties of nanomaterials like organic, inorganic, metal based or metal oxide-based nanoparticles. Semiconductor nanomaterials to carbon-based nanomaterials, nano electronics, biosensors are added applications of nanotechnology (Ramos et al., 2017; Zhao and Castranova, 2011b).

There are numerous possible uses for nanotechnology in a variety of industries. Nanotechnology is paving the way for the development of more compact and efficient electronics and computer equipment. Electronic components that operate more quickly and consume less energy can be produced by utilizing the special electrical and thermal properties of nanomaterials. Nanoelectronics is a field of nanotechnology to increase functionality and energy efficiency, electronic gadgets use materials at the nanoscale. Quantum Computing is another field where the development of quantum computer technologies for cutting-edge computing applications is made possible by nanotechnology (Nasrollahzadeh et al., 2019).

Nanotechnology is also helpful in the field of environmental remediation since it may be used to clean up contaminated places, remove toxins from water, and purify it. Public health and environmental sustainability may be significantly impacted by this. Water Purification plants or small-scale purifying spaces use nanotechnology to eliminate impurities and toxins from water. To reduce pollutants and enhance air quality, filters based on nanotechnology are utilized in Air Filtration units (Taran et al., 2021).

Nanotechnology is being used in the energy sector to build better energy storage systems, boost fuel cell performance, and increase solar panel efficiency. These developments may result in more reasonably priced and environmentally friendly energy options. Moreover, the aerospace, automotive, and construction industries use lightweight, highly strengthened materials like nanocomposites and nanocoating, which are produced using nanotechnology. Nanocomposites are advanced materials with enhanced mechanical, electrical, and thermal properties while, nanocoating improves durability, corrosion resistance, and self-cleaning properties of materials (Hussein, 2015; Kianfar, 2020).

---

Additionally, remarkable advancements in the field of nano-oncology have been made by increasing the effectiveness of conventional chemotherapy medications for a wide range of aggressive human tumors. These developments have been made possible by the application of various functional molecules, such as cytotoxic drugs, antibodies, and nanoparticles, to the tumor site. Accordingly, numerous studies have demonstrated the utility of nanomaterials alone or in combination with therapeutic compounds to influence vital biological processes such as autophagy, metabolism, or oxidative stress, thereby exhibiting anticancer activity. Therefore, nano-oncology is a very appealing use of nanoscience that enables both a major decrease in the systemic toxicity connected with conventional chemotherapy therapies and an improvement in tumor response rates. NPs are newly emerging and promising therapeutic tools that can kill tumor cells while the micron-sized particles do not affect the tumor cells. Additionally, *in vitro* studies showed that certain metal oxide NPs can preferentially kill cancer cells with minimal effects on normal cells. Nanoparticles possess a larger percentage of atoms at the exposed surface and can readily penetrate into tumor site (Chavali and Nikolova, 2019; Nasrollahzadeh et al., 2019).

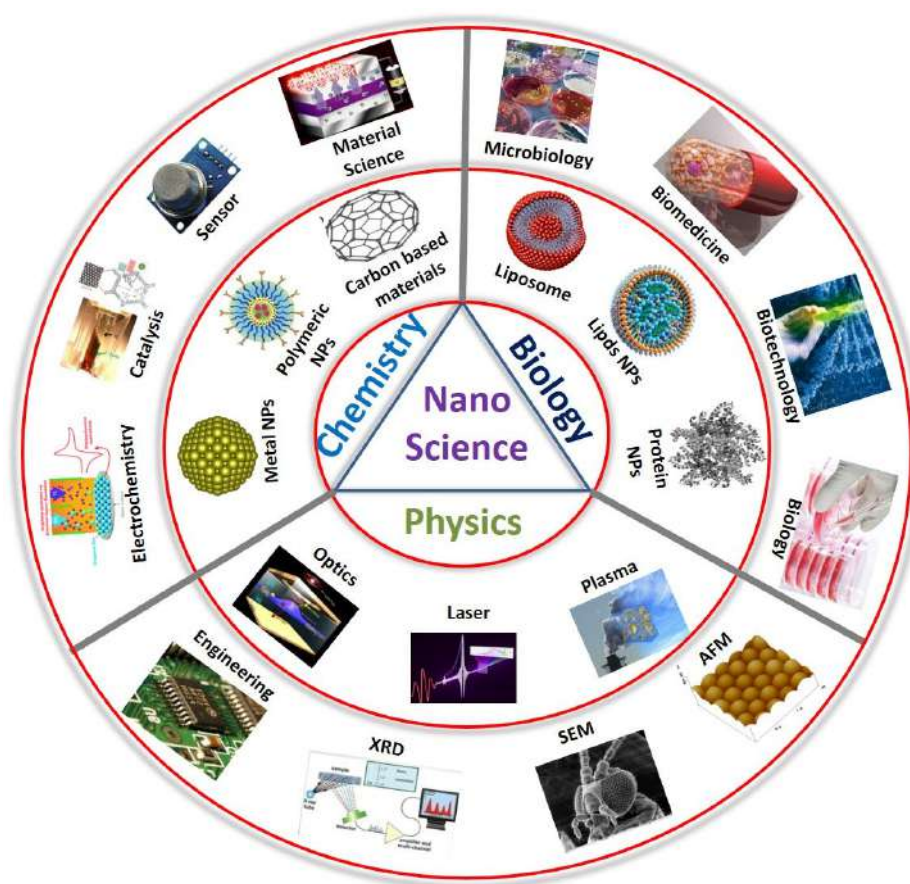
Critical factors in the therapeutic success of NPs in cancer treatment are: the stability and duration of circulation of NPs, their capacity to penetrate physiological barriers and reach afflicted anatomic locations, their bioavailability at the disease site, and their safety profile are all. Enhancing these attributes will improve the effectiveness of nanomedicines, hence aiding in their integration into the mainstream of cancer therapy. It is possible to advance particle design while simultaneously making changes to the tumour microenvironment, which can have a significant impact on particle accumulation. Concurrently, the effectiveness problem can be resolved by finding more effective APIs in combination with targeted and specific cancer treatments for which nanoparticle-based delivery offers notable benefits. The synthesis and characterization of modified NPs for cancer imaging and treatment have advanced significantly since the U.S. Food and Drug Administration (FDA) initially approved the liposomal nanomedicine Doxil® in the 1990s for Kaposi sarcoma and ovarian cancer.<sup>1,2</sup> Life-threatening toxicities linked to the active pharmaceutical ingredient (API) have been decreased by FDA-approved nano pharmaceuticals (Doxil®, Abraxane®, Marqibo®, Onyvite®, Vyxeos®, and others), and this has led to a slight improvement in patients' overall survival owing to nanotechnology intervention (Beltrán-Gracia et al., 2019; Gyanani et al., 2021).

The application of nanotechnology in medicine for targeted drug delivery, by directing medication to particular organ sites, NPs can be designed to increase medication effectiveness

---



and decrease negative effects. Tissue engineering where scaffolds for tissue regeneration and repair are made of nanomaterials, and in the field of diagnostics to increase sensitivity and accuracy of medical imaging and diagnostic instruments utilizing nanoscale materials (Gunasekera et al., 2009). Treatments with fewer adverse effects and more precision and efficacy are made possible use of NPs. Drugs can be delivered directly to cancer cells using nanoparticles as drug carriers, reducing harm to healthy cells in the process. Various nanocarriers such as liposomes, micelles, dendritic macromolecules, quantum dots, and carbon nanotubes have been employed for drug delivery in cancer therapy (Banerjee and Verma, 2008; Biswal and Yusoff, 2017; Mi et al., 2016).



**Figure 2.6** Applications of nano science in the fields of Chemistry, biology and physics

(Source: Bayda et al., 2020)

Molecular imaging is a subset of application for NPs that enables the early diagnosis of cancer. Because of their unique optical, magnetic, or structural characteristics compared to other molecules, nanoparticles are helpful in the early identification and screening of cancer cells. For instance, immune superparamagnetic iron oxide nanoparticles (SPIONs) can be targeted against cancer cell lines in magnetic resonance imaging (MRI) (Wang et al., 2008).

---

Because nanotechnology makes it possible to construct highly specific biomarkers that can swiftly and effectively diagnose tumors, it plays a crucial role in cancer biomarker screening. These biomarkers, which can be proteins, DNA, or protein fragments, are used to track or detect alterations in cancer cells, investigate cellular processes, and eventually improve our knowledge of cancers. The development of these tailored biomarkers is made possible by nanotechnology, which improves the precision and effectiveness of cancer screening procedures. Circulating Tumor Cells (CTCs) are cancer cells that have broken out from their original tumor and made their way into the circulation. They can serve as biomarkers for the detection and tracking of cancer (Jia et al., 2021). To identify and separate CTCs from blood samples, nanotechnology-based techniques have been developed, including magnetic nanoparticles and microfluidic devices. Alteration in the synthesis of specific macromolecules brought on by DNA mutations can result in unchecked cell proliferation and, eventually, giving rise to malignant tissues. Techniques based on nanotechnology, such as graphene and nanowire-based biosensors, have been developed to identify such DNA alterations in cancer cells (Gribko et al., 2019; Hou et al., 2021).

### **2.4 Zinc oxide nanoparticles (ZnONPs)**

#### **2.4.1 Biological role of Zinc (Zn)**

Zinc, a trace element found throughout the body, holds immense significance for human health. Zn needed for body comes primarily from the food because the body cannot store excess Zn. It is essential for several processes, including thyroid function, blood clotting, wound healing, immunity and essential for preserving vision. Its involvement in myriad enzymatic reactions, immune function, protein synthesis, wound healing, DNA synthesis, and cell division underscores its multifaceted impact. It is often known that Zn is a vital trace element for humans as well as other animals, plants, and even microorganisms. Emerging from the Earth's crust, zinc finds its way into the food chain via plants, animals, and water. Meat, shellfish, legumes, seeds, nuts, dairy products, and whole grains are particularly rich dietary sources. Daily intake recommendations for adults stand at 8-11 milligrams for men and 8 milligrams for women, with increased needs during pregnancy and lactation (Jiang et al., 2018; Mossink, 2020; Zhang et al., 2013).

Zn's ability to bind allows it to enter the most confined areas of the cell, where it functions as an enzyme co-factor for more than 300 different enzymes. Beyond its enzymatic prowess, Zn plays a pivotal role in gene expression. Through certain DNA interactions, it acts as a crucial cofactor for more than a thousand transcription factors, regulating the gene expression. These

---

zinc-fingered proteins play pivotal role in selecting the genes that become active and those that remain inactive, influencing differentiation, development, and environmental adaption (Wu et al., 2008).

Zn is a ubiquitous trace element that affects a wide range of biological processes beyond its function within cells. Beyond the transcriptional stage, Zn is important because it is essential to the immunological defenses. It strengthens immune cell responses and protects against invasive infections by functioning as a powerful barrier. Its antioxidant and anti-inflammatory qualities boost our defense mechanisms even more, strengthening our ability to ward off illness (Panda and Rout, 2006).

Depletion of zinc levels can lead to a cascade of adverse effects, including impaired immune function, delayed wound healing, growth retardation and cognitive impairments. Deficiency in Zn can result in an impaired immune response, leading to an increased susceptibility to infections and diseases. In severe cases, it can manifest as acrodermatitis enteropathica, characterized by skin lesions, diarrhea, and hair loss. A deficiency in Zn can result in delayed wound healing and increased susceptibility to skin infections. Pregnant and lactating women, infants, the elderly, vegetarians, and individuals with certain gastrointestinal disorders affecting zinc absorption are particularly vulnerable to deficiency (Barnes and Moynahan, 1973; Jeejeebhoy, 2007).

### **2.4.2 ZnONPs properties**

The term "zinc oxide nanoparticles" refers to the NPs of ZnO with particle sizes less than 100 nanometers. They are very catalytically active and have a larger surface area in relation to their size. The many methods used to create ZnONPs affect their precise chemical and physical characteristics. Compared to bulk ZnO, they have improved optical, electrical, and biological properties that make them valuable for use in biomedical devices, sensors, solar cells and medicine among other uses (Ijaz et al., 2020).

ZnONPs are one of the most studied materials due to their versatility in a variety of downstream applications. According to (Lakshmipriya and Gopinath, 2020), ZnONPs are the second most common metal oxide after iron. They are also safe, inexpensive, and simple to make. By altering the morphology of zinc oxide nanoparticles, one may readily modify their physical and chemical properties. This can be achieved by producing the nanomaterial utilizing alternative synthesis techniques, precursors, or materials. According to, zinc oxide nanoparticles are a type of inorganic chemical classified as a semiconductor in group II–IV for use in analytical sensing

---

---

applications. ZnONPs have grown increasingly common in a wide range of commercial items and applications, including medicine, pharmaceuticals, personal care products, paints, coatings, and numerous industrial uses. Their high surface-to-volume ratio, as well as the resulting alterations in physicochemical, optical, reactive, and electrical properties, set them apart from their bulk counterparts. ZnONPs have a wide band-gap semiconductor property and can be tailored and optimized to be used in biosensors, UV protection materials, and antibacterial agents. ZnONPs' size-dependent interactions with cancer cells have been investigated, revealing their effects on cell viability, DNA damage, ROS production, and morphological alterations. These findings emphasize ZnONPs' potential for specific biomedical applications in cancer research and therapy (Mandal et al., 2022; Zhang and Xiong, 2013).

ZnONPs can adopt different crystal structures, each with unique properties and potential applications. There are three main crystal forms of ZnONPs which are more commonly found in nature than other: Wurtzite, Sphalerite and Rock Salt (Espitia et al., 2012). The most prevalent form is wurtzite, characterized by a hexagonal arrangement of alternating zinc and oxygen layers. Wurtzite ZnONPs are prized for their piezoelectric and pyroelectric properties, making them valuable in sensors and actuators. Another, less common, crystal form is sphalerite, featuring a cubic crystal structure. ZnONPs in this form exhibit distinct optical and electronic characteristics compared to wurtzite, offering advantages in specific applications. Finally, under specific synthesis conditions or within certain nanoscale structures, ZnONPs can take on the rock salt crystal structure, characterized by a cubic arrangement of zinc and oxygen ions. This form displays properties potentially different from both wurtzite and sphalerite, depending on the ZnONPs' size and morphology. Each form holds promise in diverse fields, ranging from electronics and optics to catalysis and biomedical engineering. Understanding the crystal structure of ZnONPs is therefore critical for realizing their full potential and utilizing their distinctive characteristics in a variety of scientific and technical sectors (Decremps et al., 2003; Kuang et al., 2015).

Physical methods involve the use of physical force to break down bulk ZnO into nanoparticles. Some examples include ball milling, sputtering, physical vapor deposition, laser ablation, and electric arc deposition. Chemical methods rely on chemical reactions to produce ZnO NPs. Some common examples include sol-gel, precipitation, co-precipitation, micro-emulsion, hydrothermal, and solvothermal synthesis. Green methods use biological materials or processes

---

to synthesize ZnO NPs. Some examples include plant mediated synthesis, algae mediated synthesis, bacteria mediated synthesis, and fungi mediated synthesis (Ijaz et al., 2020).

### 2.4.3 ZnONPs synthesis route

ZnONPs have developed as an important topic of research due to their numerous applications in a variety of industries. ZnONPs can be synthesized by physical, chemical, or biological processes, each with significant advantages in terms of characteristics and uses. NP synthesis involves two primary approaches: Top-down approach and bottom-up approach.

- **Top-down approach:** The top-down technique involves shrinking bulk materials to make nanoparticles. This category includes physical methods of synthesis such as ball milling, sputtering, and laser ablation. Ball milling is a mechanical process that uses a grinding medium to reduce particles to nanoscale sizes. Sputtering is the process of striking a target substance with high-energy particles in order to dislodge atoms, which then condense and create NPs. A high-energy laser is used to ablate a target substance and generate NPs (Singh et al., 2020).
- **Bottom-up approach:** The bottom-up strategy, on the other hand, requires assembling nanoparticles from atomic or molecular species. Precipitation, vapor transport, and hydrothermal reactions are examples of chemical techniques. The precipitation method includes putting a precipitating chemical into a solution to synthesize NPs. Vapor transport produces NPs through a vapor-phase reaction, whereas hydrothermal procedures produce nanoparticles through the use of high-temperature and high-pressure water-based solutions (Xiong, 2013).

ZnONPs are extremely desirable for a variety of industries due to their adaptability and broad applications, which are largely attributed to their numerous manufacturing methods. Largely three different routes are preferred for ZnONPs synthesis universally namely: Physical synthesis, chemical synthesis, and biological synthesis.

- **Physical synthesis:** Physical methods of synthesis involve the use of mechanical and physical processes to fabricate ZnONPs. These methods can include techniques like thermal decomposition, grinding and milling. For example, in the synthesis by thermal method, the zinc salt was heated at high temperatures for the synthesis of ZnONPs, and the morphologies of the synthesized ZnONPs were determined using scanning electron microscope (SEM). Physical methods enable the direct control of particle size and distribution, leading to more

---

uniform and reproducible nanoparticles. ZnONPs are synthesized using a variety of physical techniques, each of which has unique features and allows for customization of the size, shape, and characteristics of the particles (Tsuzuki and McCormick, 2004). Typical physical techniques for synthesizing ZnONPs include:

Vapor-Phase Synthesis: In this technique, precursors containing zinc are vaporized and subsequently condensed to generate nanoparticles. ZnONPs with tunable properties are created using methods like chemical vapor deposition (CVD) and physical vapor deposition (PVD), which modify variables including temperature, pressure, and precursor concentration (Singh et al., 2013).

Mechanical Milling: Using a solid-state technique, bulk substances are ground into nanoparticles by mechanical milling. To break down zinc oxide powder for ZnONPs, it is milled using balls or other abrasive tools. This method works well for creating huge amounts of ZnONPs with a regulated distribution of particle sizes (Tsuzuki, 2009).

Laser Ablation: In order to create nanoparticles in the surrounding media, a target material is ablated using high-energy laser pulses. ZnONPs are generated by laser-irradiating a Zn compound while an appropriate media (such as water or an organic solvent) is present. Particle composition and size can be precisely controlled with this technique (Semaltianos, 2010).

Hydrothermal Synthesis: In this process, precursor materials are reacted at high pressures and temperatures inside a sealed vessel. Zinc-containing precursors are treated at high temperatures with a hydrothermal solution (such as water or an aqueous solution) to synthesize ZnONPs with precise size and shape. This method works effectively for producing ZnONPs with consistent characteristics that are well-defined (Bharti and Bharati, 2017).

- **Chemical synthesis:** ZnONPs are created via chemical synthesis techniques, which employ particular chemical processes. For the chemical production of ZnONPs, methods include the hydrothermal process, vapor transfer method, and precipitation method are frequently used. These techniques provide exact control over the nanoparticles' crystalline structure, size, and form. For example, the alkaline precipitation approach uses sodium hydroxide and zinc formate dihydrate to produce complex nanomaterials with specific morphological properties, including spherical, nanoflex, dumbbell-like, and rod-like morphologies. In order to more effectively control the dimensions and shape of the ZnONPs, surface active substances can also be used to further improve chemical synthesis. Several chemical methods are commonly used for the synthesis of ZnONPs:
-

---

**Precipitation method:** In this process, soluble Zn salts are mixed under controlled conditions with an alkaline or reducing agents to produce ZnONPs by precipitation. By modifying variables like temperature, pH, and the rate of reagent addition, one may alter the size and shape of the NPs. To control the dimensions and other physical parameters during synthesis, some stabilizers or size control agents can be added to prevent agglomeration, improve stability, and generate specific shape of NPs. These agents can be called as stabilizing agents or capping agents. Chitosan (CS), amino acids, Poly vinyl alcohol (PVA), Polyethylene glycol (PEG), starch etc. are known agents used in synthesis (Arora et al., 2014; Ghorbani et al., 2015).

**Sol-Gel Method:** This technique is based on the creation of a colloidal suspension (sol) that gels to create a solid network (gel) that contains ZnONPs. NPs synthesized with this process have variety of forms, including powders, coatings, and films, by adjusting variables including the kind of concentration of the precursor, solvent, and drying conditions (Ain Samat and Md Nor, 2013).

**Sono chemical Process:** The sono chemical process uses ultrasonic vibrations to produce cavitation in a liquid medium that contains Zn precursors. As a result of the cavitation bubbles collapsing, a sequence of chemical events occurs that result in the synthesis of ZnONPs. ZnONPs with regulated size and morphology can be synthesized quickly and effectively using this approach (Noman et al., 2020).

**Electrochemical Process:** Using an electric potential, zinc ions are reduced to create ZnONPs on an electrode surface in the electrochemical process. By varying the electrochemical conditions, this technique makes it possible to precisely regulate the size and form of nanoparticles. ZnONPs with particular characteristics can be produced for a range of applications (Chandrappa and Venkatesha, 2012).

- **Biological synthesis:** Biological entities including microbes, plants, and biomolecules can be used in biological synthesis processes to generate ZnONPs in an environmentally friendly method. These techniques control the synthesis of ZnONPs by taking leverage the capping abilities and reducing abilities of biological agents. For ZnONPs, biological synthesis techniques provide special benefits such biocompatibility, sustainability, and the possibility of regulated synthesis in controlled circumstances. These techniques are useful in a number of industries, such as nanotechnology, environmental cleanup, agriculture, and biomedicine (Ahmed et al., 2017). Several biological synthesis methods for ZnONPs include:

---

Microbial Synthesis: ZnONPs can be produced intracellularly or extracellularly by microorganisms such as bacteria, fungus, or algae. While extracellular synthesis forms the nanoparticles outside the cells, intracellular synthesis occurs inside the cells when microorganisms decrease zinc ions to generate ZnONPs. Benefits of microbial synthesis include the possibility of large-scale manufacturing, scalability, and gentle reaction conditions (Mohd Yusof et al., 2019).

Plant-Mediated Synthesis: Many phytochemicals found in plants, including terpenoids, phenolics, and flavonoids, can serve as capping and reducing agents during the production of ZnONPs. Under the right circumstances, plant extracts are combined with zinc precursors to aid in the stabilization and reduction of ZnONPs. By avoiding the use of hazardous chemicals, plant-mediated synthesis is an environmentally friendly method that may be used to create nanoparticles with particular biological properties (Jayaseelan et al., 2012).

Enzyme-Mediated Synthesis: Zinc ion reduction to produce ZnONPs can be catalyzed by enzymes sourced from biological materials. The synthesis of ZnONPs with customized properties is made possible via enzyme-mediated synthesis, which provides efficiency, specificity, and control over the reaction conditions. For the manufacture of ZnONPs, enzymes including oxidases, peroxidases, and reductases have been employed (Arib et al., 2021).

Cell-Free Extracts: Biologically derived cell-free extracts include a range of biomolecules that can help with ZnONP production. These extracts provide a straightforward and affordable method for producing ZnONPs by acting as stabilizing and reducing agents during the synthesis process (Saleha et al., 2023).

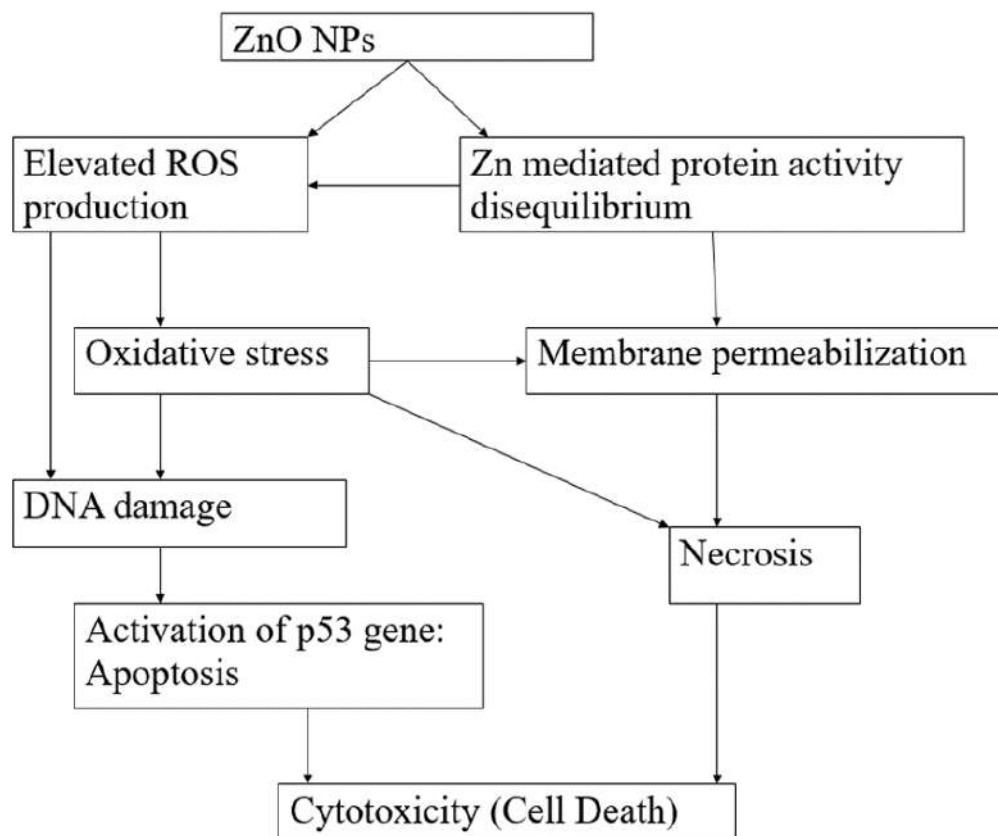
These above synthesis processes contribute significantly to the versatility and numerous uses of ZnONPs, rendering them desirable characteristics for a diverse range of industries.

#### **2.4.4 ZnONPs mechanism of action**

ZnONPs have shown promise as an anticancer agent due to their unique properties, such as biocompatibility, high selectivity, enhanced cytotoxicity, and easy synthesis [1]. Even though ZnONPs are being used in cosmetics for several years, they are indeed lately investigated as potential therapeutics for the treatment and diagnosis of cancer. What renders ZnONPs such an appealing prospect. Being able to synthesize NPs with required size and shape using array of methods makes them attractive option (Król et al., 2017).



Although the exact mechanism by which ZnONPs cause toxicity is yet known but, several studies are conducted to elucidate the underlying mechanism. From all of that study what we know is that the ZnONPs cause rapid release of free  $\text{Zn}^{+2}$  inside cells, leading to up-regulation of cellular metallothionein. ZnONPs having amphoteric nature preferentially and rapidly degrades under acidic environment like provided by cancer cell and lysosomal compartments.



**Figure 2.7** ZnONPs mechanism of action (Source: Bisht and Rayamajhi, 2016)

Once inside, the ZnONPs dissociation disrupts cellular Zn homeostasis causing lysosomal and mitochondria damage. Even though, ZnONPs are reported to possess opposing effects, probably based on the model, the cell type and the dose. Some authors reported that ZnONPs possess antioxidant effects, while others claim that ZnONPs increase reactive oxygen species (ROS) generation inside cells. This infiltrated ZnONPs inside the cancer cell membrane leads to  $\text{Zn}^{+2}$  release and liberating free radicals (Vandebriel and De Jong, 2012). This oxidative stress in cells, is one of the mechanisms of cytotoxicity causing DNA damage to cancer cells. ZnONPs have been found to cause DNA leakage from the nuclei of cancer cells, further contributing to their cytotoxic effects. Further, due to increased buildup of ROS, ZnONPs forces cells to undergo apoptosis through intrinsic or extrinsic pathway induction depending on cell-to-cell interaction (**Figure 2.7**). Apart from that ZnONPs can selectively target and kill

---

cancer cells due to their enhanced permeability and retention (EPR) effect and electrostatic interaction. Overall, the anticancer activity of ZnONPs can be attributed to their ability to produce ROS, mitochondrial damage, DNA damage creating nicks and breaks, and induce apoptosis in cancer cells, making them a promising anticancer agent. Due to this is a unique property of ZnONPs, it is possible to combine them with other chemotherapeutic agents or radiation therapy for treating various types of cancers (Nagar et al., 2022; Sirelkhatim et al., 2015).

### 2.4.5 ZnONPs anticancer application/drug delivery application

There have been studies investigating the use of ZnONPs for drug delivery, gene delivery, biosensors, and nanomedicine as well. The combination of anticancer drugs with biocompatible nanomaterials has been investigated in terms of how effectively they deliver the drugs to carcinogenic cells. Furthermore, ZnONPs have demonstrated promise in biological imaging, notably in fluorescence imaging methods. Because of their low cost and biocompatibility, they promise wide range of imaging applications, including the observation of biomolecules and cellular compartments within cells. ZnONPs are better anticancer agents compared to its bulk counterpart owing to its nanoparticle properties like small size, shape and large surface area. Interestingly, limited number of studies have shown a promising antitumor activity of ZnONPs on many human cancer cell lines including lymphoblastoid (WIL2-NS) cells and myoblastoma (C2C12) cells (Hassan et al., 2017). ZnO nanowires have demonstrated biodegradable nature and breaks down into  $\text{Zn}^{+2}$  which may later be absorbed by the body and, making them suitable as DDS. Because ZnONPs can be synthesized into hollow nanotube-type structures, it is a good alternative for drug delivery, especially delayed drug release applications. ZnONPs when coated with doxorubicin the anticancer drug, the combination of the two treatments was designed to destroy cancer cells by disrupting their cell membranes and inhibiting their growth. Doxorubicin, a powerful anti-cancer agent is being used for years in chemotherapy, works by damaging DNA in cancer cells as well as ZnONPs which by releasing free radicals ultimately leads to same fate of the cell. This damage prevents cells from dividing and also stops them from growing or repairing damaged DNA leading to death of cells. (Alavi and Meshkini, 2018) successfully created a drug loaded nanocomposite system as an alternative to traditional chemotherapy. Where mesoporous  $\text{Zn@Fe}_2\text{O}_3$  nanocomposite was made to which Methotrexate (MTX) was adsorbed. This system was PEG coated to enhance the stability of overall system. It was found that drug loaded nanocomposite was selective towards MCF-7 and T47D cells and showed more cytotoxicity in terms of ROS generation and mitochondrial

---

damage. This study also presents the use of ZnO as carrier of chemotherapeutic drug(s) which may have high potential applications.

Aminated polystyrene, zinc oxide and silver nanoparticles were checked for their cytotoxicity on HeLa cells by (Sharma, Gorey and Casey, 2018). They found out that all the nanoparticles show relatively high toxicity irrespective of the physiochemical properties they possess. They also concluded that of the three particles tested Zinc oxide nanoparticles showed the least toxicity and arrest of cell cycle in G2/M phase.

Zinc oxide quantum dots (QDs) were checked for the first time for its cytotoxicity profile against MCF-7 and MDA-MB-231 metastatic breast cancer cell lines by (Roshini et al., 2017). In the study they found out that small particle size of QDs was directly proportional to cytotoxicity generated. They also confirmed that acidic tumor microenvironment was favoring the activity of zinc oxide QDs. Even they found out that when normal cells exposed to same conditions of the cancer cells, minimum toxicity was seen compared to cancerous cells.

Chitosan-Zinc oxide nanoparticles synthesized by (Wu and Zhang, 2017) showed enhanced cytotoxicity against cervical cancer cells. Anticancer activity was seen as a result of ROS generation which, eventually lead to apoptosis and cancer cell death.

Yet another application of Zinc oxide as a drug carrier was highlighted by (Tian et al., 2017) where mesoporous Zinc oxide nanospheres were used as a drug carrier for Doxorubicin (DOX) delivery to cancer cells. The study revealed that when drug release was checked as a function of pH, at acidic pH of 5.0, controlled and large amount of drug release was seen in contrast to neutral pH of 7.4. This clearly indicates that ZnO has pH dependent activity under acidic pH and the same can be exploited in various different ways.

Micellar type core shell water dispersible ZnO nanocomposites with high payload efficiency have also been synthesized. ZnO nanoparticles were functionalized with PEG and  $\beta$ -cyclodextrin creating hydrophobic pockets for loading of curcumin. This biocompatible ZnO nanocomposite showed as imaging agent and cytotoxic agent along with curcumin on MCF-7 cells.  $\beta$ -cyclodextrin had advantage of storing large amount of hydrophobic drug and making whole system more biocompatible. Sustained drug release at acidic pH was also noted. So together the nanocomposite system showed imaging ability, anticancer activity and drug delivery system (Sawant and Bamane, 2018).

# Chapter 3

# Rationale, Aim and Objectives

---

*Rationale, Aim and Objectives*

---

**3.1 Rationale**

In case of breast cancer, there are limited treatments that specifically target hormone receptor-negative cancers and these cancers are often treated with chemotherapy and radiation therapy. MTX have a selective internalization via FAR, which are comparatively overexpressed on cancer cells than normal cells. Studies suggest that FAR may be a promising target for the development of new treatments for breast cancer cells. But MTX toxicity and resistance become one big hurdle in its application. Nanotechnology offers both passive and active targeting strategies that can enhance the intracellular concentration of drugs in cancer cells and at the same time avoid toxicity to normal cells. ZnONPs have proved its efficacy as a potential anticancer agent and drug delivery vehicle for various different cancer types in-vitro. By combining the NP based drug delivery of MTX, we anticipate that the system will enhance the therapeutic effectiveness and minimize the side effects by individual systems when used alone.

In the current study, we plan to use MTX along with ZnONPs to check its activity in vitro using breast cancer cells. Here in this study, we will be taking advantage of ZnONPs to kill cancer cells along with MTX as targeting agent. Through scientific approaches, ZnONPs role in killing cancer cells has been evaluated but, its potential along with MTX still remains to be unexplored in breast cancer.

**3.2 Aim**

To synthesize and characterize Methotrexate loaded Zinc oxide nanoparticles for efficient delivery to breast cancer cells.

**3.3 Objectives**

- 1 Synthesis and characterization of drug loaded Zinc oxide nano particles (ZnONPs)
- 2 Drug release study of drug loaded nanoparticles.
- 3 In vitro analysis of the developed system to evaluate its anti-cancer potential.
- 4 Study the Blood biocompatibility with newly developed system.
- 5 In vivo acute oral toxicity study of the newly developed system using a suitable animal model.

# Chapter 4

## Synthesis, Characterization, and drug release study of nanoparticles

---

## Synthesis, Characterization, and drug release study of nanoparticles

---

### 4.1 Introduction

The purpose of this chapter is to study the synthesis and characterization of bare and MTX loaded ZnONPs. In brief, bare ZnONPs were synthesized with chemical precipitation approach using Poly Ethylene Glycol-400 (PEG-400) as stabilizer. These bare NPs were then mixed in certain ratio with drug MTX to yield MTX-ZnONPs. Characterization of both NPs was done followed by drug release study. For characterization Ultraviolet-visible (UV-vis) absorbance spectroscopy, Fourier transform infrared spectroscopy (FTIR), X-ray diffraction (XRD), Inductively Coupled Plasma-Atomic Emission Spectrometry (ICP-AES), zeta ( $\zeta$ ) potential, Dynamic light scattering (DLS), Energy dispersive spectroscopy (EDS)-mapping and High-resolution transmission electron microscopy (HR-TEM) was used.

#### 4.1.1 Synthesis of nanoparticles

The synthesis of ZnONPs is accomplished through physical, chemical, and biological processes that employ either top-down or bottom-up strategies. The top-down technique involves breaking down larger particles into nanoscale-sized particles using grinding, cutting or attrition. This method is widely used for small-scale NP synthesis. In contrast, the bottom-up approach involves assembling pre-existing atoms/molecules into NPs using chemical and physical methods. This method is more cost-effective and time-efficient than the top-down approach. NP synthesis can be divided into three different approaches: Physical methods, chemical methods and green methods (Manoranjan Arakha, 2018; Singh et al., 2020).

The chemical method of NP synthesis involves the use of chemical reactions to create ZnONPs. This method is commonly employed due to its ability to produce NPs with controlled size, shape, and properties. Various chemical techniques can be utilized for ZnONP synthesis, including sol-gel, precipitation, co-precipitation, microemulsion, hydrothermal, and solvothermal synthesis (Espitia et al., 2012). Each of these methods involves the dissolution of ZnO precursors in a solvent, followed by a series of chemical reactions that lead to the formation of ZnONPs. The specific conditions employed in each method can be tailored to achieve the desired NP characteristics. For instance, the concentration of precursors, reaction temperature, and reaction time can be adjusted to control the size and shape of the ZnONPs. Chemical methods offer a versatile and controllable approach for the synthesis of ZnONPs, making them widely used in various research and industrial applications (Kolodziejczak-Radzimska and Jesionowski, 2014; Sabir et al., 2014).

---

### 4.1.2 Characterization of nanoparticles

NP characterization is the process of determining the physical and chemical properties of NPs. This is important for a variety of reasons for example, it is necessary to analyze multiple physicochemical characteristics of NPs which includes morphological, optical, structural, surface and elemental characterization. Not only that but it is essential to ensure the quality and consistency and understand the behavior of NPs in different environments. There are a variety of techniques that can be employed to characterize NPs but, the choice of technique also depends on the specific properties of the NPs that are being studied.

#### 4.1.2.1 UV-Vis Spectroscopy

A useful tool for characterizing NPs is UV-visible spectroscopy. It can be used for measuring the concentration, aggregation state, size, and shape of NPs. Additionally, it can be employed to determine the chemical composition of NPs. UV-visible spectroscopy works on the principle of measuring the light that gets absorbed while travelling through material. The wavelength of the light, the concentration of the sample, and the characteristics of the sample all affect how much light is absorbed. The size, shape, and chemical make-up of a NP determine its specific absorption spectrum. Various chemical groups present in sample changes how light is absorbed and changes the absorption maxima ( $\lambda_{\text{max}}$ ) i.e the wavelength at which sample absorbs maximum light.

#### 4.1.2.2 Fourier Transform Infrared (FTIR) spectroscopy

FTIR spectroscopy works on the principle of Fourier transformation which is a mathematical technique using which the data obtained from measuring the absorbance of infrared light can be transformed into a spectrum that represents the molecular vibrations present in the sample (Achebe et al., 2019). Additionally, FTIR spectroscopy works bypassing infrared light through a sample and measuring the absorption of specific wavelengths, allowing for the identification and characterization of compounds based on their unique molecular vibrations (Jose et al., 2019). FTIR is useful technique of characterization for NPs since it can provide information about the functional groups present on the NP surface and their interaction with other molecules.

#### 4.1.2.3 X-Ray Diffraction (XRD)

XRD is a technique that can be used to determine the crystal structure of NPs. XRD works by shining X-rays on a sample and measuring the diffraction pattern that is produced. The



---

diffraction pattern can be used to determine the size and shape of the crystal structures in the sample by calculating the various peaks produced by the different planes of material.

#### **4.1.2.4 Inductively coupled plasma-atomic absorption spectroscopy (ICP-AES)**

ICP-AES, an emission spectrophotometric method, take advantage of the excited electrons energy which is released at specific wavelengths upon returning to their ground state. The fundamental feature of this method is that every element emits energy at specific wavelengths that correspond to its chemical identity. The amount of energy released at the selected wavelength, corresponds to that element's concentration in the sample under study. Consequently, by identifying the emitted wavelengths and quantifying their intensities, elemental composition of the sample in relation to a reference standard can be quantified.

#### **4.1.2.5 Zeta potential and Dynamic light scattering (DLS)**

DLS is a technique that can be used to measure the size distribution of NPs. DLS works by illuminating sample by a laser beam and measuring the Brownian motion of the NPs. The Brownian motion of the NPs can be used to determine their size distribution.

Zeta potential indicates the magnitude of charge on the surface of a particle in a dispersion or solution. Zeta potential is important parameter for NP characterization because it provides valuable information about the stability of NPs in a dispersion or solution. NPs show higher stability when they have a zeta potential outside the range of +30 mV to -30 mV.

#### **4.1.2.6 Energy dispersive spectroscopy (EDS)-mapping**

EDS is one of the most useful analytical instruments for general materials analysis. Electron microscopy and elemental spectroscopy work hand in hand. When a high energy electron beam affects a material's intrinsic electron structure, EDS detects and interprets the distinctive x-rays that are produced from that substance. The foundation of elemental mapping is the collection of extremely detailed elemental composition data over a sample's surface. A qualitative representation of the elemental abundances is provided by the intensity map. Under identical electron beam illumination conditions, the abundances of the elements are correlated with the intensity of distinctive X-rays emitted by that element.

#### **4.1.2.7 High-resolution transmission electron microscopy (HR-TEM)**

High-resolution Transmission Electron Micrography (HR-TEM) is a method that allows to explore the intricate details of materials at the atomic stage. By utilizing transmitted electrons, HR-TEM presents an array of statistics about the shape and properties of diverse substances. In HR-TEM, a beam of high-electricity electrons, normally several hundred kiloelectron volts

---

(keV), is focused onto a sample placed on carbon coated copper grid. As these electrons bypass through the material, they interact with its atoms, resulting in scattering and diffraction patterns. These patterns are then captured via specialized detectors and converted into high-resolution images.

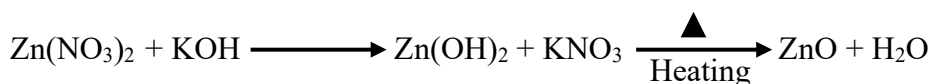
## 4.2 Materials and Methods

Zinc nitrate hexa hydrate ( $\text{Zn}(\text{NO}_3)_2 \cdot 6\text{H}_2\text{O}$ ) and Potassium hydroxide (KOH) was procured from LOBA Chemi, India. Chitosan (CS) low molecular weight, Tri ethyl amine (TEA), Acridine Orange (AO) and Ethidium bromide (EB) was procured from Sigma-Aldrich, USA. Polyethylene Glycol 400 (PEG-400), Sodium chloride (NaCl), Potassium chloride (KCl) Sodium phosphate dibasic dihydrate ( $\text{Na}_2\text{HPO}_4 \cdot 2\text{H}_2\text{O}$ ) and Potassium phosphate monobasic monohydrate ( $\text{KH}_2\text{PO}_4 \cdot \text{H}_2\text{O}$ ) was procured from Molychem, India. Dialysis Membrane-110 was used from HiMedia, Mumbai. Methotrexate (MTX) was kindly provided as gift sample from Khandelwal Laboratories Pvt. Ltd, Mumbai, India. All chemicals used are of analytical grade. All preparations of buffers/reagents were done using MilliQ water.

### 4.2.1 Synthesis of Bare ZnONPs

For synthesis of bare ZnONPs, 0.2M  $\text{Zn}(\text{NO}_3)_2 \cdot 6\text{H}_2\text{O}$  solution was prepared in 10% PEG-400 and kept for stirring in a round bottom flask till temperature reached  $85^\circ\text{C}$ . Slowly touching the wall of the flask, 20% KOH was added until the solution reaches to pH 11. After 30 minutes of reaction time at  $85^\circ\text{C}$  under stirring conditions the solution was set aside. Supernatant was discarded and particles were centrifuged at 5000 rpm for 10 minutes. The pellet was washed twice with MilliQ water and once with Ethanol, followed by drying at  $70^\circ\text{C}$  for 1 hour. Dried powder of ZnONPs was stored in dry place for further analysis.

Chemical reaction involved in synthesis is as follows:



### 4.2.2 Synthesis of Methotrexate loaded Zinc oxide nanoparticles (MTX-ZnONPs)

MTX-ZnONPs were synthesized by Ex-situ approach. Briefly, MTX solution was prepared in 0.1% TEA at final conc. of 1 mg/mL, with 0.1% Chitosan solution (CS) in the ratio of 9:1. MTX solution was then mixed with bare ZnONPs solution in the ratio of 1:20 and sonicated for 5 minutes followed by constant mixing for overnight. Next day, the solution was centrifuged, and the NPs were washed twice with MilliQ water and once with Ethanol. NPs

---

were dried at 50°C for 1 hour. Dried MTX-ZnONPs were later stored in dry place for further analysis.

### 4.2.3 MTX loading efficiency

To calculate the % loading efficiency, concentration of MTX before loading and after loading onto the NPs was determined with the help of UV-Vis spectrophotometer at 303 nm (Rahman et al., 2021). MTX loading efficiency was calculated from the equation 4.1, and the concentration of MTX was determined using the standard curve equation.

$$\% \text{ Loading efficiency} = \frac{(\text{Conc. of MTX Initial} - \text{Conc. of MTX after})}{(\text{Conc. of MTX Initial})} \times 100 \quad \dots 4.1$$

### 4.2.4 Characterization

Characterization of bare and drug loaded ZnONPs was carried out using UV-Vis spectroscopy, FTIR, XRD, ICP-AES, Zeta potential and DLS, EDS mapping, and HR-TEM analysis. In each method of characterization, comparison was made between bare and MTX loaded ZnONPs. Comparative analysis helps us understand if NPs are synthesized appropriately and MTX loading has taken place on ZnONPs.

#### 4.2.2.1 UV-Vis Spectroscopy

UV-vis absorption spectra for bulk ZnO, bare ZnONPs, MTX-ZnONPs and MTX were collected in a quartz cell having 1.0 cm path length on a Perkin Elmer Lambda 25 UV- vis spectrophotometer equipped with UVWINLAB software. Each spectrum for was analyzed to confirm the absorption spectra of NPs and successful loading of MTX on NPs. Tauc's plot was plotted using the absorption values to determine the Binding energy (eV) of ZnONPs.

#### 4.2.2.2 FTIR spectroscopy

FTIR spectra of NPs and MTX were analyzed using IRAffinity-1S, Shimadzu by ATR method. Samples were scanned in wavenumber range of 4000-400  $\text{cm}^{-1}$  for detection of functional groups. The FTIR measurements were recorded in transmission mode.

#### 4.2.2.3 XRD

The crystal structures of the synthesized NPs and MTX were recorded using XRD-7000, Shimadzu. Data was recorded with scan rate of  $2^\circ \text{ min}^{-1}$  using Cu  $K\alpha$  radiation ( $\lambda = 0.154 \text{ nm}$ ). The diffracted intensities were recorded from  $2\theta$  angles ranging from  $20^\circ$  to  $80^\circ$ . The spectra obtained was then compared and matched with reference patterns with the JCPDS database that has standard data used as the fingerprints of all the powder diffraction samples.

---

---

#### 4.2.2.4 ICP-AES

ICP-AES method was used to determine the concentration of elemental Zn in the NPs using ARCOS from M/s. Spectro Analytical Instruments GmbH, Germany. 10 mg of each sample was prepared in 2 ml of conc.  $\text{HNO}_3$  and boiled for 5 min followed by making up the volume to 10 ml using Deionized water and then analyzed.

#### 4.2.2.5 Zeta potential and DLS

Surface charge analysis and hydro dynamic diameter of the synthesized NPs was measured using Malvern Zeta Sizer Nanoseries model ZEN 3690. For Zeta potential analysis, study was performed at various pH ranging from 5-10 that was adjusted using 1% HCl and 0.1 M NaOH in MilliQ water at RT to determine the hydrodynamic diameter of the given sample.

#### 4.2.2.6 EDS-mapping

Chemical purity and spatial distribution of elements within NPs was illustrated with the help of Energy-dispersive Spectroscopy was recorded by JEOL JSM-7600F. Sample was Mounted on a conductive stub with adhesive carbon tape to ensure uniform distribution.

#### 4.2.2.7 HR-TEM

High resolution-Transmission Electron Microscopy (HR-TEM) model JEOL-JEM 2100F was used to examine the NPs to determine their size, shape, and morphology of NPs. A drop of the NPs colloidal dispersion was placed on a copper grid and dried using an infrared light under RT. After which HR-TEM and Selected area electron diffraction (SAED) pictures were recorded.

#### 4.2.2.8 Stability of NPs

NPs synthesized earlier were checked for its physical stability and colloidal stability over a period. For colloidal stability three concentrations of NPs were used viz. 10, 25 and 50  $\mu\text{g}/\text{mL}$  in deionized water. NPs were firstly sonicated in water for 7-10 minutes after which the labeled tubes were kept aside undisturbed to monitor the colloidal stability. In physical stability of NPs color, flow, aggregation, and texture was also monitored at various intervals of time.

#### 4.2.5 Drug release study of MTX-ZnONPs

The dialysis method was employed to characterize the in vitro release kinetics of MTX from ZnONPs. This technique mimics the physiological conditions in vivo, allowing for a comprehensive assessment of the drug release profile. Two buffer systems were utilized to simulate the physiological pH environment and the acidic tumor microenvironment. Phosphate buffered saline (PBS) at pH 7.4 was used to represent the physiological pH, while PBS at pH

---

5.0 mimicked the acidic tumor microenvironment. The selection of these buffer systems aimed to evaluate the influence of pH on MTX release behavior (Chen et al., 2014). The drug was tested for 24 hours in phosphate buffered saline (PBS) at pH 7.4 and 5.0 at 37 °C with moderate stirring conditions. PBS was used to suspend MTX-ZnONPs at a 5 mg/ml concentration. After that, the NP suspension was put into a dialysis bag with a 12 kDa molecular weight cutoff, which ensured NP retention while permitting MTX diffusion. This setup was submerged in 50 ml of fresh PBS buffer at the specified pH (7.4 or 5.0) and kept at 37 °C while being constantly stirred at slow speed to ensure uniform mixing. At predetermined time intervals (0 to 8 hours, and 24 hours), 1 ml aliquots were withdrawn from the dialysate and replaced with an equal volume of fresh PBS buffer. The withdrawn aliquots were analyzed using a UV-Vis spectrophotometer at 303 nm, the absorbance wavelength of MTX. The cumulative release percentage (% CR) of MTX at each time point was calculated using the below equation 4.2:

$$\%CR = \frac{D_t}{D_i} \times 100 \quad \dots 4.2$$

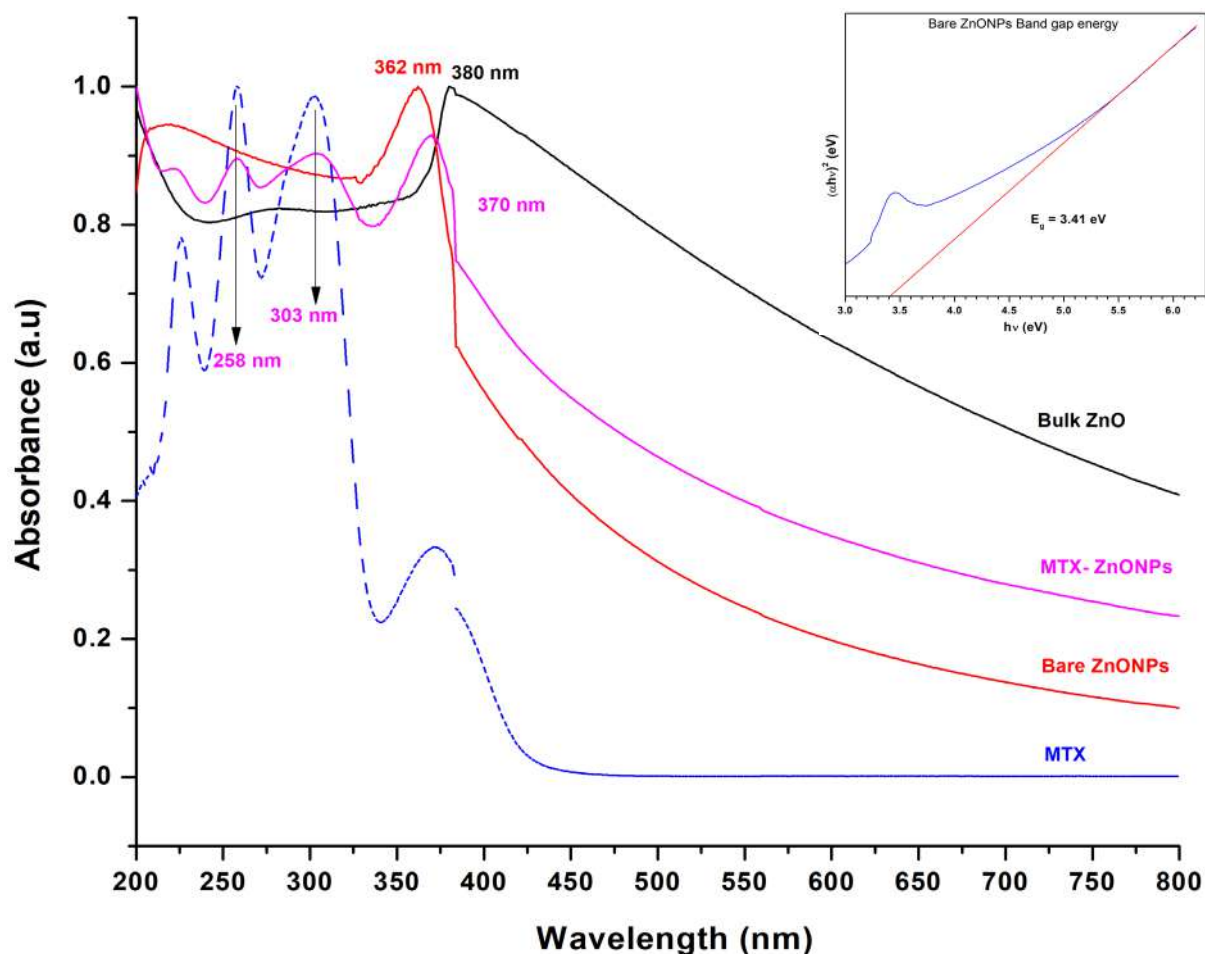
Where,  $D_t$  refers to drug released at time  $t$  and  $D_i$  refers to initial drug loaded onto the NPs. For every pH condition, the entire experiment was run in triplicate to verify the results' consistency and reliability. The MTX release profile was then visualized by plotting the average % CR values for each time point as a function of time (Nosrati H, Salehiabar M, Davaran S, Danafar H, Manjili HK, 2018; Joshi and Bhatt, 2023).

### 4.3 Results

#### 4.3.1 UV-Vis Spectroscopic analysis

Quartz cells with a 1 cm path length was used for UV-visible spectroscopic analysis to examine the absorption characteristics of bulk ZnO, bare ZnONPs, and MTX-ZnONPs in the wavelength range of 200-800 nm. As depicted in **Figure 4. 1**, bulk ZnO exhibited an absorption maximum at 380 nm, corresponding to its intrinsic bandgap energy. Interestingly, bare ZnONPs displayed an absorption maximum at 362 nm, representing a significant blue shift of 18 nm compared to bulk ZnO. As the particle size decreases, the band-gap energy of the particles increases, leading to an absorption shift to shorter wavelengths (Raoufi, 2013). This blue shift is characteristic of quantum confinement, phenomenon that arises when the NP size is comparable to the wavelength of light (Singh et al., 2017). The band gap energy ( $E_g$ ) of bare ZnONPs was determined using a Tauc plot where the square of the absorption coefficient  $(\alpha h\nu)^2$  is plotted against photon energy ( $h\nu$ ). The direct band gap energy ( $E_g$ ) for bare ZnONPs was calculated to be 3.41 eV, which is higher than that of bulk ZnO (3.26 eV). This higher

band gap energy further confirms the nanocrystalline nature of bare ZnONPs (Bhatkalkar et al., 2018; Wu et al., 2008). When compared to bare ZnONPs, MTX-ZnONPs showed two different absorption peaks one at 370 nm for ZnONPs and another one at 303 nm for MTX. The presence of the peak at 303 nm confirms the successful loading of MTX onto the ZnONPs surface. The observed blue shift in the absorption spectrum of bare ZnONPs confirms the quantum confinement effect, while the presence of the MTX peak in the MTX-ZnONPs spectrum indicates successful drug conjugation.



**Figure 4. 1** UV-Vis spectroscopic analysis of bulk ZnO, bare ZnONPs, MTX-ZnONPs and MTX showing their respective normalized spectra in the range of 200-800 nm wavelength. Inset showing Tauc's plot of bare ZnONPs for bandgap energy measurement.

#### 4.3.2 Fourier Transform Infrared Spectroscopic analysis

The Fourier Transform Infrared (FTIR) spectroscopy, a versatile analytical technique, was employed to delve into the intricate molecular architecture of both the NPs and the drug, revealing their unique vibrational signatures. The FTIR spectra were meticulously acquired within the wavenumber range of  $4000\text{ cm}^{-1}$  to  $400\text{ cm}^{-1}$  using the attenuated total reflection

(ATR) method, as complied in **Table 4.1**. Upon scrutinizing the FTIR spectrum of bare ZnONPs, characteristic peaks appeared at  $3382\text{ cm}^{-1}$ ,  $886\text{ cm}^{-1}$ , and  $420\text{ cm}^{-1}$ , corresponding to the stretching vibrations of the hydroxyl (-OH) group, the Zn-OH bond, and the Zn-O metal oxide bond, respectively clearly seen in **Figure 4.2**. The peak region between  $400\text{ cm}^{-1}$  and  $600\text{ cm}^{-1}$  is generally attributed to metal ion bonds, as documented in previous studies (AbdElhady, 2012; Lanje et al., 2013).

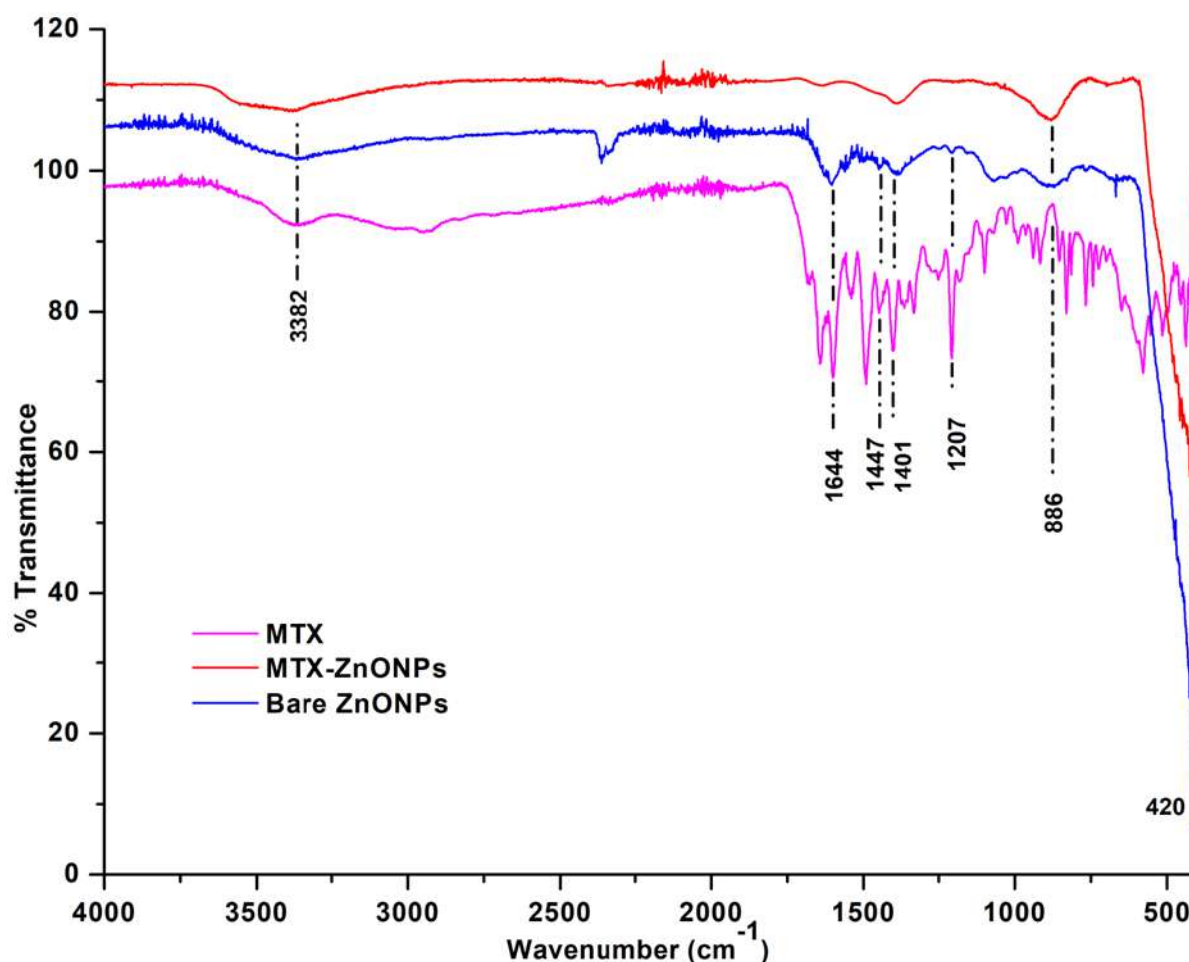
**Table 4.1** List of all the functional groups identified based on FTIR spectrum analysis of bare ZnONPs, MTX-ZnONPs and MTX.

Nanoparticle System	Wavenumber ( $\text{cm}^{-1}$ )	Functional Group
Bare ZnONPs	3382	-OH stretching
Bare ZnONPs	886	Zn-OH bond
Bare ZnONPs	420	Zn-O metal oxide bond
Bare ZnONPs	400-600	Metal ion bonds
MTX-ZnONPs	1640	-CONH group (MTX)
MTX-ZnONPs	1450	-NH amide bending (MTX)
MTX-ZnONPs	420	Zn-O metal oxide bond (ZnO)
MTX	1644	-CONH group
MTX	3387	-NH stretch
MTX	2926	-CH groups
MTX	1207	Carboxylate group (-COO)
MTX	1447	Carboxylate group (-COO)
MTX	1450	-NH amide bending

Conversely, the FTIR spectrum of pure MTX exhibited distinct peaks at  $1644\text{ cm}^{-1}$ ,  $3387\text{ cm}^{-1}$ , and  $2926\text{ cm}^{-1}$ , signifying the presence of the -CONH group, the -NH stretch, and the -CH groups embedded within the molecular structure. The carboxylate group (-COO) manifested its presence at  $1207\text{ cm}^{-1}$  and  $1447\text{ cm}^{-1}$ , while the -NH amide bending vibration of the MTX

molecule resonated at  $1450\text{ cm}^{-1}$ , as corroborated by prior literature (Chen et al., 2014; Kumari et al., 2013). When the MTX-ZnONPs was subjected to FTIR analysis, it unveiled fascinating interplay between the drug and the NPs. The characteristic peaks of MTX, namely  $1640\text{ cm}^{-1}$  and  $1450\text{ cm}^{-1}$ , remained intact, confirming the successful loading of MTX onto the ZnONPs. Additionally, the signature peak of ZnO at  $420\text{ cm}^{-1}$  persisted in the MTX-ZnONPs, emphasizing the preservation of the ZnONPs' integrity.

Collectively, the FTIR spectra of the bare ZnONPs, MTX-ZnONPs and drug, provided compelling evidence of the intimate interaction. The presence of distinct peaks corresponding to both components underscored the successful loading of MTX onto the ZnONPs, paving the way for further exploration of their synergistic properties.



**Figure 4.2** FTIR spectroscopy analysis of bare ZnONPs (red), MTX-ZNONPs (blue) and MTX (pink) showing their respective spectra when recorded in the wavelength range of  $4000\text{--}400\text{ cm}^{-1}$ .



---

### 4.3.3 X-Ray Diffraction analysis

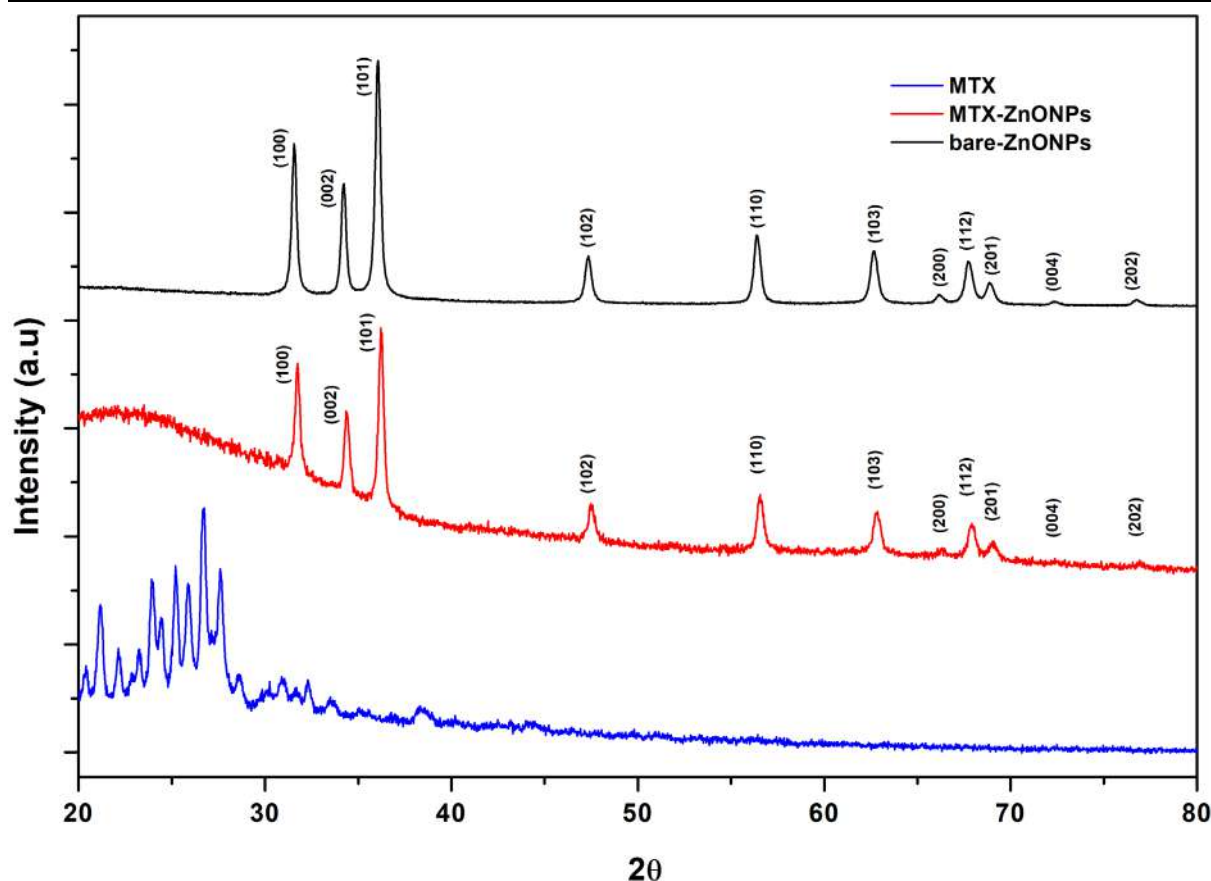
X-ray diffraction (XRD) analysis, a powerful tool for elucidating the crystalline structure of materials, was employed to investigate both bare ZnONPs and their MTX-ZnONPs along with MTX. The XRD patterns, depicted in **Figure 4.3**, revealed the highly crystalline nature of both NP systems, as evidenced by the presence of sharp and well-defined peaks.

A thorough comparison of the XRD patterns with the standard ZnO reference pattern (JCPDS card no. 00-036-1451) confirmed the hexagonal wurtzite phase of the ZnONPs. Both sets of NPs exhibited a consistent array of characteristic peaks, including (100), (002), (101), (102), (110), (103), (200), (112), and (201), corresponding to the planes of standard ZnO.

While the incorporation of MTX onto the ZnONPs resulted in subtle alterations in peak intensities, the overall XRD pattern remained largely unchanged. This observation aligns with previous studies (Buchheit et al., 2016; Raoufi, 2013; Sanmugam et al., 2017), further verifying the successful loading of MTX onto the ZnONPs.

To quantify the crystalline size of the NPs, the Scherrer equation,  $D = K\lambda / (B \cos\theta)$ , was employed, where  $D$  represents the average crystalline size in nanometers (nm),  $K$  is the Scherrer constant,  $\lambda$  is the X-ray wavelength,  $B$  is the full width at half maximum (FWHM) of the peaks, and  $\cos\theta$  is one-half of  $2\theta$  (Javed Akhtar et al., 2012; Malaikozhundan et al., 2017). The calculated crystalline sizes for the bare ZnONPs and MTX-ZnONPs were 31 nm and 40 nm, respectively. These values suggest that the MTX loading process did not significantly impact the crystalline size of the ZnONPs and also retained the crystalline phase of the ZnONPs.

In summary, the XRD analysis provided compelling evidence of the highly crystalline nature of both bare ZnONPs and MTX-ZnONPs. The consistent XRD patterns and calculated crystalline sizes underscore the successful synthesis of the NPs and the preservation of their crystalline structure upon MTX loading.



**Figure 4.3** XRD analysis of bare ZnONPs, MTX-ZnONPs and MTX revealing their respective diffraction spectrum recorded in the range of 20- 80  $2\theta$  angle.

#### 4.3.4 Inductively coupled plasma-atomic absorption spectroscopic analysis

ICP-AES is a widely employed technique for elemental analysis. The ICP-AES results revealed that the concentration of  $\text{Zn}^{+2}$  ions in bare ZnONPs was 0.352 mg/mL, while in MTX-ZnONPs, it was 0.280 mg/mL (**Table 4.2**). These findings indicate the successful incorporation of MTX onto the ZnONPs, as evidenced by the considerable decrease in  $\text{Zn}^{+2}$  ion concentration compared to bare ZnONPs.

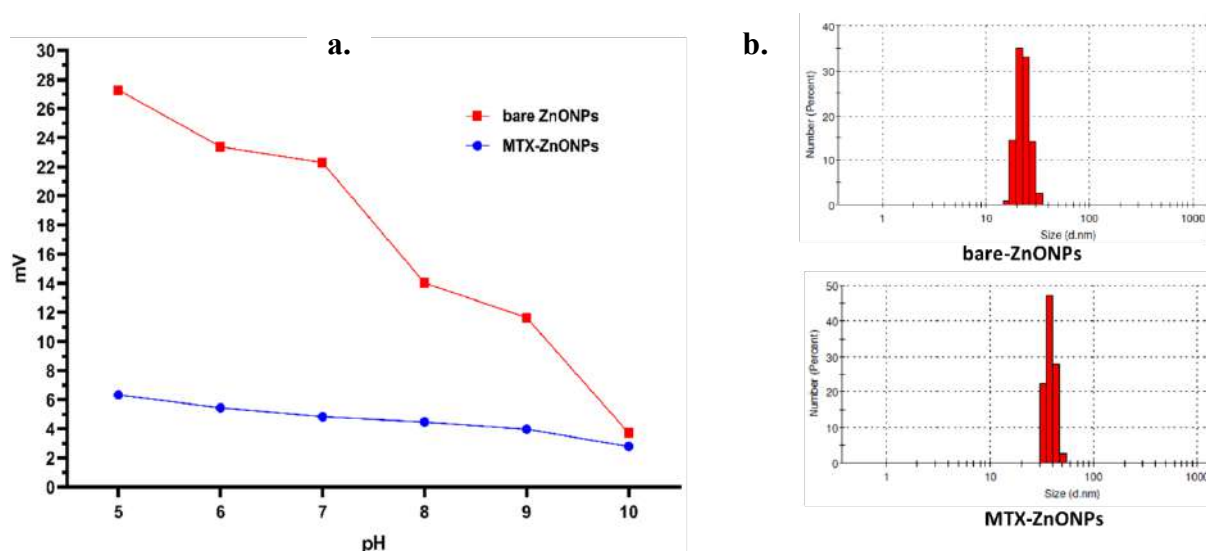
**Table 4.2**  $\text{Zn}^{+2}$  concentration determined from ICP-AES analysis of bare ZnONPs and MTX-ZnONPs

Nanoparticle System	$\text{Zn}^{+2}$ Ion Concentration (mg/mL)
Bare ZnONPs	0.352
MTX-ZnONPs	0.280

### 4.3.5 Zeta potential and DLS analysis

As depicted in **Figure 4.4a** the zeta potential of both bare ZnONPs and MTX-ZnONPs was evaluated across a pH range of 5 to 10. Bare ZnONPs maintained a high positive charge throughout the entire pH range, exhibiting a higher surface charge under acidic conditions. Interestingly, upon MTX loading via an ex-situ synthesis approach, the resultant MTX-ZnONPs led to decrease in the positive charge considerably still exhibiting a positive charge across the entire pH range. This shift in surface charge can be attributed to the presence of the negatively charged carboxyl group of MTX, coupled with its enhanced loading onto the bare ZnONPs. Overall, both NP systems demonstrated greater stability towards acidic pH conditions. The observed zeta potential shift clearly indicates the successful coating of ZnONPs with MTX, providing further evidence of MTX loading.

Additionally, DLS analysis in **Figure 4.4b** revealed an average particle size distribution of 270 nm and 285 nm for bare ZnONPs and MTX-ZnONPs, respectively. This data indicates the moderate size distribution. It is important to note that the particle size measured by DLS typically exceeds the actual particle size due to the consideration of the average hydrodynamic diameter. In conclusion, zeta potential analysis provided valuable insights into the stability and surface charge characteristics of bare ZnONPs and MTX-ZnONPs, with implications for their potential biological applications. The observed shift in zeta potential upon MTX loading confirms the successful coating process.



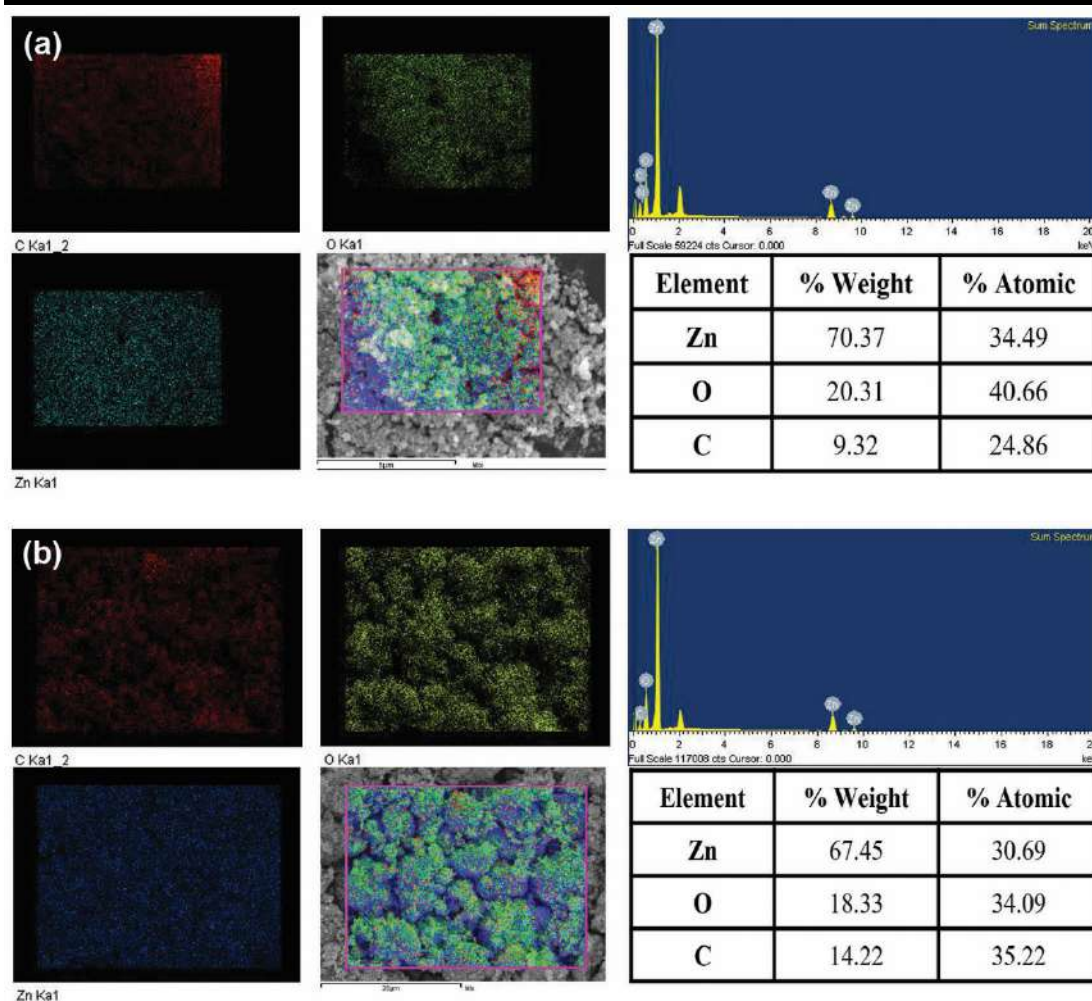
**Figure 4.4** Zeta potential and Dynamic Light Scattering (DLS) analysis of bare ZnONPs and MTX-ZnONPs. (a) Zeta potential of bare ZnONPs and MTX-ZnONPs was analyzed across

---

wide pH range and plotted, (b) DLS analysis of bare ZnONPs and MTX-ZnONPs size distribution data in histogram.

#### 4.3.6 Energy Dispersive Spectroscopy-Mapping analysis

Utilizing Energy-Dispersive X-ray Spectroscopy (EDS) mapping allows for the comprehensive determination of the chemical composition and spatial distribution of materials. To determine the distribution patterns of Zinc (Zn), Oxygen (O), and Carbon (C), a detailed elemental analysis was undertaken. **Figure 4.5a** illustrates the EDS mapping images of bare ZnONPs, revealing distinct peaks corresponding to Zinc and Oxygen, accompanied by Carbon at a weight percentage of 70.37, 20.31, and 9.32, respectively, without any discernible impurities. Conversely, in **Figure 4.5b**, portraying MTX-ZnONPs, the weight percentages of Zinc, Oxygen, and Carbon were observed as 67.45, 18.33, and 14.22. These findings collectively affirm the successful synthesis of ZnONPs in both scenarios (Ahamed and Vijaya Kumar, 2016; Boruah et al., 2016). Notably, the heightened presence of Carbon in MTX-ZnONPs can be ascribed to the loading of the drug onto the bare ZnONPs. This outcome explicitly validates the efficacious loading of MTX onto the bare ZnONPs.



**Figure 4.5** EDS mapping images of (a) bare ZnONPs; (b) MTX-ZnONPs, showing Zinc (blue), Oxygen (green) and Carbon (red). (Right) showing EDS spectrum with elemental values in table, (left) EDS micrographs showing each element mapped with different colors.

#### 4.3.7 High Resolution-Transmission Electron Microscopic analysis

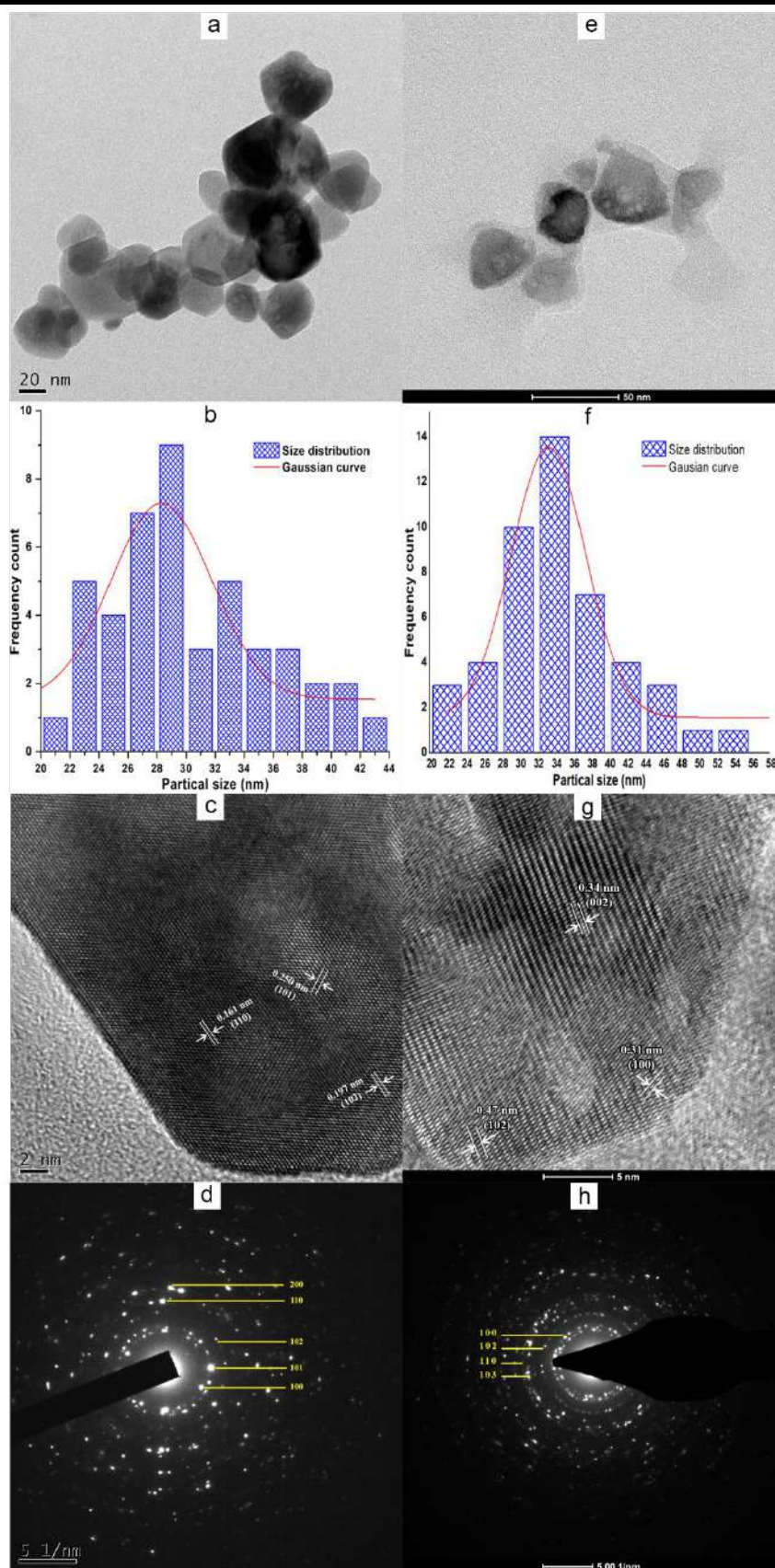
Conducting High-Resolution Transmission Electron Microscopy (HR-TEM) analysis offered insightful data into the crystalline size and planar structure of ZnONPs. The examination revealed a distinctive hexagonal crystal morphology, as depicted in **Figure 4.6a**, with an average size measuring approximately 30 nm, as illustrated in **Figure 4.6b**. MTX-ZnONPs images clearly shows the thin translucent hazy layer of drug coating around the ZnONPs **Figure 4.6e**. This evidently supports the data confirmed by other supporting methods like FTIR and UV-spectroscopic analysis about successful drug loading on the NP surface. Size distribution profile of MTX-ZnONPs is illustrated in **Figure 4.6f** revealed the average particle size in the size range of 32-34 nm in size. The crystal lattice arrangement of bare ZnONPs, vividly captured in **Figure 4.6c**, showcased the existence of various planes corresponding to

---

the Selected Area Electron Diffraction (SAED) pattern presented in **Figure 4.6d**. This intricate pattern exhibited multiple bright spots and rings aligning with the lattice structure of the crystals. HR-TEM image of MTX-ZnONPs in **Figure 4.6g** showed fine lattice fringes on the surface of MTX-ZnONPs crystal correlating with the SAED pattern observed in **Figure 4.6h**. SAED pattern clearly indicates the polycrystalline nature of MTX-ZnONPs similar to that of bare ZnONPs.

The evident bright spots in the SAED pattern indicated a highly crystalline morphology, while the diffused bands suggested the presence of aggregates within the NP ensemble. Notably, the planes described by the SAED pattern concurred with those derived from the XRD data, further confirming the crystalline nature of the particles (Liu et al., 2010; Sreevalsa et al., 2013). This comprehensive analysis not only unveils the hexagonal crystal morphology and average size of the bare ZnONPs and MTX-ZnONPs but also highlights the successful drug loading on MTX-ZnONPs with their intricate lattice structure, affirming the high degree of crystallinity in the nanomaterial.





**Figure 4.6** HR-TEM analysis of nanosystems showing HR-TEM of image of (a) bare ZnONPs and (e) MTX-ZnONPs; size distribution curve of (b) bare ZnONPs and (f) MTX-ZnONPs;

crystal lattice structure of (c) bare ZnONPs and (g) MTX-ZnONPs; SAED pattern of (d) bare ZnONPs and (h) MTX-ZnONPs.

#### 4.3.8 Stability analysis of NPs

The synthesized NPs were rigorously evaluated for their physical and colloidal stability over an extended period to ensure their suitability for various applications. Colloidal stability, a crucial factor in NP dispersibility and efficacy, was assessed using three different NP concentrations: 10, 25, and 50  $\mu\text{g/mL}$  in deionized water. Samples were subjected to sonication for 7-10 minutes to ensure proper dispersion. The labeled tubes containing the dispersed NPs were then set aside undisturbed and observed periodically to monitor their colloidal stability. Results revealed a consistent and sustained colloidal stability, demonstrating minimal aggregation/sedimentation up to 8 hours at 10 and 25  $\mu\text{g/mL}$ . 50  $\mu\text{g/mL}$  tube showed early aggregation/sedimentation.

Results of the stability assessment are recorded in **Table 4.3** revealed that the synthesized NPs exhibited admirable physical and colloidal stability over the observation period. The color, flowability, and texture of the NPs remained consistent, indicating their resistance to physical alterations. Additionally, to confirm the physical and chemical stability basic characterization techniques like UV-Vis spectroscopy and FTIR spectroscopy were utilized. No significant changes were observed in the peaks received for both the NP systems over the observation period.

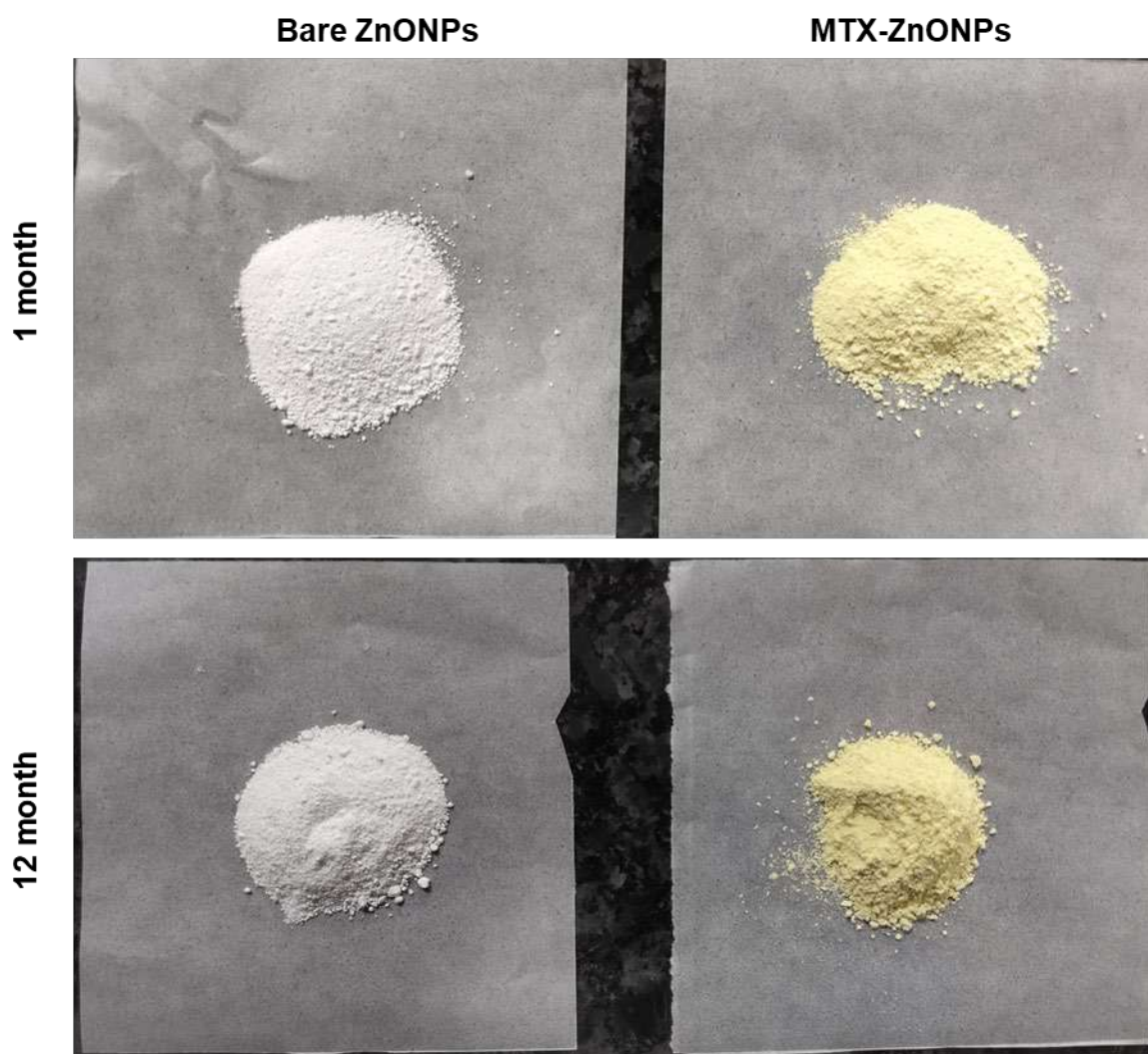
**Table 4.3** Observation table of colloidal stability study for bare ZnONPs and MTX-ZnONPs.

	Bare ZnONPs			MTX-ZnONPs		
	10 $\mu\text{g/mL}$	25 $\mu\text{g/mL}$	50 $\mu\text{g/mL}$	10 $\mu\text{g/mL}$	25 $\mu\text{g/mL}$	50 $\mu\text{g/mL}$
<b>0 hr</b>	-	-	-	-	-	-
<b>1 hr</b>	-	-	-	-	-	-
<b>2 hrs</b>	-	-	-	-	-	-
<b>3 hrs</b>	-	-	-	-	-	-
<b>4 hrs</b>	-	-	-	-	-	-
<b>5 hrs</b>	-	-	-	-	-	-
<b>6 hrs</b>	-	-	+	-	-	+
<b>7 hrs</b>	-	+	++	-	-	++
<b>8hrs</b>	-	++	++	-	+	++
<b>24 hrs</b>	+++	+++	+++	+++	+++	+++

**Key:** -No sedimentation, +Low sedimentation, ++High sedimentation, +++Highest sedimentation



Bare ZnONPs and MTX-ZnONPs were also assessed for its physical stability at interval of 1 year as depicted in **Figure 4.7**. It was appreciated that there was no considerable change observed in terms of color of the particles, flow of particles or even texture of particles. No significant impact was observed on any physical attributes of NPs over a duration stating their stability in their own way.

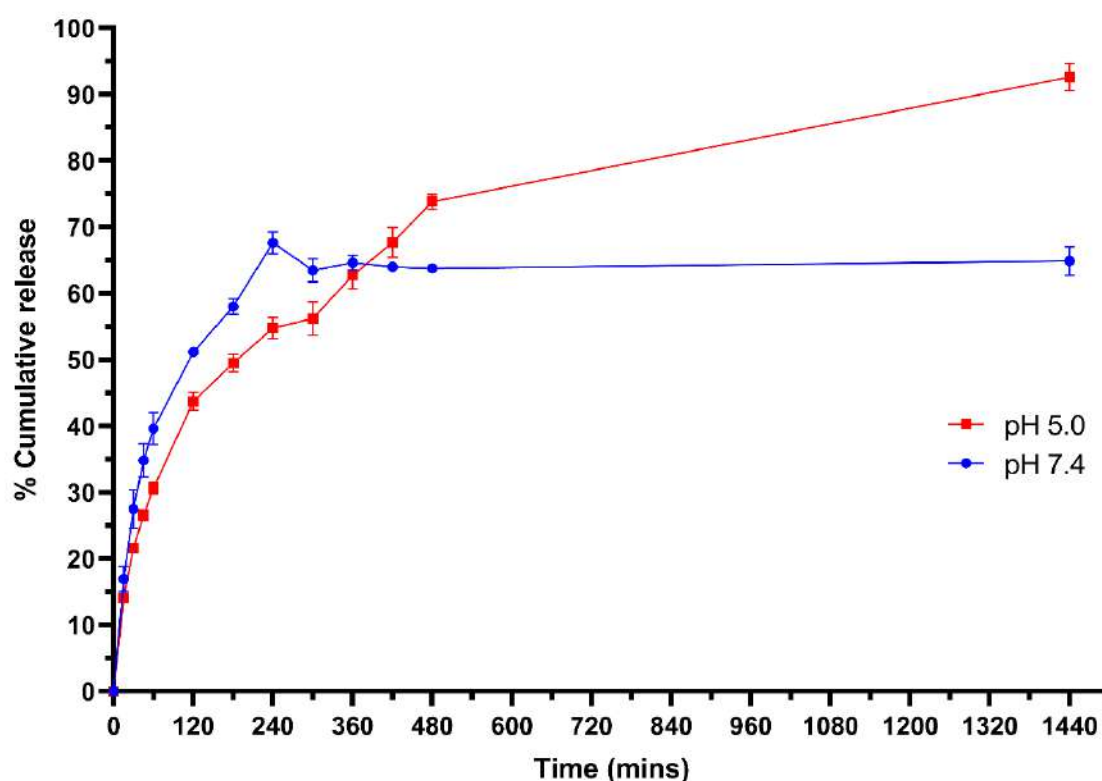


**Figure 4.7** Physical stability study for color, flow and texture study of bare ZnONPs and MTX-ZnONPs at two different time points.

#### 4.3.9 Drug release study of MTX-ZnONPs

The determination of MTX loading efficiency on ZnONPs was conducted using a UV-Vis spectrophotometer, revealing an impressive loading efficiency of 79.44%. To decipher the release dynamics of the nano-system in simulated physiological conditions, a precise drug release study was undertaken. Employing the dialysis method, the study utilized Phosphate-Buffered Saline (PBS) at pH 7.4 to replicate the normal cellular environment and, for the acidic

cancer cell milieu, PBS at pH 5.0 was employed at a temperature of 37 °C. The release profile of MTX from the MTX-ZnONPs exhibited a distinctive biphasic pattern, illustrated in **Figure 4.8**. An initial burst release within the first hour accounted for nearly 40% of drug release, followed by a steady increase observed up to the 5<sup>th</sup> hour. At pH 7.4, the drug release plateaued at no more than 65%, while at pH 5.0, a logarithmic phase persisted for up to 24 hours, resulting in notable 90% drug release. The drug release could be multiphasic, with an initial burst release followed by a sustained release. The burst release could be larger at pH 7.4 due to factors like higher solubility or faster diffusion at that pH. However, the sustained release could be slower at pH 7.4 due to stronger binding of the drug to the carrier matrix. This unequivocally demonstrates that the acidic microenvironment favors drug release, a crucial insight with significant implications for cancer cells. The subtle drug release kinetics provide valuable information for tailoring therapeutic strategies in cancer treatment.



**Figure 4.8** Drug release study of MTX-ZnONPs conducted in PBS at pH 7.4 and pH 5.0

#### 4.4 Discussion

There are various methods available to synthesize ZnONPs, each with its own set of advantages and limitations. Precipitation, sol-gel synthesis, thermal degradation, and hydrothermal synthesis are some of the most often utilized methods (Purcar et al., 2017). Precipitation

---

method involves the addition of a zinc salt to a solution containing a precipitating agent also known as reducing agent, resulting in the formation of ZnONPs. Here in the current project chemical precipitation method was chosen for the synthesis of bare ZnONPs. Also, in order to prevent agglomeration in particles while synthesis PEG was introduced as solvent, this approach is known as polyol assisted synthesis. Polyols serve as solvents for most inorganic precursors by dissolving them as metallic salts, owing to their hydrogen bonds and relatively high dielectric constant (Chieng and Loo, 2012). In addition, polyols' chelating abilities allow them to act as coordinating solvents, complexants, and surfactants, all of which adsorb on the surface of the expanding elementary particles and inhibit their aggregation (Hosni, Mongia, Samir Farhat, Mounir Ben Amar, Andrei Kanaev, Noureddine Jouini, 2015). Calcination/ dry heating is the particularly important step in final making of ZnONPs. Usually, NPs are calcined at remarkably high temperatures which provides ZnONPs their unique properties, size and shape. In the current study we dried the particles at 70°C for 1 hr to get rid of all the excess moisture trapped in NPs to give free flowing powder state. For synthesis of MTX-ZnONPs ex-situ approach was preferred considering the positive charge on bare ZnONPs and negative charge of MTX at pH 7. Chitosan (CS) is a biocompatible positively charged polymer that has metal ion coordination chemistry. This helps in the binding of MTX on the ZnONP surface easily. Hence, MTX-CS complex was mixed with previously characterized bare ZnONPs in 1:20 ratio for 24 hours under mixing condition at RT.

When characterized using various techniques it was confirmed that both the NPs were of desired characteristics. For UV-Visible spectroscopy clear quartz cuvettes were used as ZnONPs absorb in the UV range and quartz does not absorb in the UV region. When NPs are synthesized to nanoscale, they show energy change and absorption shifts towards UV region hence the shift is called as blue shift. Blue shift implies quantum confinement of NPs, where particle size decreases, the band gap of the particles increases, leading to a shift in absorption to the lower wavelengths (Raoufi, 2013; Singh et al., 2017). The blue shift in the absorption spectrum of bare ZnONPs due to size quantum size effect can be attributed to the increase in energy gap between conduction and valence bands when particle size decreases and electronic orbitals become more closed, leaving the highest occupied molecular orbital (HOMO) and the lowest occupied molecular orbital (LUMO) occupied. Consequently, the transfer of an electron from HOMO to LUMO requires the absorption of high-energy photons, resulting in the observed blue shift (Garimella et al., 2020). The difference in absorption spectra of bulk ZnO and bare ZnONPs and MTX-ZnONPs clearly suggests the size reduction under quantum

---

---

confinement principle. MTX showed 2 distinct peaks at 303 nm and 256 nm which were seen in the MTX-ZnONPs post loading. Loading results of MTX on ZnONPs were in alignment with previous literature showing same (Rozalen et al., 2020). FTIR based NP characterization was done to understand the loading of MTX on ZnONPs surface. This technique is extremely sensitive and can detect even small changes in the structure and composition of NPs. The peak between  $400\text{ cm}^{-1}$  to  $600\text{ cm}^{-1}$  is generally designated for Metal ion bonds (AbdElhady, 2012; Lanje et al., 2013) where we see the sharp peak at  $420\text{ cm}^{-1}$  indicating presence of ZnO bond. In case of MTX-ZnONPs sharp peaks of ZnO with few other organic groups coming from MTX were present indicating presence of MTX on NPs. These groups were common to pure MTX as  $1644\text{ cm}^{-1}$  for -CONH group,  $3387\text{ cm}^{-1}$  for -NH stretch,  $2926\text{ cm}^{-1}$  for -CH groups. XRD calculates the crystalline nature of material and gives diffraction peaks on bombardment of X-rays. Data of synthesized bare ZnONPs was matched with the standard ZnO JCPDS card no. 00-036-1451, identifying hexagonal wurtzite phase of the crystal structure. MTX-ZnONPs showed change in peak intensities and added noise due to the presence of MTX on its surface but, keeping its crystal phase same. These results were found to be in accordance with data reported in literature earlier (Buchheit et al., 2016; Sanmugam et al., 2017). Zeta potential is a charge present on the surface of the NPs which directly correlates to the stability of nano systems. Surface charge plays an important role in cellular internalization of these particles (Albanese et al., 2012; Yu et al., 2011). NPs with zeta potential values greater than  $\pm 30\text{ mV}$  are highly stable and those with values near iso electric point (IEP) i.e zero charge are considered to be the least stable (Sandmann et al., 2015). Bare ZnONPs and MTX-ZnONPs both showed positive zeta potential under acidic environment. In addition, PEG assisted synthesis gives particle more stability allowing them to remain suspend in the solution for longer periods of time. There was an evident shift in the surface charge when MTX was introduced indicating positive interaction between ZnONPs and MTX. Zeta potential clearly indicates the successful coating of NPs with MTX due to shift in the charge. Charge on the MTX-ZnONPs reaches close to zero under high alkaline environment. Whereas at acidic pH particles still show good charge stability. Under those conditions particles do show some amount of aggregation after some amount of time and no immediate effects can be observed. And same results were observed in stability study presented in **Table 4.3**. where we understand that at low concentrations particles do not show aggregation for initial few hours up to 6-7 hours, after which also some amount of aggregation becomes observable. For DLS study it is important to note that particle size measured by DLS is usually greater than the actual particle size as it considers the average hydrodynamic diameter. Moderate size distribution was

---

---

observed for both systems. ICP-AES is the most commonly used method for the elemental analysis, to know the precise concentration of a specific metal ion in the sample (Johari-Ahar et al., 2016; Xie et al., 2017). Both the NP systems were analyzed to know the total Zn content present in them. Amount of Zn present in bare ZnONPs was 0.352 mg/ ml and for MTX-ZnONPs it was 0.280 mg/ ml. In EDS mapping, the chemical composition and distribution of the ZnONPs was determined to quantify the Zinc, oxygen, and carbon present in them. Zinc, Oxygen and Carbon and weight percentage as 70.37, 20.31 and 9.32 were found for bare ZnONPs whereas for MTX-ZnONPs it was 67.45, 18.33 and 14.22. Change in carbon value was indicative of presence of organic backbone in sample coming from MTX. HR-TEM analysis of bare ZnONPs and MTX-ZnONPs presented highly crystalline particles with an average size of around 30 nm with size distribution of 24 nm to 36 nm, while MTX-ZnONPs presented much narrower size distribution of 28-34 nm with average particle size of 32 nm. The narrow size distribution, indicative of a well-controlled synthesis process, coupled with the small NP size, renders these ZnONPs particularly advantageous for applications that demand enhanced surface area and reactivity. The polycrystalline nature of the bare ZnONPs and MTX-ZnONPs suggests their composition which contains numerous small crystallites oriented in various directions, likely attributed to the rapid growth process. HR-TEM images of MTX-ZnONPs also evidently showcased the presence of drug coating on the surface of ZnONPs, which was absent in bare ZnONPs confirming presence of MTX. Despite their polycrystalline nature, the presence of multiple diffraction spots in the SAED pattern underscores the high degree of crystallinity exhibited by these ZnONPs. This lattice fringe distance was calculated to correlate the lattice planes with XRD peaks which were in alignment.

The drug release study data shows that the cumulative release of the drug is significantly lower in PBS pH 7.4 than in PBS pH 5.0. This suggests that the drug release is pH-dependent, with a higher release rate in acidic conditions. This is likely due to the protonation of the drug molecule in acidic conditions, which increases its hydrophilicity and facilitates its release from the NPs. Conversely, in neutral or alkaline conditions, the drug molecule is deprotonated and becomes more hydrophobic, which hinders its release from the NPs. The carrier matrix could be degrading faster at pH 5.0, leading to a slower but more prolonged drug release. This is because the degradation of the matrix would expose more drug molecules over time, allowing for their gradual release. The slower drug release rate in PBS pH 7.4 is advantageous for several reasons. First, it allows for sustained drug release over a longer period of time, which can improve the efficacy of the drug and reduce the need for frequent dosing. Second, it can help

---

to minimize systemic side effects by limiting the drug concentration in the bloodstream. Third, it can improve the targeting of the drug to specific tissues or organs, as the drug will be released more slowly from the NPs in the extracellular environment (which is typically neutral or alkaline) and more quickly in the acidic environment of intracellular compartments. It is also possible that a combination of factors, such as pH-dependent solubility, diffusion, and degradation, are contributing to the observed release profile. It is likely due to a more complex interplay of factors, such as multiphasic release, pH-dependent degradation, or a combination of both.

#### 4.5 Conclusion

MTX-ZnONPs, synthesized through a facile chemical precipitation approach, hold significant promise for targeted cancer therapy. The simple and efficient synthesis method yielded NPs with desirable characteristics, including well-defined size, high crystallinity, and efficient MTX loading. The NPs exhibited uniform dimensions. Hexagonal wurtzite crystal structure, confirmed by XRD and HR-TEM, further underscores NPs stability and potential for controlled drug release. Additionally, the moderate size distribution and stability across a range of pH values ensure effective dispersibility in biological mediums. The ex-situ synthesis method facilitated a 79% loading efficiency of MTX, ensuring a substantial payload for targeted delivery to cancer cells. The biphasic drug release profile observed in simulated physiological conditions is particularly encouraging. Notably, this enhanced biphasic release observed in the acidic environment suggests potential for selective drug delivery to cancer cells while sparing healthy tissues.

# Chapter 5

## **In-vitro study to evaluate the anti- cancer activity of Methotrexate loaded Zinc oxide nanoparticles on breast cancer cell lines**

---

## **In-vitro study to evaluate the anti-cancer activity of Methotrexate loaded Zinc oxide nanoparticles on breast cancer cell lines**

### **5.1 Introduction**

Within the field of cancer research, in vitro assays have emerged as an indispensable tool for evaluating the anti-cancer efficacy of NPs. In-vitro assays remain a crucial tool for assessing the anti-cancer potential of NPs. One of the key advantages of in vitro assays is the precise control over experimental conditions. Researchers can accurately control factors like NP concentration, exposure time, and cell type, ensuring a comprehensive evaluation of NP impact on cancer cells without encountering confusing variables prevalent in in vivo studies. This meticulous control facilitates reliable and reproducible results, critical for drawing meaningful conclusions about NP anti-cancer potential. Furthermore, in vitro assays enable the investigation of specific cellular and molecular mechanisms underlying NP mediated anti-cancer effects. In-vitro assays can also detect potential off-target effects and toxicity of nanoparticles early in the development process, allowing researchers to optimize their design and minimize potential risks before moving on to more expensive and time-consuming in-vivo studies. Techniques like flow cytometry, immunofluorescence, and protein expression analysis offer researchers a detailed understanding of how NPs interact with cancer cells at the cellular and molecular level. This mechanistic insight is crucial for comprehending the pathways involved in NP anti-cancer activity, ultimately informing the development of targeted and effective therapeutic interventions.

Additionally, employing in vitro assays aligns with ethical considerations. They allow for an initial assessment of NP safety profiles before advancing to animal or clinical studies. This approach minimizes the potential risks associated with unforeseen toxicities and ensures that only the most promising candidates progress to further research stages. A wide variety of in-vitro assays exist, each targeting specific aspects of the cancer cell biology. This allows researchers to comprehensively assess the anti-cancer potential of nanoparticles and gain a deeper understanding of their mechanisms of action.

In conclusion, the importance of utilizing in vitro assays to evaluate NP anti-cancer activity is underscored by the controlled experimental environment they provide, their significant contribution to mechanistic understanding, and their alignment with ethical considerations. As the field of nanomedicine continues to evolve, in vitro assays will remain an indispensable tool in the arsenal of cancer researchers, paving the way for the development of safer and more effective NP-based therapies.

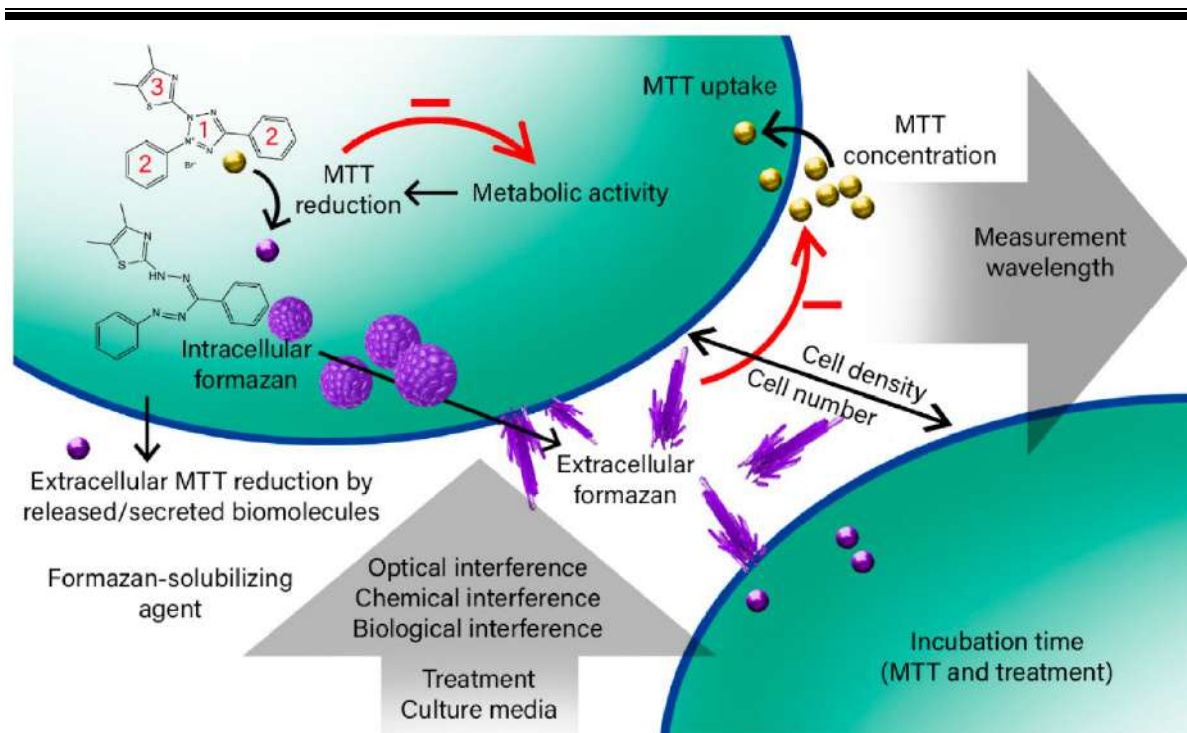
---



---

### 5.1.1 MTT Cellular viability assay

The MTT assay, or 3-(4,5-dimethylthiazol-2-yl)-2,5-diphenyltetrazolium bromide assay, plays a vital role in cancer research as a robust and widely used tool for evaluating the cytotoxicity of potential anti-cancer compounds (Kollur et al., 2021). The MTT assay is extremely sensitive, capable of detecting subtle changes in cell viability even at low concentrations of drug candidates. This allows to accurately differentiate between cytotoxic and non-cytotoxic compounds, facilitating the identification of promising anti-cancer agents. The assay utilizes a yellow tetrazolium salt called MTT, which is readily taken up by living cells. The MTT assay relies on the metabolic activity of living cells to convert a yellow tetrazolium salt (MTT) into a purple formazan product as depicted in **Figure 5.1**. This conversion is mediated by mitochondrial enzymes, specifically succinate dehydrogenase, present in viable cells. The amount of formazan formed is directly proportional to the number of metabolically active cells. By measuring the amount of formazan produced, metabolic activity of cells is quantified, providing a direct measure of cell viability and proliferation (Wang et al., 2015). This assay is particularly valuable in evaluating the cytotoxicity of NPs by determining the concentration required to inhibit cell viability by 50% (IC<sub>50</sub>). The assay allows for the determination of the dose-dependent cytotoxicity of a compound, providing valuable information about its potency and toxicity profile. The MTT assay can be used to assess the cytotoxicity of a wide range of compounds, including natural products, synthetic drugs, and nanomaterials. This versatility makes it a valuable tool for anti-cancer drug discovery and development. While the MTT assay offers numerous benefits, it is important to acknowledge its limitations. The assay does not provide information on the specific mechanism of cell death, and it may not be equally sensitive to all types of cell death. The assay only provides information on cell viability, not differentiating between cell death mechanisms like apoptosis or necrosis. The assay measures mitochondrial activity, which may not always be a perfect reflection of overall cell health. Also, the assay may underestimate the cytotoxicity of compounds that primarily target non-mitochondrial processes or metabolically inactive cells. Additionally, MTT assay can be affected by factors such as cell density and culture conditions, demanding careful control of these parameters (Ghasemi et al., 2021; Wang et al., 2010).

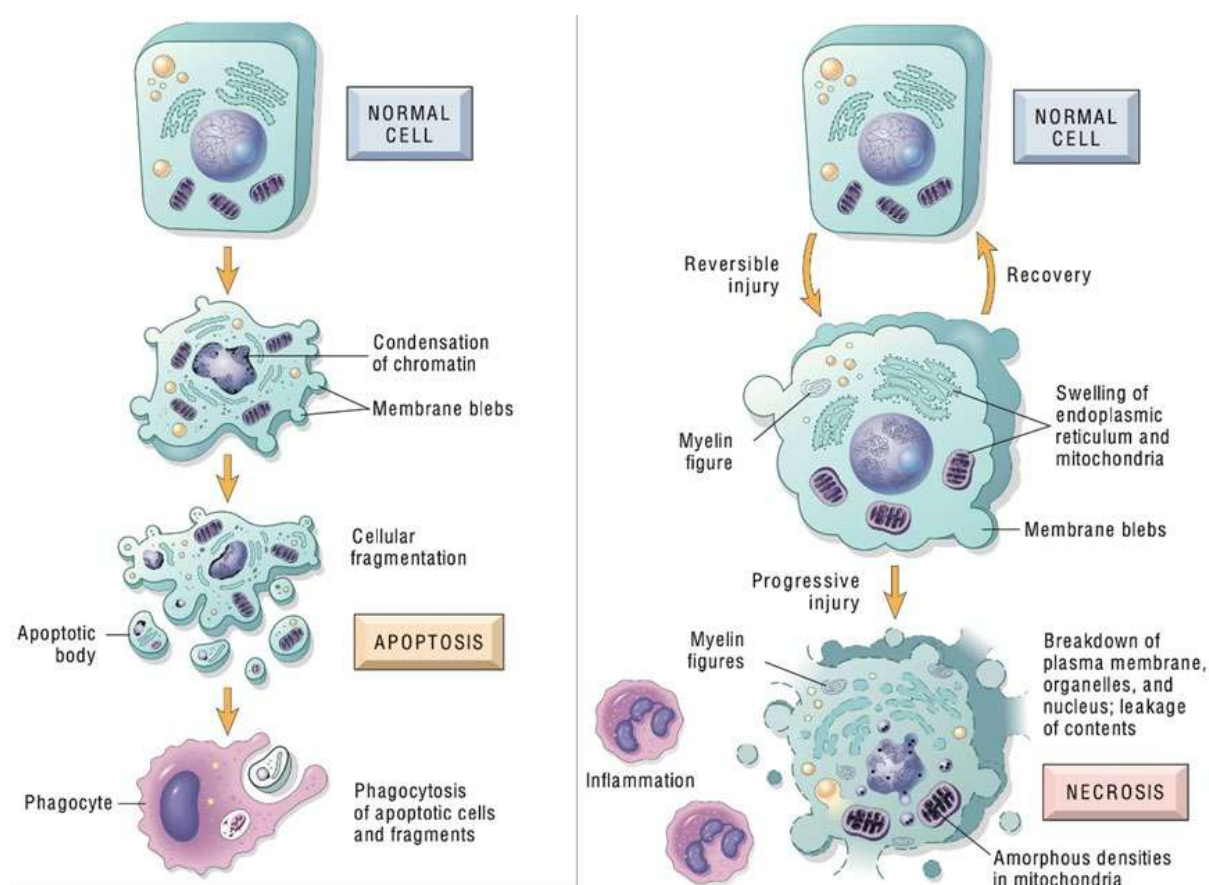


**Figure 5.1** A simplified overview of the principle behind MTT assay. Viable cells take up the yellow tetrazolium dye MTT (3-(4,5-dimethylthiazol-2-yl)-2,5-diphenyltetrazolium bromide) which is reduced to purple formazan crystals by mitochondrial dehydrogenase enzymes. Chemical structure of MTT and its reduced form, formazan. The tetrazole ring in MTT (1) is converted to a formazan by cellular enzymes. The red arrows indicate the reduction process, while the dashed lines and minus symbol represent factors that can disrupt MTT reduction or hinder uptake, leading to inaccurate OD measurements. It also illustrates various factors that can affect MTT assay measurements. (Source: Ghasemi et al., 2021)

### 5.1.2 Acridine Orange/ Ethidium Bromide (AO/EB) viability staining

AO/EB viability staining technique offers a simple and effective method to assess the health and viability of cells. This staining technique is widely used and robust method for assessing cell viability and cytotoxicity. This fluorescent staining approach relies on the contrasting DNA-binding properties of two dyes i.e., AO and EB. Principle behind the assay is to differentiate between viable and non-viable cells based on their membrane integrity (Babu et al., 2017). AO dye passively diffuses through the cell membrane and stains both viable and non-viable cells. In viable cells, AO intercalates with DNA, emitting green fluorescence, while in non-viable cells, it accumulates in the cytoplasm, emitting a less intense orange fluorescence. Whereas EB is membrane-impermeant and can only enter cells with compromised membrane integrity. In non-viable cells, EB binds to DNA, emitting a bright red fluorescence, thereby

quenching the green fluorescence from AO (Shelat et al., 2019). By observing the fluorescence patterns of stained cells under a microscope, researchers can distinguish between viable, early apoptotic, late apoptotic and necrotic cell populations. Viable cells appear green due to the green fluorescence emitted by AO-bound DNA. Their morphology remains intact with no visible signs of cell death (**Figure 5.2**). Early apoptotic cells exhibit condensed chromatin, appearing as bright green dots within the green cytoplasm stained by AO. Late apoptotic cells display a combination of green and red fluorescence due to AO staining the nucleus and EB staining the condensed chromatin. In necrotic cells, the compromised membrane allows EB to enter, staining the DNA red and quenching the green fluorescence from AO, thus cells appear orange or red due to the dominant red fluorescence coming from EB (Sanchala et al., 2018).



**Figure 5.2** Morphological difference between apoptosis and necrosis of a cell. On the left side notice the blebs being made and eaten by a phagocyte as fate of cells in apoptosis. Right hand side of image shows swelling, inflammatory response, and leak leaks everywhere which will induce inflammation and possible organ failure. (Source: Robbins and Cotran pathologic basis of disease, 9th ed.)

---

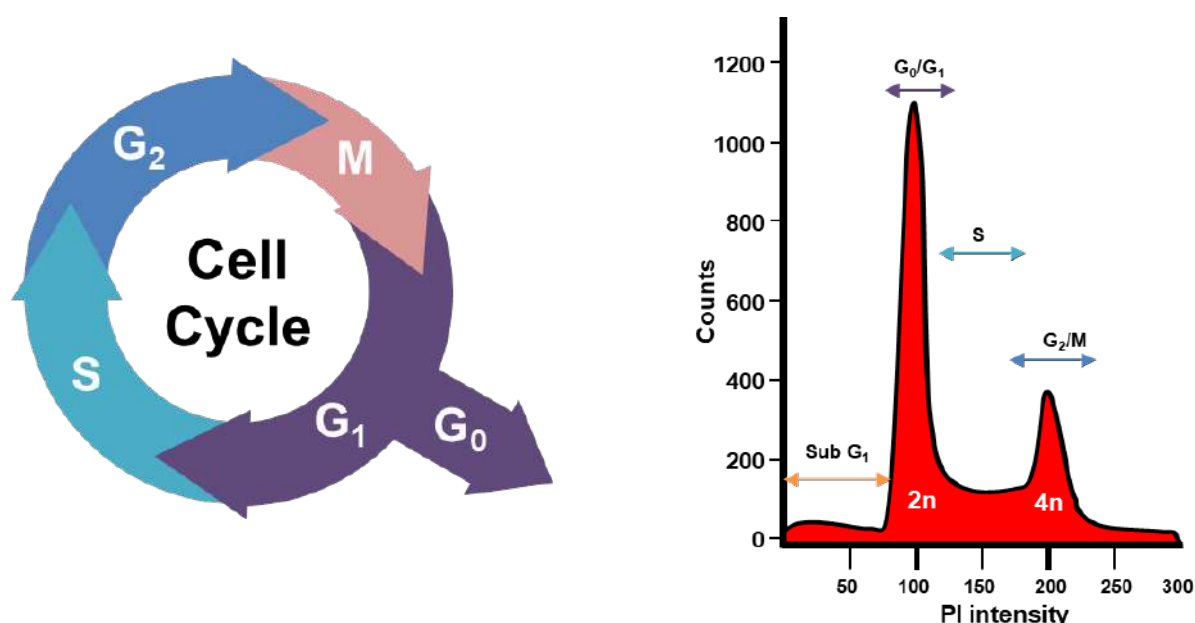
AO/EB staining is commonly used to assess the cytotoxic effects of various agents, including drugs, radiation, and environmental toxins. By quantifying the relative proportions of viable and non-viable cells, researchers can determine the potency and effectiveness of cytotoxic compounds. The staining pattern of AO/EB can provide valuable insights into the type of cell death occurring. The appearance of condensed chromatin regions and the characteristic green-to-red shift in fluorescence are indicative of apoptosis, while necrosis is characterized by a purely red staining (Nicotera et al., 1999). Necrosis and apoptosis are morphologically distinct forms of cell death. Necrosis is characterized by the swelling of organelles, plasma membrane rupture, and the release of cellular contents into the extracellular space, leading to inflammation due to the uncontrolled release of antigens (**Figure 5.2**). On the other hand, apoptosis is characterized by nuclear DNA fragmentation, condensed chromatin, and the formation of cell-bound bodies that are phagocytosed by neighboring cells without eliciting an inflammatory response (Vanden Berghe et al., 2013; Van Cruchten and Van den Broeck, 2002). While this method provides valuable visual data, the results obtained are qualitative rather than quantitative. Interpretation of the fluorescence patterns can be subjective and may vary between person to person. Despite its limitations, the AO/EB staining technique remains a valuable and widely used tool for assessing cytotoxicity. When combined with other analytical techniques, the AO/EB staining can provide valuable insights into the cytotoxic effects of various compounds, aiding in drug development, safety testing, and understanding cell death mechanisms.

### 5.1.3 Cell cycle analysis by Propidium Iodide (PI) staining

Cellular proliferation is a tightly regulated process governed by the cell cycle, a series of precisely coordinated events leading to DNA replication and cell division. This intricate process can be broadly categorized into five phases as shown in **Figure 5.3**: G<sub>0</sub> (resting), G<sub>1</sub> (growth), S (DNA synthesis), G<sub>2</sub> (preparation for mitosis), and M (mitosis and cytokinesis). Two primary control mechanisms orchestrate the cell cycle: kinase activation, responsible for sequential transitions between phases, and checkpoint control, ensuring critical events are completed flawlessly before initiating the subsequent stage (Sherr, 2000). Dysregulated cell cycle progression, or particularly uncontrolled proliferation, is a hallmark of cancer. Hence, understanding cell cycle dynamics and its regulatory mechanisms has become essential to oncology research. Understanding the cell cycle arrest induced by NPs is crucial for comprehending their anti-cancer mechanism (Gérard and Goldbeter, 2016). Hence cell cycle analysis by flow cytometry allows one to quantify the distribution of cells in different phases

---

of the cell cycle. Flow cytometers utilize fluorescent dyes to label DNA content, enabling the differentiation of cells in different phases. Analyzing the cell cycle distribution after NP treatment provides insights into whether the NPs induce cell death by inhibiting proliferation (G<sub>1</sub>/S arrest), blocking DNA synthesis (S-phase arrest), or preventing cell division (G<sub>2</sub>/M arrest). Thus, cell cycle analysis utilizing PI staining, provides valuable insights into the proportion of cells at each stage of the cycle for a given population. It also offers a simple, reliable, and widely application for analyzing cell cycle progression and its potential disruption by various agents, including cytotoxic compounds (Darzynkiewicz et al., 2001).



**Figure 5.3** The cell cycle is divided into four main phases: G<sub>1</sub> (growth phase 1), S (synthesis phase), G<sub>2</sub> (growth phase 2), and M (mitotic phase). Each phase plays a crucial role in preparing the cell for division. This histogram on right depicts the results of a cell cycle analysis using propidium iodide (PI) staining, a common method for quantifying cellular DNA content using flow cytometer. The horizontal axis represents the relative fluorescence intensity of PI, which is proportional to the amount of DNA present in each cell. The vertical axis represents the number of cells detected at each fluorescence intensity level. Cells in G<sub>1</sub> have 2n DNA content, having already duplicated their DNA in the previous cell cycle. During the S phase, DNA replication occurs, leading to a doubling of DNA content to 4n. Cells in G<sub>2</sub> maintain 4n DNA content, preparing for mitosis. Mitosis involves cell division, resulting in daughter cells with 2n DNA content each.

PI is a fluorescent cell-impermeable dye, meaning it cannot enter live cells with intact membranes. PI binds stoichiometrically to DNA, meaning the amount of PI fluorescence

---

emitted by a cell is directly proportional to the amount of DNA present within cell, thus allowing the quantification of DNA content and the identification of cells in various phases. For the same reason cells are first fixed with chilled alcohol or formaldehyde, permeabilizing the cell membrane and allowing PI to penetrate inside the cell allowing it to interact with the DNA. Since DNA content doubles during the S phase, PI staining intensity can be used to distinguish between cells in different phases of the cell cycle: G1 phase with Low DNA content, minimal staining, and low fluorescence. S phase with increased DNA content, moderate staining, and moderate fluorescence followed by G2/M phase having highest DNA content, highest staining, and highest fluorescence (Riccardi and Nicoletti, 2006).

Although PI staining method too have few shortcomings like, assay relies on fixed cells, providing a static snapshot rather than real-time dynamics of cell cycle progression. Clumping of cells can interfere with accurate measurement of PI fluorescence intensity and it cannot distinguish between resting (G0) and actively growing (G1) cells. While limitations exist, the assay's simplicity, reliability, and wide applicability make it an asset for investigating the cytotoxic effects of various agents (Crosby, 2007).

#### **5.1.4 Annexin V-FITC- Propidium Iodide assay**

The Annexin V FITC/ PI apoptosis assay provides a robust method for simultaneously identify viable, early apoptotic, late apoptotic, and necrotic cells. Assay utilizes the fluorescence as a maker to differentiate the population with the help of two fluorescence dyes namely Annexin V-FITC and PI. Annexin V-FITC is a conjugated molecule that exhibits high affinity for phosphatidylserine (PS). PS is a phospholipid typically confined to the inner leaflet of the plasma membrane in healthy cells. In the event of cell damage like early apoptosis, PS undergoes translocation from inner leaflet to the outer leaflet, serving as an early hallmark of programmed cell death. Annexin V readily binds to exposed PS, emitting green fluorescence when tagged with FITC (fluorescein isothiocyanate), thereby identifying early apoptotic cells. PI is an DNA binding dye and being membrane-impermeant it is excluded from viable cells with intact plasma membranes (Peng et al., 2001). However, during late apoptosis or necrosis, where membrane integrity is compromised, and PI gains access to the intracellular space. Upon binding to DNA, PI readily emits red fluorescence, effectively differentiating late apoptotic/necrotic cells from viable ones (Ormerod, 1998). By analyzing the combined fluorescence intensity of Annexin V-FITC and PI (**Figure 5.4**) in individual cells through flow cytometry, one can precisely distinguish between different cell populations like:

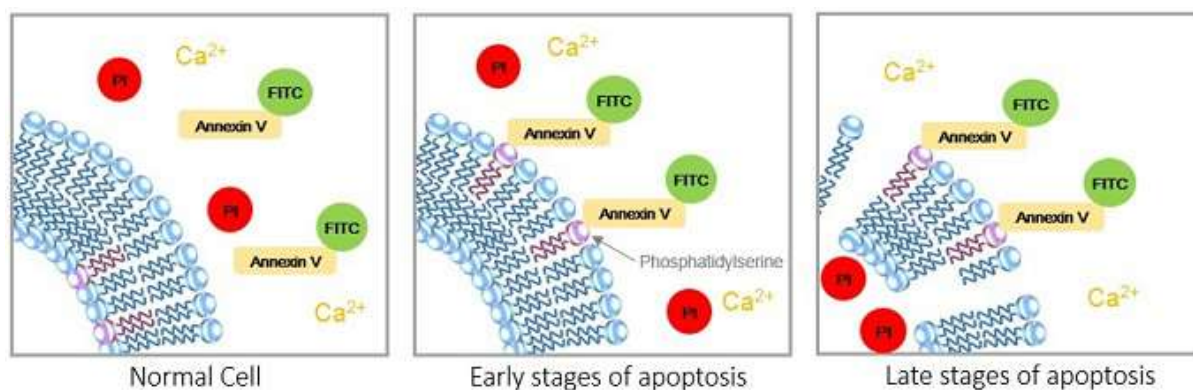


**Viable cells:** Negative for both Annexin V-FITC and PI represented by viable cells with intact membranes and functional DNA. (Lower left quadrant: Annexin V-negative/PI-negative)

**Early apoptotic cells:** Exhibit only green fluorescence due to Annexin V binding, but negative for PI. Represented by early apoptotic cells with phosphatidylserine exposure on the cell surface but intact membranes. (Lower right quadrant: Annexin V-positive/PI-negative)

**Late apoptotic/necrotic cells:** Show both green and red fluorescence, stained with both Annexin V-FITC and PI, represents late apoptotic cells with both PS exposure and compromised membranes. (Upper right quadrant: Annexin V-positive/PI-positive)

**Necrotic cells:** Exhibit only red fluorescence due to PI binding, but negative for Annexin V-FITC. Represented by necrotic cells with damaged membranes. (Upper left quadrant: Annexin V-FITC negative /PI- positive) (Miller, 2004)



**Figure 5.4** This schematic diagram illustrates the principle of Annexin V-FITC/PI staining, a common method for identifying and differentiating healthy, early apoptotic, and late apoptotic cells. (a) Illustrates a normal healthy cell membrane. The phospholipid bilayer of the cell membrane is shown as a smooth, uninterrupted structure. Neither Annexin V-FITC (green) nor PI (red) can enter the cell, resulting in no fluorescence signal, (b) Represents an early stage apoptotic cell membrane. Early in apoptosis, phosphatidylserine (PS) flips from the inner leaflet to the outer leaflet of the plasma membrane. Annexin V-FITC, with high affinity for PS, binds to the exposed PS on the cell surface, resulting in green fluorescence. PI remains excluded due to the intact plasma membrane, resulting in no red fluorescence, (c) Shows a late stage apoptotic cell membrane. In late apoptosis or necrosis, the plasma membrane loses its integrity and permeability. Both Annexin V-FITC and PI can enter the cell. Annexin V-FITC binds to PS, while PI binds to DNA, resulting in a double-positive signal with green and red fluorescence. (Source: <https://www.dojindo.com/>)

---

Understanding the differences between necrosis and apoptosis is crucial in various fields, including medicine and biology, as it helps in identifying and treating different types of cell death-related pathologies. In clinical practice, distinguishing between necrosis and apoptosis is essential for accurate diagnosis and treatment. Necrosis is distinct from apoptosis in several ways. Additionally, apoptosis results in the formation of membrane-bound apoptotic bodies, while necrosis leads to the leakage of intracellular components into the extracellular space, resulting in damage to surrounding tissues (Span et al., 2002).

This dual-staining technique offers quite a lot of advantages like, simultaneous analysis of multiple cell populations, simple and rapid protocol and quantitative data generation with broad applicability. The Annexin V-FITC/PI assay have plentiful applications to study apoptosis induction, determining the effectiveness of interventions targeting apoptosis in disease treatment and even unraveling cell death mechanisms by providing valuable insights into the intricate processes underlying cell survival and death. Despite of its limitation Annexin V-FITC/PI assay remains a powerful tool for detecting and quantifying cell death mechanism (Chen et al., 2008).

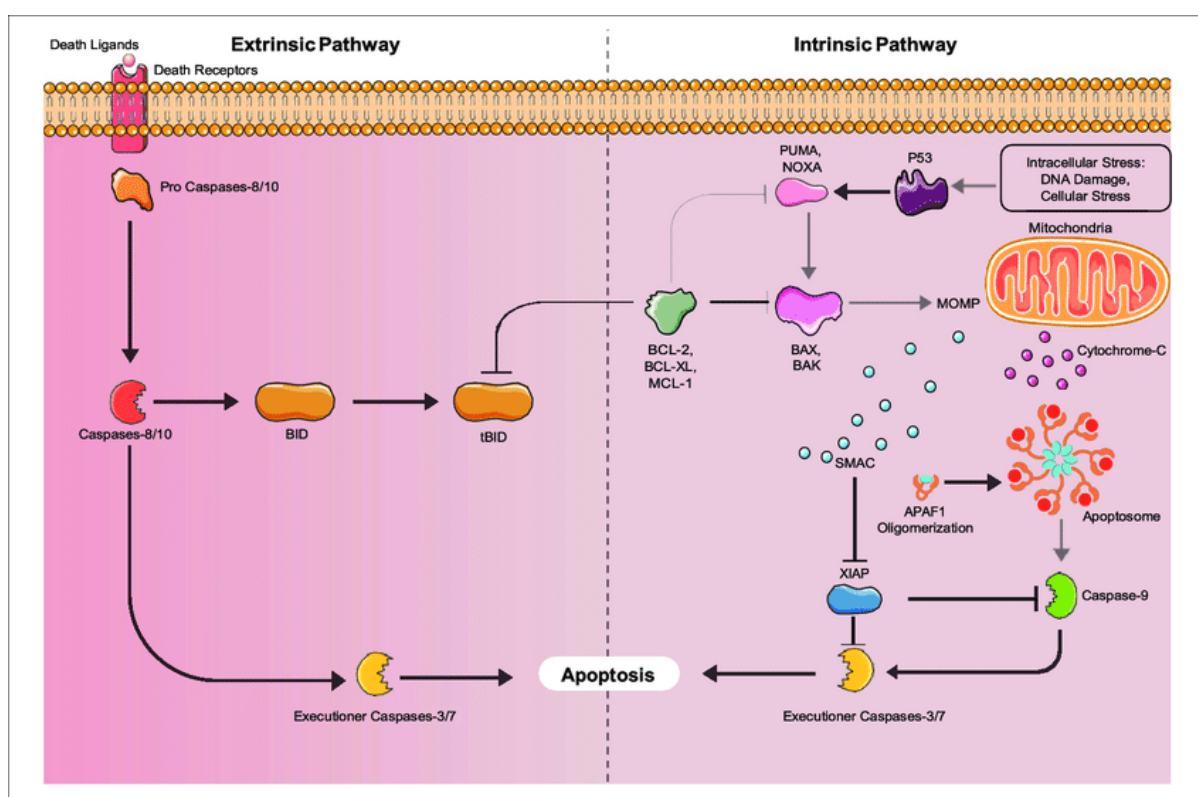
#### **5.1.5 Western blot analysis**

Western blotting, also known as immunoblotting, is a powerful analytical technique used for detection and quantification of specific proteins in a complex mixture. This method relies on the principles of both immunology and electrophoresis to achieve its remarkable sensitivity and specificity. Immunoblotting provides valuable information about specific protein identification, expression, and molecular weights. It is a multipurpose and sensitive technique widely utilized in various biomedical research and biological applications, including the study of protein interactions, disease mechanisms, and the effects of experimental treatments on expression of various protein levels. In the first step the proteins of interest are extracted from the sample and prepared for gel electrophoresis. This typically involves homogenizing the sample, lysing the cells, and extracting the proteins. Next to that protein was loaded onto polyacrylamide gel and under the influence of electrical current, proteins were separated based on their size and charge. Now, these protein bands are transferred on to the special membrane for its final probing and identification. Two types of membranes are commonly used for western blot protein transfer are Nitrocellulose membrane and polyvinylidene fluoride (PVDF) membrane. Next to this blocking agent is applied over the membrane to prevent the nonspecific binding of antibodies to the membrane. For blocking very commonly two blocking agents are used namely 5% Bovine Serum Albumin (BSA) or 5% nonfat dried milk (NFDM) which also

---



helps in reducing the background noise. Post blocking membranes are probed and incubated with highly specific monoclonal/ polyclonal antibody allowing them to specifically go and bind to that protein of interest. After washing away any unbound antibodies, enzyme-linked secondary antibody is added where two types of enzymes are commonly used horseradish peroxidase (HRP) and alkaline phosphatase (Koivunen and Krogsrud, 2006). These antibodies recognize the primary antibodies attached and amplifies the signal. Now finally, this antibody-protein complex is treated with a substrate that produces a visible signal, such as chemiluminescence or colorimetry. This signal is captured using specialized imaging equipment. In the case of a fluorophore-conjugated secondary antibody, the signal can be visualized directly under appropriate light. This powerful technique analyzes protein expression levels, offering insights into the molecular mechanisms underlying the observed cellular effects. By probing for specific signaling proteins involved in apoptosis, cell cycle regulation, and other relevant pathways, western blots can pinpoint the specific cellular targets of the NPs and shed light on their anti-cancer mechanisms. One such application can be elucidating the apoptosis or necrotic pathways and proteins that plays crucial role in regulating it (Kurien and Scofield, 2006; Ni et al., 2016).



**Figure 5.5** Intrinsic and Extrinsic Apoptosis Pathways in cell leading to apoptosis: This diagram depicts two main pathways of programmed cell death, or apoptosis: the intrinsic

---

pathway and the extrinsic pathway. Both pathways ultimately lead to the activation of caspases, which dismantle the cell's essential components, resulting in cell death. In intrinsic pathway the stress signals trigger the release of cytochrome c from the mitochondria into the cytosol. Cytochrome c binds to Apaf-1, forming a complex that activates caspase-9. Caspase-9 activates downstream caspases (caspase-3, caspase-7), leading to the execution of apoptosis. Extrinsic pathway is initiated by external signals called death ligands, such as Fas ligand or TNF- $\alpha$ , binding to their specific receptors on the cell surface. Death receptor binding induces the clustering and activation of caspase-8 or caspase-10. Similar to the intrinsic pathway, activated caspase-8/10 triggers the downstream caspases (caspase-3, caspase-7), leading to apoptosis execution. (Source: Wanner, E., Thoppil, H., & Riabowol, K. 2020).

Apoptosis, a form of programmed cell death, plays a crucial role in maintaining tissue homeostasis and eliminating unwanted/damaged cells. An intricate pathway involving Bax, Bcl-xL, and Caspase-3/7 plays a crucial role in this process, involving intricate interactions between pro and anti-apoptotic proteins plays key role in the initiation and execution of the apoptotic program as depicted in **Figure 5.5** (Li and Yuan, 2008). In the event of cellular damage caused by various expected reasons ultimately leading to activation of one of the pathways to apoptosis. Through two signaling mechanisms, caspases-specialized proteolytic enzymes that initiate and execute apoptosis-can be activated. Cell-intrinsic pathway consists of proteins from the Bcl-2 family that initiate apoptosis when cells are severely distressed; cell-extrinsic pathway triggered by extracellular ligands via cognate death receptors on target cells. The interplay between Bax, Bcl-xL, and Caspase-3/7 is crucial for the precise regulation of apoptosis. The relative levels of these proteins determine the cell's fate. In healthy cells, Bcl-xL predominates, maintaining mitochondrial integrity and preventing apoptosis. However, when Bax expression increases or Bcl-xL levels are downregulated, the balance shifts towards apoptosis. Bax then permeabilizes the mitochondrial outer membrane (MOM), releasing cytochrome c and triggering the activation of Caspase-3/7. The activated Caspase-3/7 then cleaves its downstream targets, leading to the dismantling of the cell and its eventual demise (Kavithaa et al., 2016). Bax, is a pro-apoptotic protein, acts as a gatekeeper, residing in the cytosol in an inactive state. Upon receiving a signal for cell death, Bax undergoes a conformational change, leading to its translocation to the MOM. Here, Bax oligomerizes and forms pores, disrupting the mitochondrial membrane integrity. This breach triggers the release of pro-apoptotic factors, such as cytochrome c, into the cytosol, initiating the caspase cascade (Shinoura et al., 1999). Bcl-xL, an anti-apoptotic protein, serves as a counterbalancing force to

---

---

Bax. It acts by directly binding to Bax and preventing its activation and oligomerization. This interaction inhibits Bax's ability to permeabilize the MOM, thereby delaying or preventing the initiation of apoptosis (Xu et al., 2013). Caspase-9 initiates the caspase cascade, a downstream signaling pathway involving the activation of effector caspases, such as caspase-3 and caspase-7. These effector caspases are responsible for the execution phase of apoptosis, cleaving key cellular proteins and ultimately orchestrating the demise of the cell hence they are known as executioner caspases. These are a type of cysteine proteases belonging to the caspase family, which play a central role in the execution phase of apoptosis. These enzymes are present in the cell in an inactive zymogen form. Upon activation by upstream caspases, caspase-3/7 cleave a specific set of cellular proteins, leading to morphological changes, DNA fragmentation, and ultimately, cell death. By understanding the intricate interplay between these proteins, we get valuable insights into the mechanisms of apoptosis and its role in various diseases like cancer, autoimmune disorders, and other conditions (Bai et al., 2017; Fu et al., 2014).

While apoptosis is a regulated process that does not cause inflammation, necrosis leads to inflammation due to the release of cellular contents. Necrosis is distinct from apoptosis in several ways. Necrosis can be defined as a form of cell death where the cell's structure is disrupted, leading to the release of cell contents into the surrounding tissue. Necrosis, often perceived as the 'accidental' form of cell death. This form of cell death is often caused by external factors such as infection, toxins, or trauma, physical injury, ischemia, and oxidative stress, leading to cell swelling, organelle damage, and inflammation. Although primarily associated with the initiation of apoptosis, Bax can also contribute to necrosis under specific circumstances. When activated by diverse stimuli, Bax oligomerizes and forms pores not only in the mitochondrial membrane, but also in the lysosomal membrane. Developing a deeper understanding of Bax's vital role in necrosis will have significant implications for understanding disease. In some cancer treatments, inducing controlled necrosis can be beneficial in eliminating tumor cells (Whelan et al., 2012; Ying and Padanilam, 2016).

## **5.2 Materials and Methods**

### **5.2.1 Cell lines**

This study primarily focused on elucidating the impact of newly synthesized nanoparticles on breast cancer cell lines. For this analysis, two breast cancer cell lines were employed: MCF-7 and MDA-MB-231. Additionally, non-cancerous cell lines that was included for comparison was MCF10A the immortalized mammary epithelial cell line, MCF-7 cell lines was obtained from the National Centre for Cell Sciences (NCCS), Pune. The MDA-MB-231 and MCF-10A

---

---

cell line was purchased from ATCC. This diverse selection of cell lines enabled a comprehensive assessment of the NPs effects on both malignant and healthy cells.

### 5.2.2 Chemicals and reagents

Methotrexate (MTX) was kindly provided as a gift sample from Khandelwal Laboratories Pvt. Ltd, Mumbai, India. 3-(4,5-Dimethylthiazol-2-yl)-2,5-diphenyltetrazolium bromide (MTT) was from SRL, India, while dimethyl sulphoxide (DMSO) was from SD Fine Chem, India. Propidium iodide (PI), acridine orange (AO) and ethidium bromide (EB) were purchased from Sigma- Aldrich, USA. Bovine serum albumin (BSA) was purchased from SRL Pvt. Ltd., India. RNase A was purchased from Invitrogen™, ThermoFisher Scientific, USA. All chemicals used are of analytical grade. All preparations of buffers/reagents were done using MiliQ water.

Dulbecco's Modified Eagle's Medium (DMEM), foetal bovine serum (FBS), Dulbecco's Phosphate Buffered Saline (DPBS), 0.25% Trypsin-EDTA with phenol red indicator and Trypan blue were from Gibco (Gibco™, ThermoFisher Scientific, USA). MEGM™ Mammary Epithelial Cell Growth Medium BulletKit™ media with single use aliquots of growth factors were from Lonza, Germany. Cholera toxin and Antibiotic Antimycotic solution were from Sigma-Aldrich, USA. All chemicals, reagents, buffers, media and plasticwares (SPL Life Science) used for cell culture work were of cell culture grade.

### 5.2.3 Cell culture methodology

Proper maintenance and optimal growth of the obtained cell lines were crucial for conducting successful in vitro studies. Therefore, all in vitro experiments with the cell lines were conducted in a well-equipped tissue culture laboratory, which included working within a Biosafety level 2 cabinet and other necessary facilities required for maintaining a high standard laboratory environment. Furthermore, specific procedures were followed to cultivate and sustain the cell lines as outlined below:

#### 5.2.3.1 Heat inactivation of FBS

For the heat inactivation of FBS, previously thawed bottle was placed in water bath at 56°C for 30 minutes with intermittent swirling, allowed to cool to carry out complement inactivation. Inactivated FBS was later stored at 4°C until further use. The inactivated FBS was always brought to RT whenever required for use.

---

### 5.2.3.2 Preparation of complete media

- For MCF-7/ MDA-MB-231: To 45 mL of DMEM media with 100 units/mL of penicillin and 0.1 mg/mL of streptomycin, 5 mL of heat-inactivated FBS was added to make complete medium containing 10% FBS.
- For MCF10A: It was maintained in MEM media supplemented with growth factors. As this was a serum free media, it was made complete by the addition of 100 ng/ml cholera toxin.

### 5.2.3.3 Maintenance of cell lines

To make sure the proper maintenance of cell lines following protocols were followed for maintenance, growth and freeze down the cell stock as mentioned below:

- **Revival of cell line**

The frozen cell line vial was removed from the liquid nitrogen storage tank and carefully thawed. Its contents were then transferred to a sterile 15 mL falcon tube containing pre-warmed complete medium. To remove any residual freezing media, the falcon tube was centrifuged at 1200rpm for 5 minutes at 25°C. The supernatant was discarded, and the cell pellet was resuspended in 1mL of fresh complete medium. This suspension was then transferred to a T-25 flask containing 5 mL of complete medium and placed in a CO<sub>2</sub> incubator at 37°C for subsequent growth.

- **Propagation and sub-culturing of cell line**

All media and solutions used for cell line propagation and sub-culturing were thawed and pre-warmed to 37°C to ensure optimal cell health. Once the revived cells had reached confluency of 80% or more, the culture medium from the T-25 flask was discarded. The monolayer was gently rinsed with pre-warmed DPBS, followed by the addition of 1mL of pre-warmed trypsin-EDTA solution. The flask was slightly shaken to ensure even distribution of the solution and incubated at 37°C for 3-5 minutes to facilitate cell detachment. To inactivate trypsin and collect the detached cells, complete growth medium was added to the flask, and the cell suspension was transferred to a sterile 15 mL centrifuge tube. Centrifugation at 1200 rpm for 7 minutes at 25°C separated the cells from the supernatant. The supernatant was discarded, and the cell pellet was gently resuspended in 1mL of fresh complete medium. Repeated pipetting helped create a single-cell suspension, which was then transferred to a fresh T-25 flask containing 5 mL of complete medium. Each flask was labeled with the cell line name, date, passage number,

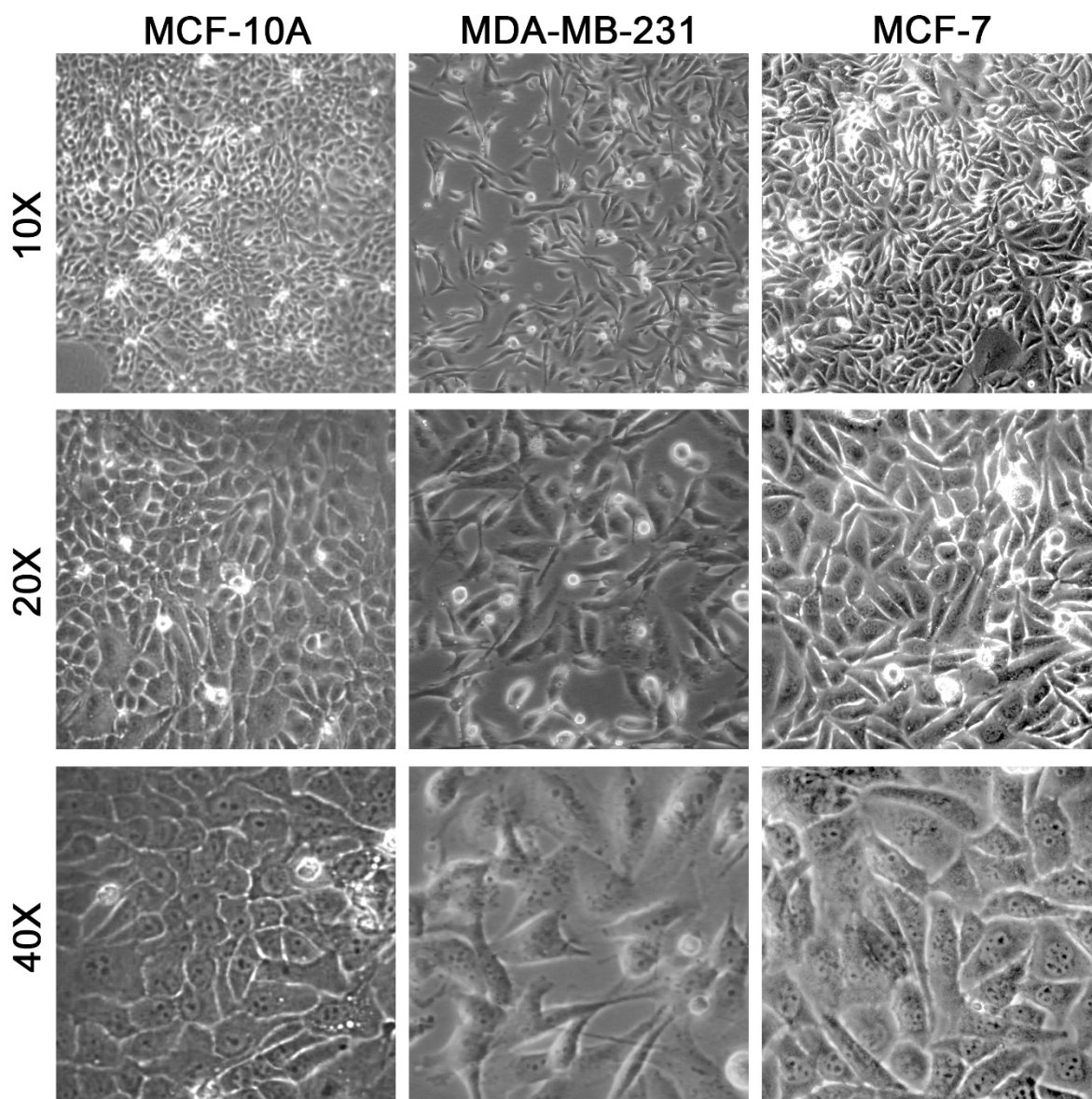
---

and initials before being placed in a CO<sub>2</sub> incubator maintained at 37°C and 5% CO<sub>2</sub>. A 1:3 split ratio was maintained for sub-culturing.

- **For MCF-10A**

MCF10A cells required a different growth medium and slightly different handling during propagation compared to the other cell lines. While the revival procedure remained the same, the incubation time with trypsin-EDTA was adjusted to 8-9 minutes. Trypsin inactivation was achieved using a specialized trypsin neutralizing medium (5% FBS in DPBS), followed by centrifugation at 1200 rpm for 7 minutes at 25 °C. After discarding the supernatant, the cell pellet was resuspended in 1mL of complete medium and transferred to a T-25 flask containing 5mL of complete medium. Proper labeling and incubation conditions followed the protocol used for the other cell lines.

These protocols ensure the successful revival, propagation, and sub-culturing of various cell lines, including the unique requirements of MCF-10A, allowing researchers to conduct diverse studies with healthy and viable cells.



**Figure 5.6** Phase contrast microscopy images of the cell lines MCF-10A, MDA-MB-231 and MCF-7 as observed under 10×, 20× and 40× magnifications.

- Freeze down of cell line

Following sub-culturing, cells were cryopreserved to ensure their availability for future experiments. This practice ensured a readily accessible stock of frozen cell lines. The freezing process mirrored the sub-culturing protocol, with specific modifications. After resuspension in complete medium, cells were stained with trypan blue and counted using a hemocytometer slide. The cell suspension was then centrifuged, and the pellet was resuspended in an appropriate volume of freezing media to achieve a final concentration of  $1.5\text{--}2 \times 10^6$  cells/ mL of freezing medium (**Table 5. 1**). Each cryo-vial was filled with approximately 1mL of this

cell-containing freezing media. Notably, the freezing media was kept at 4°C prior to use, as the cryoprotectant DMSO exhibits cytotoxicity at room temperature.

**Table 5. 1** Optimized conditions for maintenance of cell lines

Name of cell line	MCF-10A	MCF-7	MDA- MB-231
<b>Origin</b>	<i>Homo sapiens</i> ,human	<i>Homo sapiens</i> ,human	<i>Homo sapiens</i> ,human
<b>Cell type</b>	Epithelial	Epithelial	Epithelial
<b>Growth medium</b>	MEBM + growth factors+100 ng/ml Cholera toxin	DMEM+10%FBS	DMEM+10%FBS
<b>Culture properties</b>	Adherent	Adherent	Adherent
<b>Split ratio</b>	1:3	1:3	1:2
<b>Freezing media</b>	Complete growth medium supplemented with 7.5% DMSO	70% complete media + 25% FBS + 5% DMSO	65% Complete media+ 25% FBS + 10% DMSO

The cryo-vials were carefully sealed with parafilm and placed in a Mr. Frosty container filled with 100% isopropanol. This container served to maintain a gradual temperature decrease, protecting the cells from experiencing a sudden cold shock. Following this, the vials were subjected to a stepwise cooling process: 20 mins at 0°C, 1 hour at -20°C, and overnight at -80°C. The Mr. Frosty's gradual cooling prevented harmful ice crystal formation within the cells, thereby preserving their viability.

After this overnight step at -80°C, the vials were transferred to a cryo-box and submerged in liquid nitrogen for long-term storage throughout the cell culture experiments. Cells between passages 3 and 10 were typically frozen and later thawed, revived in complete medium, and propagated for conducting all the subsequent cell experiments throughout the study. This cryopreservation methodology ensured a reliable and readily available source of cells for future research endeavors.



---

### 5.2.4 MTT Cellular viability assay (in vitro cell cytotoxicity assay)

To assess the cytotoxicity of the synthesized nanosystem, a comprehensive MTT assay was conducted across three different cell lines: MCF-7, MDA-MB-231, and MCF-10A. The study aimed to investigate the dose and time-dependent effects of bare ZnONPs, MTX-ZnONPs, and MTX on these cell lines. Briefly,  $10^4$  cells per well were seeded into a 96-well plate and incubated for 24 hours at  $37^\circ\text{C}$  with 5%  $\text{CO}_2$  to allow proper attachment. Subsequently, the cells were exposed to various concentrations of bare ZnONPs (6.25, 12.5, 25, 50, and 100  $\mu\text{g/mL}$ ) and MTX-ZnONPs, alongside MTX as a positive control with equivalent concentrations of MTX equivalent to its loading concentration on NP. All systems were prepared in serum-free media. Untreated control wells received only 100  $\mu\text{L}$  of serum-free media on treatment day. Following treatment, the plates were further incubated for 24 and 48 hours under the same conditions. At the end of each incubation period, cell viability was assessed by adding 20  $\mu\text{L}$  of MTT solution (5 mg/ mL) to each well and incubating for an additional 3 hours. The resulting intracellular formazan crystals were then dissolved in 100  $\mu\text{L}$  of DMSO. The absorbance of the dissolved crystals was measured at 570 nm, with 650 nm serving as the reference wavelength, using a BioTek EPOCH 2 microplate reader. Percent cell viability was calculated using the following equation 5.1.

$$\% \text{ Cell viability} = \frac{\text{O.D of Test}}{\text{O.D of control}} \times 100 \quad \dots 5.1$$

### 5.2.5 Acridine Orange/ Ethidium Bromide (AO/EB) viability staining

To further explore the interaction of ZnONPs, MTX-ZnONPs, and MTX with different cell lines microscopically, a study was conducted using MCF-7, MDA-MB-231, and MCF-10A cells.  $10^5$  cells per well were seeded in 6-well flat-bottomed plates and incubated for 24 hours at  $37^\circ\text{C}$  with 5%  $\text{CO}_2$  under humidified condition. Based on the previously determined  $\text{IC}_{50}$  values from the MTT assay, three different concentrations of Bare ZnONPs, MTX-ZnONPs, and MTX were used for each cell line: MCF-7: 2.5, 5.0, and 7.5  $\mu\text{g/mL}$ ; MDA-MB-231: 40, 50, and 60  $\mu\text{g/mL}$ ; and MCF-10A: 10, 20, and 30  $\mu\text{g/mL}$ . Following treatment, cells were washed with DPBS and then incubated with a 1:1 mixture of AO and EB (each at 100  $\mu\text{g/mL}$  in DPBS) for less than a minute. Excess stain was removed, and the cells were readily visualized under microscope immediately. The stained cells were later visualized under an inverted fluorescent phase-contrast microscope (Zeiss, Jena, Germany).

---

### 5.2.6 Cell cycle analysis by flowcytometry

To evaluate the impact of bare ZnONPs, MTX-ZnONPs, and MTX on cell viability, a detailed flow cytometric analysis was performed. Cells were initially seeded in 6-well plates at concentration of  $10^5$  cells per well and incubated overnight for attachment. The following day, they were treated with the test systems for 24 hours, while control wells received only culture media. After treatment, cells were washed with DPBS to remove any residual media and then gently trypsinized to harvest them. Centrifugation and subsequent DPBS washes further purified the cell pellets. To prepare for flow cytometric analysis, cells were fixed with chilled 70% ethanol in PBS to preserve their internal structures. This was added dropwise with constant vortexing into the pellet, followed by storage at  $-20^{\circ}\text{C}$ . Before analysis, cells were resuspended in chilled PBS containing PI and RNase A. PI stains dead cells with compromised membranes, while RNase A degrades cellular RNA, facilitating DNA staining. After incubation in the dark for 30 minutes, a minimum of 10,000 events were acquired using a BD FACS Aria Special Order System flow cytometer.

### 5.2.7 Annexin V FITC- Propidium Iodide assay

To assess the apoptotic potential of bare ZnONPs, MTX-ZnONPs, and MTX, a modified version of the manufacturer's protocol for the FITC Annexin V Apoptosis detection kit (BD pharmingen™) was employed (Fernandes et al., 2023). Cells were seeded in 6-well plates at a density of  $10^5$  cells per well and incubated overnight for proper attachment. The following day, they were treated with the test compounds (bare ZnONPs, MTX-ZnONPs, and MTX) for 24 hours. After treatment, cells were harvested and washed to remove any residual media. The cell pellets were then resuspended in 100  $\mu\text{L}$  of chilled 1X binding buffer and stained with both Annexin V-FITC and PI according to the manufacturer's instructions. The incubation time was reduced to 10 minutes for improved efficiency. Following staining, 400  $\mu\text{L}$  of chilled 1X binding buffer was added to each sample, and they were immediately analyzed using a BD FACS Aria Special Order System flow cytometer. A minimum of 10,000 events were recorded for each sample to ensure statistically relevant data using a BD FACS Aria Special Order System flow cytometer. A heat shock control (incubated at  $55^{\circ}\text{C}$  for 20 minutes) was included to induce maximum apoptosis and serve as a positive control for Annexin V-FITC staining only. Untreated cells stained with both Annexin V-FITC and PI served as a negative control for apoptotic events.

---

### 5.2.8 Western blot analysis

To investigate the protein expression changes induced by bare ZnONPs, MTX-ZnONPs, and MTX, western blot analysis was performed following a modified protocol adapted from previous reports (Virdi and Pethe, 2022). Briefly, cells treated for 24 hours were harvested and lysed in chilled lysis buffer containing protease inhibitors on ice for 30 minutes with intermittent mixing. After centrifugation at 13,000g for 20 mins at 4°C, the protein-rich supernatant was collected, and its concentration was determined using the Bradford assay. Protein samples (20 µg) were then separated on 12% SDS-PAGE gels and transferred to PVDF membranes. The membranes were blocked with 5% NFDM in 1X Tris-buffered saline (TBST) for 1.5 hours at room temperature. Specific primary antibodies targeting key apoptotic markers such as Caspase-3, Caspase-7, Bcl-xL, Bax were used. Primary rabbit antibodies against Caspase-3, Caspase-7, Bcl-xL, Bax (Cell Signaling Technologies), were then applied and incubated overnight at 4°C. Mouse β-Actin (Sigma) was used as a loading control with its corresponding primary antibody. Following, thorough washing to remove unbound primary antibodies, secondary antibodies conjugated to HRP (GeNei™) were added for 1 hour at room temperature. After additional washes to remove unbound secondary antibodies, the blots were developed using Clarity reagent and imaged using a ChemiDoc XRS+ Gel Imaging System (Bio-Rad, USA). Finally, protein band intensities were quantified using ImageJ software to provide quantitative analysis of protein expression changes.

## 5.3 Results

### 5.3.1 MTT Cellular viability assay (in vitro cell cytotoxicity assay)

Analyzing the cytotoxic effects of MTX-ZnONPs against three breast cell lines reveals their promising potential, particularly against drug-resistant MDA-MB-231 cells. **Figure 5.7** demonstrates their time and dose dependent activity, exceeding that of MTX across all cell lines. MTX-ZnONPs exhibit exceptional potency, boasting the lowest IC<sub>50</sub> value (5 µg/mL) for MCF-7 cells, followed by MCF-10A (18 µg/mL) and MDA-MB-231 (49 µg/mL). Notably, bare ZnONPs show the highest toxicity towards MCF-10A (IC<sub>50</sub>: 13 µg/mL), highlighting the potential need for further optimization.

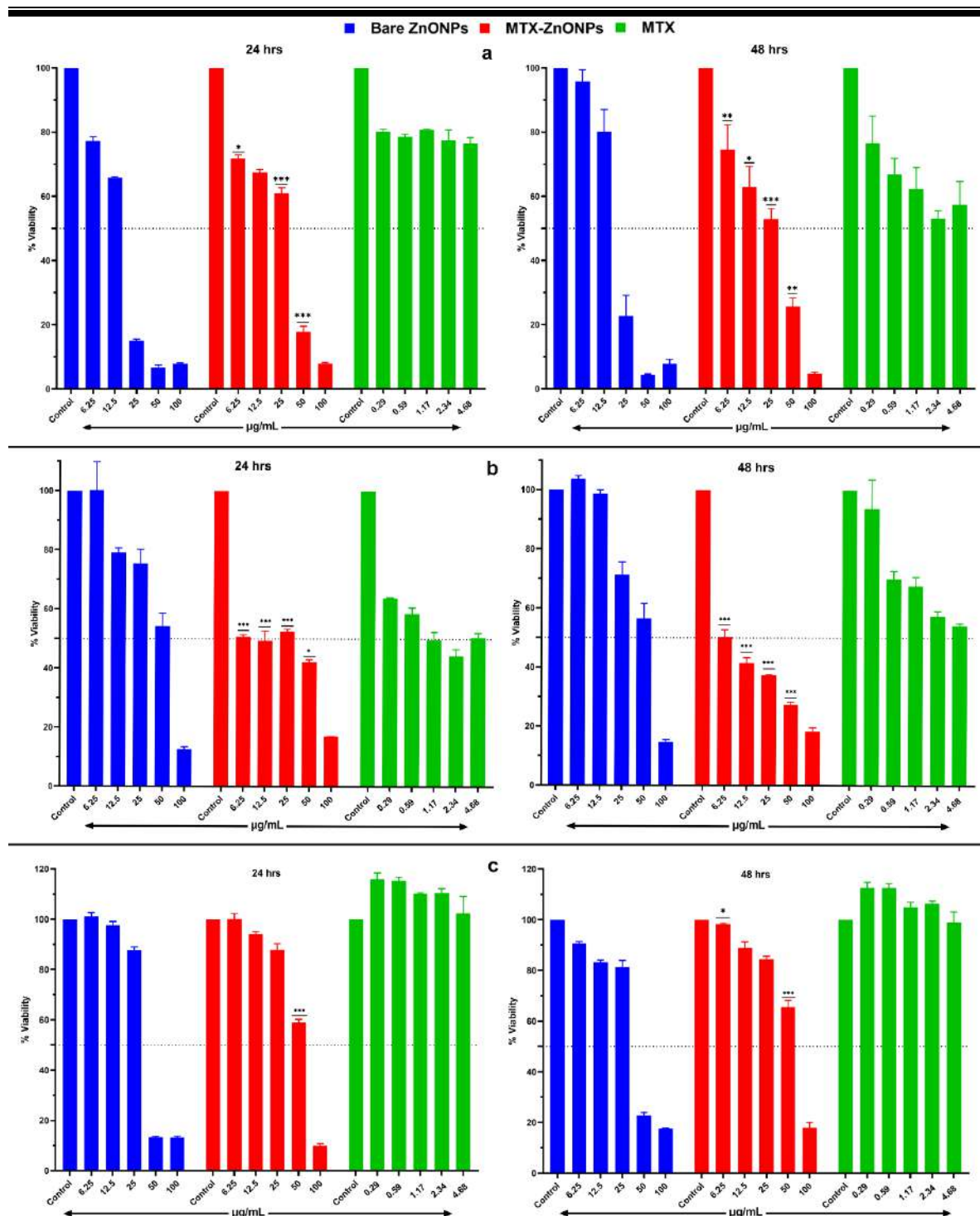
The underlying mechanism of MTX-ZnONPs toxicity likely involves Zn<sup>2+</sup> ion release in the acidic environment of cancer cells, inducing oxidative stress and releasing MTX payload (Liu et al., 2016; Xiong, 2013). This stress damages cellular components, generating ROS and triggering apoptosis (Rasmussen et al., 2010). MTX, a structural mimic of folic acid, utilizes the same transport receptor (FAR) for cellular entry. Once inside, it undergoes

---

---

polyglutamylation, activating its purine/pyrimidine synthesis inhibition, ultimately leading to cell death (Bryan, 2012). However, sensitivity varies based on FAR expression (Bath et al., 2014; Hess and Khasawneh, 2015), explaining the high MDA-MB-231 viability due to their reported MTX resistance (Corona et al., 1998; Worm et al., 2001).

Importantly, MTX-ZnONPs not only demonstrate superior efficacy against MCF-7 cells but also exhibit noteworthy activity against drug-resistant MDA-MB-231 cells, surpassing MTX alone. Furthermore, the remarkable cell viability observed in MCF-10A, a non-cancerous epithelial cell line, suggests the safe and biocompatible nature of MTX-ZnONPs and their selectivity towards cancer cells.



**Figure 5.7** Effect of bare ZnONPs, MTX-ZnONPs and MTX on mitochondrial function in (a) MCF-10A (b) MCF-7 (c) MDA-MB-231 cells. Cell viability was determined by the MTT reduction assay after 24 hrs and 48 hrs. Data presented are mean  $\pm$  SD. Asterisk above columns indicate statistically significant difference compared to bare ZnONPs (\*\*\*= $p < 0.001$ , \*\*= $p < 0.01$ , \*= $p < 0.05$ )

---

### 5.3.2 Acridine Orange/ Ethidium Bromide (AO/EB) viability staining

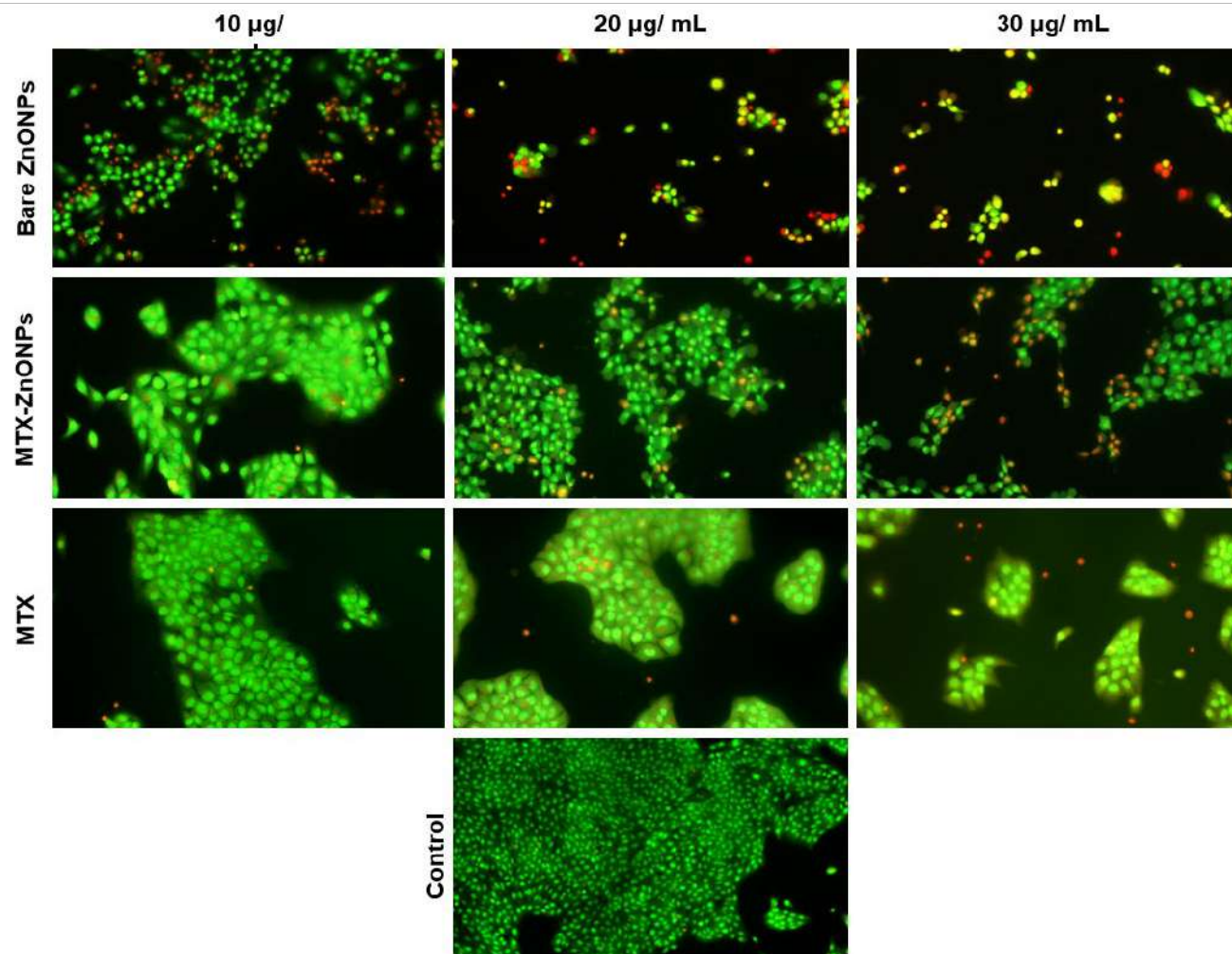
Examining the cellular morphology of treated cells reveals distinct responses across the different doses. Normal MCF-10A cells in **Figure 5.8** displayed uniform green fluorescence and intact nuclei, indicative of healthy epithelial morphology. However, dose-dependent effects were observed all doses. Bare ZnONPs, with their lower  $IC_{50}$  and higher toxicity, showed pronounced damage even at low doses, with signs of rounding, detachment, and even apoptosis and necrosis at higher concentrations. MTX-ZnONPs, due to their higher  $IC_{50}$ , exhibited less toxicity compared to bare ZnONPs. at higher doses, some necrotic cells with orange-red fluorescence were observed. Notably, both MTX-ZnONPs and MTX treatment resulted in enlarged cells with prominent nuclei, likely due to MTX's known ability to stall the cell cycle in S phase, leading to DNA/RNA accumulation and consequent cell size increase (Marika Grönroos et al., 2006; Taylor and Tattersall, 1981).

Similar observations were found in MCF-7 cells **Figure 5.9**, with MTX showing minimal damage and MTX-ZnONPs demonstrating more cytotoxicity compared to MTX alone. MTX-ZnONPs caused reduced cell confluency, condensed nuclei, and bright green granular nuclei (a hallmark of early apoptosis), progressing to loss of attachment and shrinkage at higher concentrations. MTX treatment elicited similar morphological cues. In contrast, bare ZnONPs had negligible impact on these cells, reflecting their high  $IC_{50}$  for MCF-7, while MTX also displayed damage and apoptosis alongside detachment.

Interestingly, the pattern reversed in MDA-MB-231 cells **Figure 5.10**. MTX treatment again had minimal impact, while MTX-ZnONPs displayed comparatively more cytotoxicity. Here, MTX-ZnONPs resulted in reduced confluency, condensed nuclei, and early apoptotic features, progressing to morphological changes and loss of attachment at higher concentrations. MTX also showed damage and apoptosis, similar to the other cell lines. In contrast, bare ZnONPs, while demonstrating less cytotoxicity than MTX-ZnONPs, still had higher confluency and minimal damage compared to the other treatments, reflecting their lower  $IC_{50}$  for MDA-MB-231 cells.

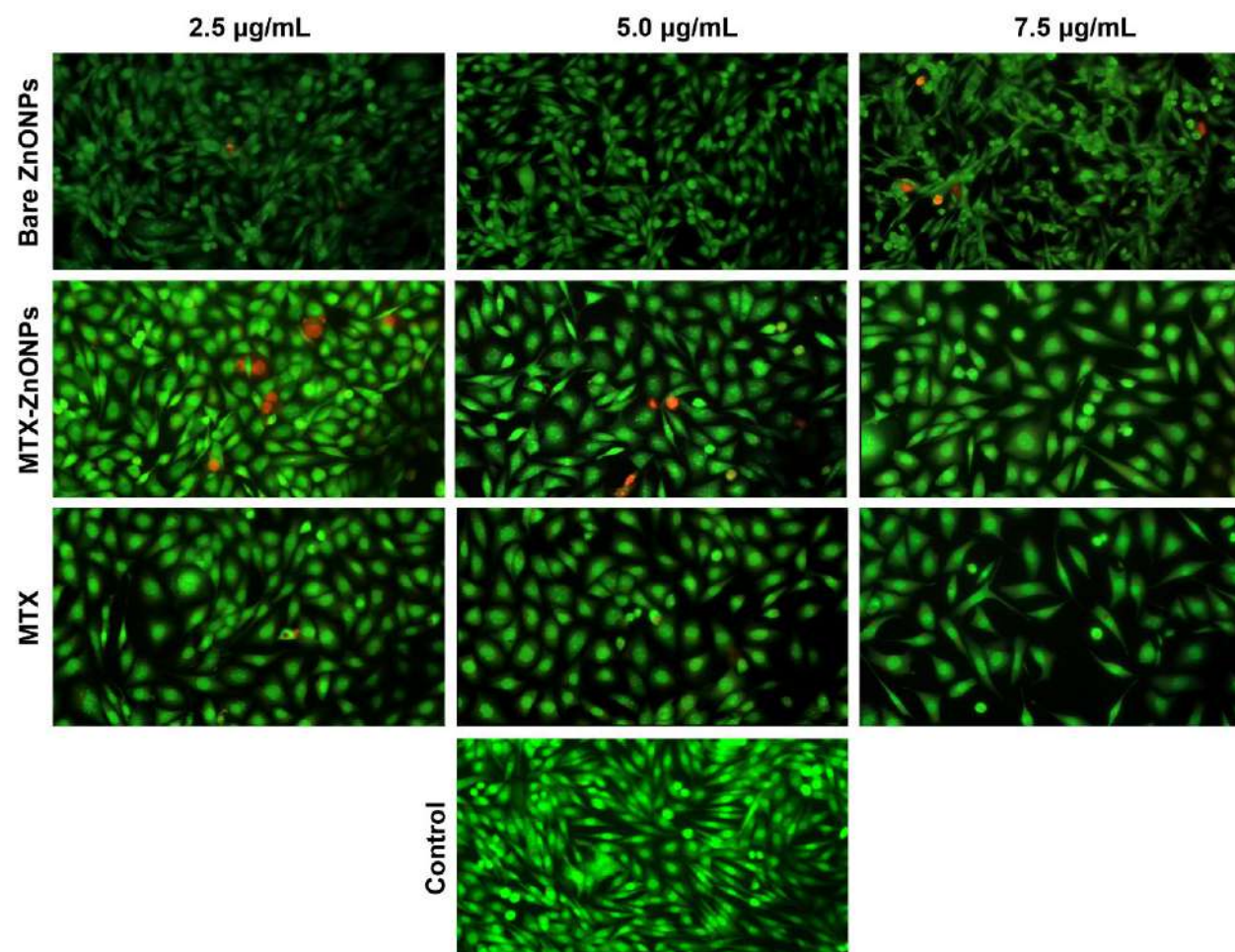
Study highlights the distinct effects of different treatments on cell morphology across all three cell lines. MTX-ZnONPs emerge as potent cytotoxic agents, particularly against MDA-MB-231 cells, while retaining some selectivity towards cancer cells over control MCF-10A cells. Bare ZnONPs, while cytotoxic, seem less selective. MTX as expected displayed cell line specific sensitivity comparable MTT results.

---



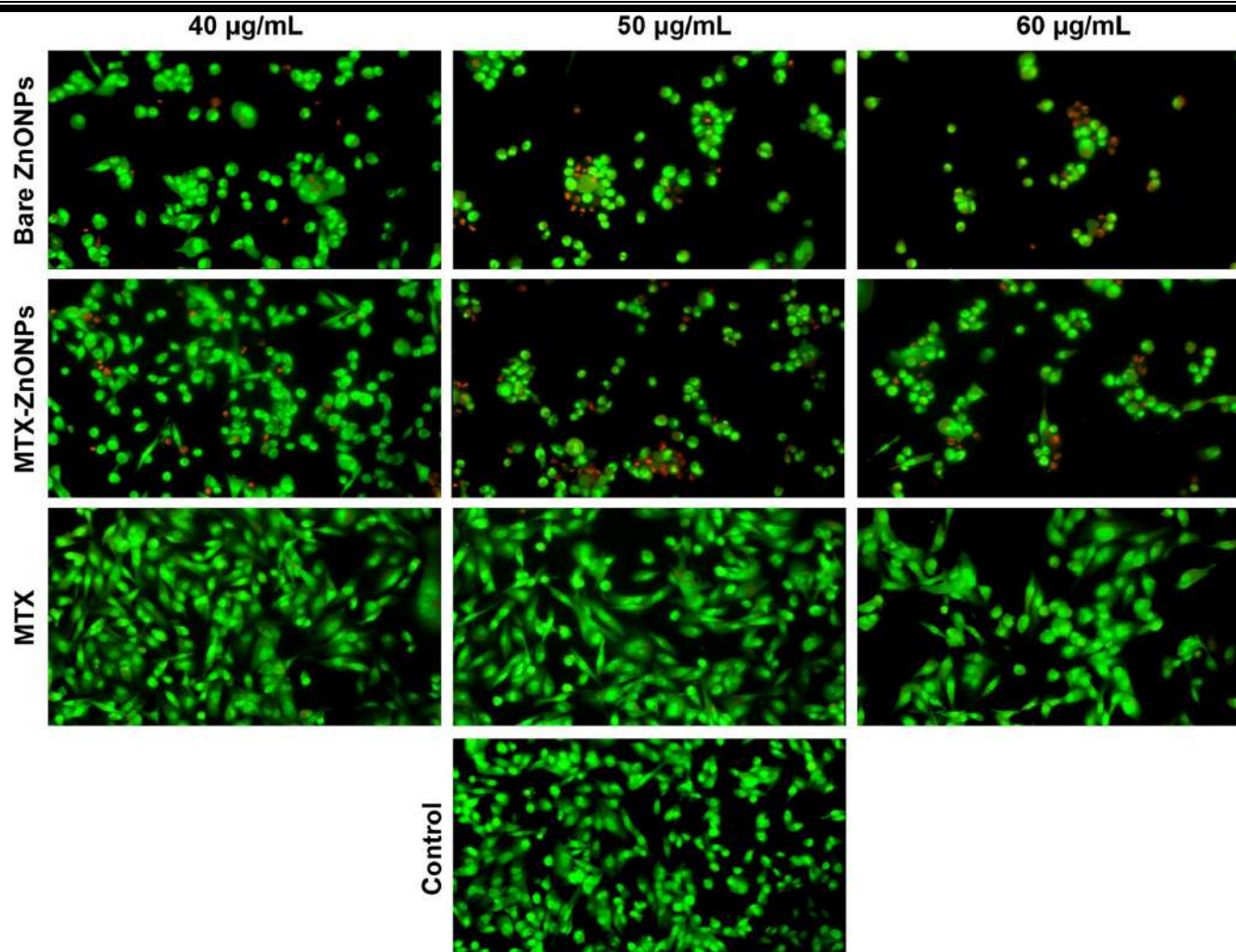
**Figure 5.8** AO/EB dual staining of MCF-10A cells for live dead cell screening treated with bare ZnONPs, MTX-ZnONPs and MTX at concentration range of 10-30  $\mu\text{g/ mL}$ . Magnification: 20X





**Figure 5.9** AO/EB dual staining of MCF-7 cells for live dead cell screening treated with bare ZnONPs, MTX-ZnONPs and MTX at concentration range of 2.5-7.5  $\mu\text{g/mL}$ . Magnification: 20



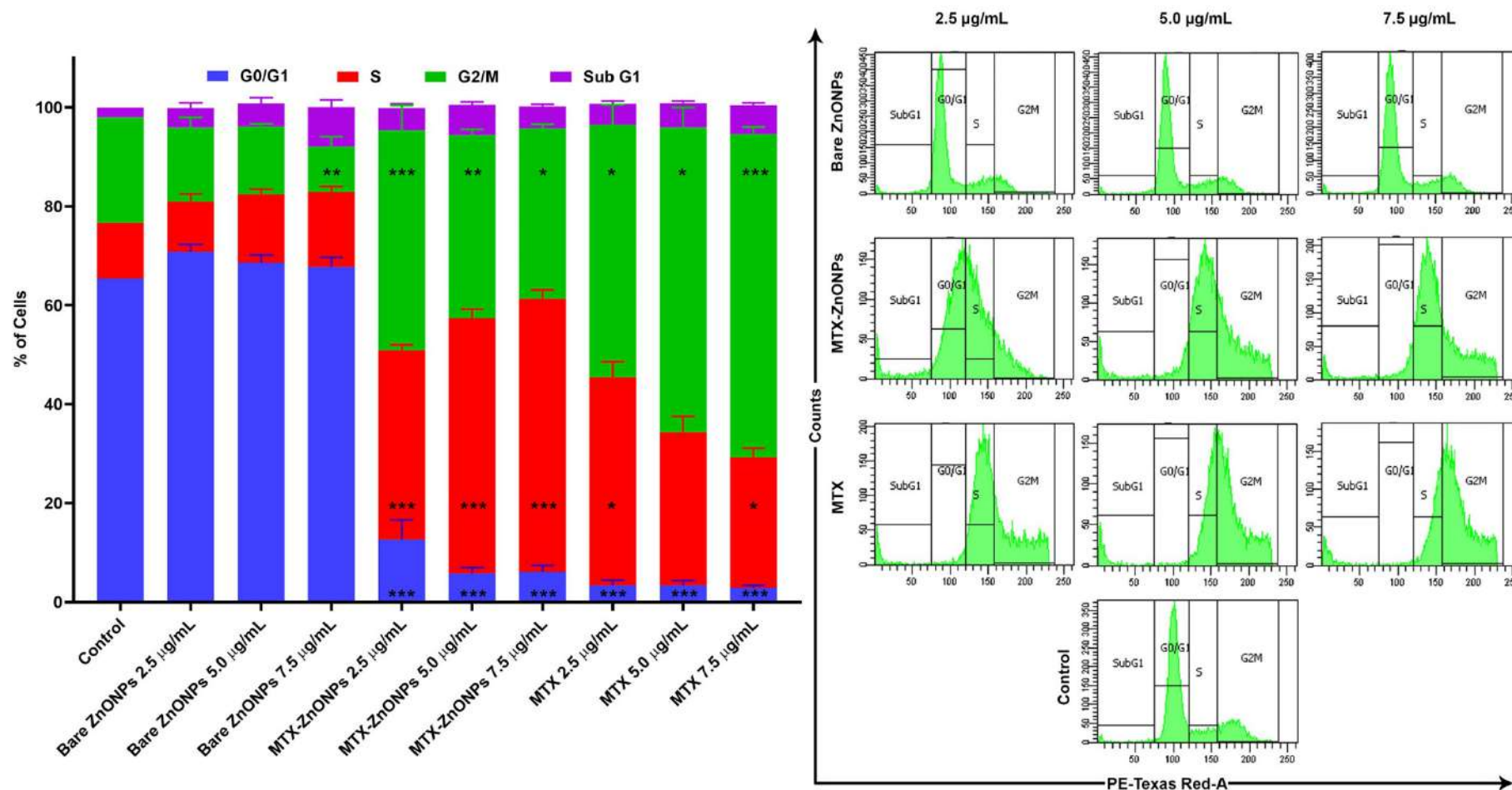


**Figure 5.10** AO/EB dual staining of MDA-MB-231 cells for live dead cell screening treated with bare ZnONPs, MTX-ZnONPs and MTX at concentration range of 40-60  $\mu\text{g/mL}$ . Magnification: 20X

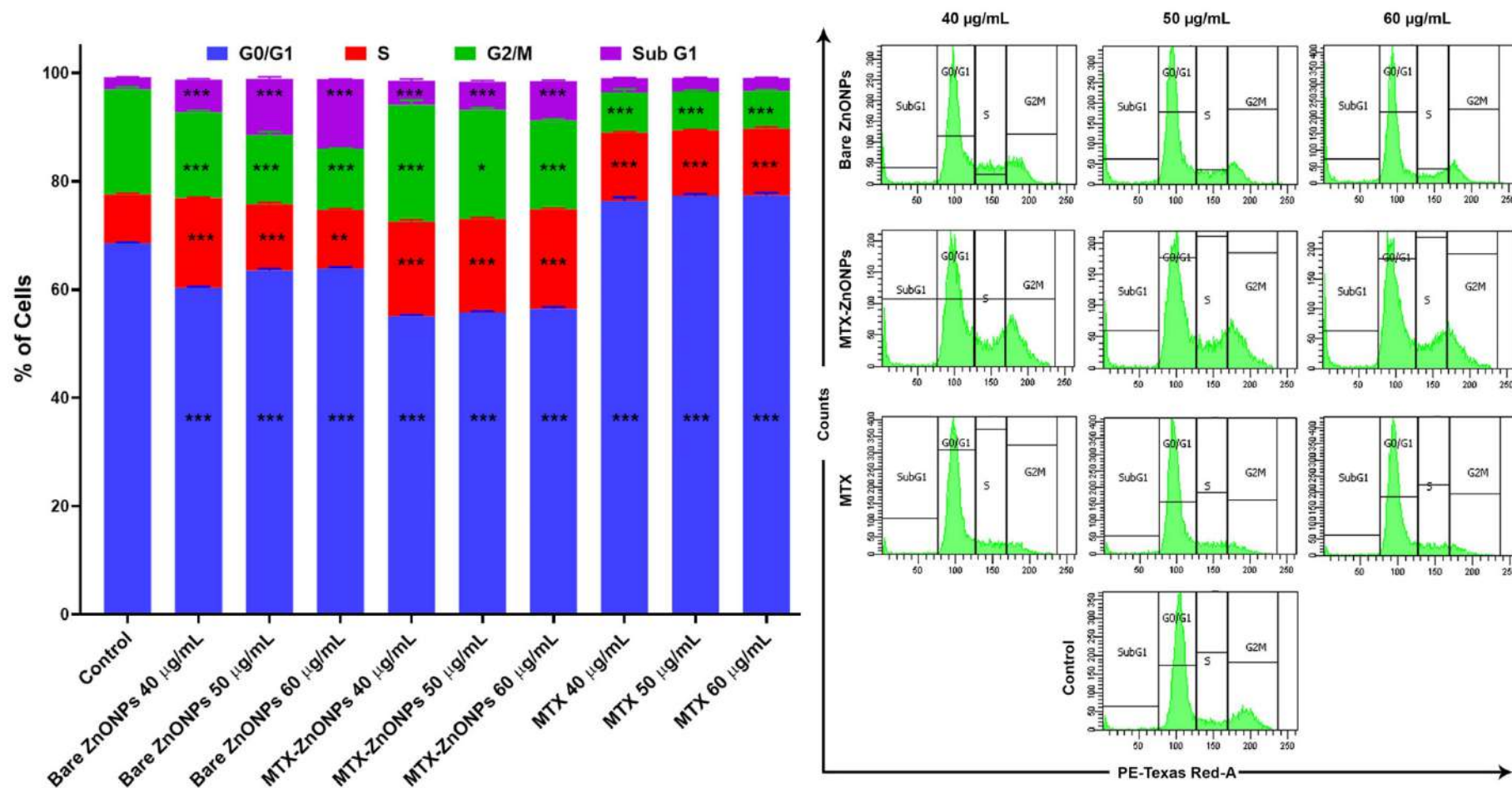
---

### 5.3.3 Cell cycle analysis by flowcytometry

Examining the cell cycle profiles of MCF-7 and MDA-MB-231 cells exposed to bare ZnONPs, MTX-ZnONPs, and MTX revealed interesting differences. Untreated and bare ZnONP-treated cells in both lines exhibited standard cell cycle progression, with a majority in the G0/G1 phase (active growth). As seen in **Figure 5.11** MTX-ZnONPs, however, displayed a distinct effect in MCF-7 cells, inducing a concentration-dependent arrest in the S phase (DNA synthesis). This S-phase arrest mirrored the activity of MTX alone, likely due to the presence of MTX within the MTX-ZnONPs. Interestingly, MTX treatment in MDA-MB-231 cells, which are known for their MTX resistance, resulted in a G0/G1 arrest, contrasting the S-phase arrest observed in MCF-7 in **Figure 5.12**. Despite this resistance, MTX-ZnONPs induced a dose-dependent shift towards the S phase in MDA-MB-231, suggesting a potentially enhanced effect compared to MTX alone. Notably, across all treatments, MTX-ZnONPs consistently displayed the lowest G0/G1 population (less than 60%), indicating a potential shift towards other phases. Additionally, a dose-dependent increase in the sub-G1 population (apoptotic cells) was observed in both bare ZnONP and MTX-ZnONP groups, suggesting cell death induction. Overall, these findings suggest that MTX-ZnONPs exhibit cell cycle-specific arrest in both MCF-7 and MDA-MB-231 cells, with MCF-7 experiencing an S-phase arrest and MDA-MB-231 exhibiting a shift towards the S phase compared to MTX alone. This difference in response highlights the potential for MTX-ZnONPs to overcome MTX resistance in certain cancer cells.



**Figure 5.11** Cell cycle analysis by PI staining for MCF-7 cells treated with bare ZnONPs, MTX-ZnONPs and MTX for 24 hrs. Data is presented as Bar graph (left) and Histogram (right). Asterisk in the columns indicate statistically significant difference compared to control group (\* $p \leq 0.05$ ; \*\* $p \leq 0.01$ ; \*\*\* $p \leq 0.001$ )



**Figure 5.12** Cell cycle analysis by PI staining for MDA-MB-231 cells treated with bare ZnONPs, MTX-ZnONPs and MTX for 24 hrs. Data is presented as Bar graph (left) and Histogram (right). Asterisk in the columns indicate statistically significant difference compared to control group (\* $p \leq 0.05$ ; \*\* $p \leq 0.01$ ; \*\*\* $p \leq 0.001$ )

---

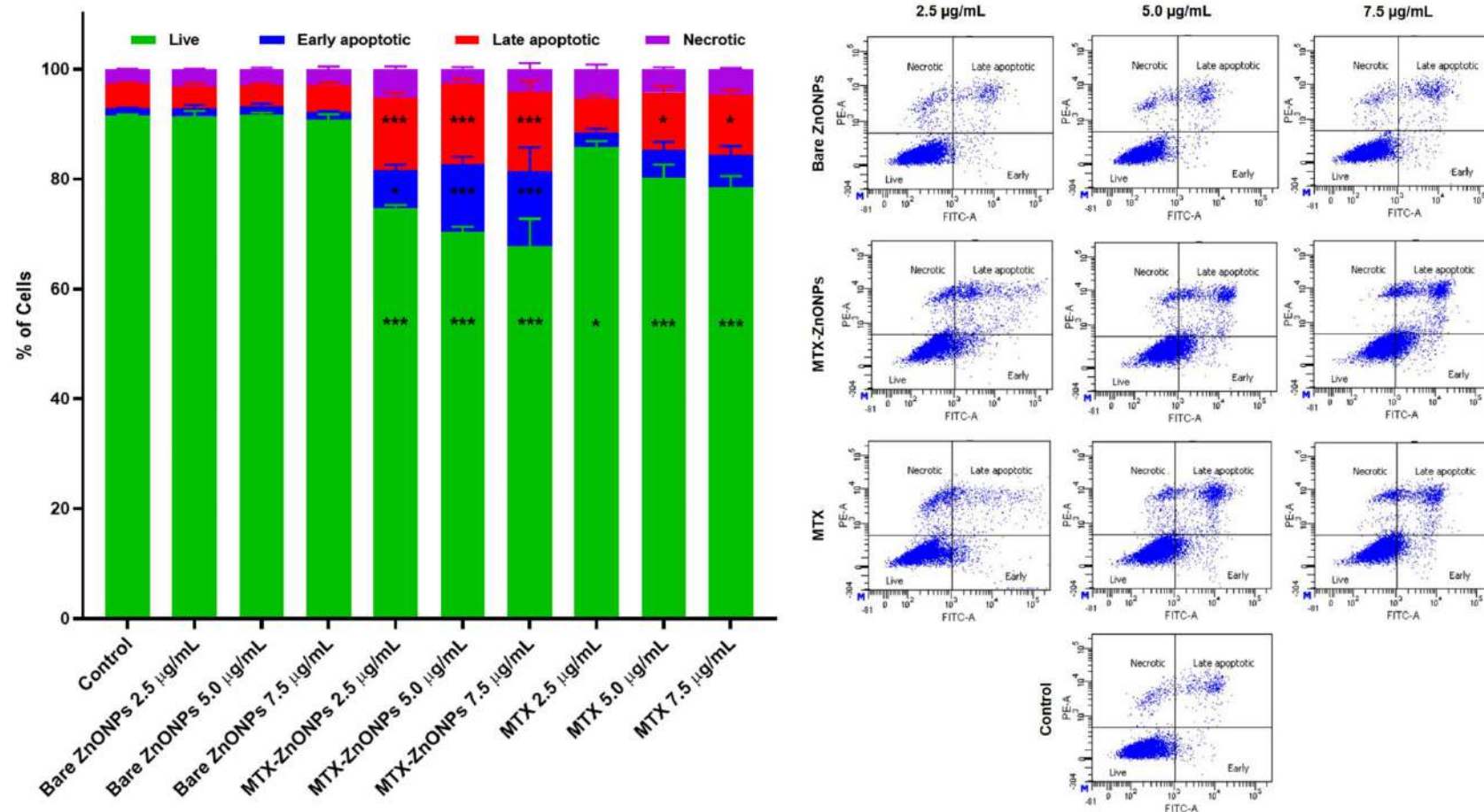
#### 5.3.4 Annexin V FITC- Propidium Iodide assay

The results of the apoptosis assay, illustrated in **Figure 5.13** and **Figure 5.14** reveal distinct vulnerabilities of the two cell lines to the various treatments. As expected, MCF-7 cells, known for their MTX sensitivity, displayed dose-dependent toxicity. This manifested as a shift from early to late apoptosis with increasing MTX concentrations. Similarly, MTX-ZnONPs induced significantly higher levels of apoptosis compared to all other groups in MCF-7 cells. In contrast, bare ZnONPs had minimal impact on MCF-7 viability, resulting in a larger proportion of live cell population comparable to that of untreated control.

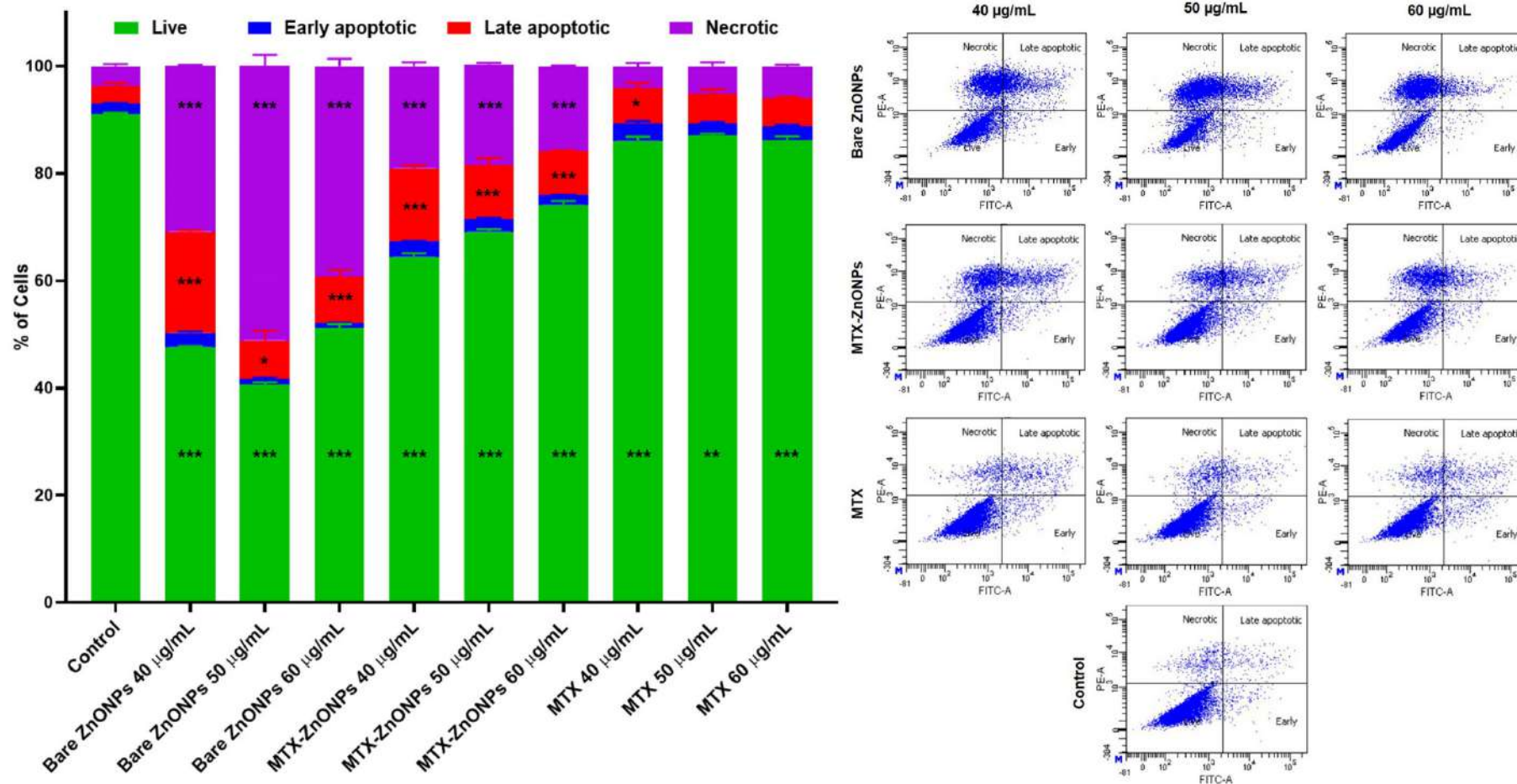
In MTX-resistant MDA-MB-231 cells, MTX at different concentrations failed to induce any significant apoptosis, confirming their inherent resistance. However, bare ZnONPs, with their lower IC<sub>50</sub> values, triggered increased cell death compared to other treatments. Both bare ZnONPs and MTX-ZnONPs led to cytotoxicity in MDA-MB-231, with majority of dead cells identified as necrotic or late apoptotic. Notably, MTX-ZnONPs exhibited a significantly higher fraction of dead cells compared to MTX alone at the same concentrations, suggesting its enhanced cytotoxic potential against even resistant cell lines.

Overall, these findings demonstrate the remarkable ability of MTX-ZnONPs to induce toxicity in both breast cancer cell lines, regardless of their MTX sensitivity, through both apoptotic and necrotic pathways. This suggests potential therapeutic advantages of MTX-ZnONPs in overcoming drug resistance and broadening treatment options for aggressive cancers.





**Figure 5.13** Apoptosis analysis by Annexin V-FITC/ PI for MCF-7 cells treated with bare ZnONPs, MTX-ZnONPs and MTX for 24 hrs. Data is presented as Bar graph (left) and Scatter plot (right). Asterisk in the columns indicate statistically significant difference compared to control group (\* $p \leq 0.05$ ; \*\* $p \leq 0.01$ ; \*\*\* $p \leq 0.001$ )



---

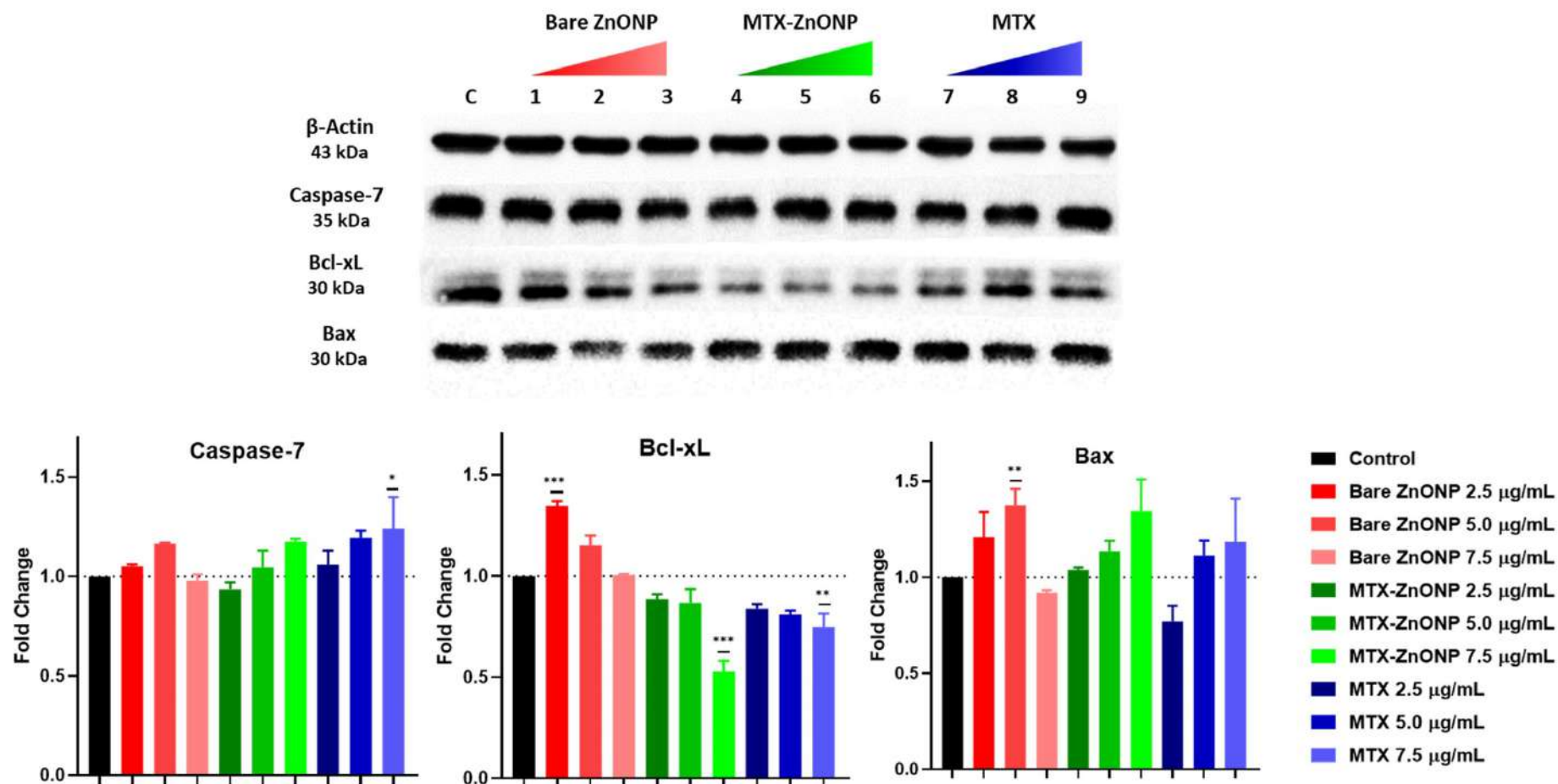
### 5.3.5 Western blot analysis

Analyzing the protein expression patterns in MCF-7 and MDA-MB-231 cells after treatment reveals distinct mechanisms of cell death induced by MTX-ZnONPs. As its visible in **Figure 5.15**, MTX-ZnONPs triggered a dose-dependent increase in Caspase-3, the key executioner caspase responsible for the final stages of apoptosis in MCF-7 cells. This was accompanied by elevated Bax levels, a pro-apoptotic protein promoting cell death by disrupting mitochondrial membranes (Roshini et al., 2017). Conversely, Bcl-xL, an anti-apoptotic protein from the same Bcl family that competes with Bax, exhibited dose-dependent downregulation (Tian et al., 2020). This classical pattern of pro-apoptotic protein upregulation and anti-apoptotic protein downregulation strongly suggests apoptosis as the predominant cell death pathway in MTX-ZnONP-treated MCF-7 cells (Xu et al., 2013).

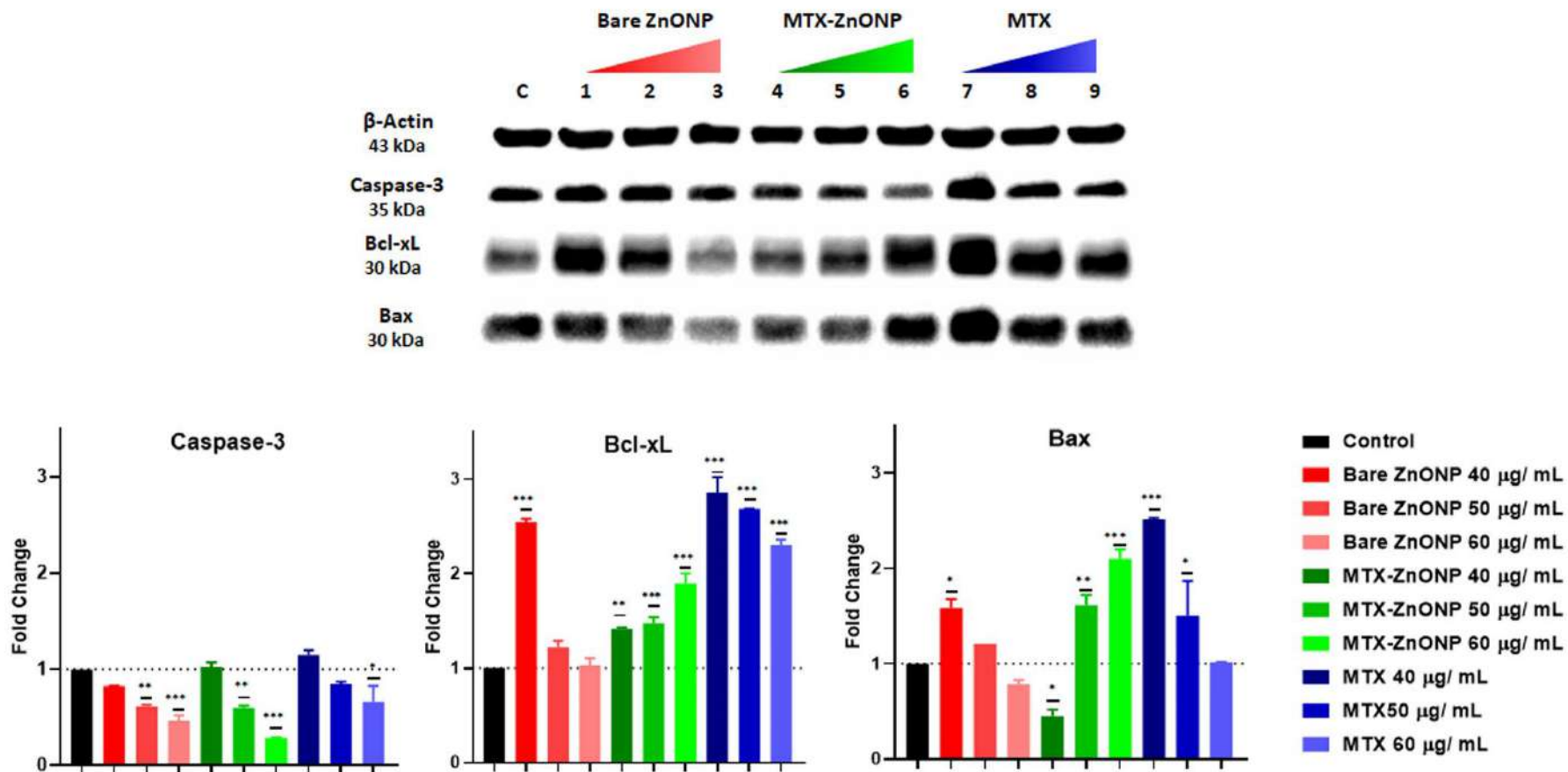
However, a different picture emerged in MDA-MB-231 cells in **Figure 5.16**. Here, Caspase-3 remained unchanged across all treatment groups, hinting at non-apoptotic cell death. Interestingly, both Bcl-xL and Bax showed dose-dependent upregulation in MTX-ZnONP-treated and, to a lesser extent, MTX-treated cells. While Bax can be associated with both apoptosis and necrosis (Jason Karch, 2018; Whelan et al., 2012), the consistent absence of Caspase-3 activation suggests necrosis as the primary mode of cell death in MDA-MB-231 cells. Additionally, the upregulation of Bcl-xL, known to suppress apoptosis and promote cell survival in response to chemotherapeutic agents (Xu et al., 2013), aligns with the known MTX resistance of MDA-MB-231 cells. Thus, it appears that Bcl-xL overexpression hinders the apoptotic pathway in these cells, allowing them to evade MTX-induced cell death and potentially contributing to their resistance.

In conclusion, MTX-ZnONPs induce distinct cell death mechanisms in MCF-7 and MDA-MB-231 cells. MCF-7 cells undergo classic apoptosis through Caspase-3 activation and Bax-mediated Bcl-xL downregulation. In contrast, MDA-MB-231 cells primarily exhibit necrosis, likely driven by Bax upregulation but lacking Caspase-3 activation. Furthermore, Bcl-xL overexpression in MDA-MB-231 cells might play a role in their MTX resistance by blocking the apoptotic pathway. These findings suggest that MTX-ZnONPs may have broad anti-cancer potential by triggering alternative cell death pathways, even in drug-resistant cells.





**Figure 5.15** Western blot analysis for MCF-7 cells treated with bare ZnONPs, MTX-ZnONPs and MTX for 24 hrs. Asterisk in the columns indicate statistically significant difference compared to control group (\* $p \leq 0.05$ ; \*\* $p \leq 0.01$ ; \*\*\* $p \leq 0.001$ )



**Figure 5.16** Western blot analysis for MDA-MB-231 cells treated with bare ZnONPs, MTX-ZnONPs and MTX for 24 hrs. Asterisk in the columns indicate statistically significant difference compared to control group (\* $p \leq 0.05$ ; \*\* $p \leq 0.01$ ; \*\*\* $p \leq 0.001$ )

---

## 5.4 Discussion

In vitro cytotoxicity assays were performed to understand the toxicity and mechanism of action of these NPs on breast cancer cells. In this study, we evaluated the impact of synthesized nano systems on cancer cell viability through comprehensive assays and staining techniques. MTT cell viability assay in MCF-7, MDA-MB-231 breast cancer cell line and MCF-10A control cell line showed high cytotoxicity of bare ZnONPs in control cells than cancer cells. As a result of MTX being present on the outer surface of MTX-ZnONPs, they demonstrated less reactivity to MCF-10A control cells compared to bare ZnONPs, which exhibited higher toxicity in MCF-10A. On the other hand, when treated with MCF-7 cells, MTX-ZnONPs in MCF-7 cells showed lower  $IC_{50}$  values due to their selectivity to cancer cells. However, when the MTX-ZnONP combination nanosystem was used to treat the MDA-MB-231 cells, which are resistant to MTX, the cells were killed at a much higher rate than they have been with MTX alone. Study conducted by Lindgren et al., focused on treatment of TNBC cell line MDA-MB-231 using cell penetrating peptide-drug conjugate which was effective in terms of killing the MTX-resistant MDA-MB-231 cells in vitro. In fact, they also showed that MDA-MB-231 cells had 100-fold resistance to MTX with the  $EC_{50}$  values as high as 18.5 mM in MDA-MB-231 cells in contrast to its counterpart MCF-7 breast cancer cells (Lindgren et al., 2006). It was noticed that due to high reactivity of bare ZnONP, it displayed lower  $IC_{50}$  values than that of MTX-ZnONPs in MDA-MB-231 cell line. In one of the recent study the effect of MTX loaded ZnONPs was studied on A549 lung cancer cells. It was interesting that the MTX loaded ZnONPs were more profound at extremely low doses compared to that of free MTX, signifying that the conjugation of MTX with ZnONPs enhanced the apoptotic effect on lung cancer cells. They also took advantage of FAR overexpression on cancer cells similar to current study and received identical results. Apart from that ZnONPs role as an efficient delivery agent was evaluated where increased MTX delivery was observed in A549 cells compared to that of pure MTX (Mishra et al., 2023). Few other research also shows when MTX was used along with some nano carrier system in combination gave better efficacy then drug alone similar to current study (Chaudhari et al., 2021; Rozalen et al., 2020). MTX-ZnONPs presented lowest  $IC_{50}$  value of 5  $\mu\text{g}/\text{ml}$  for MCF-7 cells followed by 18  $\mu\text{g}/\text{ml}$  and 49  $\mu\text{g}/\text{ml}$  for MCF-10A and MDA-MB-231 cells respectively, based on these all-further assays were conducted. AO/EB live dead cell staining was carried out visualize cytotoxicity under microscope. AO being a permeable dye tends to stain both live and dead cells hence, cells with only AO inside appears green, whereas a cell that is dead or whose membranes has been compromised, absorbs EB and therefore fluoresces red. AO/EB staining of MCF-10A, MCF-7 and MDA-MB-231 cells

---

---

treated with MTX-ZnONPs and bare ZnONPs showed fragmented nuclei, chromatin condensation blebbing of membrane and green fluorescence visual signs of cells undergoing apoptosis were evident. Additionally other features that included membrane permeability loss, swelling of cell and nuclear condensation with red color fluorescence as EtBr permeabilizes and stains necrotic cells. Necrotic cell populations were also visible in MDA-MB-231 and MCF-10A. Quite interestingly as studied by D'Souza et al., treatment with ZnOVI nanostructures exhibited pro-apoptotic effects in MDA-MB-468 TNBC cells. This was evidenced by the detection of greenish-yellow nuclear fluorescence, a hallmark of early apoptotic events, via AO/EB staining. These findings suggested the potential of ZnO nanostructures as a targeted therapeutic intervention for this aggressive breast cancer subtype (D'Souza et al., 2021). Another similar finding was noted where ZnO nanorods were used against MCF-7 cells which provoked and induced apoptosis via intrinsic pathway. Fluorescence microscopy analysis revealed a distinct phenotype in ZnO nano rods treated human breast cancer cells. Affected cells exhibited severe membrane disruption and a related loss of adherence properties. Notably, necrotic morphology characterized by intense red fluorescence, indicative of compromised membrane integrity, was also readily observed in MCF-7 cells highlighting both apoptotic and necrotic mode of death. These findings suggest that ZnO nanorods trigger detachment through membrane-altering mechanisms, potentially offering therapeutic avenues for targeting cancer cell adhesion. These results were indicative of NPs mediated apoptotic and necrotic death (Kavithaa et al., 2016). In other terms AO/EB results were in more alignment with the MTT data where sensitivity to MTX cell line was confirmed visually (Jadhav et al., 2016; Liu et al., 2015). However, it is important to note that AO/EB staining is a qualitative method and may not provide accurate quantitative data on cell viability hence further quantitative assays like apoptosis assay, immunoblotting is imperative to elucidate the findings. Normal cell cycle progression is an important function of a cell and cancer cells have some mechanism to bypass cell cycle checkpoints beyond a limit. Hence to target the cell cycle progression MTX-ZnONPs were used. It was understood that MTX-ZnONPs preferentially halt the cell cycle progression at S phase in MCF-7 and MDA-MB-231. Even though MTX alone had no effect on MDA-MB-231 cells, MTX-ZnONPs treatment at the same concentration did, implying that the combination has a cytotoxic role in resistant cell lines. Reason behind S phase inhibition was specifically due to MTX presence. Once inside the cancer cell, MTX-ZnONPs dissolve under acidic conditions, releasing  $\text{Zn}^{2+}$  ions and MTX. MTX polyglutamates and gets converted to its active form, stalling purine and pyrimidine synthesis, leading to arrest in cell cycle at synthesis phase. The mechanism of action for

---

---

ZnONPs is unknown, but it is believed to involve the release of  $\text{Zn}^{2+}$  ions under an acidic environment, causing oxidative stress and causing cellular damage (Xie et al., 2016; Hu and Du, 2020). Apoptosis is a crucial biological process that plays a significant role in the development and maintenance of tissues in multicellular organisms. Annexin V/PI staining is a widely used method for detecting apoptosis, which involves the use of fluorescently labelled annexin V and propidium iodide (PI) to identify cells that are undergoing programmed cell death. Principle of this assay is based on the fact that Annexin V binds to phosphatidylserine (PS), a lipid molecule that becomes exposed on the outer leaflet of the plasma membrane during early stages of apoptosis. PI, on the other hand, is a membrane-impermeable dye that stains cells with compromised plasma membranes, such as those in late-stage apoptosis or necrosis. By using both annexin V and PI staining, it is possible to distinguish between apoptotic cells (annexin V positive, PI negative) and necrotic cells (annexin V positive, PI positive) (Shandiz et al., 2021; Tian et al., 2020). Both bare ZnONPs and MTX-ZnONPs treated cells led to cytotoxicity in MDA-MB-231 cells and majority of the population was identified as necrotic and late apoptotic. Interestingly, MTX-ZnONP treated group had considerably higher fraction of dead population compared to MTX at those same concentrations, indicating its cytotoxic nature against MTX resistant cell line. These results were in support with the previous study of AO/EB staining where, MDA-MB-231 cells underwent necrosis more than that of MCF-7 cells. Each cell line based on its sensitivity to nanosystem reacts differentially but ultimately leading to necrosis or apoptosis. To understand the underlying mechanism behind cell death, protein expression study needs to be carried out. Caspase being member of the cysteine aspartic acid protease (caspase) family performs the function of a crucial protagonist in programmed cell death (Deng and Zhang, 2013). When cells undergo apoptosis, the pro-caspases get activated by cleavage to active caspases and show a change in protein expression. This change in expression on initiation of apoptosis was studied, where MDA-MB-231 that expresses caspase-3 and MCF-7 that expresses caspase-7 (as it is deficient in caspase-3) showed through the expression of this protein that apoptosis had been initiated (Fu et al., 2014). MTX-ZnONPs treatment in MCF-7 breast cancer cells upregulated Caspase-3 and Bax expression levels, causing apoptosis, while Bcl-xL downregulation, indicated a classical pattern of apoptotic death. Bax overexpression along with caspases is a hallmark sign for caspase mediated cell death. MDA-MB-231 cell line showed upregulation of Bcl-xL and Bax levels in MTX-ZnONP treatment, indicating non-apoptotic cell death whereas higher expression of Bcl-xL and low expression of Bax in MTX treatment group indicated resistance to chemotherapy drug. Bcl-xL

---

---

has a crucial role to play in cell survival its overexpression is associated with chemoresistance in cell lines.

### 5.5 Conclusion

Our synthesized nanocarriers, particularly MTX-ZnONPs, emerged as potent anti-cancer agent against breast cancer cells, especially MCF-7 and MTX-resistant MDA-MB-231. Attaching MTX to ZnONPs enhanced both selectivity and efficacy, surpassing MTX alone in its ability to kill MDA-MB-231 cells. This enhanced cytotoxicity was confirmed by viability assays and live/dead staining, revealing both apoptotic and necrotic cell death pathways. Notably, MTX-ZnONPs induced S-phase cell cycle arrest in both cell lines, offering a promising strategy for targeting resistant cancer cells. Further analysis using Annexin V/PI staining corroborated the apoptotic nature of MTX-ZnONPs, showing significantly higher cell death compared to MTX alone. Protein expression studies revealed upregulation of Caspase-3 and Bax in MTX-ZnONP-treated MCF-7 cells, confirming caspase-mediated apoptosis. However, MDA-MB-231 exhibited a distinct non-apoptotic pattern, characterized by Bcl-xL and Bax upregulation, suggesting a different mode of cell death.

These findings highlight the potential of MTX-ZnONPs as a promising nanotherapeutic approach for breast cancer, especially in overcoming MTX resistance. The observed cell line-specific responses emphasize the importance of personalized and targeted treatment strategies. Further research into the underlying mechanisms and in vivo studies are crucial to validate the full therapeutic potential and safety of these nano systems.

# Chapter 6

## Blood biocompatibility studies

---

## Blood biocompatibility studies

---

### 6.1 Introduction

NPs, with their unique properties and potential therapeutic applications, hold immense promise for medical diagnosis, treatment, and imaging. However, as these NPs enter the bloodstream, their interactions with blood components, particularly blood cells and proteins, become crucial considerations. Blood biocompatibility studies play a pivotal role in assessing the safety and efficacy of NP-based therapies. Blood biocompatibility studies assess the interactions between NPs and blood components, such as red blood cells, white blood cells, and platelets. These interactions can influence the fate of NPs in the body, affecting their distribution, clearance, and potential toxicity. The results of blood biocompatibility studies inform the development of safe and effective NP-based therapies, ensuring that these promising technologies can be translated into clinical applications without compromising patient safety. Blood biocompatibility studies like hemolysis assay and blood cell aggregation studies, play a pivotal role in assessing the safety and efficacy of NP-based therapies (Paul and Sharma, 2011; De La Harpe *et al.*, 2019).

One of the primary concerns associated with NPs is their potential to cause hemolysis, the rupture of RBCs leading to hemoglobin release. Hemolysis can result in anemia, impair oxygen delivery to tissues, and trigger adverse immune reactions. Blood biocompatibility studies assess the hemolytic potential of NPs to ensure their safe use in blood-contacting applications. Given the potential of NPs to induce hemolysis, it is imperative to assess their hemolytic potential before their clinical application. Blood biocompatibility studies evaluate the hemolytic activity of NPs to ensure their safe use in blood-contacting applications. The hemolytic activity of NPs is influenced by various factors, including their size, shape, surface properties, and material composition. Larger NPs with irregular shapes and positively charged surfaces tend to exhibit higher hemolytic activity compared to smaller, spherical, and negatively charged NPs (Yedgar, Barshtein and Gural, 2022).

Blood cell aggregation, refers to the clumping or stacking of Red blood cells (RBCs)/ White blood cells (WBCs) /platelets, resulting in an increase in blood viscosity. This process can have adverse effects on blood flow, oxygen delivery to tissues, and the overall functioning of the circulatory system. NPs can interact with RBCs, potentially inducing blood cell aggregation. This can lead to impaired blood flow, particularly in micro vessels, and may contribute to thrombosis or clot formation. Blood cell aggregation studies evaluate the effects of NPs on RBC aggregation to assess their potential to disrupt blood flow and increase the



---

risk of thrombosis. Blood cell aggregation studies are an essential component of the NP development process, ensuring the safety and efficacy of NP-based therapies (Tripette *et al.*, 2009; Shirsekar *et al.*, 2016).

## 6.2 Materials and Methods

To perform blood experiments, prior approval from the Institutional Ethics Committee (IEC) was received. (NMIMS/IEC/012/2020) (the approval letter attached in Appendix I).

For the study, we selected healthy volunteers and obtained their written consent (as seen in Appendix II and III). The blood was only drawn after the volunteers had read and understood the study. A trained phlebotomist drew the blood in a vacutainer. From healthy volunteers 5 ml of Ethylenediamine tetraacetic acid (EDTA)-stabilized human blood was freshly collected in a vacutainer. A total of 6 participants (n=6) with their written consent were allowed to participate in study.

### 6.2.1 Hemolysis study

After obtaining informed consent from healthy volunteers, 5 ml of EDTA-stabilized human blood was collected and centrifuged at 1200 rpm for 5 minutes. The RBC pellet was collected separately and washed twice with PBS solution and then diluted 1:4 with PBS. NPs were prepared at different concentrations of 6.5, 12.5, 25, 50 and 100 µg/ml in PBS. 0.2 ml of RBC suspension was added to 0.8 ml of NPs. A positive control was prepared by adding 0.8 ml of deionized water to 0.2 ml of RBC suspension, and a negative control was prepared by adding 0.8 ml of PBS to 0.2 ml of RBC suspension. The samples were then incubated for 2 hours at 37°C. Every 30 minutes, the samples were inverted to resuspend the RBCs and NPs. After 2 hours, all samples were centrifuged at 1200 rpm for 5 minutes. Then, 100 µL of the supernatant was transferred to a 96-well plate. Three parallel samples were used in each group, and each experiment was repeated three times. The absorbance of hemoglobin in the supernatant was measured using a BioTek EPOCH 2 Microplate Reader at 570 nm and 655 nm, with 655 nm being used as a reference. The percentage of hemolysis was calculated as follows:

$$\% \text{ Hemolysis} = \frac{(\text{Absorbance of sample} - \text{Absorbance of negative control})}{(\text{Absorbance of positive control} - \text{Absorbance of negative control})} \times 100$$

### 6.2.2 Blood cell aggregation study

A blood cell aggregation study was performed using 5 ml of EDTA-stabilized blood from a healthy individual in vacutainer. The blood was subjected to Ficoll-Hypaque separation, in which it was layered on Ficoll-Hypaque and centrifuged at 1500 rpm for 20 minutes. The

---

---

different cell components, namely RBCs, WBCs, and platelet-rich plasma (PRP), were separated into layers based on their densities. Each layer was then carefully removed, washed with phosphate-buffered saline (PBS), and diluted 1:4. NPs were prepared in PBS at a concentration of 100  $\mu\text{g/ml}$ . For the test, 0.8 ml of NPs were mixed with 0.2 ml of the RBC/WBC/PRP suspension. The positive control was 0.8 ml of polyethyleneimine (PEI), and the negative control was the same amount of PBS. Each mixture was then incubated at 37°C for 2 hours with intermittent shaking to mix the NPs.

Blood cell aggregations, if any, were observed using a phase-contrast microscope at a magnification of 40X. Three parallel samples were prepared for each group, and each experiment was repeated three times.

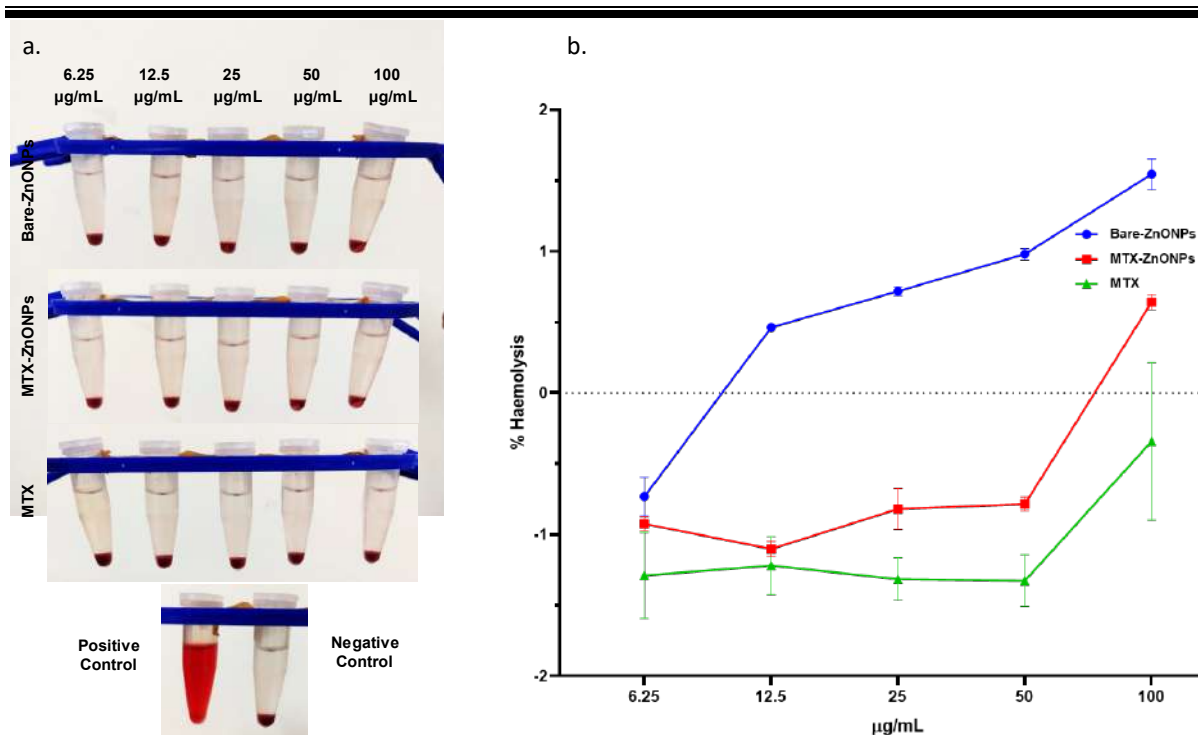
## 6.3 Results

### 6.3.1 Hemolysis study

Red blood cells, also known as RBCs responsible for major portion of our blood volume and are quite delicate in nature. As a result, they can be easily harmed by biomolecules, foreign matter or NPs that enters into the bloodstream. It is therefore decisive to investigate how these engineered nanomaterials affect RBCs.

**Figure 6.1** demonstrate that tested systems bare ZnONPs, MTX-ZnONPs and even MTX did not exhibit any hemolytic activity at concentrations tested. Even at the highest concentration NPs could not bring about the lysis of RBCs and showed signs of hemocompatibility. The percentage of hemolysis observed was, below 2% for all the systems tested. Results obtained adheres to the safety standard outlined in ASMTM F756-00. Consequently, all tested systems can be identified to be safe and biocompatible at the concentrations studied.

Our results are consistent with previous studies that have established the biocompatibility of ZnONPs and MTX (Mitra *et al.*, 2012; Rahman *et al.*, 2021). The inert nature of ZnONPs and their minimal interaction with RBCs contribute to their hemolytic inactivity. Moreover, the conjugation of MTX to ZnONPs did not alter their hemocompatible properties, suggesting that MTX-ZnONPs retain the favorable blood compatibility profile of ZnONPs.



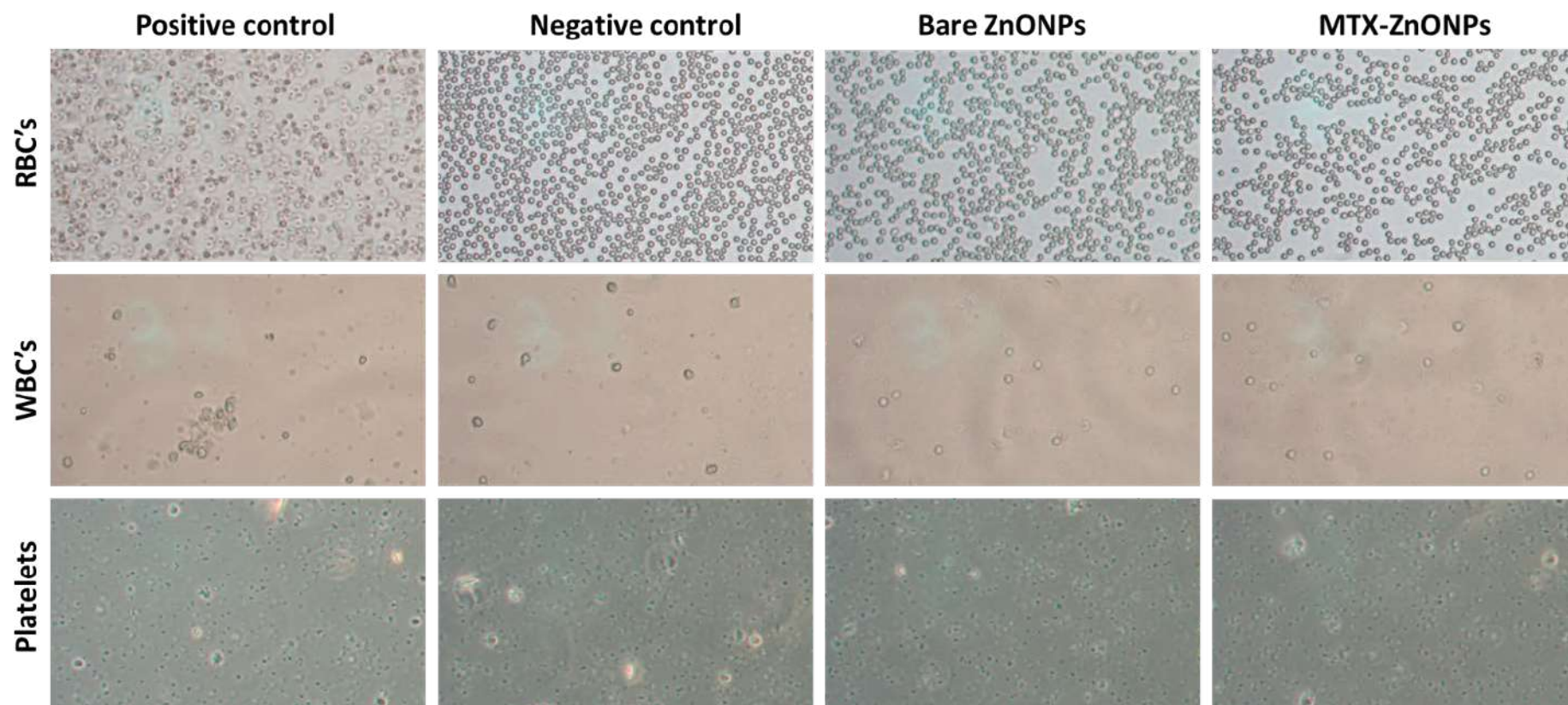
**Figure 6.1** RBC hemolysis study of Bare ZnONPs, MTX-ZnONPs and MTX. (a) visual presentation of hemolysis assay in tubes; (b) graphical presentation of % hemolysis when plotted against concentration.

---

### 6.3.2 Blood cell aggregation study

NPs are so small that they can affect the normal functions of cells in ways that larger particles cannot. When NPs enter the bloodstream, they can cause problems and harm the blood cells. Therefore, it is very important to make sure that NPs are safe for the blood before using them for medical purposes. Since NPs are smaller than micro-sized particles, they are also more physiologically active, which may enable disruption of the typical cellular biochemical milieu. Therefore, it is expected that NPs will interact with blood components, hence while designing and developing NPs with therapeutic uses, aggregation studies should be one of the top priorities.

For this study from fresh blood sample was collected and, RBCs, WBCs, and platelet rich plasma were separated. Each of these components were later then allowed to interact with bare ZnONPs and MTX-ZnONPs for specified time. For positive control, Polyethylene imine (PEI) was used whereas for negative control, saline was used. When observed under microscope PEI treated RBCs, WBC's and platelets showed clear signs of aggregations and clumping of cells whereas saline treated cells did not show any sort of clumping in the cells as observed in **Figure 6.2**. Interestingly, no observable aggregation was detected in cells treated with either bare ZnONPs or MTX-ZnONPs. These findings suggest that both ZnONPs and MTX-ZnONPs do not induce blood cell aggregation, indicating their potential biocompatibility. Our study demonstrates that ZnONPs and MTX-ZnONPs do not induce blood cell aggregation, suggesting their potential as safe and biocompatible nanomaterials for biomedical applications. These findings underscore the importance of assessing NP-blood cell interactions in the development of nanomedicines.



**Figure 6.1** Blood cell aggregation assay performed with bare ZnONPs, MTX–ZnONPs and MTX at 200  $\mu\text{g}/\text{ml}$ . Graphical presentation of % hemolysis and visual presentation of the test. (Magnification 40X)

---

## 6.4 Discussion

The above studies have investigated the blood compatibility of ZnONPs and MTX-ZnONPs by evaluating their hemolytic potential and ability to induce blood cell aggregation. Both studies provide valuable insights into the biocompatibility profile of these nanomaterials. It was observed in previous study that ZnONPs did not induce aggregation in RBCs, WBCs, or platelets. Additionally, no significant changes in cell morphology or viability were observed upon exposure to ZnONPs in study done by Salami, Khosravi and Zarei, 2022. Also, one more study conducted by Guo et al, evaluated the toxic effects of ZnONPs on liver cells and found no evidence of cellular damage or dysfunction. These findings suggest that ZnONPs may have minimal to no adverse effects on various cell types, including red blood cells, white blood cells, platelets (Guo *et al.*, 2020). However, it is important to note that NPs can have different effects depending on various factors such as concentration, duration of exposure, and specific cell type. It was observed that various physical parameters like size, shape, and surface charge of ZnONPs can influence their interaction with cells and determine their potential toxicity. One of the studies done by (Shirsekar *et al.*, 2016) highlighted the role of ZnONPs size, shape and surface area on RBCs interactions, suggesting that these factors should be taken into consideration when assessing the cytotoxicity of ZnONPs. According to the study done by Dhanka, Shetty and Srivastava, 2018, pure MTX is hemocompatible and did not show hemolysis. However, loading of MTX into chitosan NPs and liposomes induce more hemolysis as compared to blank alone. Whereas it was found that MTX loaded alginate microparticles showed less hemolysis compared to bare microparticles, which suggests that the loading of MTX into the microparticles makes them less hemolytic. This may be due to the interaction of a hemolytic group of alginates with the drug (Dhanka, Shetty and Srivastava, 2018). Interestingly, results from another in vitro study done by Kuznetsova et al. to evaluate the hemocompatibility of liposomal formulations encapsulating MTX, revealed that MTX-loaded liposomes exhibited noticeable interference with the complement and coagulation cascades. These findings suggest that the presence of MTX within the liposomal structure influenced the blood compatibility profile, particularly with regard to the activation of the complement system and the functionality of the coagulation cascade. The occurrence of aromatic amino groups and an unbound alpha-carboxyl on the exterior of the MTX prodrug molecules within the bilayer was recognized as a possible element affecting complement activation (Kuznetsova *et al.*, 2012).

---

---

## 6.5 Conclusion

This study investigated the effects of bare ZnONPs and MTX-ZnONPs on RBCs and blood cell aggregation. None of the tested systems (bare ZnONPs, MTX-ZnONPs, and MTX) exhibited significant hemolytic activity, with the percentage of hemolysis remaining below 2% at all tested concentrations. Neither bare ZnONPs nor MTX-ZnONPs induced aggregation of RBCs, WBCs, or platelets clearly indicating that they are safe, further strengthening their biocompatibility profile. These findings contribute to the advancement of nanomedicine by highlighting the importance of assessing NP interactions with blood components in the development of safe and effective nano therapies. These results suggest the potential of ZnONPs and MTX-ZnONPs as safe and biocompatible nanomaterials for biomedical applications.

# Chapter 7

## In-vivo acute oral toxicity study



---

## In-vivo acute oral toxicity study

---

### 2.1 Introduction

The Organization for Economic Co-operation and Development (OECD) Guidelines for the Testing of Chemicals comprise a comprehensive collection of approximately 150 internationally recognized testing methods used by government, business, and independent laboratories to identify and characterize the potential hazards posed by chemicals. These guidelines serve as valuable professional resources primarily employed in regulatory safety testing, chemical notification and registration processes, and chemical evaluation. They are also applicable in toxicology research for the selection and ranking of potential chemicals during the development of new chemical compounds and products. Through a series of tests, these guidelines assess the physiological effects of a substance on animals (Ukelis *et al.*, 2008).

Acute toxicity refers to the immediate or short-term adverse changes that occur after a single or brief exposure to a substance. Among other things, it also refers to the adverse effects that arise within 24 hours of taking a single dose or multiple doses consecutively. Here we refer adverse effect as, any impairment in the functioning of physical attributes and/or cellular processes that may impact the performance of specific organs or the entire organism, thereby reducing its ability to respond to additional challenges. Protocols for acute toxicity testing are employed to determine the harmful effects of a chemical on living organisms following a brief period of exposure (Walum, 1998). Typically, these tests are conducted on animals such as mice or rats, and the resulting data are used to assess the potential risks posed by these substances to humans. Specifically, in the context of oral toxicity, a chemical is considered acutely toxic if it induces adverse effects shortly after ingestion. The term "acute oral toxicity" is commonly used in relation to determine lethality and LD<sub>50</sub> values. Different testing protocols provide distinct information regarding the substance being evaluated. The LD<sub>50</sub> value, which represents the dose of a chemical expected to cause mortality in 50% of test subjects, is a critical measure of toxicity. It plays a significant role in the toxicological classification of chemicals, which involves categorizing them based on their level of toxicity. These tests aid in the identification and management of risks associated with the production, handling, and use of chemicals (Akhila *et al.*, 2007).

To ensure the confirmation of toxicity for a test substance, the OECD offers various guidelines that recommend suitable methods. One such guideline is OECD 425, titled "Acute Oral Toxicity: Up-and-Down Procedure," which was published by the OECD in 2001. The primary objective of OECD 425 is to assess the acute oral toxicity of a substance by administering a

---

---

single dose to rodents and observing both the survival rate and any adverse effects. The outcomes of this test can be utilized to classify the substance's acute toxicity according to the Globally Harmonized System (GHS) (Schrage *et al.*, 2011).

The test is conducted in two phases namely: a limit test and a main test.

- **Limit test:** The limit test is typically used when an investigator has information indicating that the material being tested is likely to be nontoxic. A single dose of 2000 mg/kg is administered to 1st animal. Under the condition where animals die main test is recommended or if animal survives, four more animals are dosed one after the other. If three or more animal survives, the substance is considered to have a LD<sub>50</sub> of greater than 2000 mg/kg and no further testing is required.
- **Main test:** This test is used to determine the LD<sub>50</sub> of a substance. Single animals are dosed sequentially, typically at fixed time interval. The first animal is given a dose that is one step below the best estimate of the LD<sub>50</sub> of the test substance. The second animal is given a lower dose if the first one dies or appears moribund. The second animal is given a higher dose if the first one survives. Dosing should begin at 175 mg/kg body weight of animal, if there is no estimate of the substance's lethality. The dose is then increased or decreased in a stepwise fashion, depending on whether the animals survive or die.

Animals are monitored individually at least once during the first 30 minutes following dosing, intermittently for the first 24 hours (with special focus given to the first 4 hours), and then every day thereafter for a total of 14 days, unless they need to be removed from the study and humanely put to death for animal welfare reasons or are discovered dead. Additional parameters to be observed are changes in the skin, fur, eyes, mucous membranes, respiratory, circulatory, autonomic, and central nervous systems, as well as somatomotor activity and behavior patterns. Tremors, convulsions, salivation, diarrhea, lethargy, sleep, and coma should all be watched for. The severity of acute toxicity can vary depending on the dose of the substance, the route of exposure, and the individual's susceptibility (Organisation for Economic Cooperation and Development, 2001).

## 7.2 Materials and Methods

### 7.2.1 Animal ethics approval

The experimental protocol was approved by the Institutional Animal Ethics Committee (IAEC) with approval no. CPCSEA/P-69/2022. Ethics approval forms are attached in Annexure I. All

procedures were performed in accordance with the guidelines set forth by the Committee for the Purpose of Control and Supervision of Experiments on Animals (CPCSEA).

Previously characterized MTX-ZnONPs were prepared in 0.5% Carboxy methyl cellulose (CMC).

### 7.2.2 Animal experimentation & housing

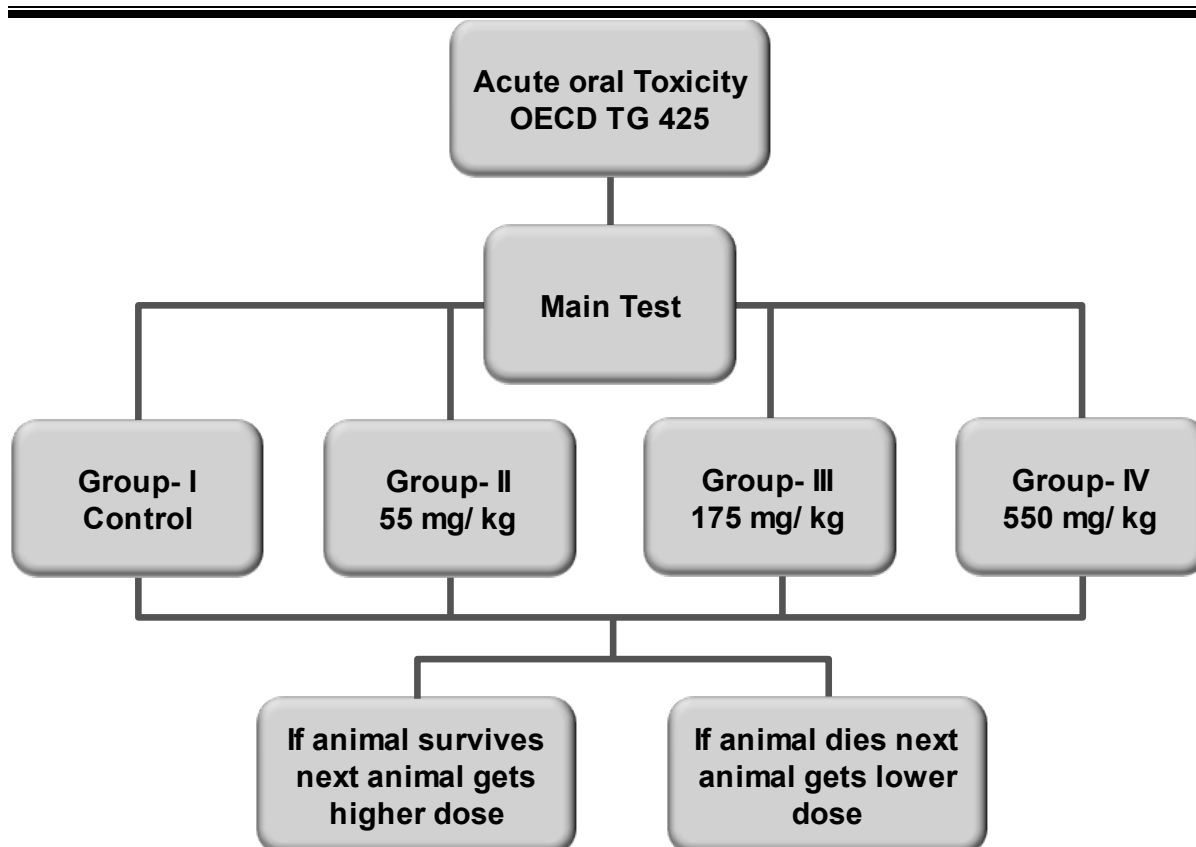
Female Swiss albino mice weighing 18–20 g was purchased from the National Institute of Biosciences in Pune, Maharashtra, India for use in the acute toxicity investigation. The animals were kept in cages in the SVKM's animal facility. The mice were acclimatized to the laboratory conditions for a week prior to the start of the study. A 12 hours light/dark cycle was maintained in an animal facility during the trial, and housing conditions were as follows: temperature of  $22\pm 2^{\circ}\text{C}$ , relative humidity  $75\pm 5\%$ , and temperature. To ensure social interaction, animals were kept in conventional polypropylene cages with a maximum of 4 mice per cage. Fresh bedding was provided, and the cages were cleaned every day. Animals were fed a basic, multi-nutrient diet and were given access to water *ad libitum*. The mice were monitored for any signs of distress or illness throughout the study period.

### 7.2.3 Experimental design

Acute oral toxicity study of MTX-ZnONPs was performed as per OECD guideline (TG 425). After a week of acclimatization, the animals were split into four groups of three animals each. Group I was control group which received only 0.5% Carboxy methyl cellulose (CMC) equivalent to dose volume, Group II received MTX-ZnONPs with the first dose being 55mg/kg, followed by 175mg/kg for group III, and finally 550 mg/kg for group IV same is presented in **Table 7.1**. Following oral treatment, animals were closely monitored for any changes in behavior and physiological appearance for the following 30 minutes, then occasionally for the following 24 hours, with a focus on the first four hours. For up to 14 days, all the groups were maintained under close supervision **Figure 7.1**.

**Table 7.1** Animal grouping scheme as per experimental protocol

No. of groups	Group-I	Group-II	Group-III	Group-IV
Doses	Control group	55 mg/ kg	175 mg/ kg	550 mg/ kg
No. of animal	n= 3	n= 3	n= 3	n= 3



**Figure 7.1** Experimental protocol used as per OCED TG 425 guideline.

#### 7.2.4 Observations

Several physical appearance-related observations, including changes to the body weight, skin, fur, eyes, and lacrimal secretion, as well as anomalies in the autonomic, somatomotor, behavioral, and respiratory systems, were recorded. Furthermore, salivation, lethargy, convulsions, diarrhea, tremors, sleep, and coma in the animals were noted.

#### 7.3 Results

Over the course of the experimental period, i.e., 14 days, the animals' behavior showed no abnormalities following a single dose of MTX-ZnONPs at all selected dose levels. In addition, no mortality or morbidity was observed following a single dose of MTX-ZnONPs. Weight data of mice taken at different time intervals up to 14 days is summarized in **Table 7.2**. The data shows that the control group mice gained weight over the course of the 14-day study, while the mice treated with MTX-ZnONPs did not gain weight or lost weight compared to day 1. Even though it was clear that at 14 day all animals showed some amount of proportional weight gain signifying healthy growth of animal's post dosing. This also substantiates the safe and biocompatible nature of MTX-ZnONPs in mice at tested dose levels. All the different physical characteristics of the animals were concerned, the eye, nose, ears, and fur of the animals

---

remained unchanged throughout the observation period along with no signs of any behavioral changes like tremors, coma, or any signs of morbidity. **Table 7.3**, **Table 7.4**, and **Table 7.5** summarizes all the data for physical characteristic and behavioral patterns. All animals were healthy and survived without showing any signs of toxicity or morbid behavior up to 14 days. Apart from this, we did not observe any sign of salivation, diarrhea, lethargy, or abnormal behavior during our observation. Based on this in vivo research, the LD<sub>50</sub> value of MTX-ZnONPs was identified to be 550 mg/kg body weight of animals with the help of ATO425 software. Clearly, this value is higher than used for in vitro testing, indicating the safety of synthesized nanosystems.

**Table 7.2** Effect of MTX-ZnONPs different doses on body weight of mice

Groups	Body weight (g)		
	1 <sup>st</sup> day	7 <sup>th</sup> day	14 <sup>th</sup> day
<b>Group- I</b> <b>Control group</b>	25.97±1.53	26.30±1.76	28.29±2.17
<b>Group- II</b> <b>55 mg/ kg</b>	25.00±0.82	25.67±2.58	28.00±2.41
<b>Group- III</b> <b>175 mg/ kg</b>	24.67±1.53	23.50±2.18	24.40±2.05
<b>Group- IV</b> <b>550 mg/ kg</b>	25.33±0.58	26.07±1.17	25.70±1.50

**Table 7.3** Observation table for physical parameters and behavioral patterns recorded for mice treated with 55 mg/ kg group.

Parameters	Group- I 55 mg/ kg of MTX-ZnONPs									
	30 minutes		4 hours		24 hours		7 days		14 days	
	CG	TG	CG	TG	CG	TG	CG	TG	CG	TG
<b>Fur &amp; Skin</b>	N	N	N	N	N	N	N	N	N	N
<b>Eyes</b>	N	N	N	N	N	N	N	N	N	N
<b>Salivation</b>	N	N	N	N	N	N	N	N	N	N
<b>Respiration</b>	N	N	N	N	N	N	N	N	N	N
<b>Urination &amp; Faeces</b>	N	N	N	N	N	N	N	N	N	N
<b>Sleep</b>	N	N	N	N	N	N	N	N	N	N
<b>Lethargy</b>	N	N	N	N	N	N	N	N	N	N
<b>Mucous membrane</b>	N	N	N	N	N	N	N	N	N	N
<b>Itching</b>	NF	NF	NF	NF	NF	NF	NF	NF	NF	NF
<b>Convulsions &amp; tremors</b>	NF	NF	NF	NF	NF	NF	NF	NF	NF	NF
<b>Coma</b>	NF	NF	NF	NF	NF	NF	NF	NF	NF	NF
<b>Mortality</b>	NF	NF	NF	NF	NF	NF	NF	NF	NF	NF

Key: CG = Control group, TG = 55 mg/ kg treatment group, N= Normal, P = Present, ↑ = Increased, N.F = Not found

**Table 7.4** Observation table for physical parameters and behavioral patterns recorded for mice treated with 175 mg/ kg group.

Parameters	Group- II 175 mg/ kg of MTX-ZnONPs									
	30 minutes		4 hours		24 hours		7 days		14 days	
	CG	TG	CG	TG	CG	TG	CG	TG	CG	TG
<b>Fur &amp; Skin</b>	N	N	N	N	N	N	N	N	N	N
<b>Eyes</b>	N	N	N	N	N	N	N	N	N	N
<b>Salivation</b>	N	N	N	N	N	N	N	N	N	N
<b>Respiration</b>	N	N	N	N	N	N	N	N	N	N
<b>Urination &amp; Faeces</b>	N	N	N	N	N	N	N	N	N	N
<b>Sleep</b>	N	N	N	N	N	N	N	N	N	N
<b>Lethargy</b>	N	N	N	N	N	N	N	N	N	N
<b>Mucous membrane</b>	N	N	N	N	N	N	N	N	N	N
<b>Itching</b>	NF	NF	NF	NF	NF	NF	NF	NF	NF	NF
<b>Convulsions &amp; tremors</b>	NF	NF	NF	NF	NF	NF	NF	NF	NF	NF
<b>Coma</b>	NF	NF	NF	NF	NF	NF	NF	NF	NF	NF
<b>Mortality</b>	NF	NF	NF	NF	NF	NF	NF	NF	NF	NF

Key: CG = Control group, TG = 175 mg/ kg treatment group, N= Normal, P = Present, ↑ = Increased, N.F = Not found

**Table 7.5** Observation table for physical parameters and behavioral patterns recorded for mice treated with 550 mg/ kg group.

Parameters	Group- III 550 mg/ kg of MTX-ZnONPs									
	30 minutes		4 hours		24 hours		7 days		14 days	
	CG	TG	CG	TG	CG	TG	CG	TG	CG	TG
<b>Fur &amp; Skin</b>	N	N	N	N	N	N	N	N	N	N
<b>Eyes</b>	N	N	N	N	N	N	N	N	N	N
<b>Salivation</b>	N	N	N	N	N	N	N	N	N	N
<b>Respiration</b>	N	N	N	N	N	N	N	N	N	N
<b>Urination &amp; Faeces</b>	N	N	N	N	N	N	N	N	N	N
<b>Sleep</b>	N	N	N	N	N	N	N	N	N	N
<b>Lethargy</b>	N	N	N	N	N	N	N	N	N	N
<b>Mucous membrane</b>	N	N	N	N	N	N	N	N	N	N
<b>Itching</b>	NF	NF	NF	NF	NF	NF	NF	NF	NF	NF
<b>Convulsions &amp; tremors</b>	NF	NF	NF	NF	NF	NF	NF	NF	NF	NF
<b>Coma</b>	NF	NF	NF	NF	NF	NF	NF	NF	NF	NF
<b>Mortality</b>	NF	NF	NF	NF	NF	NF	NF	NF	NF	NF

Key: CG = Control group, TG = 550 mg/ kg treatment group, N= Normal, P = Present, ↑ = Increased, N.F = Not found



---

## 7.4 Discussion

The results of the study on the safety of MTX-ZnONPs in animals are promising. The results of this study suggested that MTX-ZnONPs are safe for use in vivo, as they did not cause any significant toxicity or morbidity in animals. The LD<sub>50</sub> value of MTX-ZnONPs was determined to be 550 mg/kg body weight, which is higher than the value used for in vitro testing.

The lack of toxicity of MTX-ZnONPs is likely due to the fact that the MTX molecules are loaded on to the ZnONPs preventing its untimely release. The safety of MTX-ZnONPs is important because they have the potential to be used as a delivery system for MTX, a drug that is used to treat cancer and rheumatoid arthritis (Bryan, 2012). Current study showed that MTX-ZnONPs could be used to deliver MTX to tumors without causing systemic toxicity. This could improve the efficacy of MTX therapy and reduce the side effects of the drug.

The findings of earlier research on the safety of ZnONPs are congruent with the findings of this investigation. In a study done by (Kim *et al.*, 2014) rats were administered with ZnONPs with a size of 100 nm and two different surface charges (AE100(-) and AE100(+)) at doses of 500 mg/kg, 1,000 mg/kg, and 2,000 mg/kg everyday up to 14 days. It came to notice that treatment showed loss of body weight, corneal opacity and few minor signs of toxicity were observed. Only one animal was found dead in AE100(+) group but, no dead or moribund animal was observed in AE100(-) group. It was concluded that repeated oral administration of ZnONPs causes adverse effects in animals. In another study researchers administered positively charged 100 nm ZnONPs orally to the rats at doses of 0, 500, 1,000, and 2,000 mg/kg/day for 14 days. It was observed that ZnONPs showed dose dependent signs of toxicity in terms of change in body weight, feed consumption and others, while LD<sub>50</sub> for rats was determined was the highest dose tested in the study i.e 2000 mg/kg/day or above (Ko *et al.*, 2015). Compared to the previous studies in current study ZnONPs were used for much lower concentrations confirming the safety of synthesized nanosystem in animal.

## 7.5 Conclusion

In vivo study suggests that the combination of MTX and ZnONPs does not exhibit any synergistic toxicity indicating that the nanoparticles are safe for use in animals at tested dose. The results of this study suggest that MTX-ZnONPs are a safe and promising new delivery system for MTX. Although this study's findings are encouraging, more research is necessary to establish that MTX-ZnONPs are safe to use in people.

# Chapter 8

# Summary and Conclusion

---

### Summary and Conclusion

In summary, MTX-ZnONPs were synthesized using an ex-situ approach, where MTX was loaded onto previously synthesized and characterized bare ZnONPs. The resulting nanoparticles were characterized using a variety of techniques. The results of the characterization studies showed that MTX-ZnONPs had a hexagonal crystal morphology with an average size of 30 nm. The nanoparticles were also highly crystalline and had a positive Zeta potential. The drug release study showed that MTX-ZnONPs shows biphasic drug release with approx. 90% of the drug release within 24 hours. Blood biocompatibility study found that no hemolysis (rupture of red blood cells) or aggregation (clumping together) of blood cells occurred when the NPs interacted with blood cells. This indicates that the NPs are biocompatible and safe for use in blood.

Since, NPs were found biocompatible further in vitro assays were conducted to understand and study the cytotoxicity mechanism of MTX-ZnONPs on cancer cell lines. MTT cellular viability assay revealed higher cytotoxicity of MTX-ZnONPs compared to MTX in breast cancer cell lines, indicating their enhanced anticancer potential. Conversely, bare ZnONPs demonstrated increased toxicity in MDA-MB-231 cells. We also observed different IC<sub>50</sub> values for MTX-ZnONPs in MCF-7 and MDA-MB-231 cells, indicating varying efficacy against different types of breast cancer cells. Additionally, MCF-10A cells treated with MTX-ZnONPs showed high cell viability, indicating their biocompatibility and selectivity towards cancer cells. Furthermore, the AO/EB staining supported the MTT results and illustrated dose-dependent effects and unveiled distinct morphological changes associated with apoptosis and necrosis. Cell cycle analysis results revealed that bare ZnONPs had no impact on the cell cycle in MCF-7 cells, while MTX-ZnONPs specifically arrested cells in the S phase. On the other hand, S and G2/M phase specific cell cycle arrest was noted because of MTX treatment. This cell cycle-specific effect of MTX-ZnONPs on the S phase was consistent with our findings. The cell cycle progression was similarly affected by bare ZnONPs in MDA-MB-231 cells, whereas MTX had no effect. In response to MTX-ZnONP treatment, cells were arrested at the S phase and G2/M phase of cell cycle. Also, the Annexin V FITC-Propidium Iodide assay showed that MTX-ZnONPs significantly decreased the number of live MCF-7 cell population, while both bare ZnONPs and MTX-ZnONPs caused more necrosis and apoptosis in MDA-MB-231 cells. These findings demonstrate that MTX-ZnONPs enhanced cytotoxic activity in both MCF-7 and MDA-MB-231 cells irrespective of their sensitivity to MTX. Apoptosis was apparent in MCF-7 cells by the upregulation of Caspase-7 and Bax and the downregulation of Bcl-xL. In

---

case of MDA-MB-231 cells, MTX treatment resulted in an increase in Bcl-xL levels, suggesting that cell death was not driven by apoptosis. However, increased levels of Bax suggested its dual role in apoptosis and necrosis, which aligned with other findings.

Additionally, an acute oral toxicity study of MTX-ZnONPs was carried out in accordance with OECD 425 guidelines to determine its LD50. In-vivo acute oral toxicity study in mice showed no signs of toxicity or mortality in any of the animals, even at the highest dose. This suggested that MTX-ZnONPs are not acutely toxic to animals and have a LD50 of >550 mg/kg and its safe up to the given dose limit.

In conclusion, the synthesis and characterization of MTX-ZnONPs demonstrated their potential as an effective anticancer agent. In terms of anticancer activity, MTX-ZnONPs exhibited enhanced cytotoxicity compared to MTX alone in breast cancer cell lines. The selective toxicity towards cancer cells was demonstrated by high cell viability in normal breast cells. MTX-ZnONPs were found to be biocompatible and safe for use in blood. Interestingly It was observed that MTX-ZnONPs are effective against both MCF-7, MTX-sensitive and MDA-MB-231 MTX-resistant breast cancer cell line. Encouragingly, in-vivo studies also showed that MTX-ZnONPs are not acutely toxic to animals. Overall, these findings highlight the promising potential of MTX-ZnONPs as an effective and safe nanomedicine for breast cancer treatment. Further studies are required to investigate the efficacy and long-term safety of MTX-ZnONPs to evaluate its clinical role in cancer.

---



---

### Bibliography

---

AbdElhady MM. Preparation and Characterization of Chitosan/Zinc Oxide Nanoparticles for Imparting Antimicrobial and UV Protection to Cotton Fabric. *International Journal of Carbohydrate Chemistry* 2012;2012:1–6. <https://doi.org/10.1155/2012/840591>.

Abolmaali SS, Tamaddon AM, Dinarvand R. A review of therapeutic challenges and achievements of methotrexate delivery systems for treatment of cancer and rheumatoid arthritis. *Cancer Chemother Pharmacol* 2013;71:1115–30. <https://doi.org/10.1007/s00280-012-2062-0>.

Achebe CH, Obika EN, Chukwuneke JL, Ani OE. Optimisation of hybridised cane wood–palm fruit fibre frictional material. *Proceedings of the Institution of Mechanical Engineers, Part L: Journal of Materials: Design and Applications* 2019;233:2490–7. <https://doi.org/https://doi.org/10.1177/1464420719863445>.

Adams FC, Barbante C. Nanoscience, nanotechnology and spectrometry. *Spectrochimica Acta - Part B* 2013;86:3–13. <https://doi.org/10.1016/j.sab.2013.04.008>.

Ahamed AJ, Vijaya Kumar P. Synthesis and characterization of ZnO nanoparticles by co-precipitation method at room temperature. *J Chem Pharm Res* 2016;8:624–8.

Ahmed S, Annu, Chaudhry SA, Ikram S. A review on biogenic synthesis of ZnO nanoparticles using plant extracts and microbes: A prospect towards green chemistry. *J Photochem Photobiol B* 2017;166:272–84. <https://doi.org/10.1016/j.jphotobiol.2016.12.011>.

Ain Samat N, Md Nor R. Sol-gel synthesis of zinc oxide nanoparticles using *Citrus aurantifolia* extracts. *Ceram Int* 2013;39. <https://doi.org/10.1016/j.ceramint.2012.10.132>.

Ajmal M, Yunus U, Matin A, Haq NU. Synthesis, characterization and in vitro evaluation of methotrexate conjugated fluorescent carbon nanoparticles as drug delivery system for human lung cancer targeting. *J Photochem Photobiol B* 2015;153:111–20. <https://doi.org/10.1016/J.JPHOTOBIOB.2015.09.006>.

Akhila JS, Shyamjith, Deepa, Alwar MC. Acute toxicity studies and determination of median lethal dose. *Curr Sci* 2007;93:917–20. <http://www.jstor.org/stable/24099255>

Alavi AS, Meshkini A. Fabrication of poly(ethylene glycol)-coated mesoporous nanocomposite ZnO@Fe<sub>2</sub>O<sub>3</sub> for methotrexate delivery: An integrated nanoplatfrom for dual-mode cancer therapy. *European Journal of Pharmaceutical Sciences* 2018;115:144–57. <https://doi.org/10.1016/j.ejps.2018.01.027>.

---

- 
- Albanese A, Tang PS, Chan WCW. The Effect of Nanoparticle Size, Shape, and Surface Chemistry on Biological Systems. *Annu Rev Biomed Eng* 2012;14:1–16. <https://doi.org/10.1146/annurev-bioeng-071811-150124>.
- Anselmo AC, Mitragotri S. Nanoparticles in the clinic: An update. *Bioeng Transl Med* 2019;4:1–16. <https://doi.org/10.1002/btm2.10143>.
- Arib C, Spadavecchia J, de la Chapelle ML. Enzyme mediated synthesis of hybrid polyedric gold nanoparticles. *Sci Rep* 2021;11. <https://doi.org/10.1038/s41598-021-81751-1>.
- Arnold M, Morgan E, Rumgay H, Mafra A, Singh D, Laversanne M, et al. Current and future burden of breast cancer: Global statistics for 2020 and 2040. *Breast* 2022;66:15–23. <https://doi.org/10.1016/j.breast.2022.08.010>.
- Arora SK, Devi A, Jaswal VS, Singh J, Kingler M, Gupta VD. Synthesis and characterization of ZnO nanoparticles. *Oriental Journal of Chemistry* 2014;30:1671–9. <https://doi.org/10.13005/ojc/300427>.
- Arteaga C, Sliwkowski M, ... CO-N reviews C, 2012 undefined. Treatment of HER2-positive breast cancer: current status and future perspectives. *NatureCom* 2011. <https://doi.org/10.1038/nrclinonc.2011.177>.
- Babu EP, Subastri A, Suyavaran A, Premkumar K, Sujatha V, Aristatile B, et al. Size Dependent Uptake and Hemolytic Effect of Zinc Oxide Nanoparticles on Erythrocytes and Biomedical Potential of ZnO-Ferulic acid Conjugates. *Sci Rep* 2017;7:1–12. <https://doi.org/10.1038/s41598-017-04440-y>.
- Bagri NK, Ramanan Atreya, Ramanan Athimalaipet V. Dr Yellapragada SubbaRow: The forgotten figure in the history of methotrexate. *Rheumatology (United Kingdom)* 2023;62:1364–5. <https://doi.org/10.1093/rheumatology/keac520>.
- Bai D-P, Zhang X-F, Zhang G-L, Huang Y-F, Gurunathan S. Zinc oxide nanoparticles induce apoptosis and autophagy in human ovarian cancer cells. *Int J Nanomedicine* 2017;Volume 12:6521–35. <https://doi.org/10.2147/IJN.S140071>.
- Banerjee HN, Verma M. Application of nanotechnology in cancer. *Technol Cancer Res Treat* 2008;7:149–54. <https://doi.org/10.1177/153303460800700208>.
- Barnes PM, Moynahan EJ. Zinc Deficiency in Acrodermatitis Enteropathica: Multiple Dietary Intolerance Treated with Synthetic Diet. *J R Soc Med* 1973;66:327–9. <https://doi.org/10.1177/003591577306600411>.
-

- 
- Baskar R, Lee KA, Yeo R, Yeoh KW. Cancer and radiation therapy: Current advances and future directions. *Int J Med Sci* 2012;9:193–9. <https://doi.org/10.7150/ijms.3635>.
- Bath RK, Brar NK, Forouhar FA, Wu GY. A review of methotrexate-associated hepatotoxicity. *J Dig Dis* 2014;15:517–24. <https://doi.org/10.1111/1751-2980.12184>.
- Bayda S, Adeel M, Tuccinardi T, Cordani M, Rizzolio F. The history of nanoscience and nanotechnology: From chemical-physical applications to nanomedicine. *Molecules* 2020;25:112. <https://doi.org/10.3390/molecules25010112>.
- Bedoui Y, Guillot X, Sélambarom J, Guiraud P, Giry C, Jaffar-Bandjee MC, et al. Methotrexate an old drug with new tricks. *Int J Mol Sci* 2019;20. <https://doi.org/10.3390/ijms20205023>.
- Beltrán-Gracia E, López-Camacho A, Higuera-Ciapara I, Velázquez-Fernández JB, Vallejo-Cardona AA. Nanomedicine review: Clinical developments in liposomal applications. *Cancer Nanotechnol* 2019;10. <https://doi.org/10.1186/S12645-019-0055-Y>.
- Vanden Berghe T, Grootjans S, Goossens V, Dondelinger Y, Krysko D V., Takahashi N, et al. Determination of apoptotic and necrotic cell death in vitro and in vivo. *Methods* 2013;61:117–29. <https://doi.org/10.1016/j.ymeth.2013.02.011>.
- Bharti DB, Bharati A V. Synthesis of ZnO nanoparticles using a hydrothermal method and a study its optical activity. *Luminescence* 2017;32:317–20. <https://doi.org/10.1002/bio.3180>.
- Bhatkalkar SG, Kumar D, Ali A, Sachar S. Surface dynamics associated with zinc oxide nanoparticles and biomolecules in presence of surfactants. *J Mol Liq* 2018;268:1–10. <https://doi.org/10.1016/j.molliq.2018.07.037>.
- Bhattacharya B, Mukherjee S. Cancer Therapy Using Antibiotics. *J Cancer Ther* 2015;06:849–58. <https://doi.org/10.4236/jct.2015.610093>.
- Bhattacharyya S, Kudgus RA, Bhattacharya R, Mukherjee P. Inorganic nanoparticles in cancer therapy. *Pharm Res* 2011;28:237–59. <https://doi.org/10.1007/s11095-010-0318-0>.
- Bisht G, Rayamajhi S. ZnO Nanoparticles: A Promising Anticancer Agent. *Nanobiomedicine (Rij)* 2016;3:9. <https://doi.org/10.5772/63437>.
- Biswal BM, Yusoff Z. Application of Nanotechnology in Cancer Treatment. *Topics in Mining, Metallurgy and Materials Engineering* 2017:269–311. [https://doi.org/10.1007/978-3-319-29761-3\\_11](https://doi.org/10.1007/978-3-319-29761-3_11).
-

---

Boivin J -F. Second cancers and other late side effects of cancer treatment.A review. *Cancer* 1990;65:770–5. [https://doi.org/10.1002/1097-0142\(19900201\)65:3+<770::AID-CNCR2820651323>3.0.CO;2-8](https://doi.org/10.1002/1097-0142(19900201)65:3+<770::AID-CNCR2820651323>3.0.CO;2-8).

Boruah S, Mustafiza S, Saikia D, Saikia H, Saikia P, Baruah M. Synthesis of ZnO Nanoparticles from Zinc Formate and their Optical Properties. *American Chemical Science Journal* 2016;11:1–10. <https://doi.org/10.9734/ACSJ/2016/22660>.

Brown LC, Mutter RW, Halyard MY. Benefits, risks, and safety of external beam radiation therapy for breast cancer. *Int J Womens Health* 2015;7:449–58. <https://doi.org/10.2147/IJWH.S55552>.

Bryan J. From cancer to rheumatoid arthritis treatment: The story of methotrexate. *Pharmaceutical Journal* 2012;289:303–4.

Buchheit R, Acosta-Humanez F, Almanzaby O. Structural, EPR and optical studies on Cu-doped ZnO nanoparticles synthesized by the sol-gel method at different calcination temperatures. *Revista Cubana de Fisica* 2016;33:4–11.

Chabner BBA, Cancer TR-NR, 2005 U, Roberts TG. Chemotherapy and the war on cancer. vol. 5. 2005a. <https://doi.org/10.1038/nrc1529>.

Chan ESL, Cronstein BN. Mechanisms of action of methotrexate. *Bull Hosp Joint Dis* 2013;71:S5–8. [https://doi.org/10.1016/S0162-3109\(00\)00189-2](https://doi.org/10.1016/S0162-3109(00)00189-2)

Chandrappa KG, Venkatesha T V. Electrochemical Synthesis and Photocatalytic Property of Zinc Oxide Nanoparticles. *Nanomicro Lett* 2012;4:14–24. <https://doi.org/10.1007/bf03353686>.

Chaudhari R, Patel P, Meghani N, Nasra S, Kumar A. Fabrication of methotrexate-loaded gold nanoconjugates and its enhanced anticancer activity in breast cancer. *3 Biotech* 2021;11:1–13. <https://doi.org/10.1007/s13205-021-02718-7>.

Chavali MS, Nikolova MP. Metal oxide nanoparticles and their applications in nanotechnology. *SN Appl Sci* 2019;1. <https://doi.org/10.1007/S42452-019-0592-3>.

Chen J, Huang L, Lai H, Lu C, Fang M, Zhang Q, et al. Methotrexate-loaded PEGylated chitosan nanoparticles: Synthesis, characterization, and in vitro and in vivo antitumoral activity. *Mol Pharm* 2014;11:2213–23. <https://doi.org/10.1021/mp400269z>.

---



---

Chen S, Cheng AC, Wang MS, Peng X. Detection of apoptosis induced by new type gosling viral enteritis virus in vitro through fluorescein annexin V-FITC/PI double labeling. *World J Gastroenterol* 2008;14:2174–8. <https://doi.org/10.3748/wjg.14.2174>.

Chen YH, Tsai CY, Huang PY, Chang MY, Cheng PC, Chou CH, et al. Methotrexate conjugated to gold nanoparticles inhibits tumor growth in a syngeneic lung tumor model. *Mol Pharm* 2007;4:713–22. <https://doi.org/10.1021/mp060132k>.

Cheung A, Bax HJ, Josephs DH, Ilieva KM, Pellizzari G, Opzoomer J, et al. Targeting folate receptor alpha for cancer treatment. *Oncotarget* 2016;7:52553–74. <https://doi.org/10.18632/oncotarget.9651>.

Chieng BW, Loo YY. Synthesis of ZnO nanoparticles by modified polyol method. *Mater Lett* 2012;73:78–82. <https://doi.org/10.1016/j.matlet.2012.01.004>.

Chumsri, Saranya, Timothy Howes, Ting Bao, Gauri Sabnis and AB. Aromatase, aromatase inhibitors, and breast cancer. *J Steroid Biochem Mol Biol* 2011;125:13–22. <https://doi.org/10.1016/j.jsbmb.2011.02.001>

Cindy B. Matsen LAN. Breast Cancer A Review for the General Surgeon. *JAMA Surg* 2013;148:2592–618. <https://doi.org/10.1016/B978-1-4377-1757-0.00028-7>.

Corona G, Giannini F, Fabris M, Toffoli G, Biocchi M. Role of folate receptor and reduced folate carrier in the transport of 5-methyltetrahydrofolic acid in human ovarian carcinoma cells. *Int J Cancer* 1998;75:125–33. [https://doi.org/10.1002/\(SICI\)1097-0215\(19980105\)75:1<125::AID-IJC19>3.0.CO;2-F](https://doi.org/10.1002/(SICI)1097-0215(19980105)75:1<125::AID-IJC19>3.0.CO;2-F).

Corrie PG. Cytotoxic chemotherapy: clinical aspects. *Medicine* 2008;36:24–8. <https://doi.org/10.1016/j.mpmed.2007.10.012>.

Crosby ME. Cell Cycle: Principles of Control. *Yale J Biol Med* 2007;80:141. PMID: PMC2248297

Van Cruchten S, Van den Broeck W. Morphological and biochemical aspects of apoptosis, oncosis and necrosis. *Anat Histol Embryol* 2002;31:214–23. <https://doi.org/10.1046/j.1439-0264.2002.00398.x>.

Cutolo M, Sulli A, Pizzorni C, Serio B, STRAUB RH. Anti-inflammatory mechanisms of methotrexate in rheumatoid arthritis. *Ann Rheum Dis* 2001;60:729–35. <https://doi.org/10.1136/ard.60.8.729>.

---

- 
- Darzynkiewicz Z, Bedner E, Smolewski P. Flow cytometry in analysis of cell cycle and apoptosis. *Semin Hematol* 2001;38:179–93. [https://doi.org/10.1016/S0037-1963\(01\)90051-4](https://doi.org/10.1016/S0037-1963(01)90051-4).
- Das M, Datir SR, Singh RP, Jain S. Augmented anticancer activity of a targeted, intracellularly activatable, theranostic nanomedicine based on fluorescent and radiolabeled, methotrexate-folic acid-multiwalled carbon nanotube conjugate. *Mol Pharm* 2013;10:2543–57. [https://doi.org/10.1021/MP300701E/SUPPL\\_FILE/MP300701E\\_SI\\_001.PDF](https://doi.org/10.1021/MP300701E/SUPPL_FILE/MP300701E_SI_001.PDF).
- Davies SM. Therapy-related leukemia associated with alkylating agents. *Med Pediatr Oncol* 2001;36:536–40. <https://doi.org/10.1002/mpo.1126>.
- Dawood S. Triple-negative breast cancer: Epidemiology and Management Options. *Molecular Pathology of Breast Cancer* 2016;70:71–80. [https://doi.org/10.1007/978-3-319-41761-5\\_6](https://doi.org/10.1007/978-3-319-41761-5_6).
- Dawood S. Triple-negative breast cancer: Epidemiology and management options. *Drugs* 2010;70:2247–58. <https://doi.org/10.2165/11538150-000000000-00000>.
- Decremps F, Datchi F, Saitta M, Polian A, Pascarelli S, Di Cicco A, et al. Local structure of condensed zinc oxide. *Phys Rev B Condens Matter Mater Phys* 2003;68. <https://doi.org/10.1103/PhysRevB.68.104101>.
- Dehvari K, Li JD, Chang JY. Bovine Serum Albumin-Templated Synthesis of Manganese-Doped Copper Selenide Nanoparticles for Boosting Targeted Delivery and Synergistic Photothermal and Photodynamic Therapy. *ACS Appl Bio Mater* 2019;2:3019–29. [https://doi.org/10.1021/ACSABM.9B00339/SUPPL\\_FILE/MT9B00339\\_SI\\_001.PDF](https://doi.org/10.1021/ACSABM.9B00339/SUPPL_FILE/MT9B00339_SI_001.PDF).
- Deng Y, Zhang H. The synergistic effect and mechanism of doxorubicin-ZnO nanocomplexes as a multimodal agent integrating diverse anticancer therapeutics. *Int J Nanomedicine* 2013;8:1835–41. <https://doi.org/10.2147/IJN.S43657>.
- Dhanikula RS, Argaw A, Bouchard JF, Hildgen P. Methotrexate loaded polyether-copolyester dendrimers for the treatment of gliomas: Enhanced efficacy and intratumoral transport capability. *Mol Pharm* 2008;5:105–16. <https://doi.org/10.1021/mp700086j>.
- Dhanka M, Shetty C, Srivastava R. Methotrexate loaded alginate microparticles and effect of Ca<sup>2+</sup> post-crosslinking: An in vitro physicochemical and biological evaluation. *Int J Biol Macromol* 2018;110:294–307. <https://doi.org/10.1016/j.ijbiomac.2017.10.148>.
- Domingues C, Santos A, Alvarez-Lorenzo C, Concheiro A, Jarak I, Veiga F, et al. Where Is Nano Today and Where Is It Headed? A Review of Nanomedicine and the Dilemma of Nanotoxicology. *ACS Nano* 2022;16:9994–10041. <https://doi.org/10.1021/acsnano.2c00128>.
-

---

Dr.R.Sarin and ICMR group. Consensus Document for Management of Breast Cancer. Division of Publication and Information on Behalf of the Secretary DHR & DG, ICMR, New Delhi 2016;Consensus:1–40.

D’Souza JN, Prabhu A, Nagaraja GK, Navada K. M, Kouser S, Manasa DJ. Unravelling the human triple negative breast cancer suppressive activity of biocompatible zinc oxide nanostructures influenced by *Vateria indica* (L.) fruit phytochemicals. *Materials Science and Engineering C* 2021;122. <https://doi.org/10.1016/j.msec.2021.111887>.

Du L, Suo S, Luo D, Jia H, Sha Y, Liu Y. Hydroxyethylated graphene oxide as potential carriers for methotrexate delivery. *Journal of Nanoparticle Research* 2013;15:1–7. <https://doi.org/10.1007/S11051-013-1708-0/METRICS>.

Dumay A, Feugeas JP, Wittmer E, Lehmann-Che J, Bertheau P, Espié M, et al. Distinct tumor protein p53 mutants in breast cancer subgroups. *Int J Cancer* 2013;132:1227–31. <https://doi.org/10.1002/ijc.27767>.

Espitia PJP, Soares N de FF, Coimbra JS dos R, de Andrade NJ, Cruz RS, Medeiros EAA. Zinc Oxide Nanoparticles: Synthesis, Antimicrobial Activity and Food Packaging Applications. *Food Bioproc Tech* 2012;5:1447–64. <https://doi.org/10.1007/s11947-012-0797-6>.

Fabbro C, Ali-Boucetta H, Da Ros T, Bianco A, Kostarelos K, Prato M. Targeting carbon nanotubes against cancer. *Chemical Communications* 2012;48:3911–26. <https://doi.org/10.1039/c2cc17995d>.

Fan L, Duan M, Sun X, Wang H, Liu J. Injectable Liquid Metal- And Methotrexate-Loaded Microsphere for Cancer Chemophotothermal Synergistic Therapy. *ACS Appl Bio Mater* 2020;3:3553–9. [https://doi.org/10.1021/ACSABM.0C00171/ASSET/IMAGES/MEDIUM/MT0C00171\\_0008.GIF](https://doi.org/10.1021/ACSABM.0C00171/ASSET/IMAGES/MEDIUM/MT0C00171_0008.GIF).

Farkona S, Diamandis EP, Blasutig IM. Cancer immunotherapy: The beginning of the end of cancer? *BMC Med* 2016;14. <https://doi.org/10.1186/S12916-016-0623-5>.

Fasehee H, Dinarvand R, Ghavamzadeh A, Esfandyari-Manesh M, Moradian H, Faghihi S, et al. Delivery of disulfiram into breast cancer cells using folate-receptor-targeted PLGA-PEG nanoparticles: In vitro and in vivo investigations. *J Nanobiotechnology* 2016;14:1–18. <https://doi.org/10.1186/s12951-016-0183-z>.

---

- 
- Fei F, Siegal GP, Wei S. Characterization of estrogen receptor-low-positive breast cancer. *Breast Cancer Res Treat* 2021;188:225–35. <https://doi.org/10.1007/s10549-021-06148-0>.
- Feinsilber D, Leoni RJ, Siripala D, Leuck J, Mears KA. Evaluation, Identification, and Management of Acute Methotrexate Toxicity in High-dose Methotrexate Administration in Hematologic Malignancies. *Cureus* 2018;10:1–6. <https://doi.org/10.7759/cureus.2040>.
- Feng Y, Spezia M, Huang S, Yuan C, Zeng Z, Zhang L, et al. Breast cancer development and progression: Risk factors, cancer stem cells, signaling pathways, genomics, and molecular pathogenesis. *Genes Dis* 2018b;5:77–106. <https://doi.org/10.1016/j.gendis.2018.05.001>.
- Ferlay J, Colombet M, Soerjomataram I, Mathers C, Parkin DM, Piñeros M, et al. Estimating the global cancer incidence and mortality in 2018: GLOBOCAN sources and methods. *Int J Cancer* 2019;144:1941–53. <https://doi.org/10.1002/ijc.31937>.
- Fernandes SG, Gala K, Khattar E. Telomerase inhibitor MST-312 and quercetin synergistically inhibit cancer cell proliferation by promoting DNA damage. *Transl Oncol* 2023;27:101569. <https://doi.org/10.1016/j.tranon.2022.101569>.
- Feynman RP. There's plenty of room at the bottom. *Micromechanics and MEMS: Classic and Seminal Papers to 1990* 1997;2–9. <https://doi.org/10.1109/9780470545263.sect1>.
- Fitoussi AD, Berry MG, Famà F, Falcou MC, Curnier A, Couturaud B, et al. Oncoplastic breast surgery for cancer: Analysis of 540 consecutive cases. *Plast Reconstr Surg* 2010;125:454–62. <https://doi.org/10.1097/PRS.0b013e3181c82d3e>.
- Florea A-M, Büsselberg D. Breast cancer and possible mechanisms of therapy resistance. *Journal of Local and Global Health Science* 2013;1:2. <https://doi.org/10.5339/jlghs.2013.2>.
- Fu SW, Chen L, Man YG. miRNA biomarkers in breast cancer detection and management. *J Cancer* 2011;2:116–22. <https://doi.org/10.7150/jca.2.116>.
- Fu Y, Yang G, Zhu F, Peng C, Li W, Li H, et al. Antioxidants decrease the apoptotic effect of 5-Fu in colon cancer by regulating Src-dependent caspase-7 phosphorylation. *Cell Death Dis* 2014;5:e983. <https://doi.org/10.1038/cddis.2013.509>.
- Gao Y, Shang Q, Li W, Guo W, Stojadinovic A, Mannion C, et al. Antibiotics for cancer treatment: A double-edged sword. *J Cancer* 2020;11:5135–49. <https://doi.org/10.7150/jca.47470>.
-

---

Garimella LBVS, Dhiman TK, Kumar R, Singh AK, Solanki PR. One-Step Synthesized ZnO np-Based Optical Sensors for Detection of Aldicarb via a Photoinduced Electron Transfer Route. *ACS Omega* 2020;5:2552–60. <https://doi.org/10.1021/acsomega.9b01987>.

Geim AK, Novoselov KS. The rise of graphene. *Nanoscience and Technology: A Collection of Reviews from Nature Journals* 2009;11–9. [https://doi.org/10.1142/9789814287005\\_0002](https://doi.org/10.1142/9789814287005_0002).

Gérard C, Goldbeter A. Dynamics of the mammalian cell cycle in physiological and pathological conditions. *Wiley Interdiscip Rev Syst Biol Med* 2016;8:140–56. <https://doi.org/10.1002/wsbm.1325>.

Ghaderi KF, Phillips J, Perry H, Lotfi P, Mehta TS. Contrast-enhanced mammography: Current applications and future directions. *Radiographics* 2019;39:1907–20. <https://doi.org/10.1148/RG.2019190079>.

Ghasemi M, Turnbull T, Sebastian S, Kempson I. The mtt assay: Utility, limitations, pitfalls, and interpretation in bulk and single-cell analysis. *Int J Mol Sci* 2021;22:12827. <https://doi.org/10.3390/IJMS222312827/S1>.

Ghorbani HR, Mehr FP, Pazoki H, Rahmani BM. Synthesis of ZnO nanoparticles by precipitation method. *Oriental Journal of Chemistry* 2015;31:1219–21. <https://doi.org/10.13005/ojc/310281>.

Gnant M, Fitzal F, Rinnerthaler G, Steger GG, Greil-Ressler S, Balic M, et al. Duration of Adjuvant Aromatase-Inhibitor Therapy in Postmenopausal Breast Cancer. *New England Journal of Medicine* 2021;385:395–405. <https://doi.org/10.1056/NEJMOA2104162>.

Goh AM, Coffill CR, Lane DP. The role of mutant p53 in human cancer. *Journal of Pathology* 2011;223:116–26. <https://doi.org/10.1002/path.2784>.

Goss PE, Ingle JN, Pritchard KI, Robert NJ, Muss H, Gralow J, et al. Extending Aromatase-Inhibitor Adjuvant Therapy to 10 Years. *New England Journal of Medicine* 2016;375:209–19. <https://doi.org/10.1056/NEJMOA1604700>.

Gribko A, Künzel J, Wunsch D, Lu Q, Nagel S, Knauer S, et al. Is small smarter? Nanomaterial-based detection and elimination of circulating tumor cells: Current knowledge and perspectives. *Int J Nanomedicine* 2019;14:4187–209. <https://doi.org/10.2147/IJN.S198319>.

Gunasekera UA, Pankhurst QA, Douek M. Imaging applications of nanotechnology in cancer. *Target Oncol* 2009;4:169–81. <https://doi.org/10.1007/s11523-009-0118-9>.

---

- 
- Guo Z, Luo Y, Zhang P, Chetwynd AJ, Qunhui Xie H, Abdolapur Monikh F, et al. Deciphering the particle specific effects on metabolism in rat liver and plasma from ZnO nanoparticles versus ionic Zn exposure. *Environ Int* 2020;136. <https://doi.org/10.1016/j.envint.2019.105437>.
- Gyanani V, Haley JC, Goswami R. Challenges of current anticancer treatment approaches with focus on liposomal drug delivery systems. *Pharmaceuticals* 2021;14. <https://doi.org/10.3390/ph14090835>.
- Hagner N, Joerger M. Cancer chemotherapy: Targeting folic acid synthesis. *Cancer Manag Res* 2010;2:293–301. <https://doi.org/10.2147/cmar.s10043>.
- Halik PK, Koźmiński P, Gniazdowska E. Perspectives of Methotrexate-Based Radioagents for Application in Nuclear Medicine. *Mol Pharm* 2021;18:33–43. <https://doi.org/10.1021/acs.molpharmaceut.0c00740>.
- Hamed KM, Dighriri IM, Baomar AF, Alharthy BT, Alenazi FE, Alali GH, et al. Overview of Methotrexate Toxicity: A Comprehensive Literature Review. *Cureus* 2022;14. <https://doi.org/10.7759/cureus.29518>.
- Hamed Nosrati, Amir Mojtahedi, Hossein Danafar HKM. Enzymatic stimuli-responsive methotrexate-conjugated magnetic nanoparticles for target delivery to breast cancer cells and release study in lysosomal condition. *J Biomed Mater Res A* 2018;106:1646–54. <https://doi.org/https://doi.org/10.1002/jbm.a.36364>.
- Hashad D, Sorour A, Ghazal A, Talaat I. Free Circulating Tumor DNA as a Diagnostic Marker for Breast Cancer. *J Clin Lab Anal* 2012;26:467–72. <https://doi.org/10.1002/jcla.21548>.
- Hassan HFH, Mansour AM, Abo-Youssef AMH, Elsadek BEM, Messiha BAS. Zinc oxide nanoparticles as a novel anticancer approach; in vitro and in vivo evidence. *Clin Exp Pharmacol Physiol* 2017;44:235–43. <https://doi.org/10.1111/1440-1681.12681>.
- Hernando C, Ortega-Morillo B, Tapia M, Moragón S, Teresa Martínez M, Eroles P, et al. Oral selective estrogen receptor degraders (SERDs) as a novel breast cancer therapy: present and future from a clinical perspective. *MdpiCom* 2021. <https://doi.org/10.3390/ijms22157812>.
- Hess JA, Khasawneh MK. Cancer metabolism and oxidative stress: Insights into carcinogenesis and chemotherapy via the non-dihydrofolate reductase effects of methotrexate. *BBA Clin* 2015;3:152–61. <https://doi.org/10.1016/j.bbacli.2015.01.006>.
-

- 
- Hobson DW. Commercialization of nanotechnology. Wiley Interdiscip Rev Nanomed Nanobiotechnol 2009;1:189–202. <https://doi.org/10.1002/wnan.28>.
- Holohan C, Van Schaeybroeck S, Longley DB, Johnston PG. Cancer drug resistance: an evolving paradigm. Nat Rev Cancer 2013;13:714–26. <https://doi.org/10.1038/nrc3599>.
- Hosni, Mongia, Samir Farhat, Mounir Ben Amar, Andrei Kanaev, Nouredine Jouini and IHinkov. Mixing Strategies for Zinc Oxide Nanoparticle Synthesis via a Polyol Process. AIChE Journal 2015;59:1708–21. <https://doi.org/10.1002/aic.14737>.
- Hou J, Liu X, Zhou S. Programmable materials for efficient CTCs isolation: From micro/nanotechnology to biomimicry. View 2021;2. <https://doi.org/10.1002/VIW.20200023>.
- Hu C, Du W. Zinc oxide nanoparticles (ZnO NPs) combined with cisplatin and gemcitabine inhibits tumor activity of NSCLC cells. Aging 2020;12:25767–77. <https://doi.org/10.18632/aging.104187>.
- Huang Q, Luo Y, ... QZ of computer assisted radiology and, 2017 undefined. Breast ultrasound image segmentation: a survey. Springer 2017;12:493–507. <https://doi.org/10.1007/s11548-016-1513-1>.
- Hussein AK. Applications of nanotechnology in renewable energies - A comprehensive overview and understanding. Renewable and Sustainable Energy Reviews 2015;42:460–76. <https://doi.org/10.1016/j.rser.2014.10.027>.
- Hutchinson L. Breast cancer: Challenges, controversies, breakthroughs. Nat Rev Clin Oncol 2010a;7:669–70. <https://doi.org/10.1038/nrclinonc.2010.192>.
- Ijaz I, Gilani E, Nazir A, Bukhari A. Detail review on chemical, physical and green synthesis, classification, characterizations and applications of nanoparticles. Green Chem Lett Rev 2020;13:59–81. <https://doi.org/10.1080/17518253.2020.1802517>.
- Ilesanmi AE, Chaumrattanakul U, Makhanov SS. Methods for the segmentation and classification of breast ultrasound images: a review. J Ultrasound 2021;24:367–82. <https://doi.org/10.1007/s40477-020-00557-5>.
- Jadhav V, Ray P, Sachdeva G, Bhatt P. Biocompatible arsenic trioxide nanoparticles induce cell cycle arrest by p21WAF1/CIP1 expression via epigenetic remodeling in LNCaP and PC3 cell lines. Life Sci 2016;148:41–52. <https://doi.org/10.1016/j.lfs.2016.02.042>.
-

---

Janer G, Mas del Molino E, Fernández-Rosas E, Fernández A, Vázquez-Campos S. Cell uptake and oral absorption of titanium dioxide nanoparticles. *Toxicol Lett* 2014;228:103–10. <https://doi.org/10.1016/j.toxlet.2014.04.014>.

Jason Karch JDM. Regulated necrotic cell death: The passive aggressive side of Bax and Bak. *Physiol Behav* 2018;176:139–48. <https://doi.org/10.1161/CIRCRESAHA.116.305421>.

Javed Akhtar M, Ahamed M, Kumar S, Majeed Khan M, Ahmad J, Alrokayan SA. Zinc oxide nanoparticles selectively induce apoptosis in human cancer cells through reactive oxygen species. *Int J Nanomedicine* 2012;7:845–57. <https://doi.org/10.2147/IJN.S29129>.

Jayaseelan C, Rahuman AA, Rajakumar G, Santhoshkumar T, Kirthi AV, Marimuthu S, et al. Efficacy of plant-mediated synthesized silver nanoparticles against hematophagous parasites. *Parasitol Res* 2012;111:921–33. <https://doi.org/10.1007/s00436-011-2473-6>.

Jeejeebhoy KN. Human zinc deficiency. *Nutrition in Clinical Practice* 2007;22:65–7. <https://doi.org/10.1177/011542650702200165>.

Jerzy Einhorn. Nitrogen mustard: The origin of chemotherapy for cancer. *Int J Radiat Oncol Biol Phys* 1985;11:1375–8. <https://doi.org/10.4324/9780203645024>.

Jesinger RA. Breast anatomy for the interventionalist. *Tech Vasc Interv Radiol* 2014;17:3–9. <https://doi.org/10.1053/j.tvir.2013.12.002>.

Jia F, Wang Y, Fang Z, Dong J, Shi F, Zhang W, et al. Novel Peptide-Based Magnetic Nanoparticle for Mesenchymal Circulating Tumor Cells Detection. *Anal Chem* 2021;93:5670–5. <https://doi.org/10.1021/ACS.ANALCHEM.1C00577>.

Jiang J, Pi J, Cai J. The Advancing of Zinc Oxide Nanoparticles for Biomedical Applications. *Bioinorg Chem Appl* 2018;2018:1–18. <https://doi.org/10.1155/2018/1062562>.

Johari-Ahar M, Barar J, Alizadeh AM, Davaran S, Omid Y, Rashidi MR. Methotrexate-conjugated quantum dots: Synthesis, characterisation and cytotoxicity in drug resistant cancer cells. *J Drug Target* 2016;24:120–33. <https://doi.org/10.3109/1061186X.2015.1058801>.

Jose S, Cinu TA, Sebastian R, Shoja MH, Aleykutty NA, Durazzo A, et al. Transferrin-Conjugated Docetaxel-PLGA Nanoparticles for Tumor Targeting: Influence on MCF-7 Cell Cycle. *Polymers* (Basel) 2019;11:1–20. <https://doi.org/https://doi.org/10.3390/polym11111905>.

---



- 
- Joshi M, Bhatt P. Deciphering the anticancer activity of biocompatible zinc oxide nanoparticles loaded with methotrexate on breast cancer cells. *Bulletin of Materials Science* 2023;46:1–14. <https://doi.org/10.1007/s12034-023-03044-9>.
- Kakkar D, Dumoga S, Kumar R, Chuttani K, Mishra AK. PEGylated solid lipid nanoparticles: Design, methotrexate loading and biological evaluation in animal models. *Medchemcomm* 2015;6:1452–63. <https://doi.org/10.1039/c5md00104h>.
- Karami Fath M, Azargoonjahromi A, Kiani A, Jalalifar F, Osati P, Akbari Oryani M, et al. The role of epigenetic modifications in drug resistance and treatment of breast cancer. *Cell Mol Biol Lett* 2022;27. <https://doi.org/10.1186/S11658-022-00344-6>.
- Kaur S, Annu S, Shingatgeri V, Najm M. A Comprehensive Approach Towards Wnt/ $\beta$ -Catenin Signalling Pathway in Breast Cancer and Drug Resistance 2020. <https://doi.org/10.24321/2454.8642.202008>.
- Kavithaa K, Paulpandi M, Ponraj T, Murugan K, Sumathi S. Induction of intrinsic apoptotic pathway in human breast cancer (MCF-7) cells through facile biosynthesized zinc oxide nanorods. *Karbala International Journal of Modern Science* 2016;2:46–55. <https://doi.org/http://dx.doi.org/10.1016/j.kijoms.2016.01.002>.
- Ke X, Shen L. Molecular targeted therapy of cancer: The progress and future prospect. *Frontiers in Laboratory Medicine* 2017;1:69–75. <https://doi.org/10.1016/j.flm.2017.06.001>.
- Khan ZA, Tripathi R, Mishra B. Methotrexate: A detailed review on drug delivery and clinical aspects. *Expert Opin Drug Deliv* 2012;9:151–69. <https://doi.org/10.1517/17425247.2012.642362>.
- Khanna N, Berek JS. Cancer genetics. *Clinical Gynecology*, Second Edition, 2015a, p. 842–53. <https://doi.org/10.1017/CBO9781139628938.056>.
- Khanna N, Berek JS. Cancer genetics. *Clinical Gynecology*, Second Edition, 2015b, p. 842–53. <https://doi.org/10.1017/CBO9781139628938.056>.
- Kianfar E. Importance & Applications of Nanotechnology 2020.
- Kim SE, Kim WJ, Choi DS, Lee DY. Comparison of goserelin and leuprorelin for ovarian protection during chemotherapy in young patients with breast cancer. *Breast Cancer Res Treat* 2023;198:231–7. <https://doi.org/10.1007/s10549-023-06877-4>.
-

- 
- Kim YR, Park J Il, Lee EJ, Park SH, Seong NW, Kim JH, et al. Toxicity of 100 nm zinc oxide nanoparticles: A report of 90-day repeated oral administration in Sprague Dawley rats. *Int J Nanomedicine* 2014;9:109–26. <https://doi.org/10.2147/IJN.S57928>.
- Kindts I, Verhoeven K, Laenen A, Christiaens M, Janssen H, Van der Vorst A, et al. A comparison of a brachytherapy and an external beam radiotherapy boost in breast-conserving therapy for breast cancer: local and any recurrences. *Strahlentherapie Und Onkologie* 2019;195:310–7. <https://doi.org/10.1007/s00066-018-1413-0>.
- Kirkwood JM, Butterfield LH, Tarhini AA, Zarour H, Kalinski P, Ferrone S. Immunotherapy of cancer in 2012. *Wiley Online Library* 2012;62:309–35. <https://doi.org/10.3322/caac.20132>.
- Ko JW, Hong ET, Lee IC, Park SH, Park J Il, Seong NW, et al. Evaluation of 2-week repeated oral dose toxicity of 100 nm zinc oxide nanoparticles in rats. *Lab Anim Res* 2015;31:139–47. <https://doi.org/10.5625/lar.2015.31.3.139>.
- Koivunen ME, Krogsrud RL. Principles of immunochemical techniques used in clinical laboratories. *Lab Med* 2006;37:490–7. <https://doi.org/10.1309/MV9RM1FDLWAUWQ3F>.
- Kollur SP, Prasad SK, Pradeep S, Veerapur R, Patil SS, Amachawadi RG, et al. Luteolin-fabricated zno nanostructures showed PLK-1 mediated anti-breast cancer activity. *Biomolecules* 2021;11:1–21. <https://doi.org/10.3390/biom11030385>.
- Kolodziejczak-Radzimska A, Jesionowski T. Zinc oxide-from synthesis to application: A review. *Materials* 2014;7:2833–81. <https://doi.org/10.3390/ma7042833>.
- Kotsopoulos J, Lubinski J, Salmena L, Lynch HT, Kim-Sing C, Foulkes WD, et al. Breastfeeding and the risk of breast cancer in BRCA1 and BRCA2 mutation carriers. *Breast Cancer Research* 2012;14. <https://doi.org/10.1186/BCR3138>.
- Krause W. Resistance to anti-tubulin agents: From vinca alkaloids to epothilones. *Cancer Drug Resistance* 2019;1–25. <https://doi.org/10.20517/cdr.2019.06>.
- Król A, Pomastowski P, Rafińska K, Railean-Plugaru V, Buszewski B. Zinc oxide nanoparticles: Synthesis, antiseptic activity and toxicity mechanism. *Adv Colloid Interface Sci* 2017;249:37–52. <https://doi.org/10.1016/j.cis.2017.07.033>.
- Kroto HW. C60: Buckminsterfullerene, The Celestial Sphere that Fell to Earth. *Angewandte Chemie International Edition in English* 1992;31:111–29. <https://doi.org/10.1002/ANIE.199201113>.
-

---

Kuang FG, Kuang XY, Kang SY, Zhong MM, Sun XW. Ab initio study on physical properties of wurtzite, zincblende, and rocksalt structures of zinc oxide using revised functionals. *Mater Sci Semicond Process* 2015;31:700–8. <https://doi.org/10.1016/j.mssp.2014.12.068>.

Kumari SDC, Tharani CB, Narayanan N, Kumar CS. Formulation and characterization of Methotrexate loaded sodium alginate chitosan Nanoparticles. *Indian Journal of Research in Pharmacy and Biotechnology* 2013;1:915–21.

Kurien BT, Scofield RH. Western blotting. *Methods* 2006;38:283–93. <https://doi.org/10.1016/j.ymeth.2005.11.007>.

Kuznetsova NR, Sevrin C, Lespineux D, Bovin N V., Vodovozova EL, Mészáros T, et al. Hemocompatibility of liposomes loaded with lipophilic prodrugs of methotrexate and melphalan in the lipid bilayer. *Journal of Controlled Release* 2012;160:394–400. <https://doi.org/10.1016/j.jconrel.2011.12.010>.

Kyvsgaard N, Mikkelsen TS, Als TD, Christensen AE, Corydon TJ, Herlin T. Single nucleotide polymorphisms associated with methotrexate-induced nausea in juvenile idiopathic arthritis. *Pediatric Rheumatology* 2021;19:1–14. <https://doi.org/10.1186/s12969-021-00539-9>.

De La Harpe KM, Kondiah PPD, Choonara YE, Marimuthu T, Du Toit LC, Pillay V. The hemocompatibility of nanoparticles: A review of cell-nanoparticle interactions and hemostasis. *Cells* 2019;8. <https://doi.org/10.3390/cells8101209>.

Lakshmipriya T, Gopinath SCB. Introduction to nanoparticles and analytical devices. *Nanoparticles in Analytical and Medical Devices* 2020:1–29. <https://doi.org/10.1016/B978-0-12-821163-2.00001-7>.

Lanje AS, Sharma SJ, Ningthoujam RS, Ahn J-S, Pode RB. Low temperature dielectric studies of zinc oxide (ZnO) nanoparticles prepared by precipitation method. *Advanced Powder Technology* 2013;24:331–5. <https://doi.org/10.1016/j.appt.2012.08.005>.

Li CI, Malone KE, Daling JR. Differences in breast cancer stage, treatment, and survival by race and ethnicity. *ArchInternMed* 2003;163:49–56. <https://doi.org/10.1001/archinte.163.1.49>.

Li J, Yuan J. Caspases in apoptosis and beyond. *Oncogene* 2008;27:6194–206. <https://doi.org/10.1038/onc.2008.297>.

Lim HS, Jeong SJ, Lee JS, Park MH, Kim JW, Shin SS, et al. Paget disease of the breast: Mammographic, US, and MR imaging findings with pathologic correlation. *Radiographics* 2011;31:1973–88. <https://doi.org/10.1148/rg.317115070>.

---

- 
- Lindgren M, Rosenthal-Aizman K, Saar K, Eiríksdóttir E, Jiang Y, Sassian M, et al. Overcoming methotrexate resistance in breast cancer tumour cells by the use of a new cell-penetrating peptide. *Biochem Pharmacol* 2006;71:416–25. <https://doi.org/10.1016/j.bcp.2005.10.048>.
- Lipworth L, Bailey LR, Trichopoulos D. History of breast-feeding in relation to breast cancer risk: A review of the epidemiologic literature. *J Natl Cancer Inst* 2000;92:302–12. <https://doi.org/10.1093/jnci/92.4.302>.
- Liu J, Ma X, Jin S, Xue X, Zhang C, Wei T, et al. Zinc Oxide Nanoparticles as Adjuvant to Facilitate Doxorubicin Intracellular Accumulation and Visualize pH-Responsive Release for Overcoming Drug Resistance. *Mol Pharm* 2016;13:1723–30. <https://doi.org/10.1021/acs.molpharmaceut.6b00311>.
- Liu J, Park J, Park KH, Ahn Y, Park J-Y, Koh KH, et al. Enhanced photoconduction of free-standing ZnO nanowire films by L-lysine treatment. *Nanotechnology* 2010;21:485–504. <https://doi.org/10.1088/0957-4484/21/48/485504>.
- Liu K, Liu P cheng, Liu R, Wu X. Dual AO/EB Staining to Detect Apoptosis in Osteosarcoma Cells Compared with Flow Cytometry. *Med Sci Monit Basic Res* 2015;21:15. <https://doi.org/10.12659/MSMBR.893327>.
- Liu X, Qu H, Cao W, Wang Y, Ma Z, Li F, et al. Efficacy of combined therapy of goserelin and letrozole on very young women with advanced breast cancer as first-line endocrine therapy. *Endocr J* 2013;60:819–28. <https://doi.org/10.1507/endocrj.EJ12-0434>.
- Loibl S, Gianni L. HER2-positive breast cancer. *The Lancet* 2017;389:2415–29. [https://doi.org/10.1016/S0140-6736\(16\)32417-5](https://doi.org/10.1016/S0140-6736(16)32417-5).
- Lorizio W, Wu AHB, Beattie MS, Rugo H, Tchu S, Kerlikowske K, et al. Clinical and biomarker predictors of side effects from tamoxifen. *Breast Cancer Res Treat* 2012;132:1107–18. <https://doi.org/10.1007/s10549-011-1893-4>.
- Makówka A, Kotowicz B. The importance of selected biomarkers in the clinical practice of breast cancer patients. *Nowotwory* 2023;73:277–85. <https://doi.org/10.5603/njo.95605>.
- Malaikozhundan B, Vaseeharan B, Vijayakumar S, Pandiselvi K, Kalanjiam MAR, Murugan K, et al. Biological therapeutics of Pongamia pinnata coated zinc oxide nanoparticles against clinically important pathogenic bacteria, fungi and MCF-7 breast cancer cells. *Microb Pathog* 2017;104:268–77. <https://doi.org/10.1016/j.micpath.2017.01.029>.
-

- 
- Malvia S, Bagadi SA, Dubey US, Saxena S. Epidemiology of breast cancer in Indian women. *Asia Pac J Clin Oncol* 2017;13:289–95. <https://doi.org/10.1111/ajco.12661>.
- Manchanda R, Loggenberg K, Sanderson S, Burnell M, Wardle J, Gessler S, et al. Population testing for cancer predisposing BRCA1/BRCA2 mutations in the ashkenazi-jewish community: A randomized controlled trial. *J Natl Cancer Inst* 2015;107. <https://doi.org/10.1093/jnci/dju379>.
- Mandal AK, Katuwal S, Tettey F, Gupta A, Bhattarai S, Jaisi S, et al. Current Research on Zinc Oxide Nanoparticles: Synthesis, Characterization, and Biomedical Applications. *Nanomaterials* 2022;12. <https://doi.org/10.3390/nano12173066>.
- Manoranjan Arakha SJ. Nanoparticle. *Interfacial Phenomena on Biological Membranes.*, Germany: Springer International Publishing; 2018a, p. 1–36.
- Mansoori GA. *An Introduction to Nanoscience and Nanotechnology*. John Wiley & Sons.; 2017. [https://doi.org/10.1007/978-3-319-46835-8\\_1](https://doi.org/10.1007/978-3-319-46835-8_1).
- Marika Grönroos, Ming Chen, Timo Jahnukainen, Arrigo Capitanio, Roman I. Aizman and GC. Methotrexate Induces Cell Swelling and Necrosis in Renal Tubular Cells. *Pediatr Blood Cancer* 2006;46:624–9. <https://doi.org/https://doi.org/10.1002/pbc.20471>.
- Masoudipour E, Kashanian S, Maleki N. A targeted drug delivery system based on dopamine functionalized nano graphene oxide. *Chem Phys Lett* 2017;668:56–63. <https://doi.org/10.1016/J.CPLETT.2016.12.019>.
- Masuda H, Baggerly KA, Wang Y, Iwamoto T, Brewer T, Pusztai L, et al. Comparison of molecular subtype distribution in triple-negative inflammatory and non-inflammatory breast cancers. *Breast Cancer Research* 2013;15. <https://doi.org/10.1186/BCR3579>.
- Mazzaferro S, Bouchemal K, Ponchel G. Oral delivery of anticancer drugs I: General considerations. *Drug Discov Today* 2013;18:25–34. <https://doi.org/10.1016/j.drudis.2012.08.004>.
- Meng J, Wu XQ, Sun Z, Xun R De, Liu MS, Hu R, et al. Efficacy and Safety of CAR-T Cell Products Axicabtagene Ciloleucel, Tisagenlecleucel, and Lisocabtagene Maraleucel for the Treatment of Hematologic Malignancies: A Systematic Review and Meta-Analysis. *Front Oncol* 2021;11. <https://doi.org/10.3389/fonc.2021.698607>.
- Meszaros K, Patocs A. Glucocorticoids influencing Wnt/ $\beta$ -catenin pathway; multiple sites, heterogeneous effects. *Molecules* 2020;25. <https://doi.org/10.3390/molecules25071489>.
-

- 
- Mi Y, Shao Z, Vang J, Kaidar-Person O, Wang AZ. Application of nanotechnology to cancer radiotherapy. *Cancer Nanotechnol* 2016;7. <https://doi.org/10.1186/S12645-016-0024-7>.
- Miller E. Apoptosis measurement by annexin v staining. *Methods Mol Med*, vol. 88, 2004, p. 191–202. <https://doi.org/10.1385/1-59259-406-9:191>.
- Mishra P, Ali Ahmad MF, Al-Keridis LA, Saeed M, Alshammari N, Alabdallah NM, et al. Methotrexate-conjugated zinc oxide nanoparticles exert a substantially improved cytotoxic effect on lung cancer cells by inducing apoptosis. *Front Pharmacol* 2023;14:1–17. <https://doi.org/10.3389/fphar.2023.1194578>.
- Mitra S, B S, Patra P, Chandra S, Debnath N, Das S, et al. Porous ZnO nanorod for targeted delivery of doxorubicin: In vitro and in vivo response for therapeutic applications. *J Mater Chem* 2012;22:24145–54. <https://doi.org/10.1039/c2jm35013k>.
- Mohd Yusof H, Mohamad R, Zaidan UH, Abdul Rahman NA. Microbial synthesis of zinc oxide nanoparticles and their potential application as an antimicrobial agent and a feed supplement in animal industry: A review. *J Anim Sci Biotechnol* 2019;10. <https://doi.org/10.1186/s40104-019-0368-z>.
- Morris PG, Fornier MN. Microtubule active agents: Beyond the taxane frontier. *Clinical Cancer Research* 2008;14:7167–72. <https://doi.org/10.1158/1078-0432.CCR-08-0169>.
- Mossink JP. Zinc as nutritional intervention and prevention measure for COVID–19 disease. *BMJ Nutr Prev Health* 2020;3:111–7. <https://doi.org/10.1136/bmjnp-2020-000095>.
- Muhammad Z, Raza A, Ghafoor S, Naeem A, Naz SS, Riaz S, et al. PEG capped methotrexate silver nanoparticles for efficient anticancer activity and biocompatibility. *European Journal of Pharmaceutical Sciences* 2016;91:251–5. <https://doi.org/10.1016/J.EJPS.2016.04.029>.
- Mukherjee A, Basu S, Sarkar N, Ghosh A. Advances in Cancer Therapy with Plant Based Natural Products. *Curr Med Chem* 2012;8:1467–86. <https://doi.org/10.2174/0929867013372094>.
- Mukherjee N, Panda CK. Wnt/ $\beta$ -Catenin Signaling Pathway as Chemotherapeutic Target in Breast Cancer: An Update on Pros and Cons. *Clin Breast Cancer* 2020;20:361–70. <https://doi.org/10.1016/j.clbc.2020.04.004>.
- Nagar V, Singh T, Tiwari Y, Aseri V, Pandit PP, Chopade RL, et al. ZnO Nanoparticles: Exposure, toxicity mechanism and assessment. *Mater Today Proc* 2022;69:56–63. <https://doi.org/10.1016/j.matpr.2022.09.001>.
-

- 
- Nahta R, O'Regan RM. Therapeutic implications of estrogen receptor signaling in HER2-positive breast cancers. *Breast Cancer Res Treat* 2012;135:39–48. <https://doi.org/10.1007/s10549-012-2067-8>.
- Narod SA. Hormone replacement therapy and the risk of breast cancer. *Nat Rev Clin Oncol* 2011;8:669–76. <https://doi.org/10.1038/nrclinonc.2011.110>.
- Nasrollahzadeh M, Sajadi SM, Sajjadi M, Issaabadi Z. An Introduction to Nanotechnology. *Interface Science and Technology* 2019;28:1–27. <https://doi.org/10.1016/B978-0-12-813586-0.00001-8>.
- Naz F, Kumar Dinda A, Kumar A, Koul V. Investigation of ultrafine gold nanoparticles (AuNPs) based nanoformulation as single conjugates target delivery for improved methotrexate chemotherapy in breast cancer. *Int J Pharm* 2019;569:118561. <https://doi.org/10.1016/j.ijpharm.2019.118561>.
- Ni D, Xu P, Sabanayagam D, Gallagher SR. Protein blotting: Immunoblotting. vol. 2016. 2016. <https://doi.org/10.1002/9780470089941.et0803s12>.
- Nicotera P, Leist M, Ferrando-May E. Apoptosis and necrosis: Different execution of the same death. *Biochem Soc Symp*, vol. 66, 1999, p. 69–73. <https://doi.org/10.1042/bss0660069>.
- Niloufar Tavakoli Dastjerd, Nematollah Gheibi, Hossein Ahmadpour Yazdi, Hanifeh Shariatifar AF. Design and Characterization of Liposomal Methotrexate and Its Effect on BT T-474 Breast Cancer Cell Line. *Med J Islam Repub Iran* 2021;35:1–7. <https://doi.org/https://doi.org/10.4176/mjiri.35.158>.
- Nogueira E, Sárria MP, Azoia NG, Antunes E, Loureiro A, Guimarães D, et al. Internalization of Methotrexate Conjugates by Folate Receptor- $\alpha$ . *Biochemistry* 2018;57:6780–6. <https://doi.org/10.1021/acs.biochem.8b00607>.
- Noman MT, Petru M, Militkỳ J, Azeem M, Ashraf MA. One-Pot sonochemical synthesis of ZnO nanoparticles for photocatalytic applications, modelling and optimization. *Materials* 2020;13:14. <https://doi.org/10.3390/ma13010014>.
- Nosrati H, Salehiabar M, Davaran S, Danafar H, Manjili HK. Methotrexate-conjugated L-lysine coated iron oxide magnetic nanoparticles for inhibition of MCF-7 breast cancer cells. *Drug Dev Ind Pharm* 2018;44:886–94. <https://doi.org/10.1080/03639045.2017.1417422>.
-

---

Oberdörster G. Safety assessment for nanotechnology and nanomedicine: Concepts of nanotoxicology. *J Intern Med*, vol. 267, 2010, p. 89–105. <https://doi.org/10.1111/j.1365-2796.2009.02187.x>.

Organisation for Economic Cooperation and Development. Test No. 425: Acute Oral Toxicity: Up-and-Down Procedure. Guideline for Testing of Chemicals 2001:26. <https://doi.org/https://doi.org/10.1787/9789264071049-en>.

Ormerod MG. The study of apoptotic cells by flow cytometry. *Leukemia* 1998;12:1013–25. <https://doi.org/10.1038/SJ.LEU.2401061>.

Padma VV. An overview of targeted cancer therapy. *Biomedicine (Taipei)* 2015;5:1–6. <https://doi.org/10.7603/s40681-015-0019-4>.

Panda AK, Rout S. Zinc in Ayurvedic herbo-mineral products. *Natural Product Radiance* 2006;5:284–8.

Pandya S, Moore RG. Breast development and anatomy. *Clin Obstet Gynecol* 2011;54:91–5. <https://doi.org/10.1097/GRF.0b013e318207ffe9>.

Panonnummal R, Sabitha M. Anti-psoriatic and toxicity evaluation of methotrexate loaded chitin nanogel in imiquimod induced mice model. *Int J Biol Macromol* 2018;110:245–58. <https://doi.org/10.1016/J.IJBIOMAC.2017.10.112>.

Parsa Y, Mirmalek SA, Kani FE, Aidun A, Salimi-Tabatabaee SA, Yadollah-Damavandi S, et al. A Review of the Clinical Implications of Breast Cancer Biology. *Electron Physician* 2016;8:2416–24. <https://doi.org/10.19082/2416>.

Patel DB, Tiyyagura P, Patel B, Mamidipalli N, Maraju HB. Trends in Nanocarrier based Delivery Systems of Methotrexate: Update 2020. *Cancer Science & Research* 2021;4:1–7. <https://doi.org/10.33425/2639-8478.1064>.

Patel HK, Bihani T. Selective estrogen receptor modulators (SERMs) and selective estrogen receptor degraders (SERDs) in cancer treatment. *Pharmacol Ther* 2018;186:1–24. <https://doi.org/10.1016/j.pharmthera.2017.12.012>.

Paul W, Sharma CP. Blood compatibility studies of Swarna bhasma (gold bhasma), an Ayurvedic drug. *Int J Ayurveda Res* 2011;2:14–22. <https://doi.org/10.4103/0974-7788.83183>.

Peng L, Jiang H, Bradley C. Annexin V for flow cytometric detection of phosphatidylserine expression on lymphoma cells undergoing apoptosis. *Hua Xi Yi Ke Da Xue Xue Bao = Journal*

---



---

of West China University of Medical Sciences = Huaxi Yike Daxue Xuebao / [Bian Ji Zhe, Hua Xi Yi Ke Da Xue Xue Bao Bian Wei Hui] 2001;32. <https://doi.org/10.1182/BLOOD.V84.5.1415.BLOODJOURNAL8451415>.

Pérez-Herrero E, Fernández-Medarde A. Advanced targeted therapies in cancer: Drug nanocarriers, the future of chemotherapy. *European Journal of Pharmaceutics and Biopharmaceutics* 2015;93:52–79. <https://doi.org/10.1016/j.ejpb.2015.03.018>.

Pötsch N, Vatteroni G, Clauser P, Radiology TH-, 2022 undefined. Contrast-enhanced mammography versus contrast-enhanced breast MRI: a systematic review and meta-analysis. *PubsRsnaOrg* 2022;305:94–103. <https://doi.org/10.1148/radiol.212530>.

Price KD, Rao GK. Biological Therapies for Cancer. *Nonclinical Development of Novel Biologics, Biosimilars, Vaccines and Specialty Biologics*, Elsevier; 2013, p. 303–42. <https://doi.org/10.1016/B978-0-12-394810-6.00013-7>.

Purcar V, Şomoghi R, Niţu SG, Nicolae C-A, Alexandrescu E, Gîfu IC, et al. The Effect of Different Coupling Agents on Nano-ZnO Materials Obtained via the Sol-Gel Process. *Nanomaterials (Basel)* 2017;7. <https://doi.org/10.3390/nano7120439>.

Rahman M, Khan JA, Kanwal U, Awan UA, Raza A. Methotrexate-loaded PEGylated gold nanoparticles as hemocompatible and pH-responsive anticancer drug nanoconjugate. *Journal of Nanoparticle Research* 2021;23:1–13. <https://doi.org/https://doi.org/10.1007/s11051-021-05296-0>.

Ramos AP, Cruz MAE, Tovani CB, Ciancaglini P. Biomedical applications of nanotechnology. *Biophys Rev* 2017;9:79–89. <https://doi.org/10.1007/S12551-016-0246-2>.

Raoufi D. Synthesis and microstructural properties of ZnO nanoparticles prepared by precipitation method. *Renew Energy* 2013;50:932–7. <https://doi.org/10.1016/j.renene.2012.08.076>.

Rasmussen JW, Martinez E, Louka P, Wingett DG. Zinc oxide nanoparticles for selective destruction of tumor cells and potential for drug delivery applications. *Expert Opin Drug Deliv* 2010;7:1063–77. <https://doi.org/10.1517/17425247.2010.502560>.

Reddy SM, Carroll E, Nanda R. Atezolizumab for the treatment of breast cancer. *Expert Rev Anticancer Ther* 2020;20:151–8. <https://doi.org/10.1080/14737140.2020.1732211>.

---

---

Ren X, Wang Z, Yun Y, Meng G, Zhang X, Ding H, et al. Simultaneous Quantification of Methotrexate and Its Metabolite 7-Hydroxy-Methotrexate in Human Plasma for Therapeutic Drug Monitoring. *Int J Anal Chem* 2019;2019:10. <https://doi.org/10.1155/2019/1536532>.

Riccardi C, Nicoletti I. Analysis of apoptosis by propidium iodide staining and flow cytometry. *Nat Protoc* 2006;1:1458–61. <https://doi.org/10.1038/nprot.2006.238>.

Roberts C, Strauss VY, Kopijasz S, Gourley C, Hall M, Montes A, et al. Results of a phase II clinical trial of 6-mercaptopurine (6MP) and methotrexate in patients with BRCA-defective tumours. *Br J Cancer* 2020;122:483–90. <https://doi.org/10.1038/s41416-019-0674-4>.

Roshini A, Jagadeesan S, Cho YJ, Lim JH, Choi KH. Synthesis and evaluation of the cytotoxic and anti-proliferative properties of ZnO quantum dots against MCF-7 and MDA-MB-231 human breast cancer cells. vol. 81. Elsevier B.V; 2017a. <https://doi.org/10.1016/j.msec.2017.08.014>.

Roshini A, Jagadeesan S, Cho YJ, Lim JH, Choi KH. Synthesis and evaluation of the cytotoxic and anti-proliferative properties of ZnO quantum dots against MCF-7 and MDA-MB-231 human breast cancer cells. *Materials Science and Engineering C* 2017b;81:551–60. <https://doi.org/https://doi.org/10.1016/j.msec.2017.08.014>.

Rozalen M, Sánchez-Polo M, Fernández-Perales M, Widmann TJ, Rivera-Utrilla J. Synthesis of controlled-size silver nanoparticles for the administration of methotrexate drug and its activity in colon and lung cancer cells. *RSC Adv* 2020;10:10646–60. <https://doi.org/10.1039/c9ra08657a>.

Sabir S, Arshad M, Chaudhari SK. Zinc oxide nanoparticles for revolutionizing agriculture: Synthesis and applications. *Scientific World Journal* 2014;2014. <https://doi.org/10.1155/2014/925494>.

Salama EA, Adbeltawab RE, El Tayebi HM. XIST and TSIX: Novel Cancer Immune Biomarkers in PD-L1-Overexpressing Breast Cancer Patients. *Front Oncol* 2020;9. <https://doi.org/10.3389/fonc.2019.01459>.

Salami M, Khosravi M, Zarei MH. Comparative toxic effect of bulk zinc oxide (ZnO) and ZnO nanoparticles on human red blood cells. *Main Group Metal Chemistry* 2022;45:219–24. <https://doi.org/10.1515/mgmc-2022-0024>.

Saleha A, Shende SS, Ingle P, Rai M, Minkina TM, Gade A. Cell free extract-mediated biogenic synthesis of ZnONPs and their application with kanamycin as a bactericidal

---

---

combination. *World J Microbiol Biotechnol* 2023;39. <https://doi.org/10.1007/s11274-023-03777-z>.

Sanchala D, Bhatt LK, Pethe P, Shelat R, Kulkarni YA. Anticancer activity of methylene blue via inhibition of heat shock protein 70. *Biomedicine and Pharmacotherapy* 2018;107:1037–45. <https://doi.org/10.1016/j.biopha.2018.08.095>.

Sandmann A, Kompch A, Mackert V, Liebscher CH, Winterer M. Interaction of L-cysteine with zno: Structure, surface chemistry, and optical properties. *Langmuir* 2015;31:5701–11. <https://doi.org/10.1021/la504968m>.

Sanmugam A, Vikraman D, Park H, Kim H-S. One-Pot Facile Methodology to Synthesize Chitosan-ZnO-Graphene Oxide Hybrid Composites for Better Dye Adsorption and Antibacterial Activity. *Nanomaterials* 2017;7:363. <https://doi.org/10.3390/nano7110363>.

Santamaria A. Historical Overview of Nanotechnology and Nanotoxicology. *Methods in molecular biology*, vol. 926, *Methods Mol Biol*; 2012, p. 1–12. [https://doi.org/10.1007/978-1-62703-002-1\\_1](https://doi.org/10.1007/978-1-62703-002-1_1).

Sarkar MKI, Ali H, Bhuiya M, Akther L, Roy CK, Islam MR, et al. Effect of nanotechnology on cancer disease. *Journal of Bionanoscience* 2018;12:297–315. <https://doi.org/10.1166/jbns.2018.1532>.

Sawant VJJ, Bamane SRR. PEG-beta-cyclodextrin functionalized zinc oxide nanoparticles show cell imaging with high drug payload and sustained pH responsive delivery of curcumin in to MCF-7 cells. *J Drug Deliv Sci Technol* 2018;43:397–408. <https://doi.org/10.1016/j.jddst.2017.11.010>.

Schrage A, Hempel K, Schulz M, Kolle SN, Van Ravenzwaay B, Landsiedel R. Refinement and reduction of acute oral toxicity testing: A critical review of the use of cytotoxicity data. *Alternatives to Laboratory Animals* 2011;39:273–95. <https://doi.org/10.1177/026119291103900311>.

Semaltianos NG. Nanoparticles by laser ablation. *Critical Reviews in Solid State and Materials Sciences* 2010;35:105–24. <https://doi.org/10.1080/10408431003788233>.

Serrano-Olvera JA. Biological therapy of cancer. *New Approaches in the Treatment of Cancer*, 2011a, p. 33–42. <https://doi.org/10.1097/00000421-199412000-00024>.

Sha Jin KY. Targeted drug delivery for breast cancer treatment. *Recent Pat Anticancer Drug Discov* 2013;8:143–53. <https://doi.org/10.2174/1574892811308020003>.

---

---

Shah, Rupen, Kelly Rosso and SDN. Pathogenesis, prevention, diagnosis and treatment of breast cancer. *World J Clin Oncol* 2014;5:283.

Shandiz SAS, Sharifian F, Behboodi S, Ghodratpour F, Baghbani-Arani F. Evaluation of Metastasis Suppressor Genes Expression and In Vitro Anti-Cancer Effects of Zinc Oxide Nanoparticles in Human Breast Cancer Cell Lines MCF-7 and T47D. *Avicenna J Med Biotechnol* 2021;13:9. <https://doi.org/10.18502/AJMB.V13I1.4576>.

Sharma A, Gorey B, Casey A. *In vitro* comparative cytotoxicity study of aminated polystyrene, zinc oxide and silver nanoparticles on a cervical cancer cell line. *Drug Chem Toxicol* 2018;0:1–15. <https://doi.org/10.1080/01480545.2018.1424181>.

Shelat R, Bhatt LK, Khanna A, Chandra S. A comprehensive toxicity evaluation of novel amino acid-modified magnetic ferrofluids for magnetic resonance imaging. *Amino Acids* 2019;51:929–43. <https://doi.org/10.1007/S00726-019-02726-1/METRICS>.

Sherr CJ. The pezcoller lecture: Cancer cell cycles revisited. *Cancer Res* 2000;60:3689–95.

Shinoura N, Yoshida Y, Asai A, Kirino T, Hamada H. Relative level of expression of Bax and Bcl-X(L) determines the cellular fate of apoptosis/necrosis induced by the overexpression of Bax. *Oncogene* 1999;18:5703–13. <https://doi.org/10.1038/sj.onc.1202966>.

Shirsekar PP, Kanhe NS, Mathe VL, Lahir YK, Dongre PM. Interaction of zinc oxide nanoparticles with human red blood cells. *Bionano Frontier* 2016;9:99–104.

Shobhaa N, Nandab N, Nagabhushana BM. Nano ZnO and its Perspective in Anti- Cancer Activities. *Mapana Journal of Sciences* 2017;16:41–50.

Singh M, Ulbrich P, Prokopec V, Svoboda P, Šantavá E, Štěpánek F. Vapour phase approach for iron oxide nanoparticle synthesis from solid precursors. *J Solid State Chem* 2013;200:150–6. <https://doi.org/10.1016/j.jssc.2013.01.037>.

Singh S, Singh B, Sharma P, Mittal A, Kumar S, Saini GSS, et al. Amino acid functionalized zinc oxide nanostructures for cytotoxicity effect and hemolytic behavior: Theoretical and experimental studies. *Mater Des* 2017;134:10–22. <https://doi.org/10.1016/j.matdes.2017.08.020>.

Singh TA, Das J, Sil PC. Zinc oxide nanoparticles: A comprehensive review on its synthesis, anticancer and drug delivery applications as well as health risks. *Adv Colloid Interface Sci* 2020;286:102317. <https://doi.org/10.1016/j.cis.2020.102317>.

---

---

Sirelkhatim A, Mahmud S, Seeni A, Kaus NHM, Ann LC, Bakhori SKM, et al. Review on zinc oxide nanoparticles: Antibacterial activity and toxicity mechanism. *Nanomicro Lett* 2015;7:219–42. <https://doi.org/10.1007/s40820-015-0040-x>.

Smith GL, Jiang J, Buchholz TA, Xu Y, Hoffman KE, Giordano SH, et al. Benefit of adjuvant brachytherapy versus external beam radiation for early breast cancer: Impact of patient stratification on breast preservation. *Int J Radiat Oncol Biol Phys* 2014;88:274–84. <https://doi.org/10.1016/j.ijrobp.2013.07.011>.

Span LFR, Pennings AHM, Vierwinden G, Boezeman JBM, Raymakers RAP, de Witte T. The dynamic process of apoptosis analyzed by flow cytometry using Annexin-V/propidium iodide and a modified in situ end labeling technique. *Cytometry* 2002;47:24–31. <https://doi.org/10.1002/cyto.10028>.

Sreevalsa VG, Jeeju PP, Augustine MS, Anilkumar KM, Jayalekshmi S. L-Histidine-modified biocompatible zinc oxide nanocrystals. *J Exp Nanosci* 2013;8:937–46. <https://doi.org/10.1080/17458080.2011.624553>.

Stadler ZK, Salo-Mullen E, Patil SM, Pietanza MC, Vijai J, Saloustros E, et al. Prevalence of BRCA1 and BRCA2 mutations in Ashkenazi Jewish families with breast and pancreatic cancer. *Cancer* 2012;118:493–9. <https://doi.org/10.1002/cncr.26191>.

Sudhakar A. History of Cancer, Ancient and Modern Treatment Methods. *J Cancer Sci Ther* 2009;01:i–iv. <https://doi.org/10.4172/1948-5956.100000e2>.

Sun YS, Zhao Z, Yang ZN, Xu F, Lu HJ, Zhu ZY, et al. Risk factors and preventions of breast cancer. *Int J Biol Sci* 2017;13:1387–97. <https://doi.org/10.7150/ijbs.21635>.

Sung H, Ferlay J, Siegel RL, Laversanne M, Soerjomataram I, Jemal A, et al. Global Cancer Statistics 2020: GLOBOCAN Estimates of Incidence and Mortality Worldwide for 36 Cancers in 185 Countries. *CA Cancer J Clin* 2021a;71:209–49. <https://doi.org/10.3322/caac.21660>.

Sung H, Ferlay J, Siegel RL, Laversanne M, Soerjomataram I, Jemal A, et al. Global Cancer Statistics 2020: GLOBOCAN Estimates of Incidence and Mortality Worldwide for 36 Cancers in 185 Countries. *CA Cancer J Clin* 2021b;71:209–49. <https://doi.org/10.3322/caac.21660>.

Tafari M, Yamashita H, Timbres J, Kohut K, Caneppele M, Troy M, et al. DCIS and LCIS: Are the Risk Factors for Developing In Situ Breast Cancer Different? *MdpiCom* 2023. <https://doi.org/10.3390/cancers15174397>.

---

---

Takahashi-Yanaga F, Kahn M. Targeting Wnt signaling: Can we safely eradicate cancer stem cells? *Clinical Cancer Research* 2010;16:3153–62. <https://doi.org/10.1158/1078-0432.CCR-09-2943>.

Taran M, Safaei M, ... NK-... R in A, 2021 undefined. Benefits and application of nanotechnology in environmental science: an overview. *BiointerfaceresearchCom* 2021;11:7860–70. <https://doi.org/10.33263/BRIAC111.78607870>.

Taylor IW, Tattersall MHN. Methotrexate Cytotoxicity in Cultured Human Leukemic Cells Studied by Flow Cytometry. *Cancer Res* 1981;41:1549–58.

Teng YHF, Tan WJ, Thike AA, Cheok PY, Tse GMK, Wong NS, et al. Mutations in the epidermal growth factor receptor (EGFR) gene in triple negative breast cancer: Possible implications for targeted therapy. *Breast Cancer Research* 2011;13. <https://doi.org/10.1186/bcr2857>.

Terheyden M, Melchert C, Brachytherapy GKC, 2016 undefined. External beam boost versus interstitial high-dose-rate brachytherapy boost in the adjuvant radiotherapy following breast-conserving therapy in early-stage breast. *TermediaPl* 2016;8:294–300. <https://doi.org/10.5114/jcb.2016.61973>.

Thanki K, Gangwal RP, Sangamwar AT, Jain S. Oral delivery of anticancer drugs: Challenges and opportunities. *Journal of Controlled Release* 2013;170:15–40. <https://doi.org/10.1016/j.jconrel.2013.04.020>.

Tian B, Liu S, Zhang Y, Li C, Wang Z. Hydrophilic, mesoporous structural ZnO nanospheres for pH-triggered release of drug. *Mater Lett* 2017;188:165–8. <https://doi.org/10.1016/j.matlet.2016.11.029>.

Tian J, Wei X, Zhang W, Xu A. Effects of Selenium Nanoparticles Combined With Radiotherapy on Lung Cancer Cells. *Front Bioeng Biotechnol* 2020;8:1289. <https://doi.org/10.3389/fbioe.2020.598997>.

Tong CWS, Wu M, Cho WCS, To KKW. Recent advances in the treatment of breast cancer. *Front Oncol* 2018;8. <https://doi.org/10.3389/FONC.2018.00227/FULL>.

Tripette J, Alexy T, Hardy-Dessources MD, Mougenel D, Beltan E, Chalabi T, et al. Red blood cell aggregation, aggregate strength and oxygen transport potential of blood are abnormal in both homozygous sickle cell anemia and sickle-hemoglobin C disease. *Haematologica* 2009;94:1060–5. <https://doi.org/10.3324/haematol.2008.005371>.

---

---

Trotta M, Peira E, Carlotti ME, Gallarate M. Deformable liposomes for dermal administration of methotrexate. *Int J Pharm* 2004;270:119–25. <https://doi.org/10.1016/J.IJPHARM.2003.10.006>.

Tsuzuki T. Commercial scale production of inorganic nanoparticles. *Int J Nanotechnol* 2009;6:567–78. <https://doi.org/10.1504/IJNT.2009.024647>.

Ukelis U, Kramer PJ, Olejniczak K, Mueller SO. Replacement of in vivo acute oral toxicity studies by in vitro cytotoxicity methods: Opportunities, limits and regulatory status. *Regulatory Toxicology and Pharmacology* 2008;51:108–18. <https://doi.org/10.1016/j.yrtph.2008.02.002>.

Understanding Cancer - National Cancer Institute. Patient Education Publications 2016. <https://www.cancer.gov/about-cancer/understanding> (accessed January 16, 2020).

Vandebriel RJ, De Jong WH. A review of mammalian toxicity of ZnO nanoparticles. *Nanotechnol Sci Appl* 2012;5:61–71. <https://doi.org/10.2147/NSA.S23932>.

Virdi JK, Pethe P. Soft substrate maintains stemness and pluripotent stem cell-like phenotype of human embryonic stem cells under defined culture conditions. *Cytotechnology* 2022;74:479–89. <https://doi.org/10.1007/s10616-022-00537-z>.

Vivek R, Rejeeth C, Thangam R. Targeted Nanotherapeutics Based on Cancer Biomarkers. *Multifunctional Systems for Combined Delivery, Biosensing and Diagnostics* 2017:229–44. <https://doi.org/10.1016/B978-0-323-52725-5.00012-5>.

Walum E. Acute oral toxicity. *Environ Health Perspect* 1998;106:497–503. <https://doi.org/10.1289/ehp.98106497>.

Wang GH, Zhao YZ, Tan J, Zhu SH, Zhou KC. Arginine functionalized hydroxyapatite nanoparticles and its bioactivity for gene delivery. *Transactions of Nonferrous Metals Society of China (English Edition)* 2015;25:490–6. [https://doi.org/10.1016/S1003-6326\(15\)63629-9](https://doi.org/10.1016/S1003-6326(15)63629-9).

Wang P, Henning SM, Heber D. Limitations of MTT and MTS-Based Assays for Measurement of Antiproliferative Activity of Green Tea Polyphenols. *PLoS One* 2010;5:e10202. <https://doi.org/10.1371/JOURNAL.PONE.0010202>.

Wang WY, Zhao XF, Ju XH, Wang Y, Wang L, Li SP, et al. Novel morphology change of Au-Methotrexate conjugates: From nanochains to discrete nanoparticles. *Int J Pharm* 2016;515:221–32. <https://doi.org/10.1016/j.ijpharm.2016.10.022>.

---

---

Wang X, Yang L, Chen Z, Shin DM. Application of Nanotechnology in Cancer Therapy and Imaging. *CA Cancer J Clin* 2008;58:97–110. <https://doi.org/10.3322/CA.2007.0003>.

Wang Y, Tang SC. The race to develop oral SERDs and other novel estrogen receptor inhibitors: recent clinical trial results and impact on treatment options. *Cancer and Metastasis Reviews* 2022;41:975–90. <https://doi.org/10.1007/S10555-022-10066-Y>.

Wang ZL. Nanomaterials for Nanoscience and Nanotechnology. *Characterization of Nanophase Materials* 1999:1–12. <https://doi.org/10.1002/3527600094.ch1>.

Weinstein B, Muresan B, Solano S, de Macedo AV, Lee Y, Su YC, Ahn Y, Henriquez G, Camargo C, Kim GJ C DO. Efficacy and safety of innovative experimental chimeric antigen receptor (CAR) T-cells versus axicabtagene ciloleucel (Yescarta) for the treatment of relapsed. *Innov Pharm* 2021;12. <https://doi.org/10.24926/iip.v12i4.4345>

Whelan RS, Konstantinidis K, Wei AC, Chen Y, Reyna DE, Jha S, et al. Bax regulates primary necrosis through mitochondrial dynamics. *Proc Natl Acad Sci U S A* 2012;109:6566–71. <https://doi.org/10.1073/pnas.1201608109>.

Wingett D, Louka P, Anders CB, Zhang J, Punnoose A. A role of ZnO nanoparticle electrostatic properties in cancer cell cytotoxicity. *Nanotechnol Sci Appl* 2016;9:29–45. <https://doi.org/10.2147/NSA.S99747>.

Wong PT, Choi SK. Mechanisms and implications of dual-acting methotrexate in folate-targeted nanotherapeutic delivery. *Int J Mol Sci* 2015;16:1772–90. <https://doi.org/10.3390/ijms16011772>.

Worm J, Kirkin AF, Dzhandzhugazyan KN, Guldberg P. Methylation-dependent Silencing of the Reduced Folate Carrier Gene in Inherently Methotrexate-resistant Human Breast Cancer Cells. *Journal of Biological Chemistry* 2001;276:39990–40000. <https://doi.org/10.1074/jbc.M103181200>.

Wu H, Zhang J. Chitosan-based zinc oxide nanoparticle for enhanced anticancer effect in cervical cancer: A physicochemical and biological perspective. *Saudi Pharmaceutical Journal* 2017. <https://doi.org/10.1016/j.jsps.2017.12.010>.

Wu Q, Chen Xia, Zhang P, Han Y, Chen Xiaoming, Yan Y, et al. Amino acid-assisted synthesis of ZnO hierarchical architectures and their novel photocatalytic activities. *Cryst Growth Des* 2008;8:3010–8. <https://doi.org/10.1021/cg800126r>.

---



- 
- Xian M, Zhang Y, Cheng HD, Xu F, Zhang B, Ding J. Automatic breast ultrasound image segmentation: A survey. *Pattern Recognit* 2018;79:340–55. <https://doi.org/10.1016/j.patcog.2018.02.012>.
- Xie L, Zhao T, Cai J, Su Y, Wang Z, Dong W. Methotrexate induces DNA damage and inhibits homologous recombination repair in choriocarcinoma cells. *Onco Targets Ther* 2016;9:7115–22. <https://doi.org/10.2147/OTT.S116387>.
- Xie M, Zhang H, Xu Y, Liu T, Chen S, Wang J, et al. Expression of folate receptors in nasopharyngeal and laryngeal carcinoma and folate receptor-mediated endocytosis by molecular targeted nanomedicine. *Int J Nanomedicine* 2013;8:2443–51. <https://doi.org/10.2147/ijn.s46327>.
- Xie X, Liao J, Shao X, Li Q, Lin Y. The Effect of shape on Cellular Uptake of Gold Nanoparticles in the forms of Stars, Rods, and Triangles. *Sci Rep* 2017;7:1–9. <https://doi.org/10.1038/s41598-017-04229-z>.
- Xiong HM. ZnO nanoparticles applied to bioimaging and drug delivery. *Advanced Materials* 2013a;25:5329–35. <https://doi.org/10.1002/adma.201301732>.
- Xu C, Wu A, Zhu H, Fang H, Xu L, Ye J, et al. Melatonin is involved in the apoptosis and necrosis of pancreatic cancer cell line SW-1990 via modulating of Bcl-2/Bax balance. *Biomedicine and Pharmacotherapy* 2013;67:133–9. <https://doi.org/10.1016/j.biopha.2012.10.005>.
- Yang SL, Zhao FY, Song H, Shen DY, Xu XJ. Methotrexate associated renal impairment is related to delayed elimination of high-dose methotrexate. *Scientific World Journal* 2015;2015:1–9. <https://doi.org/10.1155/2015/751703>.
- Yang W, Zou Y, Meng F, Zhang J, Cheng R, Deng C, et al. Efficient and Targeted Suppression of Human Lung Tumor Xenografts in Mice with Methotrexate Sodium Encapsulated in All-Function-in-One Chimeric Polymersomes. *Advanced Materials* 2016;28:8234–9. <https://doi.org/10.1002/ADMA.201600065>.
- Yasui M, Uemura K, Yoneyama S, Kawahara T, Hattori Y, Teranishi JI, et al. Predictors of poor response to secondary alternative antiandrogen therapy with flutamide in metastatic castration-resistant prostate cancer. *Jpn J Clin Oncol* 2016;46:1042–6. <https://doi.org/10.1093/jjco/hyw110>.
-

---

Yedgar S, Barshtein G, Gural A. Hemolytic Activity of Nanoparticles as a Marker of Their Hemocompatibility. *Micromachines* (Basel) 2022;13:1–15. <https://doi.org/10.3390/mi13122091>.

Ying Y, Padanilam BJ. Regulation of necrotic cell death: p53, PARP1 and cyclophilin D-overlapping pathways of regulated necrosis? *Cellular and Molecular Life Sciences* 2016;73:2309–24. <https://doi.org/10.1007/s00018-016-2202-5>.

Yook S, Cai Z, Jeong JJ, Lu Y, Winnik MA, Pignol JP, et al. Dual-Receptor-Targeted (DRT) Radiation Nanomedicine Labeled with <sup>177</sup>Lu Is More Potent for Killing Human Breast Cancer Cells That Coexpress HER2 and EGFR Than Single-Receptor-Targeted (SRT) Radiation Nanomedicines. *Mol Pharm* 2020;17:1226–36. <https://doi.org/10.1021/acs.molpharmaceut.9b01259>.

Yu J, Baek M, Chung HE, Choi SJ. Effects of physicochemical properties of zinc oxide nanoparticles on cellular uptake. *J Phys Conf Ser*, vol. 304, 2011. <https://doi.org/https://doi.org/10.1088/1742-6596/304/1/012007>.

Zhang D, Kanakkanthara A. Beyond the paclitaxel and vinca alkaloids: Next generation of plant-derived microtubule-targeting agents with potential anticancer activity. *Cancers* (Basel) 2020;12:1–23. <https://doi.org/10.3390/cancers12071721>.

Zhang H-J, Xiong H-M. Biological Applications of ZnO Nanoparticles. *Curr Mol Imaging* 2013;2:177–92. <https://doi.org/10.2174/22115552113029990012>.

Zhang X, Achazi K, Haag R. Boronate cross-linked ATP- and pH-responsive nanogels for intracellular delivery of anticancer drugs. *Adv Healthc Mater* 2015;4:585–92. <https://doi.org/10.1002/adhm.201400550>.

Zhang Y, Nayak T, Hong H, Cai W. Biomedical Applications of Zinc Oxide Nanomaterials. *Curr Mol Med* 2013;13:1633–45. <https://doi.org/10.2174/1566524013666131111130058>.

Zhao J, Castranova V. Toxicology of nanomaterials used in nanomedicine. *J Toxicol Environ Health B Crit Rev* 2011a;14:593–632. <https://doi.org/10.1080/10937404.2011.615113>.

Zhao Y, Guo Y, Li R, Wang T, Han M, Zhu C, et al. Methotrexate Nanoparticles Prepared with Codendrimer from Polyamidoamine (PAMAM) and Oligoethylene Glycols (OEG) Dendrons: Antitumor Efficacy in Vitro and in Vivo. *Scientific Reports* 2016 6:1 2016;6:1–11. <https://doi.org/10.1038/srep28983>.

---

# Appendix-I

# Ethics

# approval

# Forms

---

**Institutional Ethics Committee (IEC) approval**


---



**SUNANDAN DIVATIA  
SCHOOL OF SCIENCE**

**SVKM's INSTITUTIONAL ETHICS COMMITTEE (IEC)**

9<sup>th</sup> March 2020

To  
Principal Investigator  
Sunandan Divatia School of Science,  
NMIMS

Sub: Project proposal No: NMIMS/IEC/012/2020

The Committee has reviewed and approved the proposal entitled "Fabrication of drug loaded polymeric zinc oxide nano carriers for targeted delivery to cancer cells" in its meeting held on 18<sup>th</sup> February 2020 for a period of three years. The progress report and final report of the proposal should be submitted to the Committee.

  
Signature of the Member-Secretary  
(Dr. Brijesh Sukumaran)

  
Signature of the Chairman  
(Dr. Rabindranath Mukhopadhyaya)

Copy forwarded to protocol applicant:  
Copy in File


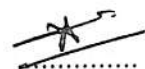

SVKM'S  
**Narsee Monjee Institute of Management Studies**  
Deemed to be UNIVERSITY  
V. L. Mehta Road, Vile Parle (West), Mumbai - 400 056, India.  
Tel: (91-22) 42355555  
Email: enquiry@nmims.edu | Web: www.nmims.edu



---

**Institutional Animal Ethics Committee (IAEC) approval****Certificate**

This is to certify that the project proposal no. CPCSEA/IAEC/P-69/2022 entitled "Fabrication of Drug Loaded Polymeric Zinc Oxide Nano Carriers for Targeted Delivery to Cancer Cells" submitted by Dr.Purvi Bhatt has been approved by the IAEC of Shri Vile Parle Kelavani Mandal in its meeting held on 24<sup>th</sup> September 2022 and 12 Albino mice have been sanctioned under this.

Authorized by	Name	Signature	Date
Chairman:	Dr.Bala Prabhakar		24 SEP 2022
Member Secretary:	Dr.Yogesh Kulkarni		24 SEP 2022
Main Nominee of CPCSEA:	Dr.Rahul Thorat		24 SEP 2022

(Kindly make sure that minutes of the meeting duly signed by all the participants are maintained by Office)

# Appendix-II

# Participant Information Sheet

---

**Participant Information Sheet**

**Title of the Project:** Synthesis and Characterization of Methotrexate Loaded Zinc Oxide Nano Particles for Efficient Delivery to Breast Cancer Cells

**Mentor for the Research Project:** Dr. Purvi Bhatt, Ph.D.

Associate Professor, Biological Sciences, Sunandan Divatia School of Science, SVKM's Narsee Monjee Institute of Management Studies (NMIMS) Deemed-to-University

**1. Aim of the Project**

The aim of the study is to synthesize and characterize Methotrexate loaded Zinc oxide nanoparticles for efficient delivery to breast cancer cells

**2. Expected Duration of the study and number of participants**

The blood collection is a part of the Ph.D. research project. Blood collection would be a one-time requirement from healthy participants. Not more than 20 participants would be involved in the study and the study would involve only one visit from you. The blood would be collected to carry out blood compatibility studies for the synthesized biocompatible arsenic trioxide nanoparticles.

Inclusion criteria:

Healthy individuals (men/women) above 18 years of age

On no medication including hormonal or infection related

Exclusion criteria:

Below 18 years of age

Any kind of medication including hormonal, or infection related.

**3. What is requested of you? And what does it involve?**

You are requested to give 5.0 ml of blood in your visit which would be only once. The blood will be drawn by a trained lab technician (phlebotomist) using a sterile disposable needle into a sterile tube. The assays conducted using the blood would include *in vitro* assays such as blood cell aggregation and hemolysis assay.

---

#### **4. Risk and Benefits of the participants**

There is no risk involved in the study. You will only feel the prick of a needle. The prick you get will heal in time. Your participation in this project would contribute towards understanding that the synthesized biocompatible arsenic trioxide nanoparticles do not affect healthy blood cells.

#### **5. Voluntary Participation**

The blood you give is strictly voluntary with no coercion with any medical, research or any social work group. You may ask any questions for the project and even may refuse to donate blood anytime even after signing your consent.

If you have any query you may contact:

#### **Principal Investigator**

##### **Dr. Purvi Bhatt, Ph.D.**

H.O.D, Associate Professor, Biological Sciences,  
Sunandan Divatia School of Science,  
SVKM's Narsee Monjee Institute of Management Studies  
(NMIMS) Deemed-to-University.  
Vile Parle (West), Mumbai-400056.  
Tel:022-42355956.



# Appendix-III

# Participant Consent Form

---

**Participant Consent Form**

---

I have been invited to participate in the study of the research project titled “Synthesis and Characterization of Methotrexate Loaded Zinc Oxide Nano Particles for Efficient Delivery to Breast Cancer Cells.”

I have understood that I have to give 5 ml of blood only once, which will be used for *in vitro* assays such as blood cell aggregation and hemolysis assay and not for any genetic analysis. The blood will be drawn by a trained lab technician (phlebotomist) using a sterile disposable needle into a sterile tube. The donation of 5 ml of blood will not produce any harm other than that I will experience a pin prick and mild pain at the site for a time point and perhaps for a short period.

In confirmation, I provide my signature below as a proof of my acceptance to participate in the study. My signature below indicates that I have read the participant information sheet, understood its meaning, have had a chance to ask questions, have had these questions answered to my satisfaction and consent to my participation in this program.

I give my consent to have 5 ml blood collected from me and necessary information on the project for the research study. My participation on the project is voluntary with no coercion from any associated medical, research or social worker on the study. I understand that I reserve the right to withdraw my participation on the project and will suffer no consequences of my withdrawal. I will be given a signed copy of this consent form.

I hereby make a donation of 5 ml of blood for the purpose of the mentioned research/study/education. I have been explained the entire procedure and purpose of this study in the language known to me. I hereby certify that I have signed the agreement freely and voluntarily without any threat and coercion and am willing to participate in this research study with a clear understanding about the likely benefits and risks involved. My signature also indicates that I have received a copy of the consent form and I also understand that in the event of my non-participation in the study or withdrawal of consent at any time, will not be affected any way.

Name of the participant:

Age of the participant:

Contact no:

Signature/thumb impression of the participant:

Name and signature of the Witness:

Relationship, if any, to the donor:

Date of consent:

Place:

# Appendix-IV

## Preparation of buffers/ solutions/ reagents

---

**Preparation of buffers/solutions/reagents**

---

**10% Acetic Acid:** Add 10 mL of glacial acetic acid to 90 mL of deionized (DI) water.

**30% Acrylamide Solution:** 29.2 g acrylamide and 0.8 g N', N'-methylene bis-acrylamide were dissolved in 50 mL of DI water, volume made up to 100 ml, filtered and stored at 4°C.

Caution: Acrylamide is a potent neurotoxin and is absorbed through skin. Wear gloves while handling.

**10% Ammonium Persulfate (APS):** 0.1 g APS was dissolved in 1 mL DI water. Fresh solution is prepared.

**5% Blocking Solution:** Dissolve 2.5 g of non-fat dry milk (NFDM) powder to 50 mL Tween TBS buffer. Mix well by keeping on rocker for few hours. Centrifuge at 2000 rpm for 5 min to remove undissolved solids and collect supernatant for its use as blocking solution.

**1 mg/mL BSA Stock Solution for Bradford Assay:** Add 10 mg of BSA to 10 ml of DI water, mix well.

**0.25% Coomassie Brilliant Blue Staining solution:** 0.25% Coomassie brilliant blue R-250 was dissolved in 45% methanol and 10% glacial acetic acid.

**Destaining Solution After Coomassie Staining:** Make solution by mixing 45% Methanol and 10% glacial acetic acid.

**100 µg/mL Ethidium Bromide (EtBr):** Dissolve 1 mg of EtBr and dissolve in 10 ml of DI water.

**70% Ethanol:** 70 mL of ethanol was taken, and volume made up to 100 ml with DI water.

**Lysis buffer:** For 30 mL of lysis buffer, dissolve 181.71 mg of Tris base (50 mM), 262.98 mg of sodium chloride (150 mM), 11.17 mg of EDTA (1 mM), 30 mg of sodium deoxycholate (0.1%), 30 mg of sodium dodecyl sulphate (0.1%), 1.26 mg of NaF (1 mM) in around 20 mL of DI water and adjust pH 7.5. Next, add 300 µL of Triton X-100 (1%), 0.00522 gm of PMSF (2 mM) (made separately in isopropanol) and make volume to 30mL and store at 4°C.

Complete cell lysis buffer contains above solution and 1X protease inhibitor cocktail (PIC).

**5mg/mL MTT:** Add 50 mg of MTT reagent to 10 mL of Dulbecco's PBS (DPBS-ATC grade) and cover the falcon with aluminum foil.

---

**Phosphate Buffered Saline (PBS):** Dissolve 8 g of NaCl, 0.2 g of KCl, 1.44 g of  $\text{Na}_2\text{HPO}_4 \cdot 7\text{H}_2\text{O}$  and 0.24 g of  $\text{KH}_2\text{PO}_4$  in 800 mL of DI water to dissolve the contents. Then adjust the pH to 7.4 using HCl and make up the volume to 1000 mL using DI water.

**Ponceau S Stain:** 0.05 g Ponceau S stain (0.1%) dissolved in 2.5 mL glacial acetic acid (5%) and make up the volume to 50 mL with DI water.

**1mg/mL Propidium Iodide:** Add 1 mg of propidium iodide to 1 mL of DPBS (ATC grade) and use the working stock by diluting it to a final concentration of 50  $\mu\text{g/mL}$ .

**10 mg/mL RNase A:** Add 20 mg of RNase A to 2 mL of sterile DI water

**10% SDS:** Dissolve 1 g SDS powder in 10 mL of DI water. Store at RT.

**Resolving Gel Buffer Solution (1.5M Tris, pH 8.8):** 18.17 g Tris base was dissolved in 70 mL of deionized water. The pH was adjusted to 8.8 with HCl and volume made up to 100 mL with DI water

**Stacking Gel Buffer Solution (0.5M Tris, pH 6.8):** 6.055 g Tris base was dissolved in 70 mL of DI water. The pH was adjusted to 6.8 with HCl and volume made up to 100 mL with DI water.

SDS-PAGE: Resolving gel and stacking gel composition

	<b>12% Resolving gel (10 ml)</b>	<b>5% stacking gel (3 ml)</b>
<b>H<sub>2</sub>O</b>	3.3 ml	2.1 ml
<b>30% acrylamide</b>	4.0 ml	0.5 ml
<b>1.5M Tris (pH 8.8)</b>	2.5 ml	-
<b>0.5M Tris (pH 6.8)</b>	-	0.38 ml
<b>10% SDS</b>	0.1 ml	0.03 ml
<b>10% APS</b>	0.1 ml	0.03 ml
<b>TEMED</b>	0.004 ml	0.003 ml

**5X SDS-PAGE Running Buffer (Tris Glycine SDS buffer, pH – 8.3)**

<b>Tris base</b>	15.1g	7.55g
<b>Glycine</b>	94g	47g
<b>10 % SDS</b>	50 mL	25 mL
<b>DI Water</b>	1000 mL	500 mL

**4X SDS-PAGE Loading Dye:** The loading dye (10 mL) was prepared by addition of the following reagents

- 0.5M Tris pH 6.8 (Stacking buffer) – 2.4 mL
- 100% Glycerol - 4 mL
- SDS – 0.8g
- $\beta$ -mercaptoethanol – 0.5 mL
- Bromophenol blue – 4mg
- DI water – 3.1 mL

**1X Transfer Buffer (for western blot):** The total volume was made up to 2000 mL using 400 mL methanol. This was stored in chilled condition (4°C).

	<b>1X 2L</b>	<b>1X 1L</b>	<b>10X 1L</b>
<b>Tris base (25mM)</b>	6.057 g	3.029 g	30.29 g
<b>Glycine (194mM)</b>	28.8 g	14.4	144 g
<b>DI Water</b>	1600 mL	800 mL	800 mL
<b>Methanol</b>	400 mL	200 mL	

---

**Tris Buffered Saline-Tween 20 buffer 10X (TBST for western blot)**

Adjust pH in range of 7.5-7.6 and make up the vol to 1L. Take 100 mL of 10X buffer add to 900 mL DI water and 1 mL of Tween-20 to make 1L of 1X TBST. Store at RT.

	<b>10X 1L</b>	<b>1X 1L</b>
<b>Tris base (20mM)</b>	24 g	2.4 g
<b>NaCl (150mM)</b>	88 g	8.8 g
<b>Tween 20 (0.1%)</b>	-	1 mL
<b>DI water</b>	900 mL	900 mL

**5% NFDM:** 2.5 g in 50 mL of TBST. Keep on shaker till all particles dissolves and then remove all particles to make sure to get homogenous solution.

1° & 2° Antibodies: Prepare in diluted NFDM OR BSA with TBST



# List of Conferences/ Workshops/ Award(s)

---

---

**List of Conferences/ Workshops/ Award(s)**

**Conferences attended.**

1. Attended “International conference on Advances in Materials Science & Applied Biology (AMSAB-2019)” at SVKM’s (NMIMS) Deemed-to-be University, Mumbai. From 8<sup>th</sup>- 10<sup>th</sup> January, 2019.
2. Presented poster titled “Synthesis and Characterization of Biocompatible Chitosan Coated Zinc Oxide Nanoparticles and it’s In vitro Cytotoxicity studies on MCF-7 and MCF-10A Cell lines- **Joshi Mitesh**, Bhatt Purvi” at “6th International Conference On Recent Trends In Bioengineering (ICRTB 2023)” held at MIT School of Bioengineering Sciences & Research, Pune on 20-21<sup>st</sup> January, 2023,

**Award(s)**

1. Awarded **3<sup>rd</sup> Prize for best poster presentation** at “International Conference on Advances in Biotechnology (ICAB-2023)” poster titled as “Synthesis, Characterization And Evaluation Of The Anti-Cancer Potential Of MTX-Loaded Zinc Oxide Nanoparticles For Breast Cancer”- **Joshi Mitesh**, Bhatt Purvi. Organized by Amity University Mumbai, 17- 18<sup>th</sup> October, 2023
2. Awarded **3rd prize** at the “**3 Minute Thesis (3MT)**” interstate event organized by the Science Club of Sunandan Divatia School of Science, SVKM’s NMIMS University, Mumbai on 28<sup>th</sup> February, 2024

**Workshops/seminar attended.**

1. Attended “19th Indo-US Cytometry Symposium & workshop” at NIRRH, Mumbai. 15-17<sup>th</sup> February, 2018
2. Attended “Popular lecture series” by Indian Women Scientists Association (IWSA) on Nanoscience and Nanotechnology, Juhu Jagruti hall, Mithibai college, Mumbai. 19<sup>th</sup> February, 2018
3. Attended guest lecture by Dr. Deepa Khushalani from TIFR on “Synthesis and characterization of template mediated formation of novel porous nanomaterials.” organized by National center for nanoscience and nanotechnology, University of Mumbai on 27<sup>th</sup> March, 2018
4. Attended annual meeting of Mumbai chapter of the “Society of Biological Chemists” at ICT, Mumbai on, 13<sup>th</sup> October, 2018

5. Attended online three-day National level workshop “USING MS WORD EFFECTIVELY FOR SCIENTIFIC REPORT WRITING”, arranged by Bombay College of Pharmacy, Mumbai on 27-29<sup>th</sup> May, 2020
6. Attended 1<sup>st</sup> International Online Flow Cytometry course by Trust for Education and Training in Cytometry (TETC) on 24-26<sup>th</sup> June 2020

# List of Publications

---

**List of Publications**

---

1. **Joshi, Mitesh**, and Purvi Bhatt. "Deciphering the anticancer activity of biocompatible zinc oxide nanoparticles loaded with methotrexate on breast cancer cells." *Bulletin of Materials Science* 46, no. 4 (2023): 192. **IF-1.8**
2. **Joshi, Mitesh**, and Purvi Bhatt. "Ameliorated in vitro anti-cancer efficacy of methotrexate loaded zinc oxide nanoparticles in breast cancer cell lines MCF-7 & MDA-MB-231 and its acute toxicity study." *Nanotechnology* 35, no. 33 (2024): 335101. **IF 3.5**
3. Patil, Dipti, Swapnil Raut, **Mitesh Joshi**, Purvi Bhatt, and Lokesh Kumar Bhatt. "PAQR4 oncogene: a novel target for cancer therapy." *Medical Oncology* 41, no. 6 (2024): 161. **IF 3.4**



# Deciphering the anticancer activity of biocompatible zinc oxide nanoparticles loaded with methotrexate on breast cancer cells

MITESH JOSHI<sup>1</sup> and PURVI BHATT\*<sup>1</sup>

Department of Biological Sciences, Sunandan Divatia School of Science, SVKM's NMIMS (Deemed-to-be University), Mumbai 400056, India

\*Author for correspondence (purvi.bhatt@nmims.edu)

MS received 1 March 2023; accepted 20 June 2023

**Abstract.** Novel nanoparticle-based therapies, in combination with cytotoxic drugs, are a new paradigm that is being explored. Methotrexate (MTX), a folic acid (FA) analog, is internalized by the folic acid receptor (FAR) which is known to be overexpressed in many cancer cells like breast cancer. MTX suppresses cell division by binding and blocking the dihydrofolate reductase, resulting in cell death due to cell cycle arrest. Thus, targeting FAR is an attractive strategy for controlling breast cancer cells. Zinc oxide nanoparticles (ZnONPs) are known biocompatible agents with anticancer and antimicrobial properties. Both MTX and ZnONPs have limitations such as nonspecific absorption and toxicity. In this study, we have attempted to use a combinatorial approach using MTX and ZnONPs, to target FAR on breast cancer cells and to improve the specificity towards cancer cells and be safe towards normal cells. Cytotoxicity of MTX–ZnONPs was assessed via MTT assay and acridine orange/ethidium bromide staining, which showed specificity and anticancer potential towards MTX-sensitive MCF-7 and MTX-resistant MDA-MB-231 cell lines, while showing less toxicity towards MCF-10A control cells. Also, the RBC haemolysis assay supports the biocompatible nature of MTX–ZnONPs, showing no haemolysis. Our results reveal MTX–ZnONPs as a novel nanosystem for showing specificity and cytotoxicity towards breast cancer cells, including MTX-resistant MDA-MB-231.

**Keywords.** Zinc oxide; methotrexate; breast cancer; folic acid receptor; biocompatible.

## 1. Introduction

Nanotechnology is a science of manipulation of material at a nanoscale level for the production of novel materials and its application in various fields. When materials are scaled down to the nano size (1–100 nm), their inherent biological, chemical and physiological properties change drastically [1,2]. Zinc oxide (ZnO) is a white-coloured powder with a large bandgap energy (3.37 eV). ZnO has also been given GRAS (Generally Regarded as Safe) status by US-FDA. Zinc oxide nanoparticles (ZnONPs) are easy to synthesize, and can be modified into various sizes and shapes. Due to its attractive properties, ZnO has found its applications in electronics, textiles, skincare and personal care products, food industry, and medicines and healthcare [3–6]. ZnO nanomaterials are an attractive candidate for targeted cancer therapy, as they are biocompatible and biodegradable. It has previously been reported that ZnO nanoparticles (NPs) were able to retain and release ligated drugs as well as loaded drugs with high selectivity, retention and controlled release. Furthermore, they crossed the therapeutic indices of currently used cancer chemotherapy agents [7,8]. It is believed that the  $\text{Zn}^{2+}$  ions released from ZnONPs cause oxidative stress and cell damage in cancer cells. An acidic pH and a

high  $\text{Zn}^{2+}$  ion concentration cause reactive oxygen species (ROS) to be generated. This leads to DNA damage followed by cell death. In addition, these released  $\text{Zn}^{2+}$  ions also inhibit certain enzymes involved in cell growth and proliferation, which contributes to their anticancer properties [9]. The stability of NPs plays a very important role in determining their activity. Diverse biological coating agents having biocompatible and biodegradable nature, such as chitosan, polyethylene glycol (PEG), polyvinyl pyrrolidone and amino acids, are used to increase the stability and functionalization of NPs. Also, PEG has a dual role where it acts as a solvent and stabilizer that limits particle growth and suppresses particle agglomeration in this application [10–13].

In certain cancer types, folic acid receptor (FAR) levels increase drastically in comparison to normal healthy cells. In such cases, targeting FAR-overexpressing cells using methotrexate (MTX), a known folic acid antagonist, is an acceptable strategy for therapeutic applications. MTX inhibits the function of the enzyme dihydrofolate reductase, which is very important for nucleotide synthesis. MTX is also been used in the treatment of many cancers including some solid tumors like breast cancer [14–16]. NP-based drug delivery is an approach that can help target the cells

more specifically and increase the therapeutic index as well as reduce the side effects by reducing nonspecific absorption. Using a combinatorial approach researchers are attempting to synthesize a drug–NP conjugate system that will be stable, biocompatible and target specific in nature showing high efficacy. Drug loading on the NP surface comes out to be a challenging task while synthesizing drug–NP conjugates [17–20].

In the present study, we report for the first time, the synthesis of biocompatible MTX–loaded ZnONPs (MTX–ZnONP) for targeting the FAR overexpressed on the surface of breast cancer cells. We report the synthesis, characterization, *in-vitro* antitumour efficacy and blood biocompatibility of MTX–ZnONPs in MCF-10A, MCF-7 and MDA-MB-231 cell lines.

## 2. Experimental

### 2.1 Materials

All the chemicals were of analytical grade, unless otherwise stated and were used as received. For all preparations, MilliQ water was used. Zinc nitrate hexahydrate  $\text{Zn}(\text{NO}_3)_2 \cdot 6\text{H}_2\text{O}$  and potassium hydroxide (KOH) were purchased from LOBA Chemi, India. Chitosan low-molecular weight, triethyl amine, acridine orange (AO) and ethidium bromide (EB) were purchased from Sigma-Aldrich, USA. Polyethylene glycol 400 (PEG-400) was procured from Molychem, India. Methotrexate (MTX) was kindly provided as a gift sample from Khandelwal Laboratories Pvt. Ltd, Mumbai, India.

Dulbecco's modified Eagle's medium, foetal bovine serum, Dulbecco's phosphate-buffered saline (DPBS), 0.25% trypsin-EDTA with phenol red indicator and trypan blue were purchased from Gibco (Gibco™, ThermoFisher Scientific, USA). The MEGM bullet kit containing the MEBM media with single-use aliquots of growth factors was from Lonza, Germany. Cholera toxin and antibiotic antimycotic solution was brought from Sigma-Aldrich, USA. 3-(4,5-Dimethylthiazol-2-yl)-2,5-diphenyltetrazolium bromide (MTT) was from SRL, India, while dimethyl sulphoxide was from SD Fine Chem, India. All chemicals, reagents, buffers, media and plasticware (SPL Life Science) used for cell culture work were of cell culture grade. Human breast cancer cell lines MCF-7 were procured from NCCS, Pune, and MCF-10A normal breast epithelial cell line was purchased from ATCC.

### 2.2 Methods

**2.2a Synthesis of bare ZnONPs and MTX–ZnONPs:** For the synthesis of bare ZnONPs, 0.2 M  $\text{Zn}(\text{NO}_3)_2 \cdot 6\text{H}_2\text{O}$

solution was prepared in 10% PEG-400 and was stirred in a round bottom flask till temperature reached 85°C and was stirred for 30 min. To this, 20% KOH was slowly added through the side wall of the flask until the pH of the solution reached to 11, after which the solution was set aside. The supernatant was discarded and particles were centrifuged for 10 min at 5000 rpm. The resulting pellet was washed with MilliQ water twice and once with ethanol. Afterwards, drying was done at 70°C for 1 h and dried powder of ZnONPs was stored in a dry place until further analysis.

Using an *ex-situ* approach, MTX–ZnONPs were synthesized. Briefly, MTX solution was prepared in 0.1% triethyl amine at a final conc. of 1 mg ml<sup>−1</sup>, with 0.1% chitosan solution in the ratio of 9:1. MTX solution was then mixed with bare ZnONPs solution in the ratio of 1:20 and sonicated for 5 min followed by constant mixing for overnight. The next day the solution was centrifuged and the NPs were washed twice with MilliQ water and once with ethanol. NPs were dried at 50°C for 1 h. Dried MTX–ZnONPs were later stored in a dry place for further analysis.

**2.2b Characterization of synthesized NPs:** Nanoparticles were characterized using different methods like UV–Vis, FTIR, XRD, Zeta potential and DLS, ICP-AES, EDS-mapping and HR-TEM. Ultraviolet-visible (UV–Vis, PerkinElmer) spectroscopy analysis was performed using Quartz cuvettes having path length of 1 cm to check the optical properties of NPs in solution. Fourier-transform infrared spectroscopy (FTIR; IRAffinity-1S, Shimadzu) analysis was done to observe different functional groups present on the NPs. FTIR was recorded in the range of 4000–400 cm<sup>−1</sup> by ATR method. X-ray diffraction (XRD-7000, Shimadzu) for all samples was recorded with scan rate of 2° min<sup>−1</sup> using Cu K $\alpha$  radiation ( $\lambda$  = 0.154 nm) in the 2 $\theta$  range of 2 $\theta$  (20°–80°) to record the XRD pattern. Zeta potential and hydrodynamic diameter were measured for all NPs in solution form (Malvern, Zetasizer Version 7.11). Zeta potential was carried out to understand the surface charge possessed by NP systems at different pH values in the range of pH 5–10. To adjust the pH, 0.1 N HCl and 0.1 N NaOH were used. The total metallic zinc content of NPs was studied by inductively coupled plasma atomic emission spectroscopy (ARCOS from M/s. Spectro Analytical Instruments GmbH, Germany). The chemical purity and elemental composition of NPs was illustrated by the help of energy-dispersive spectroscopy (EDS-mapping, JEOL JSM-7600F). High-resolution-transmission electron microscopy (JEOL-JEM 2100F) was performed to understand the size, shape and distribution of the synthesized NP.

**2.2c MTX loading efficiency:** To calculate the % loading efficiency, the concentration of MTX before loading and after loading was determined with the help of

UV–Vis spectrophotometer at 303 nm. The standard curve equation was used to determine the concentration of MTX, and loading efficiency was calculated using the below equation (1) [21,22].

$$\% \text{ Loading efficiency} = \frac{(\text{Conc. of MTX initial} - \text{Conc. of MTX after})}{(\text{Conc. of MTX initial})} \times 100 \quad (1)$$

**2.2d Drug release study:** To study the release pattern of MTX from NPs, dialysis method was employed, using two buffer systems, one at physiological pH 7.4 and another at pH 5.0 simulating an acidic tumour microenvironment. A drug release study was carried out for 24 h in phosphate-buffered saline (PBS) at pH 7.4 and 5.0 at 37°C under slow stirring conditions, respectively. An aliquot of 5 mg ml<sup>-1</sup> NPs was taken in a dialysis bag having a cutoff value of 12 kDa and immersed into 50 ml buffer under constant stirring conditions. A quantity of 1 ml aliquot was removed and replaced with fresh 1 ml of buffer. Aliquots were collected at various time points upto 8 and 24 h. Readings were taken at 303 nm using UV–Vis spectrophotometer and then analysed. The experiments were run in triplicates. The % cumulative release (% CR) of the drug at various time points was calculated using the following equation (2):

$$\% \text{CR} = \frac{D_t}{D_i} \times 100 \quad (2)$$

where  $D_t$  refers to the drug released at time  $t$  and  $D_i$  refers to the initial drug loaded onto the NPs [23].

**2.2e Cell culture:** Non-metastatic human breast cancer cell line MCF-7 was procured from NCCS, Pune. Triple-negative breast cancer (TNBC) cell line MDA-MB-231 and normal breast epithelial cell line MCF-10A were purchased from ATCC, USA. MCF-7 and MDA-MB-231 cells were cultured in Dulbecco's modified Eagle's medium media accompanied with 10% heat-inactivated foetal bovine serum, and antibiotic antimycotic solution. MCF-7 cells were maintained under humidified conditions at 37°C, 5% CO<sub>2</sub> and trypsinized using 0.25% trypsin-EDTA after attaining 80–90% confluency and maintained at 37°C in 5% CO<sub>2</sub>.

MCF-10A cells were cultured in mammary epithelial cell basal medium (MEBM) supplemented with growth factors (Lonza, USA) and 100 ng ml<sup>-1</sup> of cholera toxin (Sigma, USA). MCF-10A cells were maintained at 37°C with 5% CO<sub>2</sub> under humidified conditions and 0.25% trypsin-EDTA was used for trypsinization followed by maintenance at 37°C in 5% CO<sub>2</sub>.

**2.2f In-vitro cytotoxicity test:** To determine the cytotoxicity of the synthesized nanosystem, the above cell

lines were used to perform an MTT assay. In the MTT assay, viable cells are assessed by their ability to reduce yellow MTT tetrazolium dye into purple-coloured insoluble formazan crystals. Dying cells fail to reduce the MTT into

formazan and thus show a decrease in purple colour, indicating low viability. A cytotoxicity test was conducted to study the dose- and time-dependent activity of bare ZnONPs, MTX–ZnONPs and MTX in MCF-7, MDA-MB-231 and MCF-10A cells.

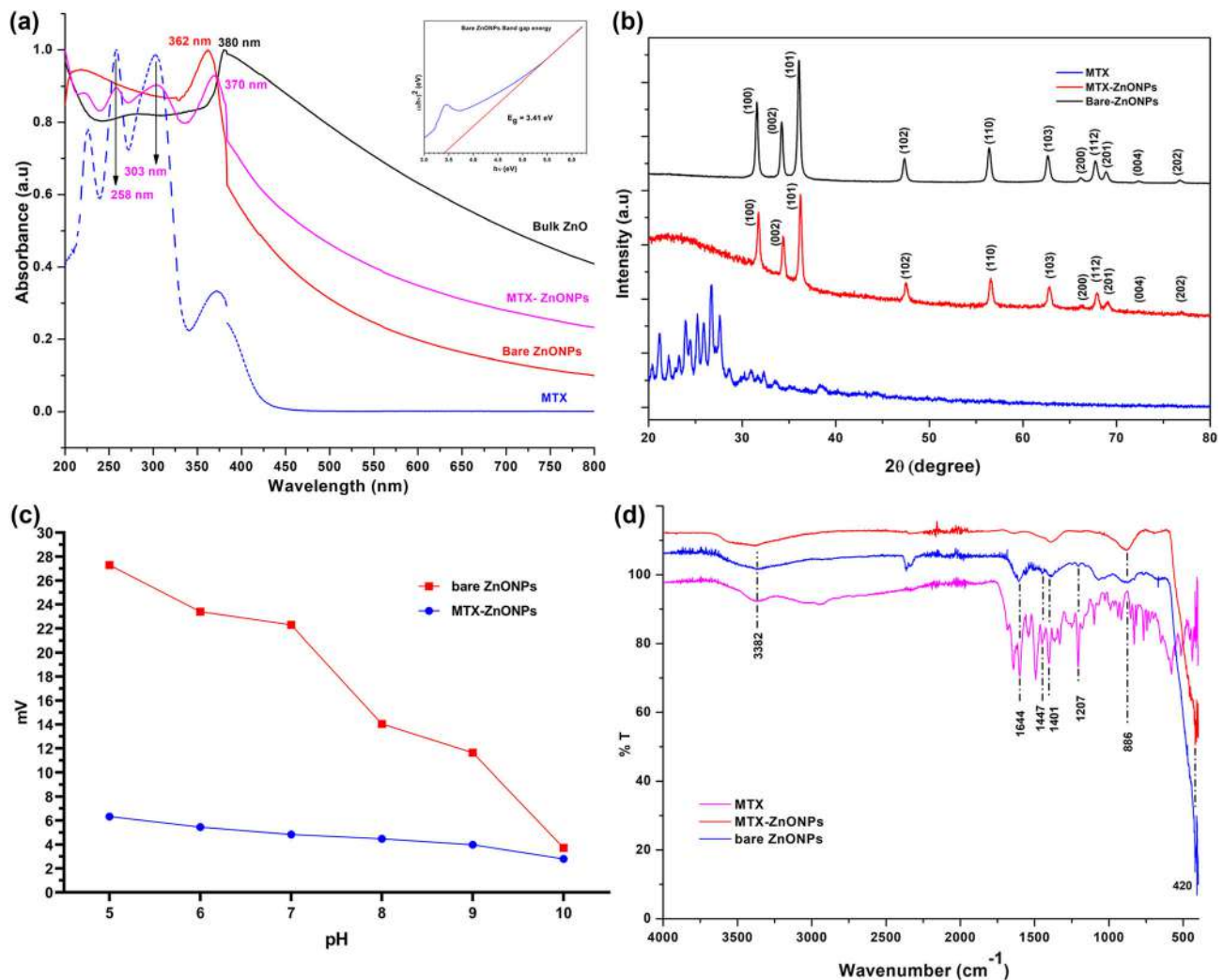
In brief, the cells were seeded at a density of 10<sup>4</sup> cells per well in a 96-well microtiter plate and allowed to attach by incubating for 24 h at 37°C in 5% CO<sub>2</sub>. Next day, cells were treated with various concentrations of the bare ZnONPs, MTX–ZnONPs and MTX. All of the systems were prepared in serum-free media. NPs were used at concentrations of 6.25, 12.5, 25, 50 and 100 µg ml<sup>-1</sup>, MTX was used as a positive control at concentrations par with its loading on MTX–ZnONPs in the following concentrations: 0.29, 0.59, 1.17, 2.34, 4.68 µg ml<sup>-1</sup>. All the dilutions were made in serum-free media. A quantity of 100 µl serum-free media was added to untreated cell control wells. Plates were further incubated at 37°C in 5% CO<sub>2</sub> for 24 and 48 h. At the end of the respective incubation time, cytotoxicity was assessed by the addition of 20 µl of MTT to each well at a concentration of 5 mg ml<sup>-1</sup> and plates were further incubated for 3 h. Formazan crystals formed intracellularly by the metabolizing cells were dissolved by the addition of 100 µl of DMSO followed by measuring the absorbance of the microtiter plate at 570 nm and 650 nm as a reference wavelength using BioTek EPOCH 2 microplate reader. Percent cell viability was calculated using the following equation (3):

$$\% \text{ Cell viability} = (\text{O. D of test})/(\text{O. D of control}) \times 100 \quad (3)$$

Three independent experiments with their triplicates were analysed for final data.

**2.2g AO/EB dual staining for live/dead cells screening:** Apoptosis and necrosis are the two ways by which cell death occurs. Both these events are quite distinct in their nature and can be morphologically visualized under the microscope. To study these morphological changes in cells, post-treatment with NPs, we carried out AO/EB dual staining. AO is nonspecific to both live and dead cells and ends up staining both the cells with green fluorescence,





**Figure 1.** Characterization data of bare ZnONPs, MTX-ZnONPs and MTX. (a) UV-vis spectrum of bulk ZnO, bare ZnONPs, MTX-ZnONPs and MTX. Inset shows the bandgap energy of bare ZnONPs. (b) XRD of bare ZnONPs, MTX-ZnONPs and MTX. (c) Zeta potential of bare ZnONPs and MTX-ZnONPs. (d) FTIR of bare ZnONPs, MTX-ZnONPs and MTX.

whereas EB stains cells red with impaired membrane permeability [24,25].

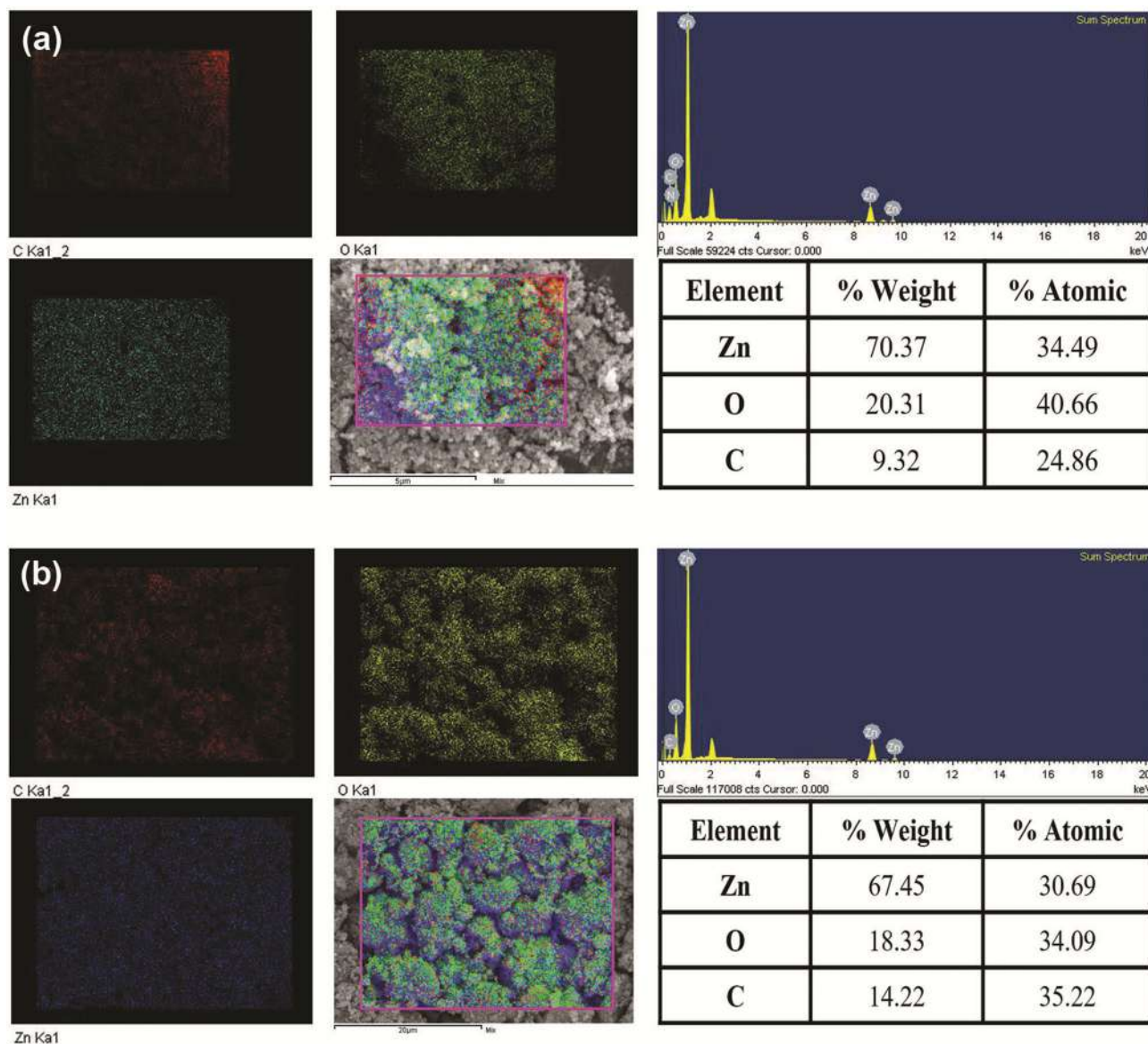
MCF-7 and MCF-10A cells were seeded in six-well flat bottom plates at a density of  $10^5$  cells per well. Cells were incubated for 24 h at  $37^\circ\text{C}$  with 5%  $\text{CO}_2$  under humidified conditions. Cells were treated with three concentrations as per  $\text{IC}_{50}$  values received in MTT for MTX-ZnONPs for both cell lines. For MCF-7 cells, 2.5, 5.0 and  $7.5 \mu\text{g ml}^{-1}$  and MCF-10A cells 10, 20 and  $30 \mu\text{g ml}^{-1}$  concentration of bare ZnONPs, MTX-ZnONPs and MTX were used for treatment for 24 h. Post-treatment, cells were washed with DPBS and cells were incubated with 1:1 AO and EB each  $100 \mu\text{g ml}^{-1}$  in DPBS for less than a min. Excess stain was removed and cells were observed under an inverted fluorescent phase contrast microscope (Zeiss, Jena, Germany).

**2.2h RBC haemolysis assay:** To study RBC haemolysis, 5 ml of fresh ethylene diamine tetra-acetic acid (EDTA)-stabilized human blood was collected. Blood was collected

from healthy individuals ( $n = 6$ ) after seeking approval from the Institutional Ethics Committee (NMIMS/IEC/012/2020). Written consent of all six participants was taken for the study.

It is of prime importance to evaluate the toxicity profile of NPs beforehand for their intravenous route of administration. To replicate the same conditions, we performed a blood compatibility test where RBC haemolysis assay was performed to understand the safe and biocompatible nature of NPs. The haemolysis study protocol was followed as described elsewhere [26].

Briefly, EDTA-stabilized 5 ml of blood was collected and centrifuged at 1200 rpm for 5 min to collect the RBC pellet. RBC pellet was collected and washed twice with PBS and diluted in a ratio of 1:4 with PBS. Suspension of NPs was made in PBS at different concentrations from 6.25, 12.5, 25, 50 and  $100 \mu\text{g ml}^{-1}$ . For the test, 0.8 ml of NPs and 0.2 ml of RBC's suspension were mixed. For positive control, 0.8 ml of distilled water and for negative control 0.8 ml of

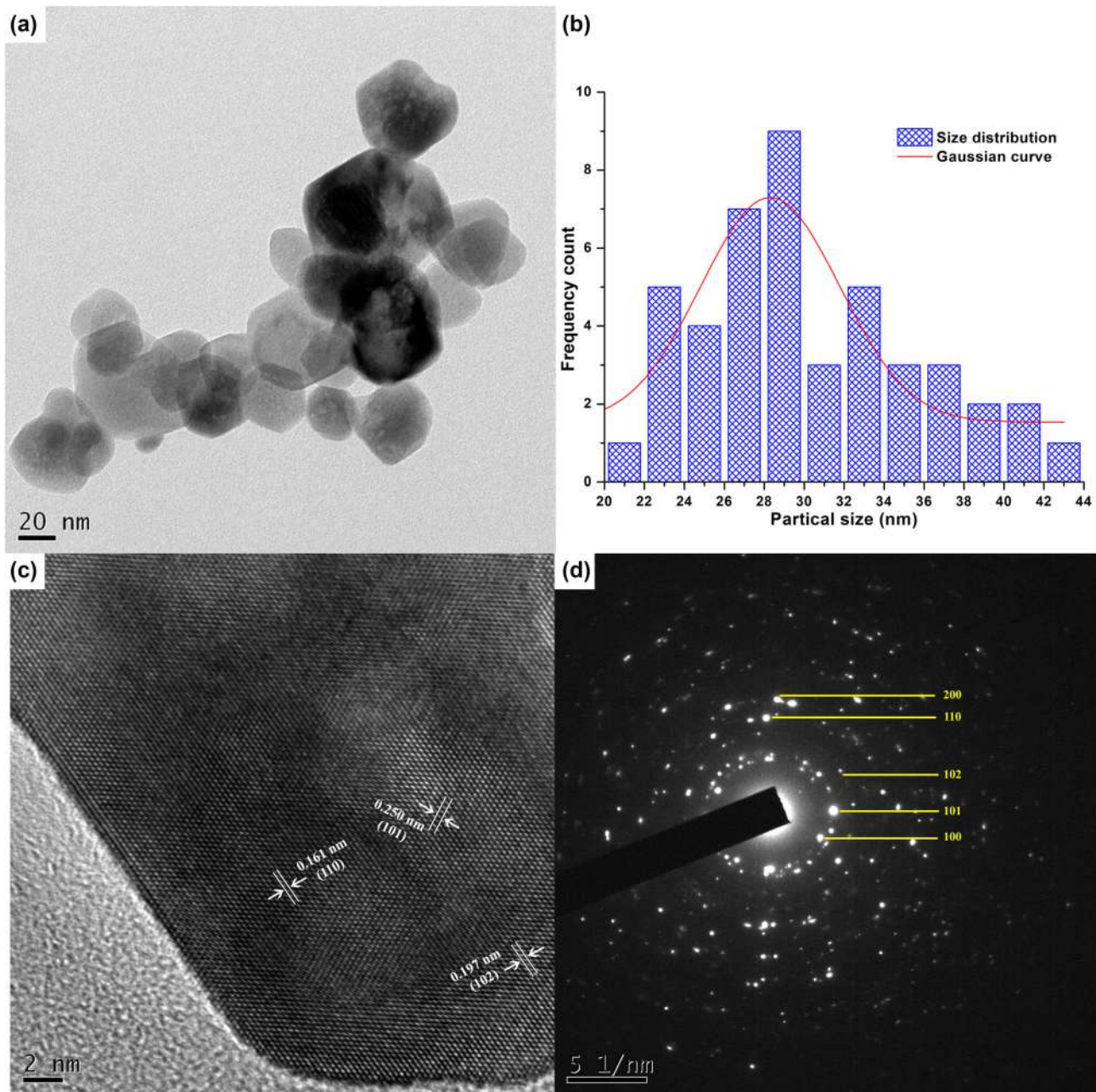


**Figure 2.** EDS mapping images of zinc in blue, oxygen in green and carbon in red. The lower right image shows the merge of all elements. Lower left image shows EDS spectrum with elemental values in the table (inset). (a) EDS mapping of bare ZnONPs and (b) MTX-ZnONPs.

PBS was mixed with 0.2 ml of RBC's suspension. All the samples were then incubated at 37°C for 2 h with intermittent mixing to resuspend the contents. After 2 h, all the tubes were centrifuged at 1200 rpm for 5 min to collect the supernatant. A quantity of 100 µl of the supernatant was

then transferred to 96-well plate. Samples were run in triplicates. The absorbance of haemoglobin in the supernatant was measured in BioTek EPOCH 2 using a 570 nm sample wavelength and 655 nm as a reference wavelength. % Haemolysis was calculated as given in equation (4):

$$\% \text{ Haemolysis} = \frac{(\text{absorbance of sample} - \text{absorbance of negative control})}{(\text{absorbance of positive control} - \text{absorbance of negative control})} \times 100 \quad (4)$$



**Figure 3.** HR-TEM micrographs of bare ZnONPs. (a) HR-TEM image of bare ZnONPs shows hexagonal nanoparticles, (b) size distribution curve of NPs, (c) crystal lattice structure of NP and (d) SAED pattern.

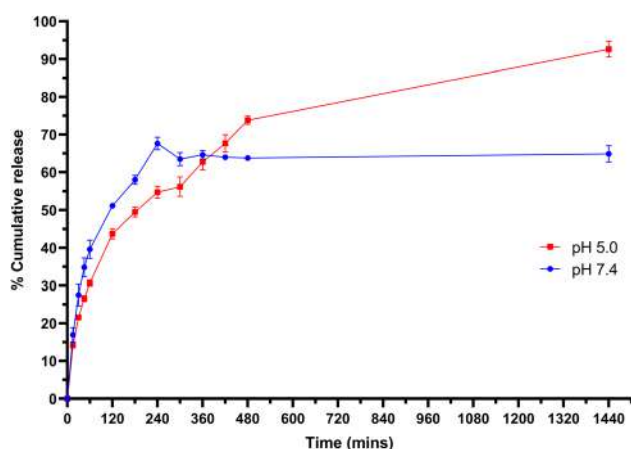
### 3. Results and discussion

#### 3.1 Characterization of synthesized NPs

All the synthesized NP systems were characterized using various techniques. UV–Visible spectroscopy of bulk ZnO, bare ZnONPs and MTX–ZnONPs was recorded in the range of 200–800 nm in Quartz cells having a 1 cm path length. Figure 1a shows the absorption spectrum of bulk ZnO and bare ZnONPs and MTX–ZnONPs. Bulk ZnO shows absorption maxima at 380 nm, whereas bare ZnONPs show absorption maxima at 362 nm, 18 nm of sharp blue shift is

seen. Blueshift indeed implies quantum confinement of NPs. When particle size decreases, the bandgap of the particles increases, leading to a shift in absorption to lower wavelengths [27,28]. Bandgap energy of bare ZnONPs was calculated using Tauc's plot by plotting the graph of  $(\alpha h\nu)^2$  vs. photon energy ( $h\nu$ ) [29]. Direct bandgap energy ( $E_g$ ) for bare ZnONPs was found to be 3.41 eV, which was higher than the bulk ZnO (3.26 eV), indicating nanocrystalline state of particles [30,31]. MTX–ZnONPs showed two characteristic peaks at 370 nm for ZnONPs and 303 nm for MTX, respectively. The peak at 303 nm implies the presence of MTX on the surface of ZnONPs.





**Figure 4.** Drug release study of MTX–ZnONPs in PBS at pH 7.4 and 5.0.

XRD for both the NPs systems bare ZnONPs, and MTX–ZnONPs showed characteristic sharp peaks, indicating the highly crystalline nature of NPs in figure 1b. All the peaks of samples matched that of the standard ZnO (JCPDS card no. 00-036-1451) showing the hexagonal wurtzite phase of the structure. Both the NPs showed the same characteristic peaks (100), (002), (101), (102), (110), (103), (200), (112) and (201) corresponding to the planes of standard ZnO. Though peak intensities change for samples containing MTX, the data obtained is in accordance with the previously reported results [27,29,32]. Sharp peaks observed indicate the highly crystalline nature of synthesized NPs. Furthermore, the crystalline size of the NPs was calculated with the help of Scherrer's formula:  $D = K\lambda / (B \cos\theta)$ , where,  $D$  is the average crystalline size in nm,  $K$  is Scherrer constant,  $\lambda$  is X-ray wavelength,  $B$  is FWHM (full-width half-maxima) of peaks and  $\cos\theta$  one-half of  $2\theta$  [33,34]. The average crystalline size calculated for NPs was 31 and 40 nm for bare ZnONPs and MTX–ZnONPs, respectively.

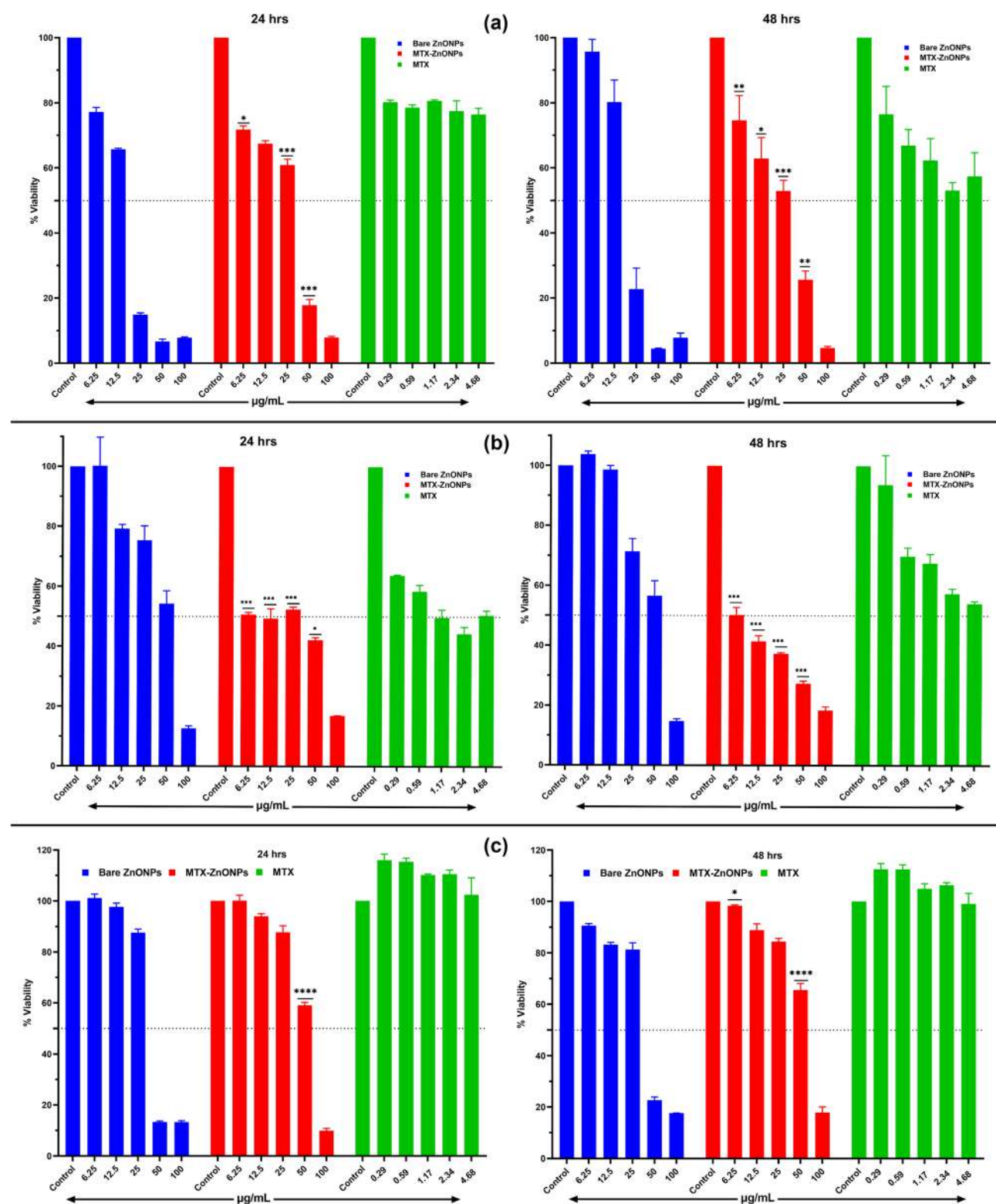
Zeta potential analysis of both the NPs was performed using Malvern, Zetasizer instrument. Zeta potential is a charge present on the surface of the NPs, which directly correlates to the stability of nanosystems. Surface charge plays a very important role in the cellular internalization of these particles [35,36]. Zeta potential values greater than  $\pm 30$  mV are considered as highly stable and values near isoelectric point, i.e., zero charge is considered as least stable [37]. Figure 1c shows the zeta potential of bare ZnONPs and MTX–ZnONPs from pH 5–10. Bare ZnONPs show a positive charge throughout the pH scale with a high surface charge under an acidic environment. At the same time when these particles were loaded with MTX during the *ex-situ* synthesis approach, they also attain a positive charge at the entire pH range. The shift of surface charge of MTX–ZnONPs can be attributed to the presence of a negative carboxyl group of MTX drug and higher loading on the surface of bare ZnONPs. Overall, all NP systems show greater stability towards the alkaline pH scale. It is observed

that PEG-stabilized bare ZnONPs have higher stability at various pH in comparison to MTX–ZnONPs. Overall, all NP systems show greater stability towards acidic pH. Also, zeta potential indicates the successful coating of NPs with MTX due to a shift in the charge. Also, DLS results gave average size distribution of 270 and 285 nm for bare ZnONPs and MTX–ZnONPs with moderate size distribution. It is important to note that particle size measured by DLS is usually greater than the actual particle size, as it considers the average hydrodynamic diameter.

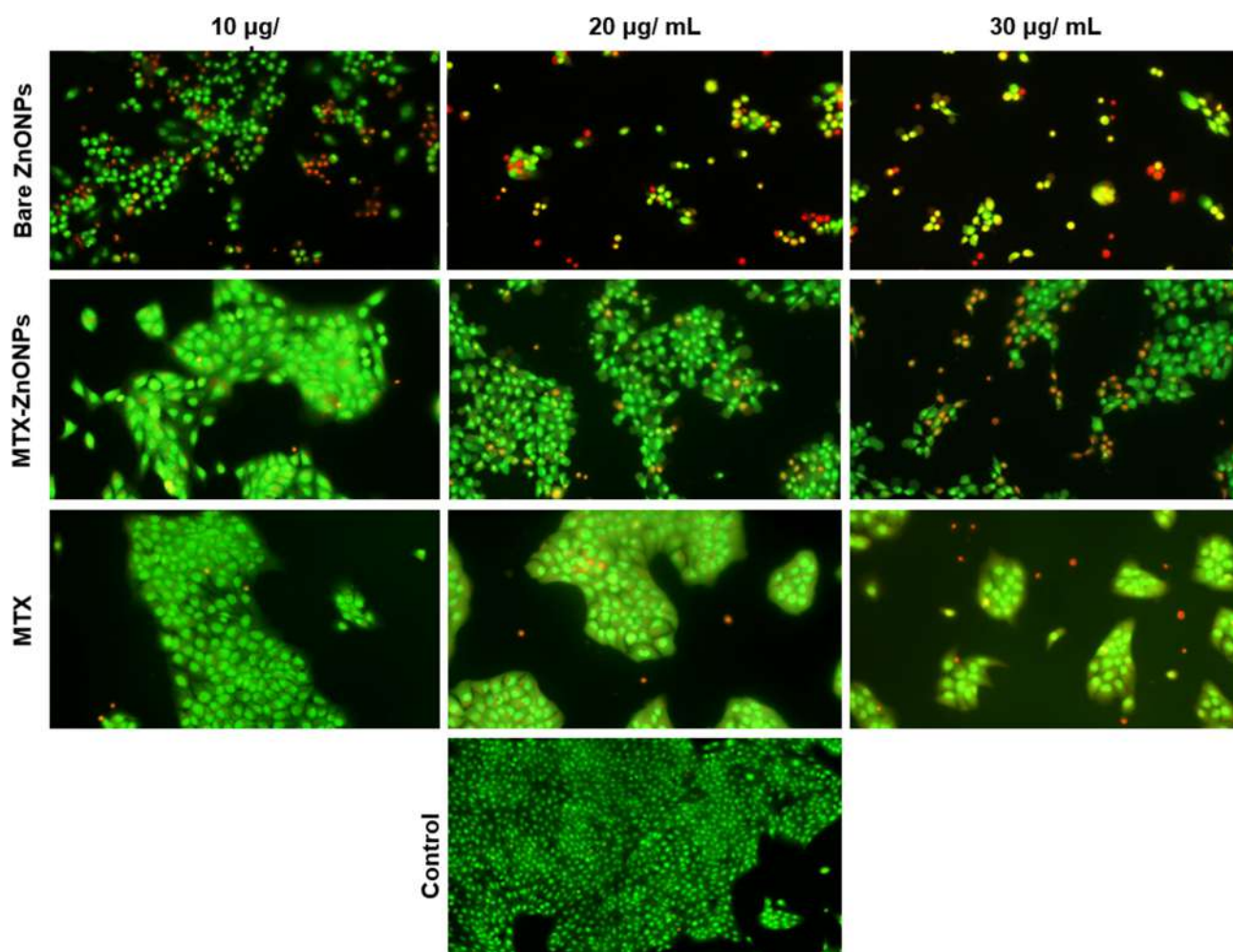
FTIR spectrum of both the NPs and drug was taken in the range of  $4000\text{--}400\text{ cm}^{-1}$  with ATR method, as shown in figure 1d. FTIR spectrum of bare ZnONPs showed characteristic peaks at  $3382$ ,  $886$  and  $420\text{ cm}^{-1}$  for  $\text{--OH}$  stretching,  $\text{Zn--OH}$  vibration and  $\text{Zn--O}$  metal oxide bond. The peak between  $400$  and  $600\text{ cm}^{-1}$  is generally designated for metal ion bonds [38,39]. In the case of pure MTX, it showed characteristic peaks at  $1644\text{ cm}^{-1}$  for  $\text{--CONH}$  group,  $3387\text{ cm}^{-1}$  for  $\text{--NH}$  stretch,  $2926\text{ cm}^{-1}$  for  $\text{--CH}$  groups present in the structure. Carboxylate group  $\text{--COO}$  presence can be seen at  $1207$  and  $1447\text{ cm}^{-1}$  designated for the  $\text{--NH}$  amide bending of the MTX molecule [23,40]. Considering MTX–ZnONPs, it also showed the presence of peaks from the MTX at  $1640$  and  $1450\text{ cm}^{-1}$  as well as peaks coming from bare ZnONPs at  $420\text{ cm}^{-1}$  for ZnO. All the above peaks confirm the loading of MTX on the bare ZnONPs.

ICP-AES is the most commonly used method for elemental analysis, to know the precise concentration of a specific metal ion in the sample [15,41]. Both the NP systems were analysed to know the  $\text{Zn}^{2+}$  concentration present in them. The amount of zinc present in bare ZnONPs was  $0.352\text{ mg ml}^{-1}$  and for MTX–ZnONPs it was  $0.280\text{ mg ml}^{-1}$ . By using EDS mapping, the chemical composition and distribution of the material can be determined. In order to determine the distribution of Zn, O and C, elemental analysis was performed. The EDS mapping images of bare ZnONPs, in figure 2a, showed sharp peaks of zinc and oxygen with carbon and weight percentage of 70.37, 20.31 and 9.32, respectively, without any impurities. Whereas in the case of MTX–ZnONPs, in figure 2b, the weight percentage of the zinc, oxygen and carbon was 67.45, 18.33 and 14.22, respectively. All the results confirm the formation of ZnONPs successfully in both systems [42,43]. Also, the increased presence of carbon in MTX–ZnONPs can be attributed to the presence of drug loading onto bare ZnONPs. This result also confirms the successful loading of MTX over bare ZnONPs.

HR-TEM analysis of bare ZnONPs was done to understand the crystalline size and plane structure of NPs. It was found that the bare ZnONPs have hexagonal crystal morphology, figure 3a, with an average size of around 30 nm in size, figure 3b. Crystal lattice arrangement is visible in figure 3c, showing the presence of different planes corresponding to SAED (selected area electron diffraction) pattern, figure 3d, which shows multiple bright spots and the



**Figure 5.** Effect of bare ZnONPs, MTX-ZnONPs and MTX on mitochondrial function in (a) MCF-10A, (b) MCF-7 and (c) MDA-MB-231 cells. Cell viability was determined by the MTT reduction assay after 24 and 48 h. Data presented are mean  $\pm$  SD. The asterisks above columns indicate statistically significant differences compared to bare ZnONPs (\*\* $p < 0.01$ , \*\*\* $p < 0.001$ , \*\*\*\* $p < 0.0001$ ).



**Figure 6.** AO/EB dual staining of MCF-10A cells for live and dead cells screening treated with bare ZnONPs, MTX–ZnONPs and MTX at the concentration range of 10–30  $\mu\text{g ml}^{-1}$ . Magnification: 20 $\times$ .

rings corresponding to the lattice structure of the crystals. Bright spots indicate highly crystalline morphology, but diffused band indicates aggregates. Planes given by SAED pattern are in accordance with the planes provided by the XRD data, which again confirms the crystalline nature of particles [44,45].

UV–vis spectrophotometer was used to calculate the MTX drug-loading efficiency on ZnONPs. The % loading efficiency of MTX was found to be 79.44%.

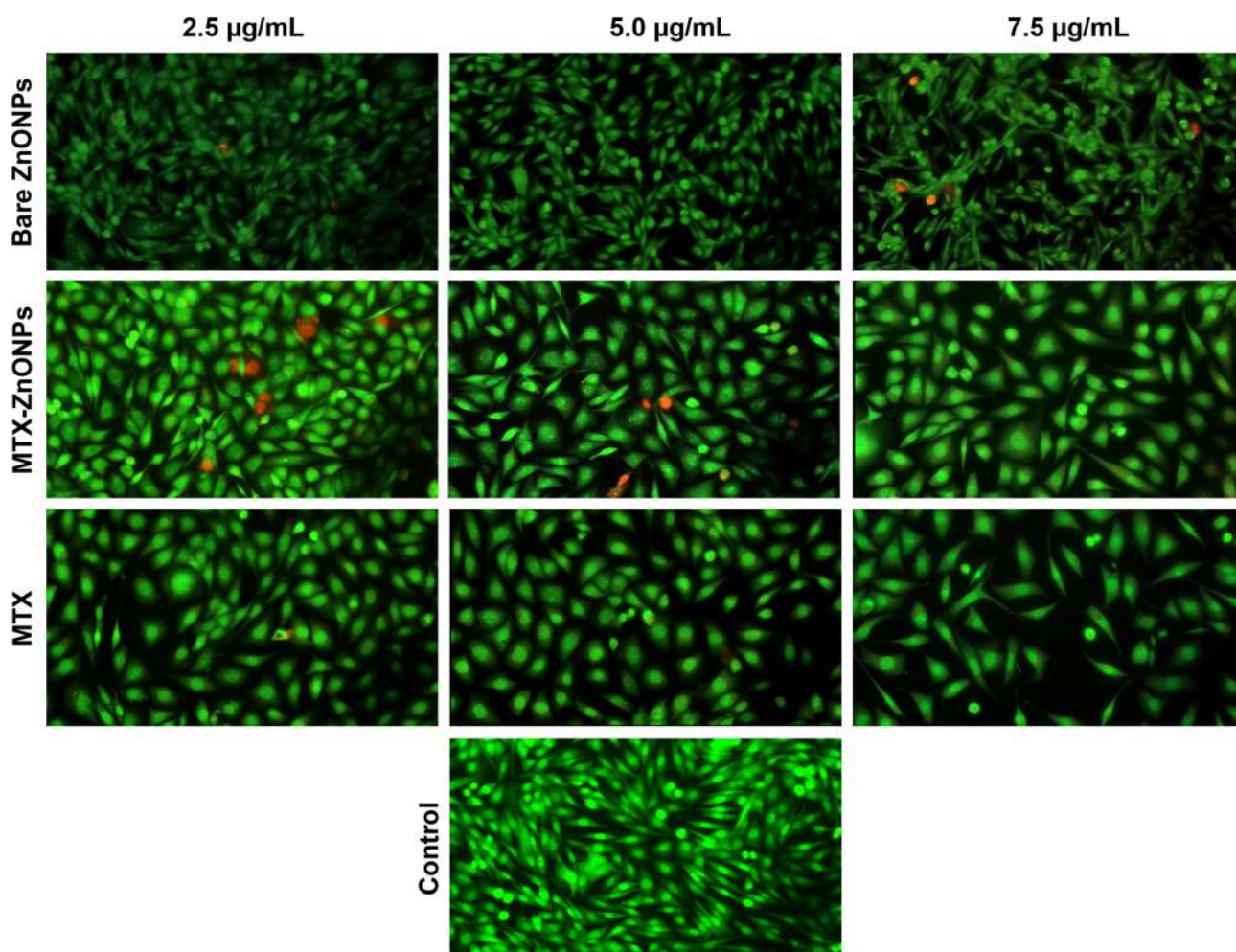
A drug release study was carried out to understand the release pattern of nanosystems under simulated physiological conditions. For the drug release study, the dialysis method was used and PBS with pH 7.4 was used to simulate a normal cellular environment and for an acidic cancer cell environment, PBS at pH 5.0 was used at 37°C. The MTX release from the NP showed a biphasic release pattern with initial burst release within 1 h, as seen in figure 4. Nearly 40% drug release was observed within 1 h and then a steady increase was observed until 5 h. At pH 7.4, no more than 65% of drug release was observed, whereas pH 5.0 kept showing the log phase upto 24 h resulting in almost 90% of

drug release. This clearly shows that under an acidic microenvironment, drug release is favoured which is significant for cancer cells.

### 3.2 In-vitro cytotoxicity test

MCF-10A, MCF-7 and MDA-MB-231 cells were used to perform dose- and time-dependent cytotoxicity studies with NPs. As seen in figure 5, MTX–ZnONPs showed time and dose-dependent activity in all three cell lines. MTX–ZnONPs were found to be highly cytotoxic towards all cell lines in comparison to MTX at all concentrations used. MTX–ZnONPs showed the lowest  $\text{IC}_{50}$  value of 5  $\mu\text{g ml}^{-1}$  for MCF-7 cells followed by 18  $\mu\text{g ml}^{-1}$  and 49  $\mu\text{g ml}^{-1}$  for MCF-10A and MDA-MB-231 cells, respectively. However, bare ZnONPs presented the highest toxicity towards control cells MCF-10A with an  $\text{IC}_{50}$  values of 13  $\mu\text{g ml}^{-1}$ , subsequently,  $\text{IC}_{50}$  value obtained for MDA-MB-231 and MCF-7 breast cancer cells were 31 and 38  $\mu\text{g ml}^{-1}$ . The mechanism of action of ZnONPs is not yet fully understood, but it is





**Figure 7.** AO/EB dual staining of MCF-7 cells for live and dead cells screening treated with bare ZnONPs, MTX–ZnONPs and MTX at the concentration range of 2.5–7.5  $\mu\text{g ml}^{-1}$ . Magnification: 20 $\times$ .

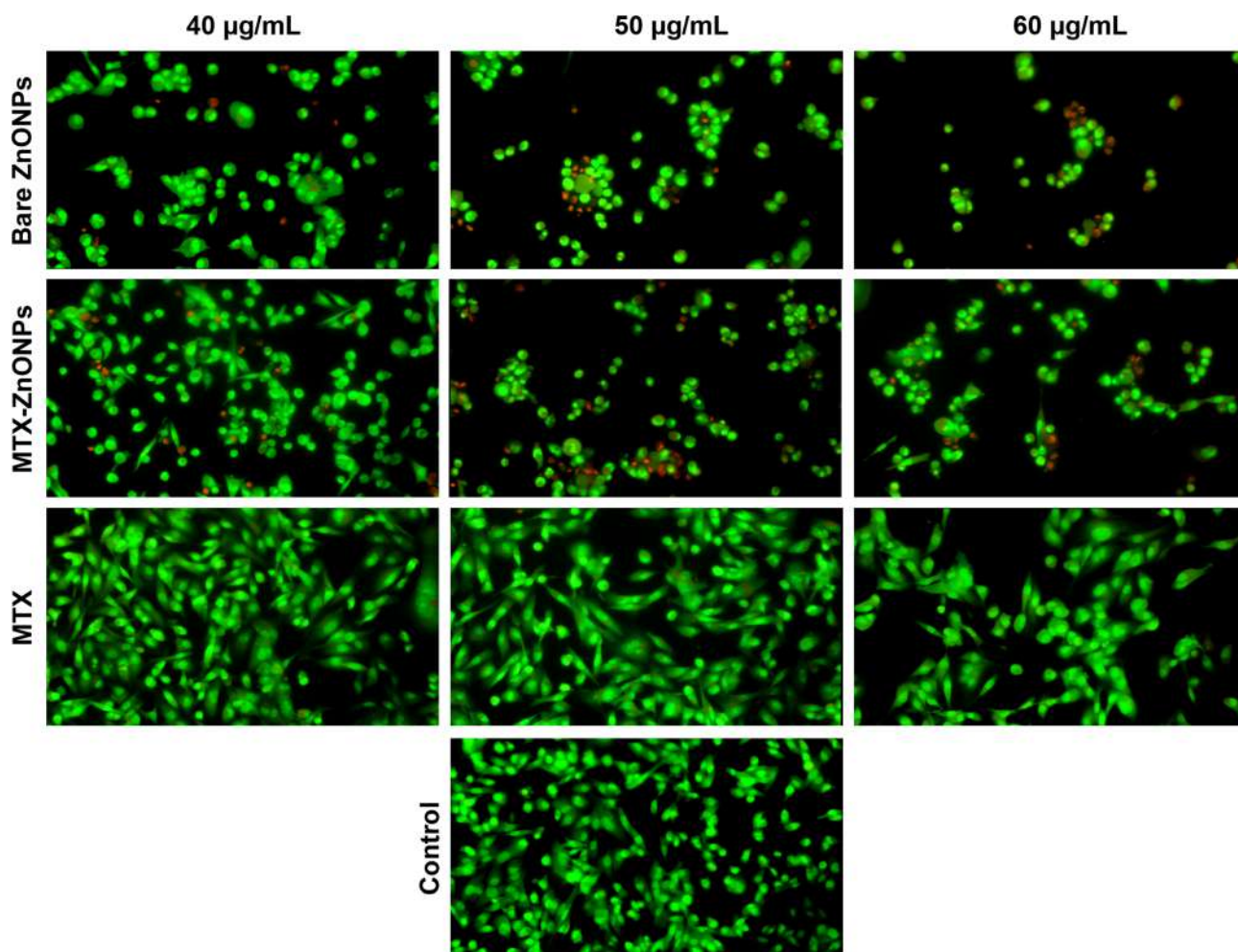
believed to involve the release of  $\text{Zn}^{2+}$  ions under an acidic environment, inducing oxidative stress and releasing any payload on it inside the cell. This oxidative stress damages the nucleic acids, proteins, enzymes and lipids leading to the generation of ROS. This damage to cellular components caused by ROS further initiates apoptosis, leading to cell death [46,47]. Once MTX–ZnONPs reach inside the cancer cell, they get exposed to its acidic cytoplasm where they dissolve under an acidic environment releasing  $\text{Zn}^{2+}$  ions and MTX [48]. MTX owing to its high structural similarity with FA gets transported in the cells using the same FAR. Once inside, MTX gets polyglutamated and gets converted to its active form stalling the purine and pyrimidine synthesis, which ultimately results in cell death [49]. However, the sensitivity of any cell line towards MTX may differ based on its expression of FAR on the surface [50,51]. MTX resistance in TNBC cell line MDA-MB-231 is widely reported [52,53], which explains the high cell viability observed for these cells. These results, therefore, indicate that synthesized MTX–ZnONPs not only show good efficacy for MCF-7 breast cancer cells, but can also show potent anticancer activity

towards drug-resistant TNBC cell line MDA-MB-231 than MTX. Subsequently, high cell viability was observed in MCF-10A cells, which control breast epithelial cell line, in contrast to breast cancer cells, implying that MTX–ZnONPs show safe and biocompatible nature towards control cells and shows specificity towards cancer cells.

Consequently, significant cell viability was seen in MCF-10A cells, which is a control breast epithelial cell line, suggesting the safe and biocompatible nature of MTX–ZnONPs and displays selectivity towards cancer cells.

### 3.3 AO/EB dual staining for live/dead cells screening

AO and EB are both DNA intercalating dyes, which differentially stain cells based on their membrane integrity. AO being a permeable dye tends to stain both live and dead cells; hence, cells with only AO inside appear green, whereas a cell that is dead or whose membranes have been compromised absorbs EB and therefore fluoresces red. The nuclei of necrotic cells appear similar to those of living



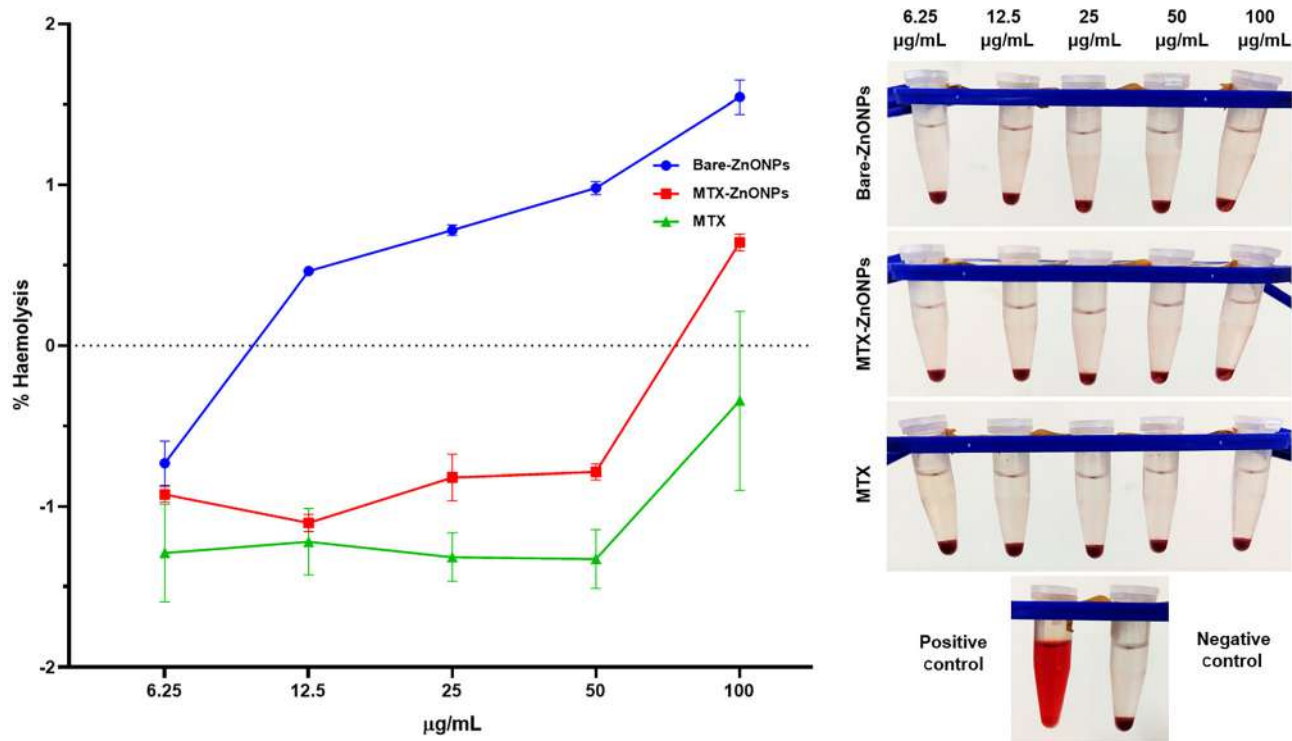
**Figure 8.** AO/EB dual staining of MDA-MB-231 cells for live and dead cells screening treated with bare ZnONPs, MTX–ZnONPs and MTX at the concentration range of 40–60  $\mu\text{g ml}^{-1}$ . Magnification: 20 $\times$ .

cells, with no condensed chromatin and have a bright orange-red fluorescence. Apoptotic cells get stained green and contain bright green granular nuclei due to nuclear fragmentation and chromatin condensation along with blebbing of cell membrane characteristics of cells undergoing apoptosis [24,54].

As shown in figure 6, MCF-10A cells which are normal breast epithelial cells showed typical epithelial morphology with uniform green fluorescence and intact nuclei in control untreated cells. Dose-dependent activity was observed for all the systems, including the positive control MTX drug. Owing to its lower  $\text{IC}_{50}$  value and high toxicity, bare ZnONPs showed increased signs of damage. Even at lower concentrations, cells lost morphology and detached due to which rounding of cells was strikingly visible. While at higher concentrations, signs of apoptosis and necrosis are visible. In contrast at lower doses MTX–ZnONPs did not show damage to cells due to its higher  $\text{IC}_{50}$  value. At higher doses, however, we could see the visible signs of apoptosis like blebbing of the cell membrane and nuclear condensation, indicating cells undergoing apoptosis due to treatment.

Also, cells with orange-red fluorescence and intact nuclei indicate cell death by necrosis. Another striking observation was the increased size of cells and large nuclei in cells treated with MTX–ZnONPs and MTX as compared to control cells. Similar observations are found in figure 7, where MCF-7 cells also showed increased cell size with MTX–ZnONPs and MTX treatment. A possible explanation behind the increased cell size could be due to the fact that MTX is known to inhibit the cell cycle in the synthesis (S) phase by disrupting purine and pyrimidine synthesis. During the S phase of the cell cycle, DNA/RNA accumulates in the cell and hence cell size may increase [55,56]. Similar to MTT data, it was observed that MTX treatment group had the least signs of cell damage in MDA-MB-231 cells, as seen in figure 8. However, MTX–ZnONPs here also showed comparatively more cytotoxicity to cells than MTX-alone group, indicating its cytotoxic behaviour towards MDA-MB-231 cells. MTX–ZnONPs-treated cells showed relatively less confluency, condensed nuclei and cellular damage signs as seen by bright green granular nuclei indicating early apoptosis. At higher concentrations,





**Figure 9.** RBC haemolysis study performed with bare ZnONPs, MTX–ZnONPs and MTX at the concentration range of 6.25–100  $\mu\text{g ml}^{-1}$ . Graphical presentation of % haemolysis and visual presentation of the test.

cells showed loss of attachment and shrinkage with morphological changes indicating a cytotoxic effect of MTX–ZnONPs. Cells treated with MTX-positive control showed similar morphological cues. Bare ZnONPs-treated cells showed relatively high confluency similar to control cells and very little signs of damage which is rationalized considering the high  $\text{IC}_{50}$  value for MCF-7 cells, whereas this pattern was reversed in MDA-MB-231 cells. MTX also showed signs of damage and apoptosis-like blebbing of the membrane, condensation of nuclei, loss of cell morphology along with detachment of cells. Control cells in all three cell lines showed high confluency and characteristic cell morphology and green fluorescence, indicating a live cell population.

### 3.4 RBC haemolysis study

RBCs are the most abundant component of the blood and are very fragile in nature. Any biomolecules or NPs entering human blood will strongly interact with the RBCs, thus it becomes imperative to study the effect of these synthesized nanomaterials on the RBCs.

As seen in figure 9, no haemolytic activity was observed for any of the tested systems when compared to the control and % haemolysis was below 2%. As per ASTM F756-00, haemolysis under 5% is considered to be safe and hence all the systems tested seem safe and biocompatible in nature at the concentration used for the study [26]. ZnONPs are

known to be safe and biocompatible in nature previously in various studies [57,58].

## 4. Conclusion

Bare ZnONPs and MTX–ZnONPs were successfully synthesized via simple chemical precipitation method and *ex-situ* synthesis approach. Further characterization with UV–vis, FTIR and zeta potential confirmed the successful MTX coating onto the NP surface. It was found that the synthesized particles were highly crystalline in nature and were in the range of 30–40 nm in size, as confirmed by XRD and HR-TEM. Loading of MTX on the surface of ZnONPs was further studied using a drug release curve under different physiological conditions, which exhibited favourable release patterns under an acidic environment. The results of the MTT assay and AO/EB staining demonstrate that the MTX–ZnONPs are preferentially toxic to breast cancer cells in comparison to MCF-10A cells that are used as controls. Also, MTX–ZnONPs not only kill drug-sensitive MCF-7 cells but also show high cellular toxicity to drug-resistant MDA-MB-231 cells. Interestingly, it was noted that bare ZnONPs were more toxic to normal breast epithelial cells MCF-10A, which implies that loading of MTX on bare NPs has increased the biocompatibility and specificity of NPs to cancer cells. RBC haemolysis assay also supports the biocompatible nature of MTX–ZnONPs, showing no haemolysis. To conclude, we say that the

MTX–ZnONPs synthesized in this study demonstrated lower IC<sub>50</sub> values, improved specificity and higher toxicity towards breast cancer cells, including drug-resistant MDA-MB-231 cells and high biocompatibility towards human RBCs. These findings indicate that the synthesized nanosystem could serve as an excellent anticancer agent for further research.

## Acknowledgements

We would like to acknowledge the Department of MEMS, IIT Bombay, for XRD analysis and SAIF, IIT Bombay, for ICP-AES, SEM-EDS and HR-TEM facilities. We also acknowledge Khandelwal Laboratories Pvt. Ltd, Mumbai, India, for providing an MTX gift sample. We would also like to thank Dr Padma V Devarajan and Dr K C Barick for their insightful suggestions in the research work.

## References

- [1] Gao X, Li X and Yu W 2005 *J. Phys. Chem. B* **109** 1155
- [2] Ravichandrika K and Kiranmayirvssnr P 2012 *Adv. Mater. Res.* **585** 154
- [3] Chang Y N, Zhang M, Xia L, Zhang J and Xing G 2012 *Materials* **5** 2850
- [4] Kim K M, Kim T H, Kim H M, Kim H J, Gwak G H, Paek S M *et al* 2012 *Toxicol. Environ. Health Sci.* **4** 121
- [5] Zhang Y, Nayak T, Hong H and Cai W 2013 *Curr. Mol. Med.* **13** 1633
- [6] Shobhaa N, Nandab N and Nagabhushana B M 2017 *Mapana J. Sci.* **16** 41
- [7] Hanley C, Layne J, Punnoose A, Reddy K, Coombs I, Coombs A *et al* 2008 *Nanotechnology* **19** 1
- [8] Puvvada N, Rajput S, Kumar B N, Sarkar S, Konar S, Brunt K R *et al* 2015 *Sci. Rep.* **5** 1
- [9] Premanathan M, Karthikeyan K, Jeyasubramanian K and Manivannan G 2011 *Nanomedicine* **7** 184
- [10] Nithya A and Jothivenkatachalam K 2015 *J. Mater. Sci. Mater. Electron.* **26** 10207
- [11] Wu H and Zhang J 2018 *Saudi Pharm. J.* **26** 205
- [12] Dragojevic S, Ryu J S and Raucher D 2015 *Molecules* **20** 21750
- [13] Chieng B W and Loo Y Y 2012 *Mater. Lett.* **73** 78
- [14] Nosrati H, Salehiabar M, Davaran S, Danafar H and Manjili H K 2017 *Drug Dev. Ind. Pharm.* **44** 886
- [15] Johari-Ahar M, Barar J, Alizadeh A M, Davaran S, Omid Y and Rashidi M R 2016 *J. Drug Target.* **24** 120
- [16] Alavi A S and Meshkini A 2018 *Eur. J. Pharm. Sci.* **115** 144
- [17] De Oliveira C P, Büttenbender S L, Prado W A, Beckenkamp A, Asbahr A C, Buffon A *et al* 2018 *Nanomaterials* **8** 24
- [18] Garg N K, Singh B, Jain A, Nirbhavane P, Sharma R, Tyagi R K *et al* 2016 *Colloids Surf. B Biointerfaces* **146** 114
- [19] Wong P T and Choi S K 2015 *Int. J. Mol. Sci.* **16** 1772
- [20] Majoros I J, Williams C R, Becker A and Baker J R 2009 *Wiley Interdiscip. Rev. Nanomed. Nanobiotechnol.* **1** 502
- [21] Rahman M, Khan J A, Kanwal U, Awan U A and Raza A 2021 *J. Nanopart. Res.* **23** 195
- [22] Agabeigi R, Rasta S H, Rahmati-Yamchi M, Salehi R and Alizadeh E 2020 *Nanoscale Res. Lett.* **15** 1
- [23] Chen J, Huang L, Lai H, Lu C, Fang M, Zhang Q *et al* 2014 *Mol. Pharm.* **11** 2213
- [24] Jadhav V, Ray P, Sachdeva G and Bhatt P 2016 *Life Sci.* **148** 41
- [25] Shinde V and Desai K 2022 *J. Biomed. Mater. Res. B Appl. Biomater.* **110** 1400
- [26] Hoonjan M, Sachdeva G, Chandra S, Kharkar P S, Sahu N and Bhatt P 2018 *Nanoscale* **10** 8031
- [27] Raoufi D 2013 *Renew. Energy* **50** 932
- [28] Singh S, Singh B, Sharma P, Mittal A, Kumar S, Saini G S *et al* 2017 *Mater. Des.* **134** 10
- [29] Buchheit R, Acosta-Humanez F and Almanzaby O 2016 *Rev. Cubana Fisica* **33** 4
- [30] Wu Q, Chen X, Zhang P, Han Y, Chen X, Yan Y *et al* 2008 *Cryst. Growth Des.* **8** 3010
- [31] Bhatkalkar S G, Kumar D, Ali A and Sachar S 2018 *J. Mol. Liq.* **268** 1
- [32] Sanmugam A, Vikraman D, Park H and Kim H-S 2017 *Nanomaterials* **7** 363
- [33] Akhtar M J, Ahamed M, Kumar S, Khan M M, Ahmad J and Alrokayan S A 2012 *Int. J. Nanomed.* **7** 845
- [34] Malaikozhundan B, Vaseeharan B, Vijayakumar S, Pandiselvi K, Kalanjiam M A, Murugan K *et al* 2017 *Microb. Pathog.* **104** 268
- [35] Yu J, Baek M, Chung H E and Choi S J 2011 *J. Phys. Conf. Ser.* **304** 012044
- [36] Albanese A, Tang P S and Chan W C W 2012 *Annu. Rev. Biomed. Eng.* **14** 1
- [37] Sandmann A, Kompch A, Mackert V, Liebscher C H and Winterer M 2015 *Langmuir* **31** 5701
- [38] Lanje A S, Sharma S J, Ningthoujam R S, Ahn J S and Pode R B 2013 *Adv. Powder Technol.* **24** 331
- [39] AbdElhady M M 2012 *Int. J. Carbohydr. Chem.* **2012** 6
- [40] Kumari S D C, Tharani C B, Narayanan N and Kumar C S 2013 *Indian J. Res. Pharm. Biotechnol.* **1** 915
- [41] Xie X, Liao J, Shao X, Li Q and Lin Y 2017 *Sci. Rep.* **7** 3827
- [42] Ahamed A J and Vijaya Kumar P 2016 *J. Chem. Pharm. Res.* **8** 624
- [43] Boruah S, Mustafiza S, Saikia D, Saikia H J, Saikia P P and Baruah M K 2016 *Am. Chem. Sci. J.* **11** 1
- [44] Sreevalsa V G, Jeeju P P, Augustine M S, Anilkumar K M and Jayalekshmi S 2013 *J. Exp. Nanosci.* **8** 937
- [45] Liu J, Park J, Park K H, Ahn Y, Park J Y, Koh K H *et al* 2010 *Nanotechnology* **21** 485
- [46] Liu J, Ma X, Jin S, Xue X, Zhang C, Wei T *et al* 2016 *Mol. Pharm.* **13** 1723
- [47] Xiong H M 2013 *Adv. Mater.* **25** 5329
- [48] Rasmussen J W, Martinez E, Louka P and Wingett D G 2010 *Expert Opin. Drug Deliv.* **7** 1063
- [49] Bryan J 2012 *Pharm. J.* **289** 303
- [50] Hess J A and Khasawneh M K 2015 *BBA Clin.* **3** 152
- [51] Bath R K, Brar N K, Forouhar F A and Wu G Y 2014 *J. Dig. Dis.* **15** 517
- [52] Worm J, Kirkin A F, Dzhandzhugazyan K N and Guldborg P 2001 *J. Biol. Chem.* **276** 39990
- [53] Corona G, Giannini F, Fabris M, Toffoli G and Boiocchi M 1998 *Int. J. Cancer* **75** 125
- [54] Liu K, Liu P, Liu R and Wu X 2015 *Med. Sci. Monit. Basic Res.* **21** 15

- [55] Taylor I W and Tattersall M H 1981 *Cancer Res.* **41** 1549
- [56] Grönroos M, Chen M, Jahnukainen T, Capitanio A, Aizman R I and Celsi G 2006 *Pediatr. Blood Cancer* **46** 624
- [57] El-Waseif A 2019 *J. Arab. Soc. Med. Res.* **14** 42
- [58] PreediaBabu E, Subastri A, Suyavaran A, Premkumar K, Sujatha V and Aristatile B 2017 *Sci. Rep.* **7** 1

# Ameliorated *in vitro* anti-cancer efficacy of methotrexate loaded zinc oxide nanoparticles in breast cancer cell lines MCF-7 & MDA-MB-231 and its acute toxicity study

Mitesh Joshi  and Purvi Bhatt\* 

Department of Biological Sciences, SVKM's NMIMS (Deemed-to-be University), Sunandan Divatia School of Science, Vile Parle (West), Mumbai 400056, India

E-mail: [purvi.bhatt@nmims.edu](mailto:purvi.bhatt@nmims.edu) and [joshimitesh777@gmail.com](mailto:joshimitesh777@gmail.com)

Received 6 February 2024, revised 27 April 2024

Accepted for publication 14 May 2024

Published 28 May 2024



## Abstract

Traditional therapies often struggle with specificity and resistance in case of cancer treatments. It is therefore important to investigate new approaches for cancer treatment based on nanotechnology. Zinc oxide nanoparticles (ZnONPs) are known to exhibit anti-cancer properties by inducing oxidative stress, apoptosis, and cell cycle arrest. Methotrexate (MTX) a known anti-folate shows specificity to folate receptors and interrupts healthy functioning of cells. This study proposes the use of previously characterized biocompatible Methotrexate loaded Zinc oxide nanoparticles (MTX-ZnONPs) as a dual action therapeutic strategy against breast cancer cell lines, MCF-7 (MTX-sensitive) and MDA-MB-231 (MTX-resistant). To elucidate the cytotoxicity mechanism of MTX-ZnONPs an in depth *In vitro* study was carried out. *In vitro* assays, including cell cycle analysis, apoptosis assay, and western blot analysis to study the protein expression were performed. Results of these assays, further supported the anti-cancer activity of MTX-ZnONPs showing apoptotic and necrotic activity in MCF-7 and MDA-MB-231 cell line respectively. *In vivo* acute oral toxicity study to identify the LD<sub>50</sub> in animals revealed no signs of toxicity and mortality up to 550 mg kg<sup>-1</sup> body weight of animal, significantly higher LD<sub>50</sub> values than anticipated therapeutic levels and safety of the synthesized nanosystem. The study concludes that MTX-ZnONPs exhibit anti-cancer potential against breast cancer cells offering a promising strategy for overcoming resistance.

Keywords: MDA-MB-231, MCF-7, Methotrexate, Bax, Bcl-xL, Zinc oxide nanoparticles, Breast cancer

## 1. Introduction

Breast cancer is one of the most prevalent and fatal top-ranking cancers globally [1, 2]. Chemotherapy be the most classical approach to treat various cancers including breast cancer. The

drawbacks of current breast cancer treatments include toxicity, resistance, and adverse effects [3]. As a result, there is a need for new novel ideas and effective approaches to address these issues. Nanotechnology based treatment strategies are the forthcoming solutions to cancer therapies. Nanotechnology based treatment strategies are the forthcoming solutions to cancer therapies. Nanotechnology is considered a multidisciplinary science that aids in solving current problems, and where

\* Author to whom any correspondence should be addressed.

its function is to manufacture nanoscale materials and specifically, nanoparticles (NPs) exhibit completely new or improved properties based on characteristics such as size, distribution, and morphology. These can be obtained from raw materials of natural origin such as proteins and polysaccharides or from inorganic precursors such as metals and salts. The use of NPs as drug delivery vehicles is one such promising strategy [4–6]. NPs have the potential to lower the toxicity and adverse effects of anticancer medications while increasing their solubility, stability, bioavailability, and selectivity [7]. Among the many different kinds of NPs, zinc oxide nanoparticles (ZnONPs), have drawn attention because of their biocompatibility, biodegradability, affordability, and ease of synthesis. ZnONPs are nanomaterials that have proven anticancer effects by causing oxidative stress, apoptosis, and cell cycle arrest in number of cancer cell lines [8, 9].

Methotrexate (MTX) is a widely used anticancer drug that inhibits the enzyme dihydrofolate reductase (DHFR), which is vital for DNA synthesis and cell proliferation. Since MTX is an analogue of folic acid, it is internalized through the folate receptors which are known to overexpress on the surface of breast cancer cells [10]. Moreover, MTX has disadvantages such as poor solubility, low bioavailability, and resistance [11, 12]. On the other hand, cancer cells may become resistant to MTX through a number of processes, including elevated DHFR expression, decreased drug uptake, or changed drug metabolism [13]. Triple negative breast cancer (TNBC) is a subtype of breast cancer that lacks the expression of estrogen receptor (ER), progesterone receptor (PR), and human epidermal growth factor receptor-2 (HER-2). TNBC is linked to poor prognosis and significant risk of metastasis [14]. MDA-MB-231 is a commonly used TNBC cell line that displays mesenchymal features and high invasiveness with known inherited resistance to MTX [15]. MCF-7 is a human mammary tumor derived cell line first established in 1970, that is hormone-responsive cell line with adherent and epithelial luminal characteristics [16].

Using dual action therapy approach, MTX-ZnONPs aims to combine the established anti-cancer drug MTX with the inherent anti-cancer properties of ZnONPs, to potentially enhance the efficacy while reducing side effects. In our previous study we synthesized bare ZnONPs by coprecipitation method and MTX-ZnONPs using an ex-situ approach for loading of MTX on NPs surface. The synthesized MTX-ZnONPs were highly crystalline in nature and were in the range of 30–40 nm in size. The successful coating of MTX onto the NP surface was confirmed by UV-vis, FTIR, zeta potential and other characterizations. The drug release study of MTX-ZnONPs under different physiological conditions exhibited favorable release patterns under an acidic environment. The synthesized NP systems were found to be safe and biocompatible in nature at the concentration used for the study. Further their efficacy and anticancer potential was confirmed by MTT cytotoxicity assay on breast cancer cell lines MCF-7 (MTX-sensitive cell line) and MDA-MB-231 (MTX-resistant cell line) using MCF-10A as control cells. Blood biocompatibility study also confirmed safe and biocompatible nature of MTX-ZnONPs to human blood [17].

To delve deeper into the anti-cancer properties of MTX-ZnONPs, a series of *in vitro* tests, including cell cycle analysis, apoptosis assay, and western blot analysis, were conducted. Additionally, the safety of the synthesized nanosystem was evaluated in animals using an acute oral toxicity study to determine its lethal dose 50 (LD<sub>50</sub>). This comprehensive investigation aimed to assess the therapeutic potential of MTX-ZnONPs against breast cancer cell lines, specifically the MTX-sensitive MCF-7 and the MTX-resistant MDA-MB-231 cell lines, while also elucidating the underlying mechanisms of action. Our hypothesis is focused on the potential of MTX-ZnONPs to increase the responsiveness of breast cancer cells to therapy, thereby demonstrating their effectiveness as an anti-cancer treatment.

## 2. Materials and methods

### 2.1. Chemicals

All chemicals were molecular biology grade and used as received. MTX was kindly provided as gift sample from Khandelwal Laboratories Pvt. Ltd, Mumbai, India. Bovine serum albumin was purchased from SRL Pvt. Ltd, India. Propidium iodide (PI) was purchased from Sigma-Aldrich, USA. RNase A was purchased from Invitrogen™, ThermoFisher Scientific, USA.

### 2.2. Cell culture

Human breast cancer cell line MCF-7 was procured from NCCS, Pune and TNBC cell line MDA-MB-231 was purchased from ATCC and cultured in Dulbecco's Modified Eagle's Medium accompanied with 10% heat inactivated fetal bovine serum (Gibco™, ThermoFisher scientific, USA) and antibiotic antimycotic solution (Sigma-Aldrich, USA). MCF-7 and MDA-MB-231 cells were maintained under humidified conditions at 37 °C, 5% CO<sub>2</sub> and trypsinized using 0.25% trypsin-EDTA (Gibco™, ThermoFisher scientific, USA) after attaining 80%–90% confluency.

**2.2.1. Experimental design.** For all further assay, cells were treated with bare ZnONPs, MTX-ZnONPs and MTX at respective concentrations based on the IC<sub>50</sub> value obtained from MTT cytotoxicity assay previously done. For MCF-7 cells concentrations used were 2.5, 5 and 7.5 µg ml<sup>-1</sup> and for MDA-MB-231 40, 50 and 60 µg ml<sup>-1</sup>, respectively. Three independent replicates were performed and analyzed for all assays.

### 2.3. Cell cycle analysis

Cells were seeded at a density of 10<sup>5</sup> cells per well in 6 well flat bottom plates and incubated overnight for attachment. Next day, cells were treated with bare ZnONPs, MTX-ZnONPs and MTX and control cells were left untreated with only media for 24 h incubation. For analysis, cells were washed twice with phosphate buffered saline (PBS) to get rid of any media traces

followed by trypsinization to harvest the cells. Cell pellets were then collected by centrifugation at 1200 rpm for 5 min and two washes of PBS were given to remove media traces. Chilled 70% Ethanol in PBS was used a fixative to fix the cells, wherein 1 ml of chilled 70% ethanol was added dropwise to the pellet with constant vortexing after which the cells were stored at  $-20^{\circ}\text{C}$ . Cells were then centrifuged at  $4^{\circ}\text{C}$  and the pellet was resuspended in  $500\ \mu\text{l}$  of chilled PBS containing PI ( $20\ \mu\text{g ml}^{-1}$ ) and RNase A ( $10\ \mu\text{g ml}^{-1}$ ). After incubating in dark for 30 min samples were analyzed using [BD (Becton, Dickson and Company) FACS Aria Special Order System, BD Biosciences, USA] flow cytometer and minimum of 10 000 events were recorded for data collection.

#### 2.4. Apoptosis assay

Apoptosis assay was performed using fluorescein isothiocyanate (FITC) Annexin V Apoptosis detection kit (BD pharmingen™) and protocol was followed as per manufacturers guidelines with some modification [18]. Briefly, cells were grown in 6 well plates with cell density of  $10^5$  cells per well and treated next day with bare ZnONPs, MTX-ZnONPs and MTX for 24 h followed by harvesting, washing and centrifugation (1200 rpm for 10 min) to obtain the cell pellets. These cell pellets were resuspended in  $100\ \mu\text{l}$  of 1X chilled binding buffer. The cells were then stained with Annexin V-FITC and PI and incubated in dark for 10 min followed by addition of  $400\ \mu\text{l}$  of 1X chilled binding buffer. Samples were immediately analyzed with [BD (Becton, Dickson and Company) FACS Aria Special Order System, BD Biosciences, USA] flow cytometer and minimum of 10 000 events were recorded for data collection. For positive control, cells were incubated at  $55^{\circ}\text{C}$  for 20 min and later stained with only Annexin V-FITC and only PI. Untreated cells served as unstained control.

#### 2.5. Western blot analysis

For western blot analysis cells were first treated with bare ZnONPs, MTX-ZnONPs and MTX for 24 h. Protein extraction and Western blot procedure was followed as reported elsewhere with minor modifications [19]. Briefly cell pellets were resuspended in chilled cell lysis buffer containing 1X protease inhibitor cocktail (Sigma Aldrich, USA) for 30 min on ice with intermittent vortexing followed by centrifugation at 13 000 g for 20 min at  $4^{\circ}\text{C}$ . Supernatant was collected and total protein concentration was estimated by Bradford assay. For separation of proteins 12% SDS-PAGE gel was prepared and 20–30  $\mu\text{g}$  of total protein was loaded per well. For protein transfer, polyvinylidene fluoride membrane (Bio-Rad, USA) was used, followed by blocking using blocking buffer (5% non-fat dry milk (NFDM) + 0.1% Tween 20 in 1X Tris-buffered saline (TBST) for 1.5 h at room temperature (RT). Proteins were later probed with primary antibodies: anti-Caspase-3 rabbit mAb, anti-Caspase-7 rabbit mAb, anti-Bcl-xL rabbit mAb, anti-Bax rabbit pAb (Cell Signaling Technologies, USA) and  $\beta$ -Actin mouse mAb (Sigma, USA) was used as housekeeping control.

Post overnight incubation at  $4^{\circ}\text{C}$  with primary antibody. Blots were washed three times with TBST for 10 min to remove unbound antibodies and incubated with respective goat anti-mouse and goat anti-rabbit HRP linked secondary antibody (GeNei™, India) for 1 h at RT. Again, three washes with TBST for 10 min were given to blots to remove any unbound secondary antibodies. Blots were later developed using Clarity (Bio-Rad, USA) reagent and imaged using ChemiDoc XRS+ Gel Imaging System (Bio-Rad, USA) and results were analyzed using ImageJ software.

#### 2.6. Animal experimentation & housing

Female *Swiss albino mice* (18–20 g) were procured from the National Institute of Biosciences, Pune, Maharashtra, India and housed in the SVKM's animal facility. Temperature of  $22^{\circ}\text{C} \pm 2^{\circ}\text{C}$ , relative humidity  $75\% \pm 5\%$ , and a 12 h light/dark cycle was maintained in an animal facility throughout the study. Animals received a basal multi-nutritional diet and purified water, *ad libitum*. The experimental protocol (CPCSEA/P-69/2022) was approved by the Institutional Animal Ethics Committee.

#### 2.7. Statistical analysis

All results were expressed as mean  $\pm$  standard deviation from three independent experiments carried out in triplicate. Statistical analysis for differences in means was performed using two-way analysis of variance (ANOVA) and 1-way ANOVA for respective set of experiments by the GraphPad Prism software (version 5.0). The p value ( $<0.05$ ) was considered statistically significant. All graphs were prepared using GraphPad Prism software (version 5.0). Image J software was used to get the area under the curve for western blot analysis.

**2.7.1. Acute oral toxicity experimental design.** Acute oral toxicity study of MTX-ZnONPs was performed as per OECD guideline (TG 425) [20]. Following a one-week acclimation period, female Swiss albino mice (18–20 g) were randomly assigned to four groups of three animals each ( $n = 3$ ). Group 1 being control group received 0.5% CMC equivalent to dose volume, group 2, 3 and 4 received MTX-ZnONPs at dose  $55\ \text{mg kg}^{-1}$ ,  $175\ \text{mg kg}^{-1}$  and  $550\ \text{mg kg}^{-1}$  *p.o.*, respectively. Animals were monitored carefully after oral dosing for any signs of change in their behavioral and physiological appearance during the first 30 min and then periodically during the first 24 h with special attention on the first 4 h. All the groups were kept under observation for 14 d.

Various observations related to the physical appearance like change in body weight, skin and fur, eyes, lacrimal secretion, autonomic, somatomotor, behavioral pattern and respiratory abnormalities were observed. Animals were also observed for tremors, convulsions, salivation, diarrhea, lethargy, sleep and coma.



### 3. Results and discussion

#### 3.1. Cell cycle analysis

For cell cycle analysis, cells were stained with PI and analyzed using flow cytometer. PI is a cell impermeable nucleic acid dye, which binds to the DNA of the cell stoichiometrically thus giving fluorescence signal, which is proportional to cellular DNA content. Using flow cytometer different percentages of cells in different phases of the cell cycle (G0/G1, S, and G2/M) were determined to study the effect of NPs treatment on cell cycle progression [16, 21]. Flow cytometry was used to study the cell cycle progression of breast cancer cells post treatment with NPs using PI staining.

As seen in figures 1 and 2, control cell population in both the cell lines MCF-7 and MDA-MB-231 indicated standard cell cycle progression, where majority of cell population was seen in G0/G1 phase indicating cells undergoing active cell division. A similar observation was made in the bare ZnONP treated group, which did not show any significant differences compared to the untreated group. In case of MCF-7 cell line, MTX-ZnONP treated group depicted significant arrest in S phase amongst all treatment groups, in concentration dependent manner in comparison to untreated cells. Likewise, MTX treated group demonstrated similar activity to MTX-ZnONPs i.e. arresting cells in S and G2/M phase of cell cycle and preventing from entering into G0/G1 phase. Cell cycle specific activity of MTX-ZnONPs to S phase can be attributed to presence of MTX, which has direct effect on nucleic acid synthesis thereby preventing cells from going into next phase [21]. However, MTX treatment in MDA-MB-231 cells evidently arrested cells in G0/G1 phase, contrary to S phase of cell cycle [22]. MDA-MB-231 cells being resistant to MTX did not show any dose dependent effect. Whereas MTX-ZnONPs being a combination showed dose dependent activity with significant shift of population to S phase compared to untreated cells and MTX alone group. Of the three systems, MTX-ZnONPs had less than 60% population in G0/G1 phase compared to others treatment groups. Also, significant amount of population was observed in Sub G1 phase signifying dose dependent cell toxicity indicating apoptotic population in bare ZnONP and MTX-ZnONPs treated groups. Overall results indicated that MTX-ZnONPs system showed cell cycle specific arrest in S phase of the cell cycle in MCF-7 and MDA-MB-231.

It was understood that MTX-ZnONPs preferentially halt the cell cycle progression at S phase in MCF-7 and MDA-MB-231. Even though MTX alone at same concentration had no effect on MDA-MB-231 cells, MTX-ZnONPs treatment at the same concentration did affect MDA-MB-231 cells, implying that the combination has a cytotoxic role in resistant cell lines. The reason behind S phase inhibition was specifically due to MTX presence. Once inside the cancer cell, MTX-ZnONPs dissolve under acidic conditions, releasing  $Zn^{2+}$  ions and MTX. MTX polyglutamates and gets converted to its active form, stalling purine and pyrimidine synthesis, leading to arrest in cell cycle at synthesis phase. The mechanism of action for ZnONPs is unknown, but it is believed to involve the release of  $Zn^{2+}$  ions under an acidic environment,

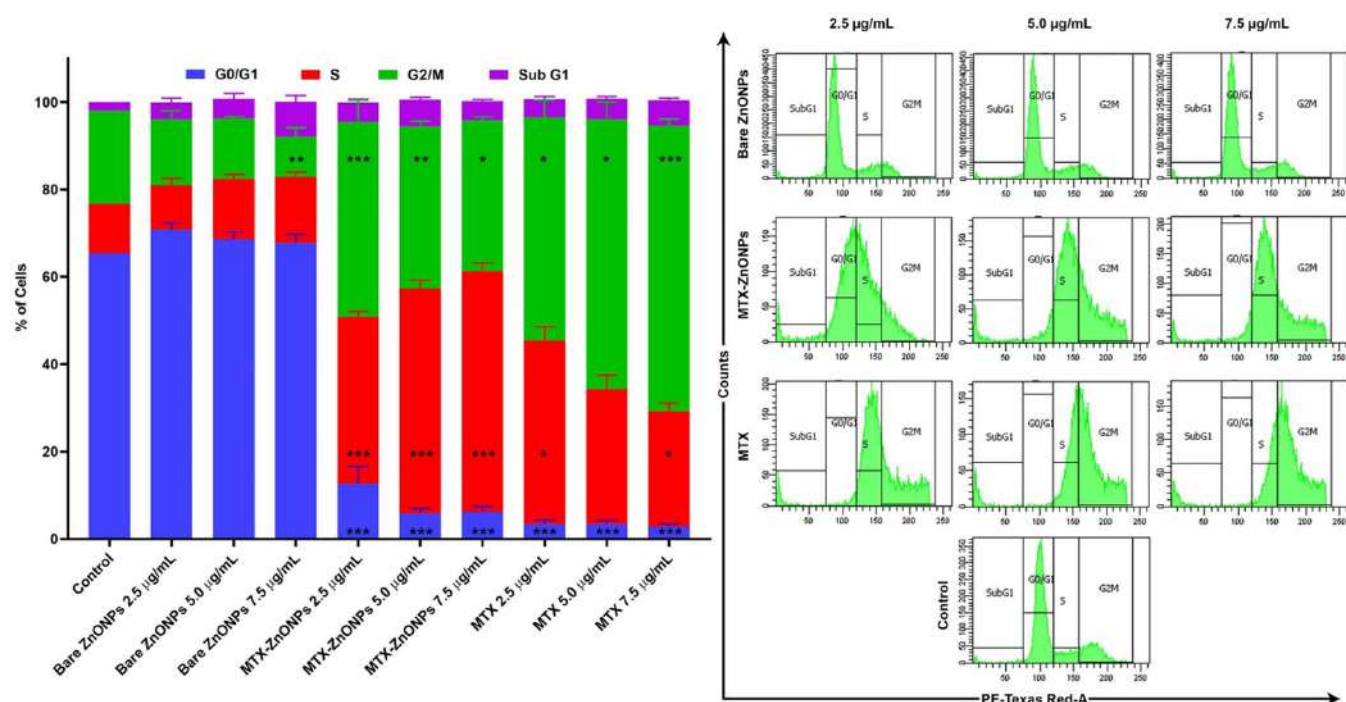
causing oxidative stress and causing cellular damage [23, 24]. In one such similar study ZnONPs were used at low dose against bladder cancer cell line T24. It was observed that low dose ZnONPs treatment led to S phase arrest in cells leading to apoptosis and suppressed the cell migration and invasion. Although, the mechanism is unclear but, it is suspected that the role of  $Zn^{2+}$  ions and ZnONPs could have contributed together and were responsible for its anti-cancer activity [25].

#### 3.2. Apoptosis assay

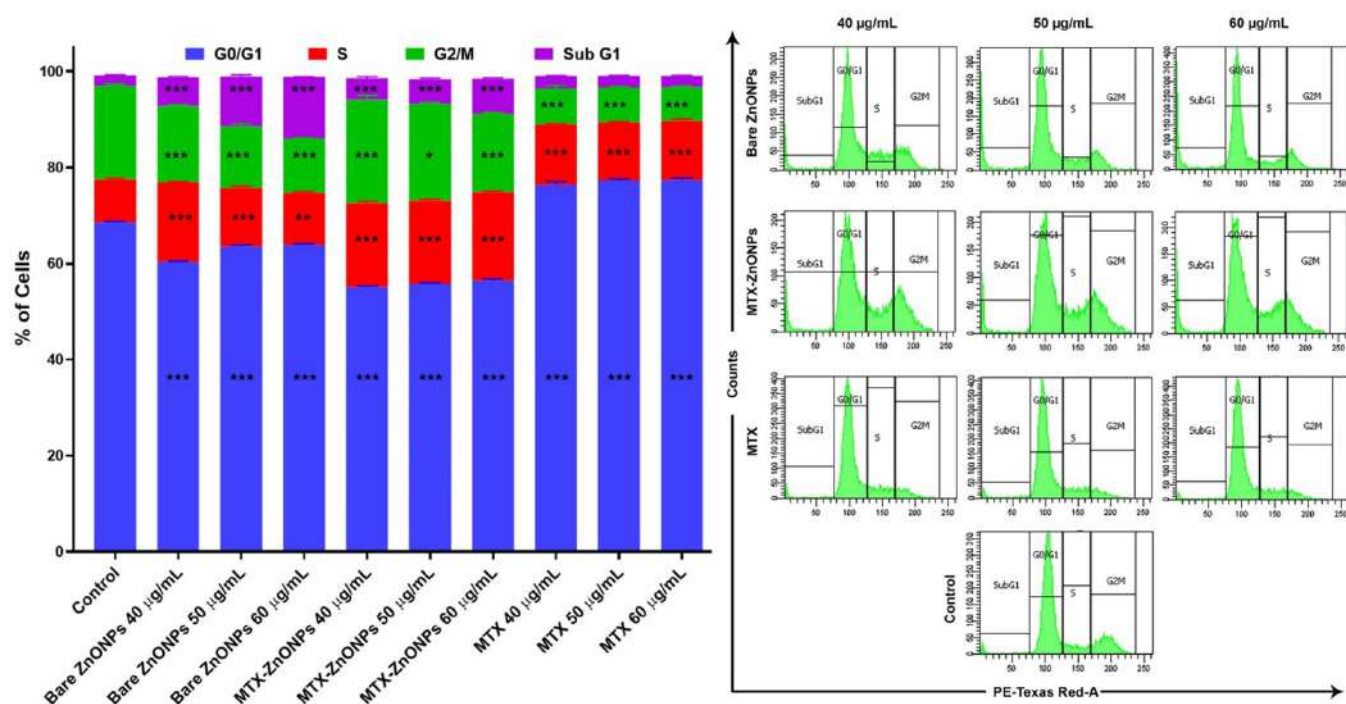
Apoptosis assay was performed using Annexin V-FITC/ PI staining as per manufacturers protocol. This method is based on the principle that, when cell undergoes apoptosis phosphatidylserine (PS) which is usually located towards inner sides of plasma membrane gets exposed to outer side of plasma membrane. Annexin V is a protein which has high affinity towards PS in presence of calcium ions, which is labeled with FITC, a fluorescent dye. Thus, makes it easier to positively stain cells with exposed PS on its surface. PI is a nuclear stain that stains DNA of the cells whose membrane integrity has been compromised, such as late apoptotic or necrotic cells. Three different types of populations can be distinguished based on this principle like, viable cells (Annexin V-FITC -negative and PI-negative), early apoptotic cells (Annexin V-FITC -positive and PI-negative), and late apoptotic or necrotic cells (Annexin V-FITC -positive and PI-positive) by using Annexin V-FITC and PI staining together [26, 27].

Results of apoptosis assay in figures 3 and 4, depicts highest percentage of live population in untreated cells of both the cell lines. MCF-7 cells being sensitive to MTX exhibited dose dependent toxicity, transitioning cells from early apoptosis to late apoptosis. Similarly, MTX-ZnONP treated group observed significantly higher percentage of cells undergoing apoptosis when compared with all other groups. On the other hand, bare ZnONPs treatment did not induce any significant toxicity to MCF-7 cells and exhibited live cell population comparable to that of untreated cells. In case of MTX resistant cell line MDA-MB-231, it was observed that MTX at different concentrations did not induce any sort of toxicity to cells, confirming the resistant behavior of the cell line. Bare ZnONP treated group owing to its lower IC50 values demonstrated increased cell death in comparison to other treatment groups. Both bare ZnONPs and MTX-ZnONPs treated cells led to cytotoxicity in MDA-MB-231 cells and majority of the population were identified as necrotic and late apoptotic. Interestingly, MTX-ZnONP treated group accounted for considerably higher fraction of dead population compared to MTX at the same concentrations, indicating its cytotoxic nature against MTX resistant cell line. All above results indicated capability of MTX-ZnONPs to induce toxicity in both the breast cancer cell lines irrespective of their sensitivity to drug via apoptotic or necrotic pathway.

When ZnONPs were used against cisplatin (DDP) resistant ovarian cancer cell line SKOV3/DDP it was observed that cell viability was dramatically reduced in SKOV3/DDP cells compared to DDP alone at same concentrations. It was con-



**Figure 1.** Cell cycle analysis by PI staining for MCF-7 cells treated with bare ZnONPs, MTX-ZnONPs and MTX for 24 h. Data is presented as bar graph (left) and histogram (right). Asterisk in the columns indicate statistically significant difference compared to control group (\* $p \leq 0.05$ ; \*\* $p \leq 0.01$ ; \*\*\* $p \leq 0.001$ ).

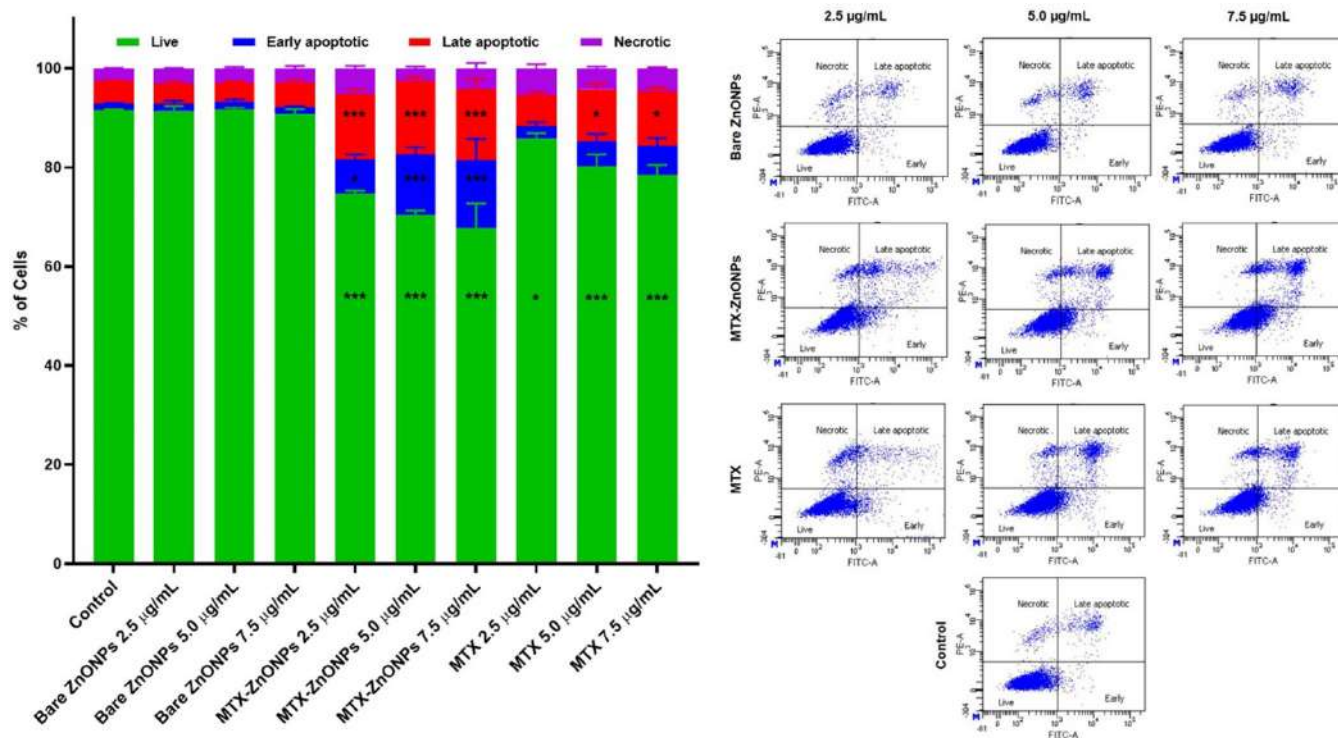


**Figure 2.** Cell cycle analysis by PI staining for MDA-MB-231 cells treated with bare ZnONPs, MTX-ZnONPs and MTX for 24 h. Data is presented as bar graph (left) and histogram (right). Asterisk in the columns indicate statistically significant difference compared to control group (\* $p \leq 0.05$ ; \*\* $p \leq 0.01$ ; \*\*\* $p \leq 0.001$ ).

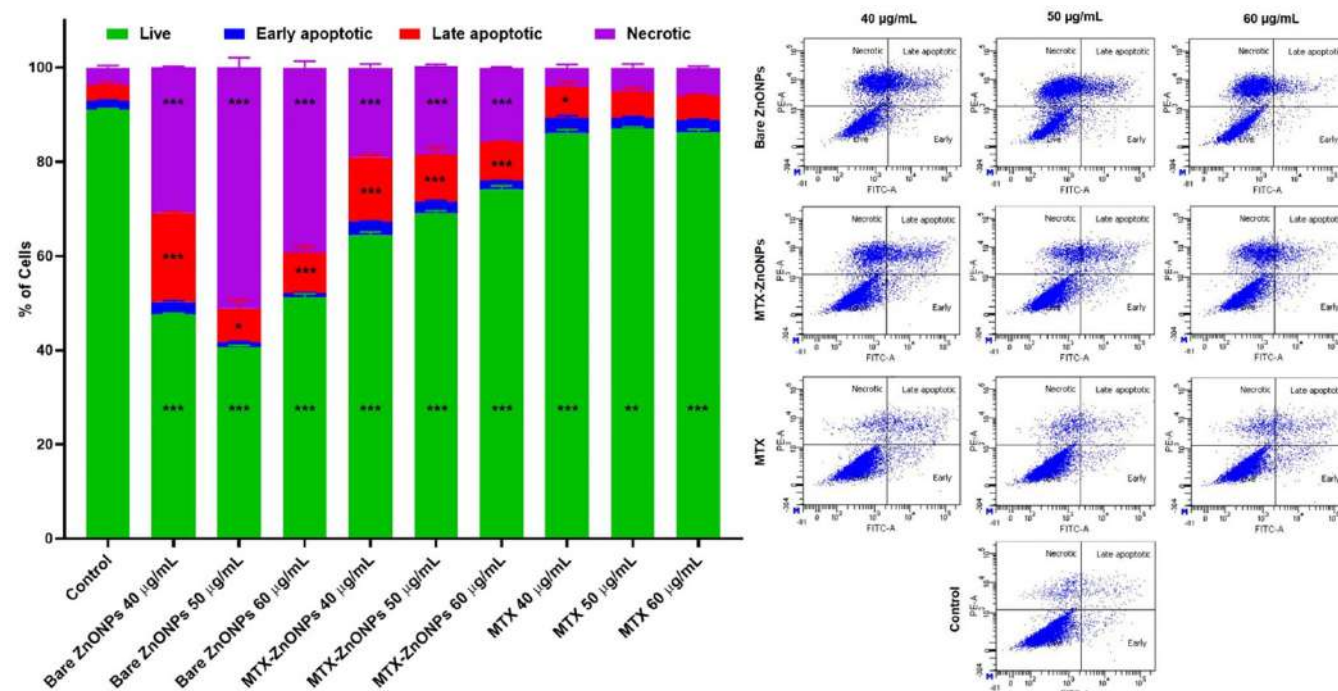
firmed through Annexin V/PI assay that the majority of the cells were undergoing apoptosis and showed higher sensitivity to ZnONPs indicating their anticancer potential against

drug-resistant cell line. They also confirmed that ZnONPs treatment induced p53 expression due to ROS and oxidative stress leading to apoptosis induction in cancer cells [28].





**Figure 3.** Apoptosis analysis by Annexin V-FITC/PI for MCF-7 cells treated with bare ZnONPs, MTX-ZnONPs and MTX for 24 h. Data is presented as bar graph (left) and scatter plot (right). Asterisk in the columns indicate statistically significant difference compared to control group (\* $p \leq 0.05$ ; \*\* $p \leq 0.01$ ; \*\*\* $p \leq 0.001$ ).

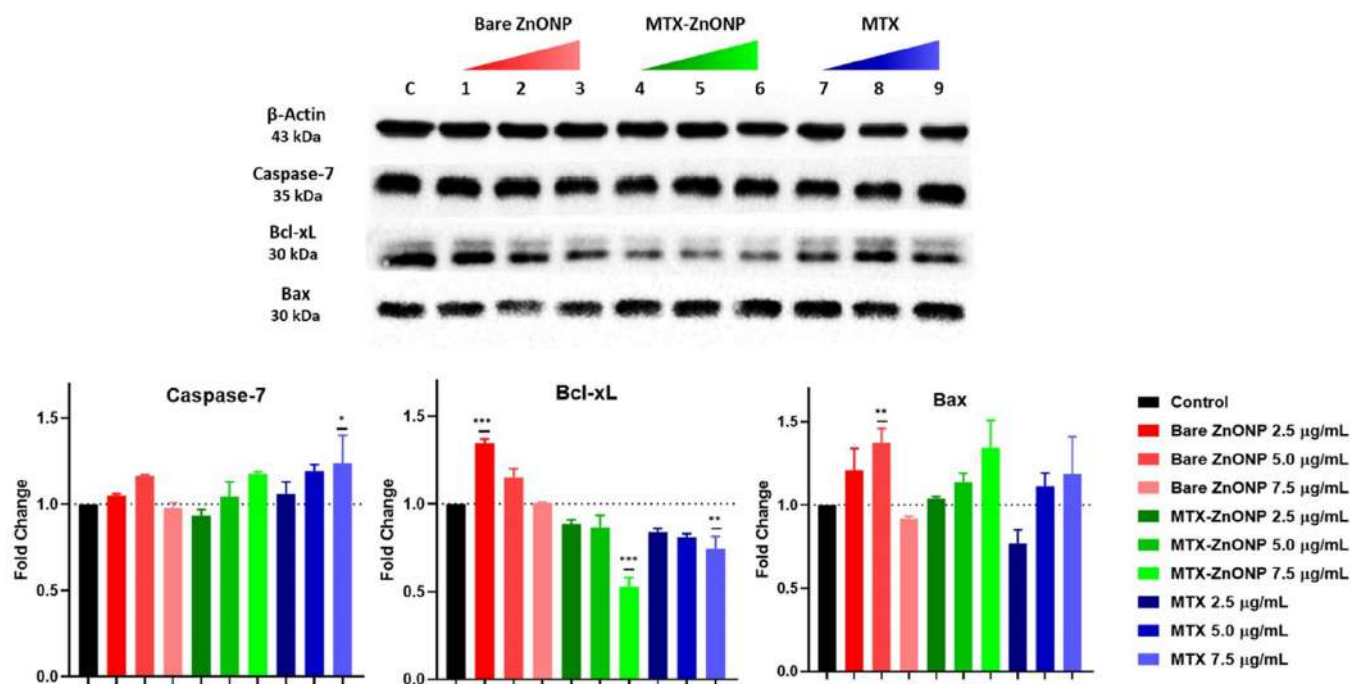


**Figure 4.** Apoptosis analysis by Annexin V-FITC/PI for MDA-MB-231 cells treated with bare ZnONPs, MTX-ZnONPs and MTX for 24 h. Data is presented as bar graph (left) and scatter plot (right). Asterisk in the columns indicate statistically significant difference compared to control group (\* $p \leq 0.05$ ; \*\* $p \leq 0.01$ ; \*\*\* $p \leq 0.001$ ).

### 3.3. Western blot analysis

Western blotting is a method to detect the specific membrane bound proteins with the help of primary and secondary

antibodies against specific protein epitope/s. Secondary antibodies are bound to an enzyme which upon converting the substrate gives out signal, which is detected over the period. In the current study, expression of proteins like Caspase 3/7, Bcl-xL



**Figure 5.** Western blot analysis for MCF-7 cells treated with bare ZnONPs, MTX-ZnONPs and MTX for 24 h. Asterisk in the columns indicate statistically significant difference compared to control group (\* $p \leq 0.05$ ; \*\* $p \leq 0.01$ ; \*\*\* $p \leq 0.001$ ).

and Bax were investigated post treatment with NPs in MCF-7 and MDA-MB-231 cells.  $\beta$ -actin was used as a housekeeping protein for loading control.

In MCF-7 breast cancer cell line (figure 5), it was observed that MTX-ZnONPs treatment led to upregulation of Caspase 3 in dose dependent manner along with Bax. Caspase-3 is a executor caspase that is activated at the last step to execute apoptosis [29]. Similarly, Bax which is a part of Bcl family, which functions as a pro-apoptotic protein whose upregulation can be associated with programmed cell death i.e. apoptosis [30]. However, Bcl-xL, also comes from the same family of Bcl has the same function as binding to Bax and preventing apoptosis, was observed to downregulate in a dose dependent manner. Downregulation of Bcl-xL which an anti-apoptotic protein and upregulation of Pro-apoptotic protein is a classical pattern observed in cells undergoing apoptotic death which is clearly seen here indicating apoptotic cell death in case of MCF-7 breast cancer cells [31].

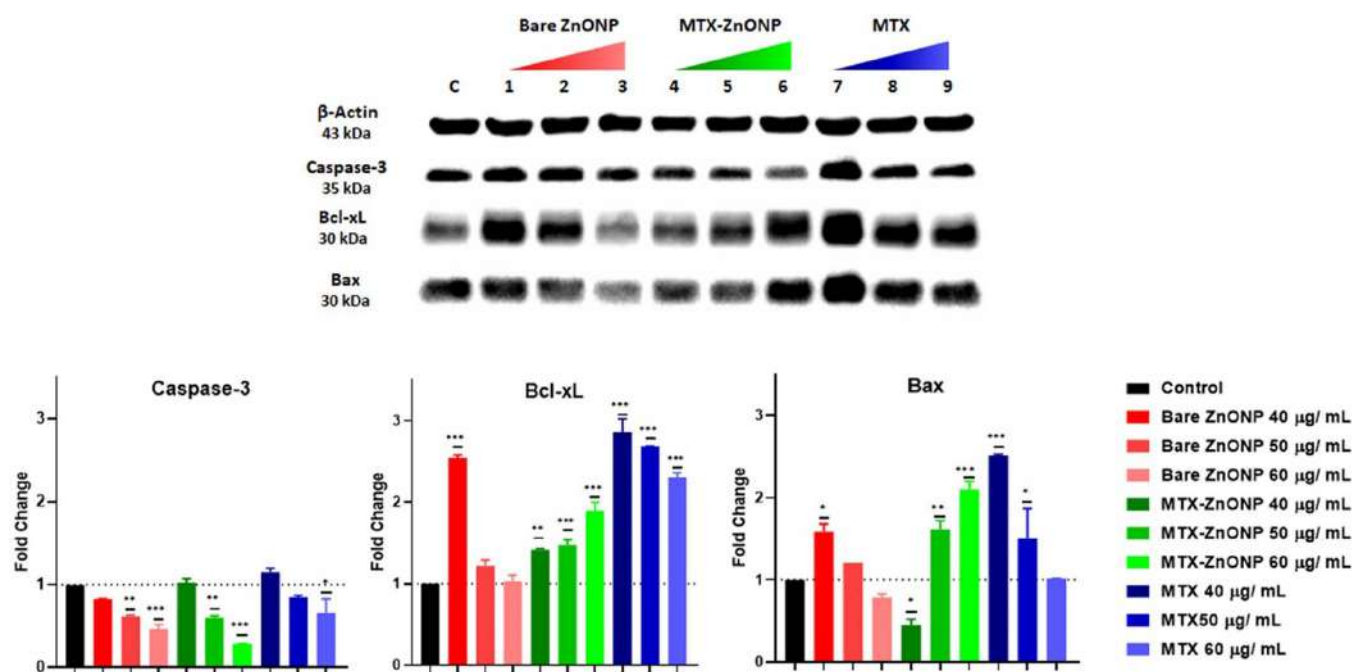
However, in case of MDA-MB-231 cell line as seen in figure 6, none of the treatment groups displayed Caspase-3 upregulation. On the other hand, Bcl-xL and Bax levels were significantly upregulated for MTX-ZnONP treatment group in dose dependent manner. Similarly, MTX treatment also depicted multifold upregulation of Bcl-xL levels upon treatment. Downregulated levels of executioner caspase and upregulation of Bcl-xL (pro-survival protein) highlights that cells are undergoing non-apoptotic cell death. Caspases are known to get upregulated and activated only under programmed cell death situation but, evidence indicates that Bax expression levels are also associated with necrotic cell death [32, 33]. Similarly, Bcl-xL upregulation in MDA-MB-231 cells with respect to MTX treatment could be associated with its drug resistance

as its observed that upregulated Bcl-xL prevents cells from undergoing apoptosis in response to chemotherapy, reducing the effectiveness of the treatment and allowing cells to survive and continue to grow.

It has been demonstrated that MTX induces apoptosis in a variety of experimental systems, such as Chinese hamster ovary cells, fibrosarcoma cells, and HL60 and Jurkat leukemic cells. The induction of p53 is linked to both growth arrest and apoptosis, especially in reaction to DNA damage or other forms of cellular stress that are frequently brought on by MTX [34]. Zinc nanorods (ZnONRs) of size range 100 nm, showed similar anticancer activity in MCF-7 breast cancer cells by increasing the expressions of Bax and reducing the levels of Bcl-xL leading to activation of apoptotic death [35]. There is limited evidence that also shows that upon ZnONPs treatment, it induces the MAPK pathways ultimately activating a cascade of events reaching to tumor necrosis factor- $\alpha$  (TNF- $\alpha$ ). TNF- $\alpha$  along with other cytokines have shown to get expressed upon NP induced inflammation [36, 37].

### 3.4. Acute oral toxicity study

During the 14 d observation period, a single dose of MTX-ZnONPs at 55 mg kg<sup>-1</sup>, 175 mg kg<sup>-1</sup> and 550 mg kg<sup>-1</sup>, did not induce any adverse effects in the animals. No mortality, morbidity, or physical abnormalities were observed. Eye, nose, ear, and fur appearance remained unchanged, and no behavioral alterations like tremors, coma, or morbidity were detected. All animals tolerated the treatment well, with no mortality, morbidity, or abnormal physical changes observed. (Supplementary-tables 1(a)–(c)) detail the findings on physical characteristics and behavior. Importantly, weight changes



**Figure 6.** Western blot analysis for MDA-MB-231 cells treated with bare ZnONPs, MTX-ZnONPs and MTX for 24 h. Asterisk in the columns indicate statistically significant difference compared to control group (\* $p \leq 0.05$ ; \*\* $p \leq 0.01$ ; \*\*\* $p \leq 0.001$ ).

were monitored (supplementary-table 2). While the control group gained weight as expected, the treated groups showed minimal to no weight gain. However, by day 14, all animals displayed proportional weight gain, suggesting healthy growth and no lasting impact of the treatment. This further supports the biocompatibility and safety of MTX-ZnONPs at tested doses in mice. Furthermore, the  $LD_{50}$  value determined using ATO425 software was  $\geq 550 \text{ mg kg}^{-1}$  body weight, exceeding the concentration used *in vitro* assays. This higher  $LD_{50}$  reinforces the safety profile of the synthesized nanosystems.

The lack of toxicity of MTX-ZnONPs is likely due to the fact that the MTX molecules are loaded on to the ZnONPs preventing its untimely release. The safety of MTX-ZnONPs is important because they have the potential to be used as a delivery system for MTX, a drug that is used to treat cancer and rheumatoid arthritis [12]. Current study showed that MTX-ZnONPs could be used to deliver MTX to tumors without causing systemic toxicity. This could improve the efficacy of MTX therapy and reduce the side effects of the drug.

#### 4. Conclusion

A combined approach utilizing MTX and ZnONPs demonstrated anti-cancer efficacy against breast cancer cells. MTX-ZnONPs effectively arrested cell cycle progression in the S/G2M phase in both cell lines. Apoptosis assays revealed differential responses, ultimately inducing cell death via apoptosis or necrosis. Western blot analysis corroborated these findings, indicating apoptotic and necrotic cell death in respective cell lines, confirming the anti-cancer activity of MTX-ZnONPs regardless of MTX sensitivity. Notably, *in-vitro* assays demonstrated superior cytotoxicity of

MTX-ZnONPs compared to MTX at equivalent concentrations. MTX-ZnONPs induced apoptosis in MCF-7 breast cancer cells, as evidenced by upregulated Caspase-3 and Bax, and downregulated Bcl-xL. Conversely, MTX-ZnONPs triggered non-apoptotic cell death in TNBC MDA-MB-231 cells, as observed by downregulated Caspase-3 and upregulated Bcl-xL. Acute oral toxicity studies revealed no signs of toxicity in animals, suggesting an  $LD_{50}$  of MTX-ZnONPs exceeding  $550 \text{ mg kg}^{-1}$  body weight, significantly higher than the effective *in vitro* concentrations. This indicates the safety of the synthesized nanosystem in animals. Inherent anti-cancer properties of ZnONPs along with the targeted delivery of MTX, offers a combination effect that helps overcome drug resistance suggesting MTX-ZnONPs as a promising novel therapeutic strategy for even drug-resistant breast cancer. Now that we have the preliminary confirmation about the anti-cancer activity of MTX-ZnONPs further bio-distribution and pharmacokinetic studies need to be conducted to understand the *in vivo* effects of the nanosystem. Along with that, long-term toxicity study needs to be performed to translate the results for clinical applications. Above findings collectively suggest MTX-ZnONPs as a promising novel therapeutic strategy for breast cancer. We anticipate that our study will pave the way for MTX-loaded ZnONPs as a novel and effective treatment for breast cancer cell lines, irrespective of drug resistance. We also hope that our study will contribute to the development of nanomedicine for the treatment and diagnosis of cancer.

#### Data availability statement

The data cannot be made publicly available upon publication because no suitable repository exists for hosting data in this



field of study. The data that support the findings of this study are available upon reasonable request from the authors.

## Acknowledgments

The authors would like to acknowledge Mrs. Madhura Joshi, Flow cytometry Facility of IIT Bombay and IRCC for all the flowcytometry analysis. We also acknowledge Khandelwal Laboratories Pvt. Ltd, Mumbai, India for providing MTX gift sample. Authors would also like to acknowledge Dr Padma V Devarajan and Dr K C Barick for their insightful suggestions in the research work.

## Author contribution

All authors contributed to the study conception and design. Material preparation, data collection and analysis were performed by [Mitesh Joshi]. The first draft of the manuscript was written by [Mitesh Joshi] and all authors commented on previous versions of the manuscript. Writing, reviewing, and editing were performed by [Mitesh Joshi, Purvi Bhatt]. All authors have read and approved the final manuscript.

## Funding

This research did not receive any specific grant from funding agencies in the public, commercial, or not-for-profit sectors.

## Conflict of interest

The authors have no competing interests to declare that are relevant to the content of this article.

## Ethics approval

The authors state that they have obtained Approval from The Institutional Animal Ethics Committee for conducting animal work (CPCSEA/P-69/2022).

## ORCID iDs

Mitesh Joshi  <https://orcid.org/0000-0003-3412-0193>

Purvi Bhatt  <https://orcid.org/0000-0001-8142-8284>

## References

- [1] Sung H, Ferlay J, Siegel R L, Laversanne M, Soerjomataram I, Jemal A and Bray F 2021 Global cancer statistics 2020: GLOBOCAN estimates of incidence and mortality worldwide for 36 cancers in 185 countries *CA Cancer J. Clin.* **71** 209–49
- [2] Chhikara B S and Parang K 2023 Global cancer statistics 2022: the trends projection analysis *Chem. Biol. Lett.* **10** 1–16
- [3] Alhalmi A, Beg S, Almalki W H, Alghamdi S and Kohli K 2022 Recent advances in nanotechnology-based targeted therapeutics for breast cancer management *Curr. Drug Metab.* **23** 587–602
- [4] Chaturvedi V K, Singh A, Singh V K and Singh M P 2018 Cancer nanotechnology: a new revolution for cancer diagnosis and therapy *Curr. Drug Metab.* **20** 416–29
- [5] Rodríguez-Félix F, López-Cota A G, Moreno-Vásquez M J, Graciano-Verdugo A Z, Quintero-Reyes I E, Del-Toro-Sánchez C L and Tapia-Hernández J A 2021 Sustainable-green synthesis of silver nanoparticles using safflower (*Carthamus tinctorius* L.) waste extract and its antibacterial activity *Heliyon* **7** e06923
- [6] Rodríguez-Félix F, Graciano-Verdugo A Z, Moreno-Vásquez M J, Lagarda-Díaz I, Barreras-Urbina C G, Armenta-Villegas L, Olguín-Moreno A, Tapia-Hernández J A and Yi D K 2022 Trends in sustainable green synthesis of silver nanoparticles using agri-food waste extracts and their applications in health *J. Nanomater.* **2022** 1–37
- [7] Cho K, Wang X, Nie S, Chen Z and Shin D M 2008 Therapeutic nanoparticles for drug delivery in cancer *Clin. Cancer Res.* **14** 1310–6
- [8] Hassan H F H, Mansour A M, Abo-Youssef A M H, Elsadek B E M and Messiha B A S 2017 Zinc oxide nanoparticles as a novel anticancer approach; *in vitro* and *in vivo* evidence *Clin. Exp. Pharmacol. Physiol.* **44** 235–43
- [9] Singh T A, Das J and Sil P C 2020 Zinc oxide nanoparticles: a comprehensive review on its synthesis, anticancer and drug delivery applications as well as health risks *Adv. Colloid Interface Sci.* **286** 102317
- [10] Thomas T P, Huang B, Choi S K, Silpe J E, Kotlyar A, Desai A M, Zong H, Gam J, Joice M and Baker J R 2012 Polyvalent dendrimer-methotrexate as a folate receptor-targeted cancer therapeutic *Mol. Pharm.* **9** 2669–76
- [11] Majoros I J, Williams C R, Becker A and Baker J R 2009 Methotrexate delivery via folate targeted dendrimer-based nanotherapeutic platform *Wiley Interdiscip. Rev. Nanomed. Nanobiotechnol.* **1** 502–10
- [12] Bryan J 2012 From cancer to rheumatoid arthritis treatment: the story of methotrexate *Pharm. J.* **289** 303–4
- [13] Lindgren M, Rosenthal-Aizman K, Saar K, Eiríksdóttir E, Jiang Y, Sassian M, Östlund P, Hällbrink M and Langel Ü 2006 Overcoming methotrexate resistance in breast cancer tumour cells by the use of a new cell-penetrating peptide *Biochem. Pharmacol.* **71** 416–25
- [14] Dawood S 2016 Triple-negative breast cancer: epidemiology and management options *Mol. Pathol. Breast Cancer* **70** 71–80
- [15] Worm J, Kirkin A F, Dzhandzhugazyan K N and Guldborg P 2001 Methylation-dependent silencing of the reduced folate carrier gene in inherently methotrexate-resistant human breast cancer cells *J. Biol. Chem.* **276** 39990–40000
- [16] Moghaddam A B, Moniri M, Azizi S, Rahim R A, Ariff A B, Navaderi M and Mohamad R 2017 Eco-friendly formulated zinc oxide nanoparticles: induction of cell cycle arrest and apoptosis in the MCF-7 cancer cell line *Genes* **8** 1–15
- [17] Joshi M and Bhatt P 2023 Deciphering the anticancer activity of biocompatible zinc oxide nanoparticles loaded with methotrexate on breast cancer cells *Bull. Mater. Sci.* **46** 1–14
- [18] Fernandes S G, Gala K and Khattar E 2023 Telomerase inhibitor MST-312 and quercetin synergistically inhibit cancer cell proliferation by promoting DNA damage *Transl. Oncol.* **27** 101569
- [19] Viridi J K and Pethe P 2022 Soft substrate maintains stemness and pluripotent stem cell-like phenotype of human embryonic stem cells under defined culture conditions *Cytotechnology* **74** 479–89
- [20] Organisation for Economic Cooperation and Development 2022 *Test No. 425: Acute Oral Toxicity: Up-and-Down Procedure (OECD Guideline for Testing of Chemicals, Section 4)* (OECD Publishing) (<https://doi.org/10.1787/9789264071049-en>)

- [21] Yamauchi A, Ichimiya T, Inoue K, Taguchi Y, Matsunaga N, Koyanagi S, Fukagawa T, Aramaki H, Higuchi S and Ohdo S 2005 Cell-cycle-dependent pharmacology of methotrexate in HL-60 *J. Pharmacol. Sci.* **99** 335–41
- [22] Chaudhari R, Patel P, Meghani N, Nasra S and Kumar A 2021 Fabrication of methotrexate-loaded gold nanoconjugates and its enhanced anticancer activity in breast cancer 3 *Biotech* **11** 1–13
- [23] Xie L, Zhao T, Cai J, Su Y, Wang Z and Dong W 2016 Methotrexate induces DNA damage and inhibits homologous recombination repair in choriocarcinoma cells *Onco. Targets Ther.* **9** 7115–22
- [24] Hu C and Du W 2020 Zinc oxide nanoparticles (ZnO NPs) combined with cisplatin and gemcitabine inhibits tumor activity of NSCLC cells *Aging* **12** 25767–77
- [25] Zhang T, Du E, Liu Y, Cheng J, Zhang Z, Xu Y, Qi S and Chen Y 2020 Anticancer effects of zinc oxide nanoparticles through altering the methylation status of histone on bladder cancer cells *Int. J. Nanomed.* **15** 1457–68
- [26] Amgalan D *et al* 2020 A small-molecule allosteric inhibitor of BAX protects against doxorubicin-induced cardiomyopathy *Nat. Cancer* **1** 315–28
- [27] Premanathan M, Karthikeyan K, Jeyasubramanian K and Manivannan G 2011 Selective toxicity of ZnO nanoparticles toward Gram-positive bacteria and cancer cells by apoptosis through lipid peroxidation *Nanomedicine* **7** 184–92
- [28] Gu W and Yang C 2023 Zinc oxide nanoparticles inhibit malignant progression and chemotherapy resistance of ovarian cancer cells by activating endoplasmic reticulum stress and promoting autophagy *Exp. Ther. Med.* **26** 1–17
- [29] Tian J, Wei X, Zhang W and Xu A 2020 Effects of selenium nanoparticles combined with radiotherapy on lung cancer cells *Front. Bioeng. Biotechnol.* **8** 1289
- [30] Roshini A, Jagadeesan S, Cho Y-J, Lim J-H and Choi K H 2017 Synthesis and evaluation of the cytotoxic and anti-proliferative properties of ZnO quantum dots against MCF-7 and MDA-MB-231 human breast cancer cells *Mater. Sci. Eng. C* **81** 551–60
- [31] Xu C, Wu A, Zhu H, Fang H, Xu L, Ye J and Shen J 2013 Melatonin is involved in the apoptosis and necrosis of pancreatic cancer cell line SW-1990 via modulating of Bcl-2/Bax balance *Biomed. Pharmacother.* **67** 133–9
- [32] Jason Karch J D M 2018 Regulated necrotic cell death: the passive aggressive side of Bax and Bak *Physiol. Behav.* **176** 139–48
- [33] Whelan R S *et al* 2012 Bax regulates primary necrosis through mitochondrial dynamics *Proc. Natl Acad. Sci. USA* **109** 6566–71
- [34] Hattangadi D K, DeMasters G A, Walker T D, Jones K R, Di X, Newsham I F and Gewirtz D A 2004 Influence of p53 and caspase 3 activity on cell death and senescence in response to methotrexate in the breast tumor cell *Biochem. Pharmacol.* **68** 1699–708
- [35] Kavithaa K, Paulpandi M, Ponraj T, Murugan K and Sumathi S 2016 Induction of intrinsic apoptotic pathway in human breast cancer (MCF-7) cells through facile biosynthesized zinc oxide nanorods *Karbala Int. J. Mod. Sci.* **2** 46–55
- [36] Nagarajan M, Maadurshni G B, Tharani G K, Udhayakumar I, Kumar G, Mani K P, Sivasubramanian J and Manivannan J 2022 Exposure to zinc oxide nanoparticles (ZnO-NPs) induces cardiovascular toxicity and exacerbates pathogenesis—role of oxidative stress and MAPK signaling *Chem. Biol. Interact.* **351** 109719
- [37] Jeong S H, Kim H J, Ryu H J, Ryu W I, Park Y-H, Bae H C, Jang Y S and Son S W 2013 ZnO nanoparticles induce TNF- $\alpha$  expression via ROS-ERK-Egr-1 pathway in human keratinocytes *J. Dermatol. Sci.* **72** 263–73



# PAQR4 oncogene: a novel target for cancer therapy

Dipti Patil<sup>1</sup> · Swapnil Raut<sup>1</sup> · Mitesh Joshi<sup>2</sup> · Purvi Bhatt<sup>2</sup> · Lokesh Kumar Bhatt<sup>1</sup>

Received: 18 January 2024 / Accepted: 6 April 2024 / Published online: 20 May 2024

© The Author(s), under exclusive licence to Springer Science+Business Media, LLC, part of Springer Nature 2024

## Abstract

Despite decades of basic and clinical research and trials of promising new therapies, cancer remains a major cause of morbidity and mortality due to the emergence of drug resistance to anticancer drugs. These resistance events have a very well-understood underlying mechanism, and their therapeutic relevance has long been recognized. Thus, drug resistance continues to be a major obstacle to providing cancer patients with the intended “cure”. PAQR4 (Progestin and AdipoQ Receptor Family Member 4) gene is a recently identified novel protein-coding gene associated with various human cancers and acts through different signaling pathways. PAQR4 has a significant influence on multiple proteins that may regulate various gene expressions and may develop chemoresistance. This review discusses the roles of PAQR4 in tumor immunity, carcinogenesis, and chemoresistance. This paper is the first review, discussing PAQR4 in the pathogenesis of cancer. The review further explores the PAQR4 as a potential target in various malignancies.

**Keywords** Cancers · PAQR4 · miRNA · Tumor immunity · Therapeutic target

## Introduction

Cancer is a well-known disease defined by the growth of cells that have managed to evade core endogenous regulating systems. It is a leading contributor to death, posing a significant threat to people’s well-being and imposing a substantial economic burden on society [1]. According to assessments from the World Health Organization (WHO) in 2019, cancer is the third or fourth main cause of mortality and morbidity before the age of 70 in 23 countries. Based on current incidence rates, there will be 28.4 million new cancer cases worldwide by 2040. Despite recent advances in cancer therapeutic techniques, effective cancer treatment remains challenging due to heterogeneities and the frequent incidence of chemoresistance.

When cancerous cells become drug-tolerant, resistance to chemotherapy often occurs. Chemoresistance is a major

obstacle in cancer treatment. It occurs due to diverse reasons, including various intrinsic and extrinsic factors [2]. The most prevalent anticancer drug resistance mechanisms are drug-dependent, target-dependent, and target-independent. Overexpression of detoxifying enzymes and efflux drug transporters causes drug-dependent multidrug resistance (MDR) [3]. Translocation, deletion, mutation, and amplification in target cause target-dependent MDR. Drug target-independent MDR is caused by genetic or epigenetically altered cell–cell communication, thereby desensitizing targets [4]. Understanding the processes involved in treatment resistance in different types of cancer is crucial, including drug efflux, DNA mutations, drug inactivation, drug target alteration, DNA damage repair, cell death inhibition, and the epithelial–mesenchymal transition (EMT) and metabolic alterations that hinder drug effectiveness.

To recognize new markers for early detection and drug-gable targets for efficient therapy, it is crucial to unravel the molecular pathways that are often engaged in various forms of cancer. Thus, for the identification of precise molecular targets to enhance cancer detection and therapy, public databases like The Cancer Genome Atlas (TCGA) have been used. From such targets, researchers have recently identified the Progestin and AdipoQ Receptor (PAQR) family gene that plays a role in various forms of cancer. PAQR is the 11-member gene family consisting of PAQR1 to PAQR11.

✉ Lokesh Kumar Bhatt  
bhatt.lokesh@gmail.com

<sup>1</sup> Department of Pharmacology, SVKM’s Dr. Bhanuben Nanavati College of Pharmacy, Vile Parle (West), Mumbai 400056, India

<sup>2</sup> Department of Biological Sciences, Sunandan Divatia School of Science, SVKM’s NMIMS (Deemed-to-be University), Vile Parle (West), Mumbai, India

PAQR genes have been implicated in the carcinogenesis of breast cancer [5], prostate cancer [6], liver cancer [7], and gastric cancer [8]. This review discusses PAQR4's role in carcinogenesis through various signaling pathways and its function and expression in several cancer types. This paper is the first review, discussing PAQR4 in the pathogenesis of cancer.

## Structure and function of PAQR4

The PAQR family proteins encompass a group of transmembrane proteins that consist of species from eubacteria, archaea, *Caenorhabditis elegans*, and humans [9]. Unlike the usual classification of G-protein-coupled receptors, it has been approximated that each protein belonging to the PAQR family possesses seven transmembrane domains. These domains consist of an intracellular N-terminus and an exterior C-terminus [9, 10]. PAQR4 gene has a 7-transmembrane domain which is similar to ADIPOR1 and ADIPOR2 (Fig. 1) [11]. Adiponectin is a crucial adipokine that has a role in regulating glucose metabolism. PAQR1, also known as AdipoR1, and PAQR2, also known as AdipoR2, have been identified as receptors for adiponectin [12]. However, Progesterone receptors have been identified as PAQR5, PAQR7, and PAQR8 [13–15]. Tang and colleagues reported that the PAQR4 gene contains 3 coding exons [11].

It is important to note that the PAQR family has been shown to exhibit abnormal expression in several solid tumors, leading to the development and advancement of cancer by regulating cellular biology and metabolism [11, 18]. Earlier studies have revealed that PAQR4, a member

of the PAQR family, exhibits significant expression in both cancer tissues and cell lines [5]. Suppression of PAQR4 significantly decreased the ability of cancer cells to migrate, proliferate, invade, and undergo epithelial–mesenchymal transition (EMT), while also inducing cell death [8].

## Role of PAQR4 in various cancers

### Role of PAQR4 in breast cancer

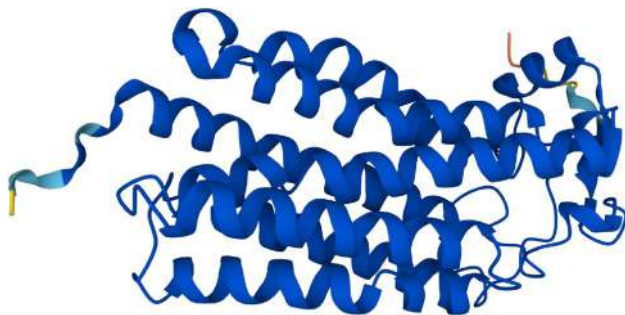
#### Role in cell proliferation

Data from cancer statistics 2022 reports revealed that breast cancer accounts for 50% of women's cancer diagnoses, along with other major malignancies that often affect women including lung cancer and colorectal cancer [19]. Zhang et al. investigated the carcinogenic effect of PAQR4 in breast cancer and reported suppression of cell proliferation in human breast cancer cells SUM159 and MCF7 after the knockdown of PAQR4 gene [5]. In terms of the cell cycle's G1-to-S transition, PAQR4 modulates the steady state level of cyclin-dependent kinase 4 (CDK4), which was examined by its amount of ubiquitination in breast cancer cells in the presence and absence of a proteasome inhibitor, MG132 (Table 1). From both the breast cancer cells, MCF7 and SUM159, PAQR4 knockdown increased CDK4 ubiquitination in the presence of MG132, whereas overexpressed cells inhibited this process [5].

Changes in sphingolipid metabolism may be the cause of the advancement of a variety of cancers, including liver, colon, endometrial, and breast cancer [24]. It has been observed that breast tumor has considerable downregulation of the sphingolipid pathway's metabolite, such as ceramidase and sphingosine-1-phosphate compared to normal tissue, and PAQR4 is recognized for its ceramidase activity. To investigate further, researchers used the homology model of PAQR4 using the crystal structure of PAQR2. An aspartic acid residue (Asp219) from histidine residues, which are present with the zinc ion, facilitates the cleavage of ceramide into sphingosine. Further, PAQR4-depleted cells showed lower ceramidase activity compared to normal cells. Ceramide induces apoptosis, and the precursors of de novo sphingolipid synthesis accumulate as a result of PAQR4 depletion [25].

#### Role in metastasis

Zhang and colleagues demonstrated a correlation between elevated PAQR4 expression and a higher risk of breast cancer metastasizing to lymph nodes in patient samples [5]. Although a specific mechanism was not established in their



**Fig. 1** Three-dimensional structures from AlphaFold (predicted) for PAQR4 Gene [16, 17]. Progesterin and adipoQ receptor family member 4 protein tertiary structure was predicted by using AlfaFold through Genecard.org. The core alpha helices regions and loops of the predicted protein were modeled to high accuracy (Blue highlighted with the predicted local distance difference test (pLDDT) > 90). There were a few regions towards the terminal N- and C-terminal of the protein that exhibited medium confidence (90 > pLDDT > 70 and highlighted in skyblue), Low confidence (70 > pLDDT > 50 and highlighted in yellow), and very low confidence (pLDDT < 50 and highlighted in orange) [16, 17]

**Table 1** Studies investigating the effects of PAQR4 gene modulation on different cancers

Sr. No.	Drug name	Category	Model	Outcomes	Result	References
1. Breast cancer						
i.	MG132	Proteasome inhibitor	(i) PQR4 KO breast cancer cells (MCF7 and SUM159) (ii) PAQR4 overexpressed breast cancer cells SUM159	(i) Increased CDK4 ubiquitination (ii) Decreased CDK4 ubiquitination	PAQR4 can control the ubiquitination and degradation of CDK4	[5]
2. Hepatocellular carcinoma						
i.	LY294002	PI3K inhibitor	PAQR4-overexpressing Huh-7	Blocked the increase in cell viability brought on by PAQR4 overexpression	PAQR4 plays a critical role in the development and spread of HCC tumors by controlling the PI3K/AKT pathway	[20]
3. Non-small cell lung cancer						
i.	MG132	Proteasome inhibitor	PAQR4 knockdown SPC-A1 and GLC-82 cells	Protein levels of Nrf2 were upregulated	PAQR4 suppresses the production of Nrf2 at the posttranslational level in a proteasome–ubiquitination-dependent manner	[21]
ii.	Palbociclib	Reversible cyclin-dependent kinase (CDK) inhibitor	Transfected with pLKO.1-PAQR4	Diminished the promoting effect of PAQR4 on cell proliferation, and migration	The CDK4-pRB-E2F1 pathway is involved in NSCLC	[22]
4. Prostate cancer						
i.	Breviscapine	Flavonoid derived from the Erigeron breviscapus (Vant.) Hand-Mazzis	Prostate cancer cells PC3 and DU145 transfected with PAQR4	(i) Downregulation in the protein level of PAQR4 (ii) Reduced the PAQR4-induced activation of the PI3K/Akt pathway	In prostate cancer, BRE may have an anti-tumor impact by disrupting the PAQR4-mediated PI3K/Akt pathway	[6]
ii.	Bisphenol A	Synthetic plasticizer	Male neonatal Sprague–Dawley rats	Reduced promoter gene methylation	PAQR4 is crucial for cellular metabolism and has been linked to a higher risk of prostate cancer when expressed abnormally	[23]



study, significant ( $p = 0.001$ ) lymph node metastasis was associated with the mRNA level of PAQR4 [5].

## Role of PAQR4 in hepatocellular carcinoma

### Role in cell proliferation

Hepatocellular carcinoma (HCC) is one of the world's most deadly malignancies, accounting for the fourth highest cause of cancer-related death worldwide [26–28]. It is the fourth most common cancer in men which in turn has a higher risk of developing liver cancer in men than women. The global male-to-female HCC incidence ratio is 2.8:1 [29]. Shi et al. identified the expression of oncoproteins vascular endothelial zinc finger 1 (VEZF1), which regulates several cancers [30]. Through the PI3K/Akt pathway, VEZF1 accelerates HCC growth by entering the nucleus and transcriptionally activating PAQR4. Additionally, VEZF1 is known to be a substrate of stress-inducible phosphoprotein 1 homology and U-box-containing protein 1 (STUB1), and its stability is impacted by STUB1-mediated ubiquitination degradation [31]. It is possible that new information about the STUB1/VEZF1/PAQR4 mechanism can help direct early detection and treatment of HCC patients.

Zhao and colleagues reported that Hep3B cells with knocked-down PAQR4 had decreased cell growth, which was associated with the prevention of the G1/S cell cycle transition [20]. PAQR4 knockdown decreased phosphorylation of AKT and p85 which further blocked PI3K/AKT pathway activation. Conversely, HCC cells (Huh-7 cells) that had PAQR4 overexpression showed the inverse effect. Table 1 shows the results of the study that tested the link between the PI3K/AKT pathway and PAQR4 activity in the progression of HCC using the PI3K inhibitor LY294002 [32, 33]. Overexpression of PAQR4 caused the cell cycle to develop more rapidly, whereas LY294002 stopped this. Researchers looked at the relationship between PAQR4 expression and PAQR4 methylation and reported a substantial negative association, indicating that PAQR4 hypomethylation may be one of the causes of the increase in PAQR4 expression [34, 35].

### Role in metastasis

Zhao and colleagues investigated the role of PAQR4 gene in HCC metastasis. Their study showed positive correlations between highly expressed PAQR4 and tumor size, stage, lymph node metastasis, and distant metastasis. The study concluded that the PAQR4 gene promotes cell growth and metastasis by activating the PI3K/AKT pathway [20]. Wang et al. reported that in the intrahepatic HCC implantation model, overexpression of PAQR4 markedly

increased the establishment of intrahepatic metastatic foci in comparison to the control group [36].

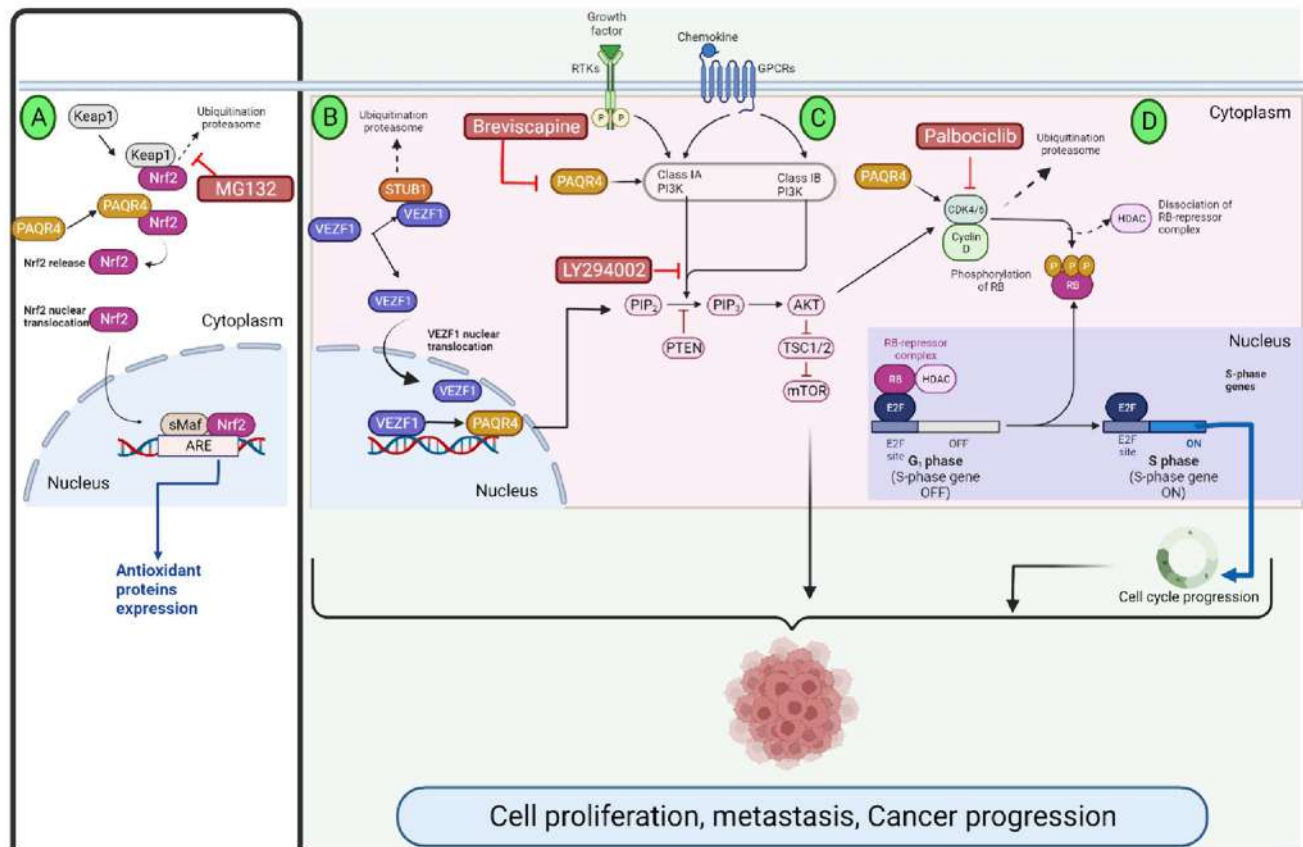
## Role of PAQR4 in non-small cell lung cancer

### Role in cell proliferation

While PAQR4 has been linked to breast cancer in humans, its function in NSCLC in humans is yet unknown. Worldwide, NSCLC ranks high among respiratory neoplasms and is a leading cause of cancer-related death and disability. Wu and Liu reported higher expression of PAQR4 in NSCLC tissue than in normal tissue. PAQR4 enhances cell proliferation, migration, and invasion by decreasing CDK4 ubiquitination and degradation or by blocking the CDK4/pRB-E2F1 pathway [5].

Additionally, in NSCLC cells, overexpression of PAQR4 also physically interacts with nuclear factor-erythroid 2 p45-related factor 2 (Nrf2), preventing Nrf2 from being ubiquitinated by Kelch-like ECH-associated protein 1 (Keap1) and disrupting the interaction between Nrf2 and Keap1 [21]. When it comes to managing oxidative and electrophilic stress, as well as maintaining cellular and tissue homeostasis, the Nrf2 signaling pathway is indispensable [37]. Nrf2 is a master transcriptional activator that drives the cellular response to a variety of stimuli, including electrophilic insults, proteotoxic stress, and oxidative stress [38–40]. Keap1 normally ubiquitinates Nrf2 constantly and facilitates its proteasome route degradation [39]. When cells experience oxidative stress, Keap1 becomes inactive and Nrf2 becomes stabilized. Once Nrf2 binds to the antioxidant response element (ARE), it moves into the nucleus and activates the transcription of several genes that code for detoxifying enzymes and proteins with antioxidant characteristics, as shown in Fig. 2 [40]. On the other hand, lung cancer has been found to be associated with a number of Keap1 mutations or loss of heterozygosity [41].

An increasing body of evidence suggests that Nrf2 is constitutively stabilized in certain human cancers [42–44], and that tumors exhibiting elevated Nrf2 levels are associated with a poor prognosis [42, 44]. The influence of Nrf2 on the efficacy of cisplatin in the treatment of ovarian cancer has been demonstrated [45]. Furthermore, evidence suggests a relationship between lung cancer and various mutations or loss of heterozygosity in the Keap1 gene [41]. Consequently, finding new components of the Keap1-Nrf2 signaling pathway may help future NSCLC patients who are resistant to treatment. This provides more evidence that PAQR4 reduction might make cancer cells more responsive to treatment.



**Fig. 2** **A** Signaling pathway of Keap1 and Nrf2: At normal conditions, Keap1 regulates the Nrf2 protein level. Keap1 forms a complex named E3 ubiquitin ligase, which causes ubiquitin–proteasome degradation of Nrf2. Due to electrophiles, reactive oxygen species (ROS), or endoplasmic reticulum stress, the Nrf2 protein level upregulates. PAQR4 competes with Keap1 and binds to the site on Nrf2. Nrf2 is then bound to the antioxidant response elements (AREs), which then translocate into the nucleus, generate heterodimers with proteins called sMAF, and activate ARE-related genes. MG132, a proteasome inhibitor, inhibits proteasome ubiquitination of Nrf2. **B** VEZF1 is the substrate of stress-inducible phosphoprotein 1 homology and U-box containing protein 1 (STUB1), which further causes ubiquitin–proteasome degradation of VEZF1. VEZF1 translocates to the nucleus when there is no ubiquitination and then activates PAQR4, which further actuates the major pathway responsible for the cancer progres-

sion. **C** PAQR4 exerts its oncogenic function in cancer by regulating PI3K/AKT pathway, which activates PI3K (Class IA PI3k and Class IB) and converts phosphatidylinositol-4, 5-bisphosphate (PIP2) into phosphatidylinositol-3, 4, 5-triphosphate (PIP3), which activates AKT, Tuberous sclerosis proteins 1 and 2 (TSC1/2), mammalian target of rapamycin (mTOR), which are mainly responsible for cell cycle proliferation and differentiation thus eventually causes cancer. Brevistapine acts on PAQR4 thus downregulates its protein levels and inhibits cancer progression by inhibiting the PI3K/AKT pathway. **D** The tumor suppressor protein, retinoblastoma (Rb), is phosphorylated by the CDK4/6-cyclin D1 complex. Palbociclib, a CDK4/6 inhibitor, inhibits the CDK4-pRB-E2F1 pathway, which lessens the effect of PAQR4’s stimulation of cell proliferation and migration

### Role in metastasis

Wu and Liu explored the role of the PAQR4 gene in NSCLC. They discovered a correlation between PAQR4 expression and pathological characteristics such as lymph node metastases, tumor size, and TNM stage. They concluded that in non-small cell lung cancer, PAQR4 stimulates cell division and metastasis via the CDK4-pRB-E2F1 pathway [5].

### Role of PAQR4 in prostate cancer

Among male cancers, prostate cancer is second only to lung cancer in terms of mortality rate. More than one million new cases are reported annually, making it a major public health concern [46]. Researchers identified PAQR4 as a key player in prostate cancer cell lines and tissues. PAQR4 knockdown in PC3 and DU145 cell lines inhibited cell growth, cell migration, and epithelial–mesenchymal transition [6].

Further, in in-vivo studies, breviscapine treatment inhibited the PAQR4-mediated PI3K/Akt pathway in prostate cancer, which in turn inhibited cell growth and metastasis [6].

## PAQR4 in drug resistance

### Mechanisms of drug resistance

Cancer cells use different mechanisms to develop drug resistance. The following are the main mechanisms by which cancer cells develop drug resistance.

#### Drug inactivation

For numerous anticancer drugs to be effective, metabolic activation is essential. It is important to consider that cancer cells may develop resistance to treatments due to decreased drug activation. Previous studies have identified drug efflux transporters/multidrug resistance pumps, uridine diphosphoglucuronosyltransferase (UGT) superfamily, cytochrome P450s, and Glutathione S-transferases (GSTs) as some classical drug resistance target(s) in cancer chemotherapy [47, 48]. GST expression levels are linked with higher tumor drug resistance. Another GST-specific isoenzyme called Glutathione S-transferases P is ubiquitous in nature and showed elevated levels in non-drug-resistant and drug-resistant cancers [49].

When treating and preventing breast cancer, irinotecan, a topoisomerase I inhibitor, is effective when uridine diphosphate glucuronosyltransferase 1A1 gene (UGT1A1) is inactive. Epigenetic alterations that boost UGT1A1 levels could lead to resistance to irinotecan and other drugs [50, 51]. For example, thymidine phosphorylase transforms the fluoropyrimidine prodrug capecitabine into 5-fluorouracil (5-FU). The thymidine phosphorylase gene can be methylated, which results in capecitabine resistance. When cellular enzyme activity such as Dihydropyrimidine dehydrogenase is low, 5-FU cannot be transformed into its most potent forms [52, 53].

Changes in epigenetics before transcription can impact the activity of genes through various regulatory mechanisms, such as DNA methylation, histone modification, and chromatin remodeling, regardless of the genetic code sequence [54–56]. DNA methyltransferases (DNMTs) and demethylases maintain CpG site methylation, which can be inherited via cell divisions [57]. DNA methylation changes chromatin structure and prevents transcription factors or co-activators from attaching to their specific locations, reducing gene expression. Methylation can also attract methyl-binding proteins (MBPs) that interact with co-repressors to inactivate chromatin at the DNA level [58, 59].

### Drug target modification

Drug targets may be altered by secondary protein mutations or epigenetic changes in expression levels. Exempli gratia, epidermal growth factor receptor (EGFR) tyrosine kinase inhibitors (TKIs) like erlotinib, and gefitinib for non-small cell lung cancer (NSCLC) have a high first response rate [60, 61]. Within a year, over 50% of responding patients developed a T790M EGFR mutation, making them resistant to the first and second generations of TKIs. The mutation from threonine to methionine changed EGFR conformation, increasing ATP binding affinity and decreasing gefitinib/erlotinib kinase binding [62–64].

#### Drug efflux

Membrane transporters are the unique proteins that assist in the transfer of ions, micro, and macromolecules through biological membranes. These transporters are comprised of ATP hydrolysis-driven pumps, secondary transporters including solute carrier transporters (SLCs), and ion channels that actively convey against the concentration gradient [65]. Under normal physiological conditions, the kidney, liver, and epithelial tissues that protect the small intestine, placenta, blood–brain barrier, and testes express efflux pumps to eliminate endogenous waste and xenobiotics [66, 67]. Efflux pumps in eukaryotes are divided into five groups Monocarboxylate transporter (MCT), Multidrug resistance protein (MDR, P-glycoprotein), Multidrug resistance-associated proteins (MRPs), Peptide transporters (PEPTs), and Na<sup>+</sup> + phosphate transporters (NPTs). ATP-driven transmembrane P-glycoprotein (P-gp) efflux pumps are a primary cause of cancer multidrug resistance [68].

### Gene modification

Drug resistance often begins with either the expression or mutation of the drug target protein. Within mammals, B-cell lymphoma-2 (Bcl-2) family proteins such as Bcl-2, Bcl-xL, Bcl-w, Mcl-1, and A1 play a role in apoptosis. With the exception of Bim, Bid, and Bad, which are BH3-only proteins, Bcl-2 proteins consist of four homologous domains (BH1, BH2, BH3, and BH4) [69–72]. Alterations in genetics associated with cancer and the development of tumors frequently impact the control of cell death to stimulate cell proliferation. These genetic changes are either passed down through generations or caused by the cell cycle. Examples include genomic amplification, rearrangements, and DNA fragment substitutions, insertions, and deletions [73, 74]. Gene mutations in the BCL-2 family can lead to the overexpression of proteins that either suppress or induce apoptosis. Bcl-2 is commonly found to be overexpressed in numerous breast and prostate tumors. Studies have shown

that mutations in the BCL-2 gene's coding sequence at diagnosis were linked to a quicker progression to aggressive lymphoma and premature death from it. Bcl-2 boosts lung metastasis in mice and promotes cell migration and invasion in breast cancer cell lines [75–77]. Several non-small cell lung carcinomas exhibit high levels of BCL-2, MCL-1, and BCL-XL. Analysis of somatic copy number alterations in around 3000 cancer samples across 26 different types reveals the amplification of genes similar to Bcl-2, such as MCL-1 and BCL-XL, as well as the deletion of BOK and PUMA [78–81]. When Bcl-2 is overexpressed in breast cancer cells, it leads to the formation of polyploid cells that exhibit multidrug resistance [82].

### Role of PAQR4 gene in drug resistance

Recent studies suggested the role of PAQR gene in the development of drug resistance. Wang and colleague have performed a systematic pan-cancer analysis of the PAQR gene [83]. They used Cancer Genome Atlas to study the association between PAQR4 and clinical phenotypes, and tumor immune response. Tumor microsatellite instability analysis for the PAQR gene showed a positive correlation in adrenocortical carcinoma, cervical squamous cell carcinoma and endocervical adenocarcinoma, kidney Chromophobe, stomach adenocarcinoma, and uterine corpus endometrial carcinoma cohorts. Positive correlation in microsatellite instability analysis predicts resistance to certain drug therapy [84]. Thus, the results from this study predict a correlation between the PAQR gene and drug resistance.

Xu et al. investigated the association between the PAQR gene and prognosis of non-small cell lung cancer [21]. Using NSCLC cells, they examined the impact of PAQR4 on colony formation, xenograft tumor formation, and cell proliferation. Results showed that PAQR4 expression was elevated in cancer cell lines in NSCLC patients, and PAQR4 mutations were observed in non-small cell lung cancer tissues. The study concluded that PAQR4 increases chemoresistance by preventing the protein degradation of nuclear factor-erythroid 2-related factor 2 (Nrf2), in non-small cell lung cancer [21].

### Targeting PAQR4 for the treatment of cancer

In cancer prevention and treatment, natural chemicals are promising. They influence cell growth and cell cycle arrest with model effects and low toxicity. Breviscapine has broad physiological and pharmacological effects. The main active ingredients in breviscapine are baicalein and 4, 5, 6-tetrahydroxy flavone-7-glucoside acid [85, 86]. Breviscapine induces apoptosis and inhibits cell proliferation, reducing tumor growth, by inhibiting the

PAQR4-mediated PI3K/Akt pathway in prostate cancer to reduce proliferation and metastasis. In addition, PI3K/Akt pathway inactivation drastically reduced N-cadherin and Vimentin protein levels and increased E-cadherin expression. In contrast, upregulating PAQR4 and inhibiting PI3K/Akt pathway reduced the above effects [6].

According to computational research, a few natural substances increase cancer survival by changing PAQR4 expression. The rosemary extract, Withaferin A, and Eusynstyelamide B change PAQR4 expression, which influences survival in kidney renal clear cell carcinoma, kidney renal papillary cell carcinoma, and liver hepatocellular carcinoma patients with low/medium expression [87]. Researchers found that PAQR4 and FLYWCH1, a transcription modulator, directly bind nuclear  $\beta$ -catenin, suppressing transcriptional activity and downregulating genes related to cell migration and morphology [88]. PAQR4 also interacts with ASB2, an ankyrin repeat-containing protein that suppresses cytokine signaling box-2 and impacts growth and chromatin condensation [89].

MicroRNAs (miRNAs) are single-stranded, non-coding RNAs whose function is to control biological processes by targeting a variety of messenger RNAs (mRNAs) [90]. Depending on the level of complementarity, miRNA may bind to the 3'-untranslated regions (3'UTRs) of target mRNAs and cause cleavage of mRNA or suppresses the translational mechanism [91, 92]. Through controlling key signaling molecules, such as various transcription factors, pro-apoptotic and anti-apoptotic, cytokines, and growth factors, proteins, miRNAs play crucial roles in many fundamental biological processes, which include cell apoptosis, metabolism, cell differentiation, cell proliferation, and development [93, 94]. Through controlling their mRNA targets, miRNAs have been demonstrated to act as oncogenes or tumor suppressor genes in a variety of malignancies, including, breast cancer, HCC, non-small cell lung cancer, prostate cancer, gastric cancer, and endometrial cancer [95–98].

While increasing apoptotic cell death, lowering the levels of either hnRNPK or LINC00162 inhibited colony formation and proliferation [99]. According to small RNA sequencing and antisense oligonucleotide pulldown, LINC00162 directly combines with miR-485-5p, which can decrease tumor growth by reducing colony formation and cell proliferation while enhancing apoptotic cell death. Due to direct binding to the 3'-untranslated region of PAQR4 mRNA, miR-485-5p reduced the expression of PAQR4.

The level of functional miR-485-5p rose when hnRNPK and LINC00162 were knocked down, suggesting that LINC00162 may compete with miR-485-5p to derepress PAQR4 expression. Results showed that a regulatory prototype including hnRNPK, LINC00162, miR-485-5p, and PAQR4



is a viable cancer target and plays a significant role in cell proliferation and death [100].

MiR-125b-5p has been demonstrated to be considerably downregulated in breast, HCC, and bladder cancer [101–103]. As a result, scientists have shown that miR-125b-5p is downregulated and inversely linked with PAQR4 expression in HCC, suggesting that this may be another possible mechanism for PAQR4 to be upregulated. This study indicates that miR-125b-5p downregulation and PAQR4 hypomethylation may be potential pathways for PAQR4 overexpression in HCC. PAQR4 overexpression in HCC may be caused by PAQR4 hypomethylation and miR-125b-5p downregulation [101]. After miR-647 knockdown, the PAQR4 mRNA level significantly rose, while after miR-647 overexpression, it significantly dropped. Additionally, circNOLC1 overexpression in PC cells dramatically increased PAQR4 mRNA and protein levels [7].

Stomach cancer is still a significant malignancy that ranks fifth for incidence and fourth for fatality globally [104]. 50% of the world's population has been found to have *H. pylori* infection [105], and the regional variance of this infection is reasonably correlated with the occurrence of stomach cancer. miRNAs have a significant role in the genetic network involved in pathophysiological events, such as the development and spread of cancer [106]. Furthermore, new research demonstrates that miRNAs are crucial in regulating other GC occurrence and development processes, including cell proliferation, apoptosis, invasion, and metastasis [107–109].

To highlight the usefulness of PAQR4 in GC, experiments were performed using luciferase plasmids with either wild-type (WT) or mutant PAQR4 3'UTR, which demonstrated that overexpression of miR-370 decreased WT PAQR4 reporter activity [8]. In SGC-7901 cells, miR-370 knockdown enhanced PAQR4 expression, whereas miR-370 introduction dramatically decreased PAQR4 expression. These results demonstrated that 3'-UTR sequence binding by miR-370 controlled PAQR4 expression in GC cells directly [8]. Overexpression of miR-370 dramatically decreased PAQR4 expression and suppressed malignant signals such as EMT, invasion, and proliferation. A similar result was seen in SGC-7901 cells after PAQR4 was knocked down. Further evidence proposes that miR-370 suppressed GC cell proliferation, invasion, and EMT via regulation of PAQR4 expression. PAQR4 may play crucial roles in the development and metastasis of GC. Restoring PAQR4 also reversed the inhibitory effects of miR-370 [8].

## Future perspective

PAQR4 has a significant influence on multiple proteins that are part of the PI3K/Akt pathway. It also affects the activity of ceramidase and FLYWCH1, which play a role in the

development of chemoresistance in cancer cells. Through the exploration of different natural and synthetic compounds, along with the current chemotherapy, there is potential to mitigate the development of chemoresistance in various types of cancer by targeting the PAQR4. Drugs that can suppress the function of PAQR4 can be explored for their potential to enhance the effectiveness of cancer treatment. Further, the role of PAQR4 in cancer metastasis and drug needs to be further explored to enhance our understanding.

## Conclusion

PAQR4 gene, a member of the PAQR family, is a recently identified oncogene. PAQR4 activates the PI3K/Akt signaling cascade, a major oncogenic axis in human cancers, to promote carcinogenesis. Previous research has demonstrated that PAQR4 plays a role in the pathogenesis of a variety of cancer types, including breast cancer, hepatocellular carcinoma, NSCLC, and prostate cancer. PAQR4's expression and role in other prevalent cancer types, however, is yet unknown. Data from various studies suggest that targeting PAQR4 can be a potential approach for the treatment of cancer, however, further clinical and mechanistic studies are warranted to enhance our understanding of PAQR4.

**Author contributions** Dipti Patil: Writing—Original draft preparation, Swapnil Raut: Writing—Original draft preparation, Mitesh Joshi: Writing—Original draft preparation, Purvi Bhatt: Conceptualization, Writing—Reviewing and Editing, Lokesh Kumar Bhatt: Conceptualization, Writing—Reviewing and Editing. All authors read and approved the final manuscript.

**Funding** The authors declare that no funds, grants, or other support were received during the preparation of this manuscript.

**Data availability** Data sharing is not applicable to this article as no datasets were generated or analyzed during the current study.

## Declarations

**Competing interests** The authors have no relevant financial or non-financial interests to disclose.

**Ethical approval** Not applicable.

**Consent to participate** Not applicable.

**Consent to publication** Not applicable.

## References

1. Ferlay J, Colombet M, Soerjomataram I, Parkin DM, Piñeros M, Znaor A, et al. Cancer statistics for the year 2020: an overview. *Int J Cancer*. 2021;149:778–89.

2. Ramos A, Sadeghi S, Tabatabaeian H. Battling chemoresistance in cancer: root causes and strategies to uproot them. *Int J Mol Sci.* 2021;22:9451.
3. Bukowski K, Kciuk M, Kontek R. Mechanisms of multidrug resistance in cancer chemotherapy. *Int J Mol Sci.* 2020;21:3233.
4. Emran TB, Shahriar A, Mahmud AR, Rahman T, Abir MH, Siddique MF-R, et al. Multidrug resistance in cancer: understanding molecular mechanisms, immunoprevention and therapeutic approaches. *Front Oncol.* 2022. <https://doi.org/10.3389/fonc.2022.891652/full>.
5. Zhang H, Han R, Ling Z-Q, Zhang F, Hou Y, You X, et al. PAQR4 has a tumorigenic effect in human breast cancers in association with reduced CDK4 degradation. *Carcinogenesis.* 2018;39:439–46.
6. Ye J, Gao M, Guo X, Zhang H, Jiang F. Brevescapine suppresses the growth and metastasis of prostate cancer through regulating PAQR4-mediated PI3K/Akt pathway. *Biomed Pharmacother.* 2020;127: 110223.
7. Chen W, Cen S, Zhou X, Yang T, Wu K, Zou L, et al. Circular RNA CircNOLC1, upregulated by NF-KappaB, promotes the progression of prostate cancer via miR-647/PAQR4 axis. *Front Cell Dev Biol.* 2021. <https://doi.org/10.3389/fcell.2020.624764>.
8. Feng Y, Sun T, Yu Y, Gao Y, Wang X, Chen Z. MicroRNA-370 inhibits the proliferation, invasion and EMT of gastric cancer cells by directly targeting PAQR4. *J Pharmacol Sci.* 2018;138:96–106.
9. Lei L, Ling Z-N, Chen X-L, Hong L-L, Ling Z-Q. Characterization of the Golgi scaffold protein PAQR3, and its role in tumor suppression and metabolic pathway compartmentalization. *Cancer Manag Res.* 2020;12:353–62.
10. Yi JK, Xu R, Obeid LM, Hannun YA, Airola MV, Mao C. Alkaline ceramidase catalyzes the hydrolysis of ceramides via a catalytic mechanism shared by Zn<sup>2+</sup>-dependent amidases. *PLoS ONE.* 2022;17:e0271540.
11. Tang YT, Hu T, Arterburn M, Boyle B, Bright JM, Emtage PC, et al. PAQR proteins: a novel membrane receptor family defined by an ancient 7-transmembrane pass motif. *J Mol Evol.* 2005;61:372–80.
12. Melchionna MV, Gullett JM, Bouveret E, Shrestha HK, Abraham PE, Hettich RL, et al. Bacterial homologs of progesterone and AdipoQ receptors (PAQRs) affect membrane energetics homeostasis but not fluidity. *J Bacteriol.* 2022. <https://doi.org/10.1128/jb.00583-21>.
13. Yang M, Li JC, Tao C, Wu S, Liu B, Shu Q, et al. PAQR6 upregulation is associated with AR signaling and unfavorable prognosis in prostate cancers. *Biomolecules.* 2021;11:1383.
14. Galindez SM, Keightley A, Koulen P. Differential distribution of steroid hormone signaling networks in the human choroid-retinal pigment epithelial complex. *BMC Ophthalmol.* 2022;22:406.
15. McGlade EA, Miyamoto A, Winuthayanon W. Progesterone and inflammatory response in the oviduct during physiological and pathological conditions. *Cells.* 2022;11:1075.
16. Jumper J, Evans R, Pritzel A, Green T, Figurnov M, Ronneberger O, et al. Highly accurate protein structure prediction with AlphaFold. *Nature.* 2021;596:583–9.
17. Varadi M, Anyango S, Deshpande M, Nair S, Natassia C, Yordanova G, et al. AlphaFold protein structure database: massively expanding the structural coverage of protein-sequence space with high-accuracy models. *Nucleic Acids Res.* 2022;50:D439–44.
18. Wu HG, Zhang WJ, Ding Q, Peng G, Zou ZW, Liu T, et al. Identification of PAQR3 as a new candidate tumor suppressor in hepatocellular carcinoma. *Oncol Rep.* 2014;32:2687–95.
19. Siegel RL, Miller KD, Fuchs HE, Jemal A. Cancer statistics, 2022. *CA Cancer J Clin.* 2022;72:7–33.
20. Zhao G, Shi X, Sun Z, Zhao P, Lu Z. PAQR4 promotes the development of hepatocellular carcinoma by activating PI3K/AKT pathway. *Acta Biochim Biophys Sin.* 2021;53:1602–13.
21. Xu P, Jiang L, Yang Y, Wu M, Liu B, Shi Y, Shen Q, Jiang X, He Y, Cheng D, Xiong Q. PAQR4 promotes chemoresistance in non-small cell lung cancer through inhibiting Nrf2 protein degradation. *Theranostics.* 2020;10(8):3767.
22. Wu B, Liu R. PAQR4 promotes cell proliferation and metastasis through the CDK4-pRB-E2F1 pathway in non-small-cell lung cancer. *OncoTargets Ther.* 2019;12:3625–33.
23. Prins GS, Ye S-H, Birch L, Zhang X, Cheong A, Lin H, et al. Prostate cancer risk and DNA methylation signatures in aging rats following developmental BPA exposure: a dose-response analysis. *Environ Health Perspect.* 2017;125:77007.
24. Fernández LP, Gomez de Cedron M, Ramirez de Molina A. Alterations of lipid metabolism in cancer: implications in prognosis and treatment. *Front Oncol.* 2020;10:577420.
25. Pedersen L, Panahandeh P, Siraji MI, Knappskog S, Lønning PE, Gordillo R, et al. Golgi-localized PAQR4 mediates antiapoptotic ceramidase activity in breast cancer. *Cancer Res.* 2020;80:2163–74.
26. Lam KL, Yang KL, Sunderasan E, Ong MT. Latex C-serum from *Hevea brasiliensis* induces non-apoptotic cell death in hepatocellular carcinoma cell line (HepG2). *Cell Prolif.* 2012;45:577–85.
27. Chen Y, Hu W, Lu Y, Jiang S, Li C, Chen J, et al. A TALEN-based specific transcript knock-down of PIWIL2 suppresses cell growth in HepG2 tumor cell. *Cell Prolif.* 2014;47:448–56.
28. Ohno M, Otsuka M, Kishikawa T, Shibata C, Yoshikawa T, Takata A, et al. Specific delivery of microRNA93 into HBV-replicating hepatocytes downregulates protein expression of liver cancer susceptible gene MICA. *Oncotarget.* 2014;5:5581–90.
29. Kulik L, El-Serag HB. Epidemiology and management of hepatocellular carcinoma. *Gastroenterology.* 2019;156:477–491.e1.
30. Shi X, Zhao P, Zhao G. VEZF1, destabilized by STUB1, affects cellular growth and metastasis of hepatocellular carcinoma by transcriptionally regulating PAQR4. *Cancer Gene Ther.* 2022;30:256.
31. Liu Y, Zhou H, Tang X. STUB1/CHIP: new insights in cancer and immunity. *Biomed Pharmacother.* 2023;165: 115190.
32. Ma X-L, Shen M-N, Hu B, Wang B-L, Yang W-J, Lv L-H, et al. CD73 promotes hepatocellular carcinoma progression and metastasis via activating PI3K/AKT signaling by inducing Rap1-mediated membrane localization of P110 $\beta$  and predicts poor prognosis. *J Hematol Oncol J Hematol Oncol.* 2019;12:37.
33. Chen H, Wong C-C, Liu D, Go MY, Wu B, Peng S, et al. APLN promotes hepatocellular carcinoma through activating PI3K/Akt pathway and is a druggable target. *Theranostics.* 2019;9:5246–60.
34. Yang T, Liu X, Kumar SK, Jin F, Dai Y. Decoding DNA methylation in epigenetics of multiple myeloma. *Blood Rev.* 2022;51: 100872.
35. Eden A, Gaudet F, Waghmare A, Jaenisch R. Chromosomal instability and tumors promoted by DNA hypomethylation. *Science.* 2003;300:455–455.
36. Wang W, Huang Q, Liao Z, Zhang H, Liu Y, Liu F, et al. ALKBH5 prevents hepatocellular carcinoma progression by post-transcriptional inhibition of PAQR4 in an m6A dependent manner. *Exp Hematol Oncol.* 2023;12:1.
37. Song M-Y, Lee D-Y, Chun K-S, Kim E-H. The role of NRF2/KEAP1 signaling pathway in cancer metabolism. *Int J Mol Sci.* 2021;22:4376.
38. Feng L, Li J, Yang L, Zhu L, Huang X, Zhang S, et al. Tamoxifen activates Nrf2-dependent SQSTM1 transcription to promote endometrial hyperplasia. *Theranostics.* 2017;7:1890–900.

39. Xu K, Ma J, Hall SRR, Peng R-W, Yang H, Yao F. Battles against aberrant KEAP1-NRF2 signaling in lung cancer: intertwined metabolic and immune networks. *Theranostics*. 2023;13:704–23.
40. Tian Y, Liu H, Wang M, Wang R, Yi G, Zhang M, et al. Role of STAT3 and NRF2 in tumors: potential targets for antitumor therapy. *Molecules*. 2022;27:8768.
41. Remigante A, Spinelli S, Marino A, Pusch M, Morabito R, Dos-sena S. Oxidative stress and immune response in melanoma: ion channels as targets of therapy. *Int J Mol Sci*. 2023;24:887.
42. Guo Q, Liu L, Chen Z, Fan Y, Zhou Y, Yuan Z, et al. Current treatments for non-small cell lung cancer. *Front Oncol*. 2022. <https://doi.org/10.3389/fonc.2022.945102>.
43. Pouremamali F, Pouremamali A, Dadashpour M, Soozangar N, Jeddi F. An update of Nrf2 activators and inhibitors in cancer prevention/promotion. *Cell Commun Signal*. 2022;20:100.
44. Dhawan A, Pifer PM, Sandulache VC, Skinner HD. Metabolic targeting, immunotherapy and radiation in locally advanced non-small cell lung cancer: where do we go from here? *Front Oncol*. 2022. <https://doi.org/10.3389/fonc.2022.1016217>.
45. Tossetta G, Fantone S, Montanari E, Marzoni D, Goteri G. Role of NRF2 in ovarian cancer. *Antioxidants*. 2022;11:663.
46. Sandhu S, Moore CM, Chiong E, Beltran H, Bristow RG, Williams SG. Prostate cancer. *Lancet*. 2021;398:1075–90.
47. McCubrey JA, Abrams SL, Fitzgerald TL, Cocco L, Martelli AM, Montalto G, et al. Roles of signaling pathways in drug resistance, cancer initiating cells and cancer progression and metastasis. *Adv Biol Regul*. 2015;57:75–101.
48. Choi C-H. ABC transporters as multidrug resistance mechanisms and the development of chemosensitizers for their reversal. *Cancer Cell Int*. 2005;5:30.
49. Zhang J, Grek C, Ye Z-W, Manevich Y, Tew KD, Townsend DM. Pleiotropic functions of glutathione S-transferase P. *Adv Cancer Res*. 2014;122:143–75.
50. Holohan C, Van Schaeybroeck S, Longley DB, Johnston PG. Cancer drug resistance: an evolving paradigm. *Nat Rev Cancer*. 2013;13:714–26.
51. Gagnon J-F, Bernard O, Villeneuve L, Têtu B, Guillemette C. Irinotecan inactivation is modulated by epigenetic silencing of UGT1A1 in colon cancer. *Clin Cancer Res*. 2006;12:1850–8.
52. Malet-Martino M, Martino R. Clinical studies of three oral prodrugs of 5-fluorouracil (capecitabine, UFT, S-1): a review. *Oncologist*. 2002;7:288–323.
53. Kosuri KV, Wu X, Wang L, Villalona-Calero MA, Otterson GA. An epigenetic mechanism for capecitabine resistance in mesothelioma. *Biochem Biophys Res Commun*. 2010;391:1465–70.
54. Greally JM. A user's guide to the ambiguous word "epigenetics." *Nat Rev Mol Cell Biol*. 2018;19:207–8.
55. Gayon J. From Mendel to epigenetics: History of genetics. *C R Biol*. 2016;339:225–30.
56. Wang H, Cao G, Wang G, Hao H. Regulation of mammalian UDP-glucuronosyltransferases. *Curr Drug Metab*. 2018;19:490–501.
57. Bird A. DNA methylation patterns and epigenetic memory. *Genes Dev*. 2002;16(1):6–21.
58. Jaenisch R, Bird A. Epigenetic regulation of gene expression: how the genome integrates intrinsic and environmental signals. *Nat Genet*. 2003;33:245–54.
59. Kouzarides T. Chromatin modifications and their function. *Cell*. 2007;128:693–705.
60. Tang J, Salama R, Gadgeel SM, Sarkar FH, Ahmad A. Erlotinib resistance in lung cancer: current progress and future perspectives. *Front Pharmacol*. 2013;4:15.
61. Gridelli C, De Marinis F, Di Maio M, Cortinovis D, Cappuzzo F, Mok T. Gefitinib as first-line treatment for patients with advanced non-small-cell lung cancer with activating epidermal growth factor receptor mutation: review of the evidence. *Lung Cancer Amst Neth*. 2011;71:249–57.
62. Bell DW, Gore I, Okimoto RA, Godin-Heymann N, Sordella R, Mulloy R, et al. Inherited susceptibility to lung cancer may be associated with the T790M drug resistance mutation in EGFR. *Nat Genet*. 2005;37:1315–6.
63. Ma C, Wei S, Song Y. T790M and acquired resistance of EGFR TKI: a literature review of clinical reports. *J Thorac Dis*. 2011;3:10–8.
64. Chan BA, Hughes BGM. Targeted therapy for non-small cell lung cancer: current standards and the promise of the future. *Transl Lung Cancer Res*. 2015;4:36–54.
65. Rang HP, Dale MM, Ritter JM, Flower RJ, Henderson G. Rang & Dale's pharmacology. Amsterdam: Elsevier; 2011.
66. Hagenbuch B, Gao B, Meier PJ. Transport of xenobiotics across the blood-brain barrier. *Physiology*. 2002;17(6):231–4. <https://doi.org/10.1152/nips.01402.2002>.
67. Dahan A, Sabit H, Amidon GL. Multiple efflux pumps are involved in the transepithelial transport of colchicine: combined effect of p-glycoprotein and multidrug resistance-associated protein 2 leads to decreased intestinal absorption throughout the entire small intestine. *Drug Metab Dispos*. 2009;37:2028–36.
68. Wang H, Gao Z, Liu X, Agarwal P, Zhao S, Conroy DW, et al. Targeted production of reactive oxygen species in mitochondria to overcome cancer drug resistance. *Nat Commun*. 2018;9:562.
69. Lovell JF, Billen LP, Bindner S, Shamas-Din A, Fradin C, Leber B, et al. Membrane binding by tBid initiates an ordered series of events culminating in membrane permeabilization by bax. *Cell*. 2008;135:1074–84.
70. Moore VDG, Brown JR, Certo M, Love TM, Novina CD, Letai A. Chronic lymphocytic leukemia requires BCL2 to sequester prodeath BIM, explaining sensitivity to BCL2 antagonist ABT-737. *J Clin Invest*. 2007;117:112–21.
71. Youle RJ, Strasser A. The BCL-2 protein family: opposing activities that mediate cell death. *Nat Rev Mol Cell Biol*. 2008;9(1):47–59.
72. Delgado Y, Torres A, Milián M. Apoptosis' activation associated to BH3 only domain and BCL-2 homology domain proteins: new way to design anti-cancer drugs. *J Cancer Prev Curr Res*. 2019. <https://doi.org/10.15406/jcpcr.2019.10.00391>.
73. Chakravarthi BVSK, Nepal S, Varambally S. Genomic and epigenomic alterations in cancer. *Am J Pathol*. 2016;186:1724–35.
74. Campbell KJ, Tait SWG. Targeting BCL-2 regulated apoptosis in cancer. *Open Biol*. 2018;8: 180002.
75. Callagy GM, Pharoah PD, Pinder SE, Hsu FD, Nielsen TO, Ragaz J, et al. Bcl-2 is a prognostic marker in breast cancer independently of the nottingham prognostic index. *Clin Cancer Res*. 2006;12:2468–75.
76. SD C. BCL-2 in prostate cancer: a minireview. *Apoptosis*. 2003;8:29–37.
77. Correia C, Schneider PA, Dai H, Dogan A, Maurer MJ, Church AK, et al. BCL2 mutations are associated with increased risk of transformation and shortened survival in follicular lymphoma. *Blood*. 2015;125:658–67.
78. Hata AN, Engelman JA, Faber AC. The BCL2 family: key mediators of the apoptotic response to targeted anticancer therapeutics. *Cancer Discov*. 2015;5:475–87.
79. Du C, Zhang X, Yao M, Lv K, Wang J, Chen L, et al. Bcl-2 promotes metastasis through the epithelial-to-mesenchymal transition in the BCap37 medullary breast cancer cell line. *Oncol Lett*. 2018;15:8991.
80. Ikegaki N, Katsumata M, Minna J, Tsujimoto Y. Expression of bcl-2 in small cell lung carcinoma cells1. *Cancer Res*. 1994;54:6–8.

81. Beroukhi R, Mermel CH, Porter D, Wei G, Raychaudhuri S, Donovan J, Barretina J, Boehm JS, Dobson J, Urashima M, Mc Henry KT. The landscape of somatic copy-number alteration across human cancers. *Nature*. 2010;463(7283):899–905.
82. Yuan B, Hao J, Zhang Q, Wang Y, Zhu Y. Role of Bcl-2 on drug resistance in breast cancer polyploidy-induced spindle poisons. *Oncol Lett*. 2020;19:1701–10.
83. Wang K, Meng J, Wang X, Yan M, Liu S, Yang S, et al. Pan-cancer analysis of the prognostic and immunological role of PAQR4. *Sci Rep*. 2022;12:21268.
84. Baretta M, Le DT. DNA mismatch repair in cancer. *Pharmacol Ther*. 2018;189:45–62.
85. Kumazaki M, Noguchi S, Yasui Y, Iwasaki J, Shinohara H, Yamada N, et al. Anti-cancer effects of naturally occurring compounds through modulation of signal transduction and miRNA expression in human colon cancer cells. *J Nutr Biochem*. 2013;24:1849–58.
86. Lou X-Y, Cheng J-L, Zhang B. Therapeutic effect and mechanism of breviscapine on cisplatin-induced nephrotoxicity in mice. *Asian Pac J Trop Med*. 2015;8:873–7.
87. Monticcolo F, Chiusano ML. Computational approaches for cancer-fighting: from gene expression to functional foods. *Cancers*. 2021;13:4207.
88. Muhammad BA, Almozan S, Babaei-Jadidi R, Onyido EK, Saadeddin A, Kashfi SH, Spencer-Dene B, Ilyas M, Lourdasamy A, Behrens A, Nateri AS. FLYWCH1, a novel suppressor of nuclear  $\beta$ -catenin, regulates migration and morphology in colorectal cancer. *Mol Cancer Res*. 2018;16(12):1977–90.
89. Guibal FC, Moog-Lutz C, Smolewski P, Gioia YD, Darzynkiewicz Z, Lutz PG, et al. ASB-2 inhibits growth and promotes commitment in myeloid leukemia cells\*. *J Biol Chem*. 2002;277:218–24.
90. Menon A, Abd-Aziz N, Khalid K, Poh CL, Naidu R. miRNA: a promising therapeutic target in cancer. *Int J Mol Sci*. 2022;23:11502.
91. Raut JR, Schöttker B, Holleczer B, Guo F, Bhardwaj M, Miah K, et al. A microRNA panel compared to environmental and polygenic scores for colorectal cancer risk prediction. *Nat Commun*. 2021;12:4811.
92. Yu X, Li Z, Shen J, Wu WKK, Liang J, Weng X, et al. MicroRNA-10b promotes nucleus pulposus cell proliferation through RhoC-Akt pathway by targeting HOXD10 in intervertebral disc degeneration. *PLoS ONE*. 2013;8:e83080.
93. Huang J, Zhang S-Y, Gao Y-M, Liu Y-F, Liu Y-B, Zhao Z-G, et al. MicroRNAs as oncogenes or tumour suppressors in oesophageal cancer: potential biomarkers and therapeutic targets. *Cell Prolif*. 2014;47:277–86.
94. Miao T-W, Chen F-Y, Du L-Y, Xiao W, Fu J-J. Signature based on RNA-binding protein-related genes for predicting prognosis and guiding therapy in non-small cell lung cancer. *Front Genet*. 2022. <https://doi.org/10.3389/fgene.2022.930826>.
95. Younas M, Hano C, Giglioli-Guivarch N, Abbasi BH. Mechanistic evaluation of phytochemicals in breast cancer remedy: current understanding and future perspectives. *RSC Adv*. 2018;8:29714–44.
96. Li N, Jiang S, Shi J, Fu R, Wu H, Lu M. Construction of a potential microRNA, transcription factor and mRNA regulatory network in hepatocellular carcinoma. *Transl Cancer Res*. 2020;9:5528–43.
97. Jadoon SS, Ilyas U, Zafar H, Paiva-Santos AC, Khan S, Khan SA, et al. Genomic and epigenomic features of glioblastoma multiforme and its biomarkers. *J Oncol*. 2022;2022:1–16.
98. Lee HK, Finniss S, Cazacu S, Bucris E, Ziv-Av A, Xiang C, et al. Mesenchymal stem cells deliver synthetic microRNA mimics to glioma cells and glioma stem cells and inhibit their cell migration and self-renewal. *Oncotarget*. 2013;4:346–61.
99. Lee WJ, Shin CH, Ji H, Jeong SD, Park M-S, Won H-H, et al. hnRNP-regulated LINC00263 promotes malignant phenotypes through miR-147a/CAPN2. *Cell Death Dis*. 2021;12:290.
100. Lee WJ, Ji H, Jeong SD, Pandey PR, Gorospe M, Kim HH. LINC00162 regulates cell proliferation and apoptosis by sponging PAQR4 -targeting miR-485-5p. *J Cell Physiol*. 2022;237:2943–60.
101. Qu C, Ma T, Yan X, Li X, Li Y. Overexpressed PAQR4 predicts poor overall survival and construction of a prognostic nomogram based on PAQR family for hepatocellular carcinoma. *Math Biosci Eng*. 2022;19:3069–90.
102. Tang C, Wu Y, Wang X, Chen K, Tang Z, Guo X. LncRNA MAFG-AS1 regulates miR-125b-5p/SphK1 axis to promote the proliferation, migration, and invasion of bladder cancer cells. *Hum Cell*. 2021;34:588–97.
103. Hu B, Yang X-B, Yang X, Sang X-T. LncRNA CYTOR affects the proliferation, cell cycle and apoptosis of hepatocellular carcinoma cells by regulating the miR-125b-5p/KIAA1522 axis. *Aging*. 2021;13:2626–39.
104. Sung H, Ferlay J, Siegel RL, Laversanne M, Soerjomataram I, Jemal A, et al. Global cancer statistics 2020: GLOBOCAN estimates of incidence and mortality worldwide for 36 cancers in 185 countries. *CA Cancer J Clin*. 2021;71:209–49.
105. Hooi JKY, Lai WY, Ng WK, Suen MMY, Underwood FE, Tanyingoh D, et al. Global prevalence of helicobacter pylori infection: systematic review and meta-analysis. *Gastroenterology*. 2017;153:420–9.
106. Kloosterman WP, Plasterk RHA. The diverse functions of microRNAs in animal development and disease. *Dev Cell*. 2006;11:441–50.
107. Wang X, Liu B, Wen F, Song Y. MicroRNA-454 inhibits the malignant biological behaviours of gastric cancer cells by directly targeting mitogen-activated protein kinase 1. *Oncol Rep*. 2017;
108. Kang W, Huang T, Zhou Y, Zhang J, Lung RWM, Tong JHM, et al. miR-375 is involved in Hippo pathway by targeting YAP1/TEAD4-CTGF axis in gastric carcinogenesis. *Cell Death Dis*. 2018;9:92.
109. Fan H, Jiang M, Li B, He Y, Huang C, Luo D, et al. MicroRNA-let-7a regulates cell autophagy by targeting Rictor in gastric cancer cell lines MGC-803 and SGC-7901. *Oncol Rep*. 2018. <https://doi.org/10.3892/or.2018.6194>.



**Publisher's Note** Springer Nature remains neutral with regard to jurisdictional claims in published maps and institutional affiliations.

Springer Nature or its licensor (e.g. a society or other partner) holds exclusive rights to this article under a publishing agreement with the author(s) or other rightsholder(s); author self-archiving of the accepted manuscript version of this article is solely governed by the terms of such publishing agreement and applicable law.



## Synopsis

**SYNOPSIS OF THE THESIS TO BE SUBMITTED  
TO THE UNIVERSITY OF NMIMS (DEEMED-TO-BE-UNIVERSITY) FOR THE DEGREE OF  
DOCTOR OF PHILOSOPHY (BIOLOGICAL SCIENCES)**

<b>NAME OF CANDIDATE:</b>	<b>Mitesh Joshi</b>
<b>DOCTORAL COMMITTEE:</b>	<b>1. Dr. Kanhu Charan Barick</b> Scientific Officer, Chemistry Division, BARC <b>2. Dr. Padma Devarajan</b> Professor, Pharmaceutics, FMAS Dean, Research and Innovation, ICT
<b>NAME AND DESIGNATION OF MENTOR:</b>	<b>Dr. Purvi Bhatt,</b> I/C Dean, Associate Professor & HOD- Biological Sciences Department of Biological Sciences SDSOS NMIMS
<b>TITLE OF THESIS:</b>	Fabrication of Drug Loaded Polymeric Zinc Oxide Nano Carriers for Targeted Delivery to Cancer Cells
<b>PLACE OF RESEARCH:</b>	Sunandan Divatia School of Science, SVKM's NMIMS University, Vile Parle (W), Mumbai- 400 056
<b>NUMBER AND DATE OF REGISTRATION:</b>	75109160001/ 25 <sup>th</sup> September, 2017
<b>DATE OF SUBMISSION OF SYNOPSIS:</b>	12 <sup>th</sup> July, 2023
<b>SIGNATURE OF THE CANDIDATE:</b>	
<b>SIGNATURE OF THE MENTOR:</b>	

## INDEX

S. No.	Table of Contents	Page Number
1	<b>Chapter 1:</b> Introduction	1-2
2	<b>Chapter 2:</b> Review of Literature	2-5
3	<b>Chapter 3:</b> Rationale, Aim and Objectives	5-6
4	<b>Chapter 4:</b> Synthesis and characterization of bare Zinc oxide nanoparticles (ZnONPs) and Methotrexate loaded Zinc oxide nanoparticles (MTX-ZnONPs) with drug release study	6-9
5	<b>Chapter 5:</b> In-vitro study to evaluate the anti-cancer activity of MTX-ZnONPs on breast cancer cell lines	9-12
6	<b>Chapter 6:</b> Blood biocompatibility studies	12
7	<b>Chapter 7:</b> In-vivo acute oral toxicity study	13
8	<b>Chapter 8:</b> Discussion	13-19
9	<b>Chapter 9:</b> Summary and Conclusion	19-21
10	Publication(s) and Poster Presentation(s)	21
11	References	22-26

### Chapter 1: Introduction

Breast cancer is a type of cancer that starts in the breast. It is the most common cancer among women, and the second leading cause of cancer death among women after lung cancer. Early detection and treatment of breast cancer are important for improving the chances of survival (Sung *et al.*, 2021). Chemotherapy is used to kill cancer cells throughout the body. Chemotherapy may be given before or after surgery, or it may be used as a treatment for advanced breast cancer. Major challenges contributing towards cancer mortality are metastasis and neoplasm resistance to various therapeutic strategies. Amongst the different types in Breast cancer, Triple negative (TNBC) is the most difficult to treat as presently no known targeted therapy is available for the same (Necela *et al.*, 2015). Of various treatment modalities available, chemotherapy has gained much attention due to vast abundance of molecules targeting all possible molecular and chemical targets. Conventional chemotherapeutic agents used to date have several limitations such as non-specific distribution, side effects and resistance in cancer cells. Though a number of treatment strategies have surfaced like Personalized vaccines (Sahin and Türeci, 2018), cell therapy (Miliotou and Papadopoulou, 2018), combination therapy (Mokhtari *et al.*, 2017), gene editing (Baylis and McLeod, 2017) and microbiome treatments (McQuade *et al.*, 2019) are the promising treatment options with their own limitations. Through combination therapy, two (or more) agents targeting different genes, disease pathways or cell-cycle checkpoints in cancer are targeted to maximize the odds to stop further growth of cancer cells. Combination approaches show synergistic or additive effects and significantly enhance the efficacy of standard single-agent treatments (Xu *et al.*, 2015). Folic acid receptor (FAR) are best molecular markers available on cancer cells whose expression increases 20-30 folds in certain cancers like ovarian, breast, cervical etc. By targeting FAR, antitumor agent can be specifically delivered to FAR overexpressing cancer cells and avoiding non-specific tissue absorption (Cheung *et al.*, 2016). Methotrexate (MTX) is a commonly used chemotherapy drug that works by inhibiting the growth of cancer cells. However, its effectiveness can be limited due to drug resistance and toxicity. MTX has been explored for its role in targeting FAR overexpressing cells (Johari-Ahar *et al.*, 2016).

## Synopsis

Nanotechnology offers both passive and active targeting strategies that can enhance the intracellular concentration of drugs in cancer cells and at the same time avoid toxicity to normal cells (Sarkar *et al.*, 2018). Several nanoparticles (NPs) that have been tested in vitro; Zinc oxide nanoparticles (ZnONPs) has proved its efficacy as a potential anti-cancer agent for various different cancer types. ZnONPs offers attractive properties such as easy synthesis, biocompatibility and preferential killing of cancer cells, by ROS generation leading to apoptosis (Singh, Das and Sil, 2020). By combining the ZnONPs and MTX, as novel system, we anticipate that the system will enhance the therapeutic effectiveness and minimize the side effects by individual systems when used alone. Therefore, this study has the potential to contribute significantly towards the development of more targeted and efficient cancer treatments. Using series of characterizations, in-vitro and in-vivo analysis we aim to study the efficacy and anti-cancer potential of this combination system against breast cancer cells.

## Chapter 2: Review of Literature

### 2.1 Breast cancer

As per Globocan data of 2020, breast cancer (11.7%) features on top of the list from its former position followed by lung cancer (11.4%) (Sung *et al.*, 2021). There are two main types of breast cancer: invasive and non-invasive. Invasive breast cancer is cancer that spreads from the lining of the milk ducts or lobules to other parts of the breast. Non-invasive breast cancer is cancer that does not spread beyond the lining of the milk ducts or lobules. The most common type of invasive breast cancer is ductal carcinoma in situ (DCIS). Another type of invasive breast cancer is lobular carcinoma in situ (LCIS) (Sharma, Jain and Sareen, 2013). The treatment for breast cancer depends on the stage of the cancer, the patient's age and overall health, and the patient's preferences. Treatment options may include surgery, radiation therapy, chemotherapy, hormone therapy, or targeted therapy. Chemotherapy is used to kill cancer cells that have spread to other parts of the body. Chemotherapy can be given before surgery to shrink the tumor, or after surgery to kill any cancer cells that may have been left behind. With early detection and treatment, most women with breast cancer can live long and healthy lives (Trayes and Cokenakes, 2021).

Based on receptor status on breast cancer cells they can be classified in different types. Estrogen receptor-positive (ER-positive) and Progesterone receptor-positive (PR-positive)

## Synopsis

breast cancer having receptor site for respective hormone present on the cells. Human epidermal growth factor receptor 2 (HER2) positive breast cancer cells have too many receptors for the HER2 protein. HER2 is a growth factor receptor that can stimulate the growth of cancer cells (Anita Khokhar, 2012). Triple-negative breast cancer (TNBC) cells do not have receptors for ER, PR, or HER2. TNBC is the most aggressive type of breast cancer and is often more difficult to treat (Avery, 2018). However, all of them still have few other receptors too present on cell surface for easy targeting like FAR and transferrin receptor which seem to be overexpressed in breast cancer cells (Soleymani *et al.*, 2018; Wang *et al.*, 2022).

## 2.2 Methotrexate (MTX)

MTX belongs to anti-folate class of drug, under antimetabolite family. MTX is an analogue of folic acid molecule with minor changes in the structure, it also binds to the same site of folic acid on FAR and internalized in the cell. Many cancer cells overexpress FAR on its surface which makes it easy to target. Hence it is recommended drug for many cancers like breast, prostate, ovarian and Acute Lymphoblastic Leukemia (ALL) to name a few (Bryan, 2012). In cells, MTX binds to di hydro folate reductase (DHFR) enzyme and inhibits the purine and thymidylate synthesis, ultimately leading to death of cell. MTX has its effect on rapidly growing cells and thus it also targets the normal body cells like hematopoietic cells and bone marrow cells. This poses serious side effects like myelosuppression and decreased immunity in patients. It has also been demonstrated that long-term use of MTX can cause liver damage and renal damage in normal cells expressing FAR. Issues associated with MTX include poor solubility, poor bioavailability, short half-life of 3-10 hours and serious side effects, which limits the use of MTX in many conditions (Bath *et al.*, 2014; Wong and Choi, 2015; Yang *et al.*, 2015). NPs based MTX delivery systems using gold nanoparticles, iron oxide nanoparticles, polymeric nanoparticles and others have already been explored in-vitro, against breast cancer cell lines like MCF-7 and MDA-MB-231. These studies have suggested a positive correlation of MTX targeting in FAR over expressing cancer cell lines proving its potential application for anticancer targeted treatment (Kukowska-Latallo *et al.*, 2005).

## Synopsis

### 2.3 Zinc oxide nanoparticles (ZnONPs)

Zinc (Zn), zinc oxide (ZnO), and zinc oxide nanoparticles (ZnONPs) are all different forms of Zn. Zn is an essential mineral that plays a role in many cellular processes, including cell growth, division, and apoptosis. ZnO is a white, odourless powder that is used in a variety of products, including sunscreen, cosmetics, and paints (R, 2016). ZnONPs are tiny particles of zinc oxide that are smaller than 100 nanometres. ZnONPs have proved its efficacy as a potential anticancer agent for various different cancer types in vitro. ZnONPs are cytotoxic as they release soluble  $\text{Zn}^{+2}$  ions in the surrounding environment which is the major factor involved into ZnONPs related toxicity. ZnONPs being positively charged, are selectively attracted to cancer cells leading to membrane destabilization and impaired permeability of cells. Increased ions in the cell leads to generation of reactive oxygen species (ROS) in the cell which generates oxidative stress on the cell and DNA damage, protein damage and ultimately apoptosis of cell. ZnONPs have been proven to be efficacious in delivering the chemotherapeutic drugs to various cancer cells (Wang *et al.*, 2017; Singh, Das and Sil, 2020).

### 2.4 Nanotechnology and its applications in cancer

Nanotechnology is the application of materials and systems at the nanometre scale (1 nanometre = 1 billionth of a meter). By offering new ways to identify, target, and administer therapies to cancer cells, nanotechnology has the potential to revolutionize the way cancer is treated (Yao *et al.*, 2020). It is known that NPs are known to possess unique properties such as, high surface area, tuneable optical and electronic properties, and the ability to interact with biological systems, that are not found in larger particles. These properties make NPs promising candidates for a wide range of applications. Nanotechnology holds the potential for controlled and targeted drug delivery of therapeutic molecules to diseased tissues which could drastically reduce toxic side effects on healthy cells (Parvanian, Mostafavi and Aghashiri, 2017). NPs can also be functionalized with various molecules or coatings to enhance their properties or enable specific applications. Nanoplatfroms are advancing and they are being developed to deliver different type of chemical drugs, antibodies, small peptides, small molecule inhibitors, biomolecular drugs like (DNA, small interfering RNA (siRNA) and mRNA) and even radio nuclei to cancer sites alone or in combination of more than one agent together to work in a synergistic manner to improve the efficacy of system

## Synopsis

(Gurunathan *et al.*, 2018).

Number of NPs-based formulations have shown enhanced efficacy against cancer and received approvals. E.g. Doxorubicin (Doxil®) got approved by US Food and Drug Administration (US-FDA) in year 1995 and became first NP based drug similarly, Albumin based NP formulation of Paclitaxel (Abraxane®) in the year 2005 got approval. MEPACT liposomal mifamurtide for Osteosarcomas got approval by European Medicines Agency in 2009 and many more are still under investigation at different stages of clinical trials (Sanna, Pala and Sechi, 2014; Anselmo and Mitragotri, 2019).

## Chapter 3: Rationale, Aim and Objectives

### 3.1 Rationale

In case of breast cancer, there are limited treatment options available that specifically target hormone receptor-negative cancers and these cancers are often treated with chemotherapy and radiation therapy. MTX have a selective internalization via FAR, which are comparatively overexpressed on cancer cells than normal cells. Studies suggest that FAR may be a promising target for the development of new treatments for breast cancer cells. But, MTX toxicity and resistance become one big hurdle in its application. Nanotechnology offers both passive and active targeting strategies that can enhance the intracellular concentration of drugs in cancer cells and at the same time avoid toxicity to normal cells. ZnONPs have proved its efficacy as a potential anticancer agent and drug delivery vehicle for various different cancer types in-vitro. By combining the NP based drug delivery of MTX, we anticipate that the system will enhance the therapeutic effectiveness and minimize the side effects observed when used alone.

Our primary aim was to use MTX along with ZnONPs to check its activity in vitro using breast cancer cells. The study aimed to take advantage of ZnONPs to kill cancer cells along with MTX as targeting agent. Through scientific approaches, ZnONPs role in killing cancer cells has already been evaluated but, its potential along with MTX still remains to be unexplored in breast cancer.

## Synopsis

### 3.2 Aim and Objectives

#### 3.2.1 Aim

To study the anti-cancer activity of drug loaded zinc oxide nanocarrier entrapped in a biocompatible polymer on breast cancer cells.

#### 3.2.2 Objectives

1. Synthesis and characterization of drug loaded Zinc oxide nano particles (ZnONPs)
2. Drug release study of drug loaded nanoparticles.
3. In vitro analysis of the developed system to evaluate its anti-cancer potential.
4. Study the Blood biocompatibility with newly developed system.
5. In vivo acute oral toxicity study of the newly developed system using a suitable animal model.

## Chapter 4: Synthesis and characterization of bare Zinc oxide nanoparticles (ZnONPs) and Methotrexate loaded Zinc oxide nanoparticles (MTX-ZnONPs) with drug release study

This chapter deals with synthesis of bare ZnONPs and MTX-ZnONPs using a simple and cost-effective method and characterization of the same. For the synthesis precursors used were Zinc nitrate hexa hydrate  $\text{Zn}(\text{NO}_3)_2 \cdot 6\text{H}_2\text{O}$ , Potassium hydroxide (KOH) and for drug loading MTX was used. NPs were characterized using Ultraviolet-visible (UV-vis) absorbance spectroscopy, Fourier transform infrared spectroscopy (FTIR), X-ray diffraction (XRD), Inductively Coupled Plasma-Atomic Emission Spectrometry (ICP-AES), zeta ( $\zeta$ ) potential, Dynamic light scattering (DLS), Energy dispersive spectroscopy (EDS)-mapping and High-resolution transmission electron microscopy (HR-TEM) method. Interpretations of the same are described below. Along with characterization, we also report the drug release study of MTX-ZnONPs.

### 4.1 Synthesis of bare ZnONPs and MTX-ZnONPs

We have used simple chemical precipitation method with polyol assisted synthesis approach for bare ZnONPs synthesis. Bare ZnONPs were synthesised in 10% PEG-400 solvent using



## Synopsis

Zn(NO<sub>3</sub>)<sub>2</sub>·6H<sub>2</sub>O as Zn precursor and KOH as reducing agent. For MTX loading ex-situ synthesis approach was used where MTX with previously synthesised and characterized bare ZnONPs were mixed in the ratio of 1:20 to get the final MTX-ZnONPs with loading efficiency of ~79%. Both the particles were centrifuged, washed and dried in oven to get the dry powder.

## 4.2 Characterization of NPs

The characterization of NPs is a critical step in the development of NP. NPs must be characterized for their size, shape, surface properties, composition, and dispersibility. This information is used to ensure that the NP are produced to the desired specifications and that they will perform as expected in the intended application.

### 4.2.1 UV-Vis Spectroscopy

This method was used to understand the change in absorption spectrum for NPs. Bulk ZnO is a non-nanomaterial form of ZnO which shows characteristic  $\lambda_{\text{max}}$  peak at 380 nm. Whereas bare ZnONPs and MTX-ZnONPs had their characteristic  $\lambda_{\text{max}}$  at 362 nm and 370 nm respectively. MTX peaks at 303 nm was also reported in pure MTX as well as MTX-ZnONPs. Band gap energy for bare ZnONPs was calculated based on Tauc's plot as 3.41 eV.

### 4.2.2 FTIR spectroscopy

This method was applied to study the various functional group present on NP system and study the interaction between them. Bare ZnONPs revealed characteristic peaks at 3382 cm<sup>-1</sup>, 886 cm<sup>-1</sup>, and 420 cm<sup>-1</sup> for -OH stretching, Zn-OH vibration, and Zn-O metal oxide bond, respectively. Pure MTX exhibited characteristic peaks at 1644 cm<sup>-1</sup> for the -CONH group, 3387 cm<sup>-1</sup> for the -NH stretch, 2926 cm<sup>-1</sup> for the presence of -CH groups and 1447 cm<sup>-1</sup> designated for the -NH amide bending in the structure. MTX-ZnONPs exhibited MTX peaks like 1640 cm<sup>-1</sup> and 1450 cm<sup>-1</sup>, as well as bare ZnONP peaks like 420 cm<sup>-1</sup> for ZnO.

### 4.2.3 X-ray diffraction (XRD)

XRD can be used to determine the crystal structure of NPs. XRD analysis of bare ZnONPs and MTX-ZnONPs revealed sharp peaks indicating highly crystalline hexagonal wurtzite phase. These peaks matched standard ZnO planes, with varying intensities for MTX-ZnONPs samples.

## **Synopsis**

The average crystalline size was 31 nm for bare ZnONPs and 40 nm for MTX-ZnONPs, consistent with previous reports.

### **4.2.4 Inductively coupled plasma-atomic absorption spectroscopy (ICP-AES)**

ICP-AES of NPs was carried out in order to estimate the Zn content present in the NPs. Bare ZnONPs and MTX-ZnONPs had 350 ppm and 280 ppm of Zn present in them respectively.

### **4.2.5 Zeta potential and Dynamic light scattering (DLS)**

Zeta potential is a charge on NPs' surface, affecting their stability. Bare ZnONPs show greater positive charge under acidic conditions. Although, ZnONPs when loaded with MTX, led to reduction in Zeta potential in comparison to bare ZnONPs. All NP systems exhibit greater stability towards acidic pH.

DLS results show Z-average of 270 nm and 285 nm with average peak size to be 39 nm and 58 nm for bare ZnONPs and MTX-ZnONPs, with moderate size distribution was observed.

### **4.2.6. Energy dispersive spectroscopy (EDS)-mapping**

EDS mapping was performed to determine the chemical composition of material and its distribution. The EDS mapping of bare ZnONPs gave sharp peaks of zinc and oxygen with carbon and weight percentages of 70.37, 20.31, and 9.32, respectively, without any impurities. Whereas in the case of MTX-ZnONPs, the weight percentages of zinc, oxygen, and carbon were 67.45, 18.33, and 14.22, respectively.

### **4.2.7 High-resolution transmission electron microscopy (HR-TEM)**

HR-TEM analysis is a powerful tool for characterizing the structure and morphology of NPs at the atomic scale. This technique allowed to determine the particle size, shape and crystal structure. HR-TEM analysis of bare ZnONPs revealed hexagonal crystal morphology with an average size of 30 nm. The crystal lattice arrangement, SAED pattern, and XRD data confirm the crystalline nature of the particles.

## Synopsis

### 4.3 Drug release study of MTX-ZnONPs

A drug release study was conducted to understand MTX release patterns under simulated physiological conditions from MTX-ZnONPs. The study used dialysis method and PBS with pH 7.4 for normal cellular environment and pH 5.0 for acidic cancer cell environments. Results presented a biphasic release pattern, with 40% drug release within 1 hour and a steady increase up to 90% was seen until 24 hours.

## Chapter 5: In-vitro study to evaluate the anti-cancer activity of MTX-ZnONPs on breast cancer cell lines

In this chapter we have conducted series of in-vitro tests to quantify the effect of MTX-ZnONPs on breast cancer cell lines MCF-7 (MTX-sensitive) and MDA-MB-231 (MTX-resistant). The cytotoxicity of the MTX-ZnONPs on these above cell lines was assessed by performing MTT (3-(4,5-Dimethylthiazol-2-yl)-2,5-diphenyltetrazolium bromide) assay using MCF-10A as control cell line. Further, Acridine Orange/ Ethidium Bromide (AO/EB) staining, cell cycle analysis, Annexin V FITC- Propidium Iodide assay and immunoblotting assays was conducted on breast cancer cell lines MCF-7 and MDA-MB-231 with MTX-ZnONPs. The results suggests that the MTX-ZnONPs had a significant anti-cancer activity on both cell lines, indicating their anti-cancer potential.

Breast cancer cell lines used were MCF-7 and MDA-MB-231 (TNBC) along with normal breast epithelial cell line MCF-10A as control cell line. MCF-7 and MDA-MB-231 cells were cultured in DMEM media accompanied with 10% heat inactivated FBS, and antibiotic antimycotic solution. The MCF-10A cells were cultured in mammary epithelial cell basal medium (MEBM) media supplemented with growth factors (Lonza, USA) and 100 ng/ ml of Cholera toxin. Cells were maintained under humidified conditions at 37 °C, 5% CO<sub>2</sub> and trypsinized after attaining 80–90% confluency and maintained at 37 °C in 5% CO<sub>2</sub>.

### 5.1 Cellular viability assay (MTT)

Cell viability was conducted in order to determine the IC<sub>50</sub> value for synthesized nano systems and study its effect on cell viability of cancer cells. For MTT assay test concentration range selected was 6.25, 12.5, 25, 50 and 100 µg/ml. For positive control MTX was used at

## Synopsis

concentration par with its loading amount on MTX-ZnONPs. The study assessed cytotoxicity of bare ZnONPs, MTX-ZnONPs and MTX on MCF-10A, MCF-7, and MDA-MB-231 cells. MTX-ZnONPs were found to be highly cytotoxic compared to MTX at all concentrations used in case of breast cancer cell lines. At the same time in MCF-10A control cell line, bare ZnONPs were highly cytotoxic compared to MTX-ZnONPs proving biocompatibility with control breast epithelial cells. The IC<sub>50</sub> value of MTX-ZnONPs in MCF-7 and MDA-MB-231 cell line was 5 µg/ml and 49 µg/ml respectively. Additionally, bare ZnONPs led to higher cytotoxicity in MDA-MB-231 cell line, than that of MCF-7 cell line. The results suggest that synthesized MTX-ZnONPs exhibit good efficacy for MCF-7 breast cancer cells and more potent anticancer activity towards drug-resistant TNBC cell line MDA-MB-231 than MTX. Cell viability was increased and higher in MCF-10A cells treated with MTX-ZnONPs, suggesting a safe and biocompatible nature of MTX-ZnONPs and selectivity towards cancer cells.

### 5.2 Acridine Orange/ Ethidium Bromide (AO/EB) viability staining

AO/EB dual fluorescent staining helps detecting basic morphological changes in cells undergoing apoptosis. Moreover, it allows to distinguish between healthy cells, early and late apoptotic cells, and necrotic cells. Control group in all three cell lines had high confluency and characteristic cell morphology with green fluorescence indicating live cell population. Dose-dependent activity was observed for all systems, including the positive control MTX drug. bare ZnONPs showed increased damage signs, while MTX-ZnONPs did not show damage at lower doses in MCF-10A and MDA-MB-231. Higher doses of MTX-ZnONPs showed cells undergoing apoptosis and necrosis in all three cell lines. MTX treatment presented minimal cell damage signs in MDA-MB-231 cells, comparison to MTX-ZnONPs. While in case of MCF-7 cells MTX-ZnONPs had clear signs of toxicity showing cells with condensed and fragmented nuclei, blebbing of plasma membrane and loss of attachment. Cells had reduced confluency, apoptosis, and morphological changes at higher concentrations.

### 5.3 Cell cycle analysis

The study was conducted to gain an understanding of how NPs treatment would affect cancer cell cycle progression. Untreated group of MCF-7 cell line exhibited a standard cell cycle pattern, with the majority of the cell population in the G<sub>0</sub>/G<sub>1</sub> phase, indicating actively

## **Synopsis**

dividing cells. Similarly, bare ZnONPs treatment group showed an identical pattern of cell cycle after treatment, indicating no effect on the cell cycle at the tested concentrations. Interestingly, MTX-ZnONPs treatment group arrested cells in the S phase of the cell cycle, while MTX treatment group led to cell cycle arrest in the S and G2/M phases, preventing cells from moving to the G0/G1 phase. This confirmed that, MTX-ZnONPs have a cell cycle-specific effect on the S phase of the cell cycle in MCF-7 cells.

In untreated MDA-MB-231 cell line control group, the cell population was observed in G0/G1 phase, indicating actively dividing cells. MTX-ZnONPs treatment group showed majority of population arrested in the S and G2/M phases. Bare ZnONPs treatment also had similar effects as MTX-ZnONPs. Although, MTX did not alter the cell cycle in MDA-MB-231 cells considering their inherent resistance to MTX; with cells remaining in the active G0/G1 phase of the cell cycle. Thus, it can be inferred that MTX-ZnONPs exhibit cell cycle specific inhibitory effect on the S phase of the cell cycle and exhibits significant cell arrest compared to MTX in both the breast cancer cell line MCF-7 and MDA-MB-231.

## **5.4 Annexin V FITC- Propidium Iodide assay**

This assay provides quantitative and qualitative information on the extent and kinetics of apoptosis, as well as the mode of cell death. By using both annexin V and PI staining, it is possible to distinguish between apoptotic cells and necrotic cells. More than 90% of cell population in control group were live in both the cell lines. Bare ZnONPs having higher IC50 value for MCF-7 cells did not show any cell toxicity. MTX-ZnONPs treatment significantly reduced live cell population in MCF-7 cells, while MTX alone was less toxic compared to MTX-ZnONP combination.

MDA-MB-231 cells showed increased necrosis and apoptosis in bare ZnONP and MTX-ZnONPs treated groups, with bare ZnONPs showing higher toxicity. While MTX group did not show significant toxicity in MDA-MB-231 cell line. MTX-ZnONPs show greater cytotoxicity towards both sensitive MCF-7 and resistant MDA-MB-231 cell lines.

## **5.5 Western blot analysis**

For quantification of cellular protein levels of Bax, Bcl-xL, Caspase-3 and Caspase-7 immunoblotting was performed, post treatment with MTX-ZnONPs. Blots were probed with

## **Synopsis**

primary antibodies of anti- $\beta$ -actin, anti-Caspase-3, anti-Caspase-7, anti-Bcl-xL, and anti-Bax antibodies. MCF-7 cells showed upregulation of Caspase-7 and Bax which are known to take part in programmed cell death process. Similarly, Bcl-xL which is known as an (anti-apoptotic family of protein) showed downregulation in MCF-7 cells indicating cells undergoing apoptosis.

In case of MDA-MB-231 cells it was observed that MTX treatment led to increase in Bcl-xL levels. Interestingly, downregulation of Caspase-3 (executor caspase) indicates the cell death is not due to apoptosis. But, increased levels of Bax are indicative of their dual role in apoptosis and necrosis which was evident with Annexin V- PI assay. Hence, we can confirm that MTX-ZnONPs and bare ZnONPs both have cytotoxicity towards cancer cells but, MTX-ZnONP combination has proven to be effective anticancer agent showing increased cytotoxicity towards breast cancer cells.

## **Chapter 6: Blood biocompatibility studies**

This chapter discusses about studying the interaction of NPs with blood cell components like, red blood cells (RBCs), white blood cells (WBCs) and platelets. Institutional Ethics Committee (IEC) approval was taken before collecting human blood samples with approval no. (NMIMS/IEC/012/2020).

### **6.1 Hemolysis study**

In this study bare ZnONPs, MTX-ZnONPs and MTX were allowed to interact with the human RBCs at 37 °C for specific amount of time and later readings were taken on EPOCH 2 machine. Distilled water was used as positive control and saline was used as negative control for the study. No hemolysis was observed upon interaction with any NP systems indicating safe and biocompatible nature of NP system.

### **6.2 Blood cell aggregation study**

For this study RBCs, WBCs and platelets were collected from fresh blood samples and interacted with bare ZnONPs and MTX-ZnONPs for specified time and observations were made under microscope. For positive control Poly ethylene imine (PEI) and negative control

## **Synopsis**

saline was used. No aggregation was observed for any of the NP systems indicating safe and biocompatible role of synthesised NPs.

## **Chapter 7: In-vivo acute oral toxicity study**

To conduct in vivo acute oral toxicity study in mice model, Institutional Animal Ethics committee (IAEC) permission was taken from with (project proposal no. CPCSEA/IAEC/P-69/2022). MTX-ZnONPs were tested as per the Acute Oral Toxicity-Up-and-Down-Procedure guideline by OECD 425. For dosing, three concentrations of doses were selected i.e. 55, 175 and 550 mg/ Kg of body weight of animal. For evaluation, behavioural changes were observed for the first 4 hours after administration of the dose and animals were monitored for next 14 days for various signs of toxicity.

No signs of toxicity were reported for any animal dosed at given concentrations and no mortality was observed throughout the study duration. All animals were found healthy and survived without showing any signs of toxicity or morbid behaviour up to 14 days. As per guideline, LD50 for MTX-ZnONPs was identified to be >550 mg/ Kg body weight of animal.

## **Chapter 8: Discussion**

Current treatment strategy available for cancer treatment involves surgery, radiation therapy, chemotherapy, hormonal therapy and targeted therapy. Treatment options are selected based on the various factors like the age, sex, stage and grade of cancer and type of cancer. Chemotherapy is used as an adjuvant therapy along with other types of therapy and occasionally as a part of monotherapy regime to minimize the risk of cancer relapse. Anti-cancer drugs are mainly of three types cytotoxic, hormonal and biological. Cytotoxic drugs kills the cancer cells by interfering with nucleotide synthesis and cell division, which not only harms the cancer cells but kills normal cells as well.

Nanotechnology based approaches have gained attention in the biomedical field due to the advantages it provides small size, superior efficiency and increased physiochemical properties. They can be synthesized from various metals, non-metals & polymers. NPs effectively builds up the therapeutic index, delivers the material across the membrane, reduces the side effects. Metal oxide NPs like gold, silver, zinc, iron are reported for various

## Synopsis

biomedical applications including cancer. A number of NPs based platforms are available for example metal NPs, liposomes, dendrimers, nanocomposites, nanocarriers etc. (Aslan *et al.*, 2013; Markman *et al.*, 2013). Despite the fact that ZnONPs are being used in cosmetics for several years, they are indeed lately investigated as potential therapeutics for the treatment and diagnosis of cancer.

There are various methods available to synthesize ZnONPs, of which precipitation method was chosen and involves the addition of a zinc salt to a solution containing a precipitating agent also known as reducing agent, resulting in the formation of ZnONPs. In the current project chemical precipitation method was chosen for the synthesis of bare ZnONPs. Also, in order to prevent particle agglomeration during synthesis, PEG was introduced as solvent, this approach is known as polyol assisted synthesis. Polyols serve as solvents for most inorganic precursors by dissolving them as metallic salts, owing to their hydrogen bonds and relatively high dielectric constant. In addition, polyols' chelating abilities allow them to act as coordinating solvents, complexants, and surfactants, all of which adsorb on the surface of the expanding elementary particles and inhibit their aggregation (Hosni, Mongia, Samir Farhat, Mounir Ben Amar, Andrei Kanaev, Noureddine Jouini, 2015). For synthesis of MTX-ZnONPs ex-situ approach was preferred considering the positive charge on bare ZnONPs and negative charge of MTX at pH 7. Drug loading on the NPs was calculated as, concentration of MTX before loading and after loading with the help of UV-Vis spectrophotometer at 303 nm and was found out to be 79.44%.

Drug release study was carried out to understand the release pattern of nano systems under simulated physiological conditions. The MTX release from the NP indicated biphasic release pattern with initial burst release within 1 hr and remaining 90% of drug release was seen up to 24 hrs. It was also noted that release was more in the acidic conditions. It is very well documented that cancer cells have faster metabolism and hypoxic conditions causing cancer cells to adopt anaerobic glycolysis, causing lactic acid buildup resulting in lower pH (Mokhtari *et al.*, 2017). ZnONPs being amphoteric in nature dissolves faster in acidic environment releasing  $Zn^{+2}$  ions, ultimate causative factor behind ZnONPs related toxicity. As ZnONPs starts to dissolve MTX is released which further shows toxicity to cells.



## Synopsis

When characterized using various different techniques it was confirmed that both the NPs were of desired characteristics. When NPs are synthesised, they show energy change and absorption shifts towards UV region called as blue shift, which implies quantum confinement of NPs. When particle size decreases, the band gap of the particles increases, leading to a shift in absorption to lower wavelengths (Raoufi, 2013; Singh *et al.*, 2017). The difference in absorption spectra of bulk ZnO, bare ZnONPs and MTX-ZnONPs clearly suggests the size reduction under quantum confinement principle. MTX displays two distinct peaks at 303 nm and 256 nm which were seen in the MTX-ZnONPs post loading. Loading results of MTX on ZnONPs were in alignment with previous literature showing the same (Rozalen *et al.*, 2020). FTIR and XRD based NP characterization confirmed the presence of characteristic peaks of functional groups indicating successful loading of MTX on bare ZnONPs surface and highly crystalline hexagonal wurtzite phase of the structure. These results were found to be in accordance with data reported in literature earlier (Buchheit, Acosta-Humaney and Almanzaby, 2016; Sanmugam *et al.*, 2017). Zeta potential is a charge present on the surface of the NPs which directly correlates to the stability of nano systems. Surface charge plays a very important role in cellular internalization of these particles (Yu *et al.*, 2011; Albanese, Tang and Chan, 2012). NPs with zeta potential values greater than  $\pm 30$  mV are considered to be highly stable and those with values near iso electric point (IEP) i.e zero charge are considered to be the least stable (Sandmann *et al.*, 2015). Bare ZnONPs and MTX-ZnONPs both revealed positive zeta potential under acidic environment. There was an evident shift in the surface charge when MTX was introduced indicating positive interaction between ZnONPs and MTX. Zeta potential clearly indicates the successful coating of NPs with MTX due to shift in the charge. For DLS study, It is important to note that particle size measured is usually greater than the actual particle size as it considers the average hydrodynamic diameter. Moderate size distribution was observed for both of the systems. ICP-AES is the most commonly used method for the elemental analysis, to know the precise concentration of a specific metal ion in the sample (Johari-Ahar *et al.*, 2016; Xie *et al.*, 2017). Both the NP systems were analyzed to know the total Zn content present in them. Amount of Zn present in bare ZnONPs was 0.352 mg/ ml and for MTX-ZnONPs it was 0.280 mg/ ml. In EDS mapping, the chemical composition and distribution of the ZnONPs was determined to quantify the Zinc, oxygen and carbon present in them. Zinc, Oxygen and Carbon and weight percentage as 70.37, 20.31 and 9.32 were found for bare ZnONPs where as for MTX-ZnONPs it was 67.45,

## Synopsis

18.33 and 14.22. Change in carbon value was indicative of presence of organic backbone in sample coming from MTX. HR-TEM analysis found out highly crystalline particles with an average size of around 30 nm with size distribution of 24 nm to 36 nm. NPs have hexagonal crystalline phase with sharp lattice structure visible. These lattice fringes distance was calculated to correlate the lattice planes with XRD peaks which were in alignment.

In vitro cytotoxicity assays were performed to understand the toxicity and mechanism of action of these NPs on breast cancer cells. In this study, we evaluated the impact of synthesized nano systems on cancer cell viability through comprehensive assays and staining techniques. MTT cell viability assay in MCF-7, MDA-MB-231 breast cancer cell line and MCF-10A control cell line showed high cytotoxicity of bare ZnONPs in control cells than cancer cells. As a result of MTX being present on the outer surface of MTX-ZnONPs, they demonstrated less reactivity to MCF-10A control cells compared to bare ZnONPs, which exhibited higher toxicity in MCF-10A. On the other hand, when treated with MCF-7 cells, MTX-ZnONPs in MCF-7 cells showed lower IC<sub>50</sub> values due to their selectivity to cancer cells. However, when the MTX-ZnONP combination nanosystem was used to treat the MDA-MB-231 cells, which are resistant to MTX, the cells were killed at a much higher rate than they have been with MTX alone. Although, bare ZnONPs had lower IC<sub>50</sub> values than that of MTX-ZnONPs in MDA-MB-231 cell line attributing to their high reactivity. Few other research also shows when MTX was used along with some nano carrier system in combination gave better efficacy than drug alone similar to current study (Rozalen *et al.*, 2020; Chaudhari *et al.*, 2021). MTX-ZnONPs presented lowest IC<sub>50</sub> value of 5 µg/ ml for MCF-7 cells followed by 18 µg/ ml and 49 µg/ ml for MCF-10A and MDA-MB-231 cells respectively, based on these all-further assays were conducted. AO/EB live dead cell staining was carried out visualize cytotoxicity under microscope. AO being a permeable dye tends to stain both live and dead cells hence, cells with only AO inside appears green, whereas a cell that is dead or whose membranes has been compromised, absorbs EB and therefore fluoresces red. AO/EB staining of MCF-10A, MCF-7 and MDA-MB-231 cells treated with MTX-ZnONPs and bare ZnONPs showed fragmented nuclei, chromatin condensation blebbing of membrane and green fluorescence visual signs of cells undergoing apoptosis were evident. Additionally other features that included membrane permeability loss, swelling of cell and nuclear condensation with red color fluorescence as EtBr permeabilizes and stains necrotic cells. Necrotic cell populations were also visible in MDA-

## Synopsis

MB-231 and MCF-10A. These results were indicative of NPs mediated apoptotic and necrotic death. In other terms AO/EB results were in more alignment with the MTT data where sensitivity to MTX cell line was confirmed visually (Liu *et al.*, 2015; Jadhav *et al.*, 2016). Normal cell cycle progression is a very important function of a cell and cancer cells have some mechanism to bypass cell cycle checkpoints beyond a limit. Hence to target the cell cycle progression MTX-ZnONPs were used. It was understood that MTX-ZnONPs preferentially halt the cell cycle progression at S phase in MCF-7 and MDA-MB-231. Even though MTX alone had no effect on MDA-MB-231 cells, MTX-ZnONPs treatment at the same concentration did, implying that the combination has a cytotoxic role in resistant cell lines. Reason behind S phase inhibition was specifically due to MTX presence. Once inside the cancer cell, MTX-ZnONPs dissolve under acidic conditions, releasing  $Zn^{2+}$  ions and MTX. MTX polyglutamates and gets converted to its active form, stalling purine and pyrimidine synthesis, leading to arrest in cell cycle at synthesis phase. The mechanism of action for ZnONPs is unknown, but it is believed to involve the release of  $Zn^{2+}$  ions under an acidic environment, causing oxidative stress and causing cellular damage (Xie *et al.*, 2016; Hu and Du, 2020). Apoptosis is a crucial biological process that plays a significant role in the development and maintenance of tissues in multicellular organisms. Annexin V/PI staining is a widely used method for detecting apoptosis, which involves the use of fluorescently labelled annexin V and propidium iodide (PI) to identify cells that are undergoing programmed cell death. Principle of this assay is on the fact that annexin V binds to phosphatidylserine (PS), a lipid molecule that becomes exposed on the outer leaflet of the plasma membrane during early stages of apoptosis. PI, on the other hand, is a membrane-impermeable dye that stains cells with compromised plasma membranes, such as those in late-stage apoptosis or necrosis. By using both annexin V and PI staining, it is possible to distinguish between apoptotic cells (annexin V positive, PI negative) and necrotic cells (annexin V positive, PI positive) (Tian *et al.*, 2020; Shandiz *et al.*, 2021). Both bare ZnONPs and MTX-ZnONPs treated cells led to cytotoxicity in MDA-MB-231 cells and majority of the population was identified as necrotic and late apoptotic. Interestingly, MTX-ZnONP treated group had considerably higher fraction of dead population compared to MTX at those same concentrations, indicating its cytotoxic nature against MTX resistant cell line. These results were in support with the previous study of AO/EB staining where, MDA-MB-231 cells underwent necrosis more than that of MCF-7 cells. Each cell line based on its sensitivity to nanosystem reacts differentially but ultimately leading to necrosis or apoptosis. To

## Synopsis

understand the underlying mechanism behind cell death, protein expression study needs to be carried out. Caspase being member of the cysteine aspartic acid protease (caspase) family performs the function of a crucial protagonist in programmed cell death (Deng and Zhang, 2013). When cells undergo apoptosis, the pro-caspases get activated by cleavage to active caspases and show a change in protein expression. This change in expression on initiation of apoptosis was studied, where, MDA-MB-231 that expresses caspase-3 and MCF-7 that expresses caspase-7 (as it is deficient in caspase-3) showed through the expression of this protein that apoptosis had been initiated (Fu *et al.*, 2014). MTX-ZnONPs treatment in MCF-7 breast cancer cells upregulated Caspase-3 and Bax expression levels, causing apoptosis, while Bcl-xL downregulation, indicated a classical pattern of apoptotic death. Bax overexpression along with caspases is a hallmark sign for caspase mediated cell death. MDA-MB-231 cell line showed upregulation of Bcl-xL and Bax levels in MTX-ZnONP treatment, indicating non-apoptotic cell death whereas higher expression of Bcl-xL and low expression of Bax in MTX treatment group indicated resistance to chemotherapy drug. Bcl-xL has a crucial role to play in cell survival its overexpression is associated with chemoresistance in cell lines.

Blood biocompatibility is an essential property of NPs that needs to be verified as they are intended to be used for medical applications. Incompatibility of NPs can result in severe issues including hemolysis, clotting or even inflammation. NPs that are safe for use in the body can be used as imaging agents, drugs delivery platform and other therapies to patients. In our study of hemolysis and blood cell aggregation assay we found that both bare ZnONPs and MTX-ZnONPs are safe and does not lead to hemolysis or aggregation of blood cells. As ZnO already known to have Generally Recognized as Safe (GRAS) status by US-FDA and MTX is also very well studied clinically used drug biocompatibility status is high (R, 2016).

Acute oral toxicity studies are important to evaluate the potential harm of a substance when ingested. OECD 425 test involves administering a single dose of the substance to a group of animals and monitoring their behaviour and health for a pre-determined period of time. The results are then used to determine the LD50, or the dose at which 50% of the animals die. This information is crucial for determining safe levels of exposure for humans and animals alike (Organisation for Economic Cooperation and Development, 2001). In current study animal behaviour remained normal for 14 days, with no mortality or morbidity observed.

## Synopsis

MTX-ZnONPs showed high LD50 (>550 mg/kg body weight), indicating safe nanosystem use in animals. Considering Zinc is one of the essential mineral nutrients for animal and considering its biosafety profile earlier it can be attributed that excess of Zinc is readily eliminated from body and hence in acute toxicity study no side effects could be noted.

Our findings suggest that MTX-ZnONPs have potential as effective anticancer agents, especially against drug-resistant TNBC cells and other breast cancer cells, while demonstrating biocompatibility and selectivity towards cancer cells.

## Chapter 9: Summary and Conclusion

In summary, MTX-ZnONPs were synthesized using an ex-situ approach, where MTX was loaded onto previously synthesized bare ZnONPs. The resulting NPs were characterized using a variety of techniques. The results of the characterization studies indicated that MTX-ZnONPs had a hexagonal crystal morphology with an average size of 30 nm. The NPs were also highly crystalline and had a positive Zeta potential. The drug release study revealed that MTX-ZnONPs shows biphasic drug release with approx. 90% of the drug release within 24 hours. Blood biocompatibility study found that no hemolysis (rupture of red blood cells) or aggregation (clumping together) of blood cells occurred when the NPs were interacted with blood cells. This indicates that the NPs are biocompatible and safe for use in blood. MTT cell viability assay results revealed the higher cytotoxicity of MTX-ZnONPs compared to MTX in breast cancer cell lines, indicating their enhanced anticancer potential. Conversely, bare ZnONPs demonstrated increased toxicity in MDA-MB-231 cells. We also observed different IC50 values for MTX-ZnONPs in MCF-7 and MDA-MB-231 cells, indicating varying efficacy against different types of breast cancer cells. Additionally, MCF-10A cells treated with MTX-ZnONPs exhibited high cell viability, indicating their biocompatibility and selectivity towards cancer cells. Furthermore, the AO/EB staining supported the MTT results and illustrated dose-dependent effects and unveiled distinct morphological changes associated with apoptosis and necrosis. Cell cycle analysis results revealed that bare ZnONPs had no impact on the cell cycle in MCF-7 cells, while MTX-ZnONPs specifically arrested cells in the S phase. On the other hand, MTX treatment led to cell cycle arrest in both the S phase and G2/M phases. This cell cycle-specific effect of MTX-ZnONPs on the S phase was consistent with our findings. The cell cycle progression was similarly affected by bare ZnONPs in MDA-MB-231 cells, whereas MTX

## Synopsis

had no effect. Cell cycle arrest at the S phase and G2/M phase checkpoints was observed after treatment with MTX-ZnONPs. Also, the Annexin V FITC-Propidium Iodide assay disclosed that MTX-ZnONPs significantly decreased the number of live MCF-7 cell population, while both bare ZnONPs and MTX-ZnONPs caused more necrosis and apoptosis in MDA-MB-231 cells. These findings demonstrate that MTX-ZnONPs enhanced cytotoxic activity in both MCF-7 and MDA-MB-231 cells irrespective of their sensitivity to MTX. Apoptosis was apparent in MCF-7 cells by the upregulation of Caspase-7 and Bax and the downregulation of Bcl-xL. In case of MDA-MB-231 cells, MTX treatment resulted in an increase in Bcl-xL levels, suggesting that cell death was not driven by apoptosis. However, increased levels of Bax suggested its dual role in apoptosis and necrosis, which aligned with other findings. In-vivo acute oral toxicity study in mice presented no signs of toxicity or mortality in any of the animals, even at the highest dose. This suggested that MTX-ZnONPs are not acutely toxic to animals and have a LD50 of 550 mg/Kg.

In conclusion, the synthesis and characterization of MTX-ZnONPs demonstrated their potential as an effective anticancer agent. In terms of anticancer activity, MTX-ZnONPs exhibited enhanced cytotoxicity compared to MTX alone in breast cancer cell lines. The selective toxicity towards cancer cells was demonstrated by high cell viability in normal breast cells. MTX-ZnONPs were found to be biocompatible and safe for use in blood. Interestingly It was observed that MTX-ZnONPs are effective against both MCF-7, MTX-sensitive and MDA-MB-231 MTX-resistant breast cancer cell line. Encouragingly, in-vivo studies also supports that MTX-ZnONPs are not acutely toxic to animals. Overall, these findings highlight the promising potential of MTX-ZnONPs as an effective and safe nanomedicine for breast cancer treatment. Further studies are required to investigate the efficacy and long-term safety of MTX-ZnONPs to evaluate its clinical role in cancer.

## Publications and Presentations

### Publications

1. **Joshi Mitesh, Bhatt Purvi** “Deciphering The Anti-Cancer Activity of Biocompatible Zinc Oxide Nanoparticles Loaded With Methotrexate (MTX-ZnONPs) On Breast Cancer Cells”, Bulletin of Materials Science- IF 1.8 (**Accepted and in Press**)

## Synopsis

2. Manuscript titled “In vitro and In vivo Efficacy and Safety of MTX-ZnONPs against Breast Cancer” is at final editing stage and will be submitted soon to journal.

## Conferences and poster presentations

1. Presented poster titled “Synthesis and Characterization of Biocompatible Chitosan Coated Zinc Oxide Nanoparticles and it’s In vitro Cytotoxicity studies on MCF-7 and MCF-10A Cell lines”- **Joshi Mitesh, Bhatt Purvi**” at **“6<sup>th</sup> INTERNATIONAL CONFERENCE ON RECENT TRENDS IN BIOENGINEERING (ICRTB 2023)”** held at MIT School of Bioengineering Sciences & Research, held on 20<sup>th</sup> - 21<sup>st</sup> January 2023 in Pune.
2. Attended **“INTERNATIONAL CONFERENCE ON ADVANCES IN MATERIALS SCIENCE & APPLIED BIOLOGY (AMSAB 2019)”** held on 8<sup>th</sup>-10<sup>th</sup> January 2019 at NMIMS, Mumbai.

## References

1. Albanese, A., Tang, P. S. and Chan, W. C. W. (2012) 'The Effect of Nanoparticle Size, Shape, and Surface Chemistry on Biological Systems', *Annual Review of Biomedical Engineering*, 14(1), pp. 1–16. doi: 10.1146/annurev-bioeng-071811-150124.
2. Anita Khokhar (2012) 'Breast Cancer in India: Where Do We Stand and Where Do We Go?', *Asian Pacific Journal of Cancer Prevention Asian Pacific J Cancer Prev*, 13(1310), pp. 4861–4866. doi: 10.7314/APJCP.2012.13.10.4861.
3. Anselmo, A. C. and Mitragotri, S. (2019) 'Nanoparticles in the clinic: An update', *Bioengineering & Translational Medicine*, 4(3), pp. 1–16. doi: 10.1002/btm2.10143.
4. Aslan, B. et al. (2013) 'Nanotechnology in cancer therapy.', *Journal of Drug Targeting*, 21(10), pp. 904–13. doi: 10.3109/1061186X.2013.837469.
5. Avery, T. P. (2018) *Triple-Negative Breast Cancer, Changing Paradigms in the Management of Breast Cancer*. doi: 10.1007/978-3-319-60336-0.
6. Bath, R. K. et al. (2014) 'A review of methotrexate-associated hepatotoxicity', *Journal of Digestive Diseases*, 15(10), pp. 517–524. doi: 10.1111/1751-2980.12184.
7. Baylis, F. and McLeod, M. (2017) 'First-in-human Phase 1 CRISPR Gene Editing Cancer Trials: Are We Ready?', *Current Gene Therapy*, 17(4), pp. 309–319. doi: 10.2174/1566523217666171121165935.
8. Bryan, J. (2012) 'From cancer to rheumatoid arthritis treatment: The story of methotrexate', *Pharmaceutical Journal*, 289(7723), pp. 303–304. Available at: [pharmaceutical-journal.com/news-and-analysis/from-cancer-to-rheumatoid-arthritis-treatment-the-story-of-methotrexate/11106439.article](http://pharmaceutical-journal.com/news-and-analysis/from-cancer-to-rheumatoid-arthritis-treatment-the-story-of-methotrexate/11106439.article).
9. Buchheit, R., Acosta-Humanez, F. and Almanzaby, O. (2016) 'Structural, EPR and optical studies on Cu-doped ZnO nanoparticles synthesized by the sol-gel method at different calcination temperatures', *Revista Cubana de Fisica*, 33(1), pp. 4–11.
10. Chaudhari, R. et al. (2021) 'Fabrication of methotrexate-loaded gold nanoconjugates and its enhanced anticancer activity in breast cancer', *3 Biotech*, 11(4), pp. 1–13. doi: 10.1007/s13205-021-02718-7.
11. Cheung, A. et al. (2016) 'Targeting folate receptor alpha for cancer treatment', *Oncotarget*, 7(32), pp. 52553–52574. doi: 10.18632/oncotarget.9651.



## Synopsis

12. Deng, Y. and Zhang, H. (2013) 'The synergistic effect and mechanism of doxorubicin-ZnO nanocomplexes as a multimodal agent integrating diverse anticancer therapeutics', *International Journal of Nanomedicine*, 8, pp. 1835–1841. doi: 10.2147/IJN.S43657.
13. Fu, Y. *et al.* (2014) 'Antioxidants decrease the apoptotic effect of 5-Fu in colon cancer by regulating Src-dependent caspase-7 phosphorylation', *Cell Death and Disease*, 5(1), p. e983. doi: 10.1038/cddis.2013.509.
14. Gurunathan, S. *et al.* (2018) 'Nanoparticle-mediated combination therapy: Two-in-one approach for cancer', *International Journal of Molecular Sciences*, 19(10), pp. 1–37. doi: <https://doi.org/10.3390/ijms19103264>.
15. Hosni, Mongia, Samir Farhat, Mounir Ben Amar, Andrei Kanaev, Nouredine Jouini, and I. Hinkov. (2015) 'Mixing Strategies for Zinc Oxide Nanoparticle Synthesis via a Polyol Process', *AIChE Journal*, 59, pp. 1708–1721. doi: 10.1002/aic.14737.
16. Hu, C. and Du, W. (2020) 'Zinc oxide nanoparticles (ZnO NPs) combined with cisplatin and gemcitabine inhibits tumor activity of NSCLC cells', *Aging*, 12(24), pp. 25767–25777. doi: 10.18632/aging.104187.
17. Jadhav, V. *et al.* (2016) 'Biocompatible arsenic trioxide nanoparticles induce cell cycle arrest by p21WAF1/CIP1 expression via epigenetic remodeling in LNCaP and PC3 cell lines', *Life Sciences*, 148, pp. 41–52. doi: 10.1016/j.lfs.2016.02.042.
18. Johari-Ahar, M. *et al.* (2016) 'Methotrexate-conjugated quantum dots: Synthesis, characterisation and cytotoxicity in drug resistant cancer cells', *Journal of Drug Targeting*, 24(2), pp. 120–133. doi: 10.3109/1061186X.2015.1058801.
19. Kukowska-Latallo, J. F. *et al.* (2005) 'Nanoparticle targeting of anticancer drug improves therapeutic response in animal model of human epithelial cancer', *Cancer Research*, 65(12), pp. 5317–5324. doi: 10.1158/0008-5472.CAN-04-3921.
20. Liu, K. *et al.* (2015) 'Dual AO/EB Staining to Detect Apoptosis in Osteosarcoma Cells Compared with Flow Cytometry', *Medical Science Monitor Basic Research*, 21, p. 15. doi: 10.12659/MSMBR.893327.
21. Markman, J. L. *et al.* (2013) 'Nanomedicine therapeutic approaches to overcome cancer drug resistance', *Advanced Drug Delivery Reviews*, 65(13–14), pp. 1866–1879. doi: 10.1016/j.addr.2013.09.019.
22. McQuade, J. L. *et al.* (2019) 'Modulating the microbiome to improve therapeutic response in cancer', *The Lancet Oncology*, 20(2), pp. 77–91. doi: 10.1016/S1470-2045(18)30952-5.

## Synopsis

23. Miliotou, A. N. and Papadopoulou, L. C. (2018) 'CAR T-cell Therapy: A New Era in Cancer Immunotherapy', *Current Pharmaceutical Biotechnology*, 19(1), pp. 5–18. doi: 10.2174/1389201019666180418095526.
24. Mokhtari, R. B. *et al.* (2017) 'Combination therapy in combating cancer', *Oncotarget*. Impact Journals LLC, pp. 38022–38043. doi: 10.18632/oncotarget.16723.
25. Necela, B. M. *et al.* (2015) 'Folate receptor- $\alpha$  (FOLR1) expression and function in triple negative tumors', *PLoS ONE*, 10(3). doi: 10.1371/journal.pone.0122209.
26. Organisation for Economic Cooperation and Development (2001) 'Test guideline 425: acute oral toxicity - Up-and-Down Procedure', *Guideline for Testing of Chemicals*, (December), p. 26.
27. Parvanian, S., Mostafavi, S. M. and Aghashiri, M. (2017) 'Multifunctional nanoparticle developments in cancer diagnosis and treatment', *Sensing and Bio-Sensing Research*, 13, pp. 81–87. doi: 10.1016/j.sbsr.2016.08.002.
28. R, S. (2016) 'A Simple Method for Preparation of Nano-sized ZnO', *Research & Reviews: Journal of Chemistry*, 5(2), pp. 45–49. Available at: <https://www.rroj.com/open-access/a-simple-method-for-preparation-of-nanosized-zno-.pdf> (Accessed: 30 October 2017).
29. Raoufi, D. (2013) 'Synthesis and microstructural properties of ZnO nanoparticles prepared by precipitation method', *Renewable Energy*, 50, pp. 932–937. doi: 10.1016/j.renene.2012.08.076.
30. Rozalen, M. *et al.* (2020) 'Synthesis of controlled-size silver nanoparticles for the administration of methotrexate drug and its activity in colon and lung cancer cells', *RSC Advances*, 10(18), pp. 10646–10660. doi: 10.1039/c9ra08657a.
31. Sahin, U. and Türeci, Ö. (2018) 'Personalized vaccines for cancer immunotherapy', *Science*, 359(6382), pp. 1355–1360. doi: 10.1126/science.aar7112.
32. Sandmann, A. *et al.* (2015) 'Interaction of L-cysteine with zno: Structure, surface chemistry, and optical properties', *Langmuir*, 31(21), pp. 5701–5711. doi: 10.1021/la504968m.
33. Sanmugam, A. *et al.* (2017) 'One-Pot Facile Methodology to Synthesize Chitosan-ZnO-Graphene Oxide Hybrid Composites for Better Dye Adsorption and Antibacterial Activity', *Nanomaterials*, 7(11), p. 363. doi: 10.3390/nano7110363.

## Synopsis

34. Sanna, V., Pala, N. and Sechi, M. (2014) 'Targeted therapy using nanotechnology: Focus on cancer', *International Journal of Nanomedicine*, 9(1), pp. 467–483. doi: 10.2147/IJN.S36654.
35. Sarkar, M. K. I. *et al.* (2018) 'Effect of nanotechnology on cancer disease', *Journal of Bionanoscience*, 12(3), pp. 297–315. doi: 10.1166/jbns.2018.1532.
36. Shandiz, S. A. S. *et al.* (2021) 'Evaluation of Metastasis Suppressor Genes Expression and In Vitro Anti-Cancer Effects of Zinc Oxide Nanoparticles in Human Breast Cancer Cell Lines MCF-7 and T47D', *Avicenna Journal of Medical Biotechnology*, 13(1), p. 9. doi: 10.18502/AJMB.V13I1.4576.
37. Sharma, A., Jain, N. and Sareen, R. (2013) 'Nanocarriers for diagnosis and targeting of breast cancer', *BioMed Research International*, 2013, pp. 1–11. doi: 10.1155/2013/960821.
38. Singh, S. *et al.* (2017) 'Amino acid functionalized zinc oxide nanostructures for cytotoxicity effect and hemolytic behavior: Theoretical and experimental studies', *Materials and Design*, 134, pp. 10–22. doi: 10.1016/j.matdes.2017.08.020.
39. Singh, T. A., Das, J. and Sil, P. C. (2020) *Zinc oxide nanoparticles: A comprehensive review on its synthesis, anticancer and drug delivery applications as well as health risks*, *Advances in Colloid and Interface Science*. Elsevier B.V. doi: 10.1016/j.cis.2020.102317.
40. Soleymani, J. *et al.* (2018) 'Probing the specific binding of folic acid to folate receptor using amino-functionalized mesoporous silica nanoparticles for differentiation of MCF 7 tumoral cells from MCF 10A', *Biosensors and Bioelectronics*, 115, pp. 61–69. doi: 10.1016/j.bios.2018.05.025.
41. Sung, H. *et al.* (2021) 'Global Cancer Statistics 2020: GLOBOCAN Estimates of Incidence and Mortality Worldwide for 36 Cancers in 185 Countries', *CA: A Cancer Journal for Clinicians*, 71(3), pp. 209–249. doi: 10.3322/caac.21660.
42. Tian, J. *et al.* (2020) 'Effects of Selenium Nanoparticles Combined With Radiotherapy on Lung Cancer Cells', *Frontiers in Bioengineering and Biotechnology*, 8, p. 1289. doi: 10.3389/fbioe.2020.598997.
43. Traves, K. P. and Cokenakes, S. E. H. (2021) 'Breast Cancer Treatment', *American family physician*, 104(2), pp. 171–178. doi: 10.12968/bjon.1995.4.8.431.
44. Wang, G. *et al.* (2022) 'Intraductal administration of transferrin receptor-targeted immunotoxin clears ductal carcinoma in situ in mouse models of breast cancer—a

## Synopsis

- preclinical study', *Proceedings of the National Academy of Sciences of the United States of America*, 119(24), pp. 1–10. doi: 10.1073/pnas.2200200119.
45. Wang, J. *et al.* (2017) 'Exploration of Zinc Oxide Nanoparticles as a Multitarget and Multifunctional Anticancer Nanomedicine', *ACS Applied Materials and Interfaces*, 9(46), pp. 39971–39984. doi: 10.1021/acsami.7b11219.
46. Wong, P. T. and Choi, S. K. (2015) 'Mechanisms and implications of dual-acting methotrexate in folate-targeted nanotherapeutic delivery', *International Journal of Molecular Sciences*, 16(1), pp. 1772–1790. doi: 10.3390/ijms16011772.
47. Xie, L. *et al.* (2016) 'Methotrexate induces DNA damage and inhibits homologous recombination repair in choriocarcinoma cells', *OncoTargets and Therapy*, 9, pp. 7115–7122. doi: 10.2147/OTT.S116387.
48. Xie, X. *et al.* (2017) 'The Effect of shape on Cellular Uptake of Gold Nanoparticles in the forms of Stars, Rods, and Triangles', *Scientific Reports*, 7(1), pp. 1–9. doi: 10.1038/s41598-017-04229-z.
49. Xu, X. *et al.* (2015) 'Cancer nanomedicine: From targeted delivery to combination therapy', *Trends in Molecular Medicine*. Elsevier Ltd, pp. 223–232. doi: 10.1016/j.molmed.2015.01.001.
50. Yang, S. L. *et al.* (2015) 'Methotrexate associated renal impairment is related to delayed elimination of high-dose methotrexate', *Scientific World Journal*, 2015. doi: 10.1155/2015/751703.
51. Yao, Y. *et al.* (2020) 'Nanoparticle-Based Drug Delivery in Cancer Therapy and Its Role in Overcoming Drug Resistance', *Frontiers in Molecular Biosciences*, 7(August), pp. 1–14. doi: 10.3389/fmolb.2020.00193.
52. Yu, J. *et al.* (2011) 'Effects of physicochemical properties of zinc oxide nanoparticles on cellular uptake', in *Journal of Physics: Conference Series*. doi: <https://doi.org/10.1088/1742-6596/304/1/012007>.